Towards an understanding of the graphite anode surfaces and their relationship at low-temperature in Li-ion batteries

You Shin Yoon

Doctor of Philosophy

Department of Chemical & Biological Engineering

University of Sheffield

December 2021

Acknowledgement

Abstract

The Li-ion battery tends to show reduced performance or fail at temperatures below room temperature. Hence, it is important to know why the battery performance drops with the decrease in temperature. A solid electrolyte interface (SEI) is a passive layer that forms on the electrode after the first charging cycle due to the electrolyte undergoing reduction at the anode surface during the first charge in the Li-ion battery system. The main scope of this thesis is to investigate and to understand the formation of the SEI layer and understand its relationship with the temperature in Li-ion battery systems. Temperatures were fixed to 0^oC, -5^oC, -10^oC, and -15^oC. The compositions of the SEI layer is mainly determined by the compositions of the electrolyte used within the system being studied. The physical properties such as freezing and melting points are highly dependable by the temperature. At a certain low temperature, partial freezing of the electrolyte can occur resulting in significantly poor ionic conductivity compared to room temperature because it loses the role of electrolyte that is a liquid to transport the Li-ions from the cathode to the anode and vice versa.

The SEI layer is crucial in the Li-ion battery system especially for the low-temperature battery cycle because without the SEI layer, poor battery performance is seen. The battery can have much better low temperature performance when the SEI layer is formed on the graphite anode, the majority of this is formed in the first cycle but sometimes, it continuously occurs for up to a few cycles (30 cycles) to obtain a stable robust SEI layer. Although the SEI layer is formed by having few cycles at room temperature, the battery can still have poor low temperature performance mostly due to the reduced ionic conductivity of the battery electrolyte. The decisive, and performance parameters including capacity, coulombic efficiency, irreversible capacity loss, and capacity retention are important to assess the battery performance in general. At low temperatures, these parameters can decrease which results in poor low temperature battery performance. FEC additive can slightly improve the low temperature performance by reducing the capacity retention and obtaining good coulombic efficiency, but it had minimal effect on the capacity produced.

Using a diverse range of experimental techniques available to us (EIS, ATR-FTIR, and AFM), the behaviour of the SEI layer, and the temperature can be determined. EIS is used to find out the possible resistance of the SEI layer (R_{sei}) and gain quantitative information. ATR-FTIR is used to determine possible SEI components. Based on the FTIR data, these are the possible SEI components formed on graphite anode; $(CH_2OCO_2Li)_2$, Li_2CO_3, and ROLi because EC based electrolyte is mainly used throughout this study. When an FEC additive is used, possibly LiF is included into to the SEI component observed. AFM analysis gives further insight into the SEI layer formed on the graphite electrode to visualises the scanned surface of the sample.

Abbreviation table

Abbreviation	Meaning
AC	Alternating Current
AFM	Atomic force microscopy
ATR-FTIR	Attenuated total reflection-FTIR
CC	Constant Current
DC	Direct Current
DEC	Diethyl carbonate
DMC	Dimethyl carbonate
EC	Ethylene carbonate
EIS	Electrochemical impedance spectroscopy
EMC	Ethyl methyl carbonate
FTIR	Fourier- transform infrared spectroscopy
IPA	Isopropyl alcohol
Li	Lithium
$LiBF_4$	Lithium tetrafluoroborate
$LiCoO_2$	Lithium Cobalt Oxide
$LiNiO_2$	Lithium Nickel Oxide
$LiPF_6$	Lithium hexafluorophosphate
LP30	1.0M $LiPF_6$ in EC/DMC=50/50 (v/v)
LTO	Spinel lithium titanate
MCMB	Mesocarbon microbeads
NiCd	Nickel-cadmium battery
NiMH	Nickel-metal-hydride battery
NMC	Lithium Nickel Manganese Cobalt oxide battery
PC	Propylene carbonate
R	Resistor
RMS	Root mean square
SEI	Solid Electrolyte Interphase
SEM	Scanning electron microscope

Table of Contents

Chapter 1 - Introduction

As people seek an efficient and better lifestyle, their thought of energy was completely changed into produce, recycling, and storing the energy whereas in the past it was simply produced and used. Especially, storing electrical energy became crucial due to usage in its diverse application for portable electronic devices such as laptops, smartphones, cameras, and the future renewable energy industry. The electrical storage system became a promising aspect of energy storage such as batteries and capacitors. They both use electrical energy but store it into different energy; the battery stores chemical energy and the capacitor stores it as surface charge [1].

Although the study of battery has been carried out for about 100 years and researchers are still investigating it, still, there is no ideal battery available because most of the batteries do not fulfil a wanted condition. For example, an ideal battery can be described as cost-effective, non-degradable, and environmentally safe to use. Amongst different types of battery such as lead-acid, nickel-based, and sodium battery, Li-ion battery is close to the possible ideal battery and that is why it is the most commonly used secondary battery even now due to long cycle life with easy to charge / discharge, high voltage and energy density, and low self-discharge. By comparing with other batteries, it can be recharged multiple times in good stability and produce nominal voltage up to 3.6 V. However, the battery casing and protection are key issues in terms of the safety aspect. There is a possibility that a battery can catch fire or explode on its own either as the toxic gas is generated from inside a battery or the battery case is damaged and leakage of electrolyte. In addition, ageing is another issue for Li-ion batteries because the battery degradation takes place after a certain battery cycle has undergone.

Further research on Li-ion batteries is needed because there are a lot of issues to solve in future. The development study has been already started to overcome the drawbacks of Li-ion batteries. For example, graphene and carbon nanotubes were tested as an electrode because they are flat and can be aligned vertically together to boost the battery efficiency having better battery life and power. A low-temperature electrolyte is further developed to create a battery that can withstand a cold environment, especially in military and space applications. When the battery is used in a cold environment normally 0^oC or below, the battery starts to fail and either the power goes off or it leads to short battery life due to not having enough power available. The importance of low-temperature battery study is still needed because many batteries are not well functioned in such a cold environment. These are just an example of which factors that researchers are currently focusing on to create an ideal Li-ion battery. However, they are not having a deeper investigation on the SEI layer because it is difficult to analyse due to the small thickness existence on graphite anode. A lot of studies has been done related to both anode and cathode electrode, electrolyte, and cycling conditions of Li-

ion battery due to better availability and accessibility of experimental techniques such as AFM, SEM, TEM, XRD, XPS, NR, Ellipsometry and so on. Of course, SEI layer study can be done using these techniques, but it will be time managing and might not produce the expected results.

This particular thesis is especially focused on SEI layer investigation formed on graphite anode in a cold environment. Since the formation of the SEI layer and low temperature is a good reason for Li-ion battery failure, it needs to be studied further. It can be hypothesised that it is not clear which factor affects the low-temperature battery performance the most. Therefore, the behaviour of the SEI layer at low temperature must be done. Aims and objectives are introduced to understand and explain qualitative and quantitative results to develop knowledge about the Li-ion battery system, low-temperature behaviour, and SEI layer. In this thesis specific experiment, I attempt to clarify these proposals by observing the behaviour of the SEI layer in the low-temperature range (down to -15°C).

Aims

- To understand the mechanisms of the SEI layer of the Li-ion battery system (Li/graphite half-cell) and familiarise them.
- To understand its battery performance and investigate the behaviour of the SEI layer based on cycling temperature conditions (from 25°C to -15°C). It can be determined whether the SEI is a temperature-dependent layer or not.
- To classify the relationship of the formation of SEI layer on graphite anode with the low-temperature conditions (from 25°C to -15°C), the number of cycles (1 – 100) of the battery, the effect of cycle number at room temperature (SEI formation), the rest period (0 and 8 hours), and the battery electrolyte (LiPF$_6$ salt with EC-based electrolyte; DMC, DEC, EMC) with additive (FEC).
- To look and find out the information about SEI layer in Li/graphite half-cell such as the components and resistance.

Objective

- Li/graphite half-cell will be cycled at room temperature so that this data can be compared with low-temperature data to find out the effect of cycling temperature on battery performance. At this stage, the battery will be built with exactly the same materials (Artificial graphite and LP30 electrolyte) in Chapter 4.
- Then, the composition of the Li/graphite half-cell may alter based on the key aspects including temperature conditions, cycle number, rest period, and battery electrolyte (with additive) in Chapter 5.

1. The only aspect that in common is the anode material – Artificial graphite.

2. The cycle number will vary from 1-100 at room temperature and low-temperature (specifically mentioned in Chapter 4 and 5)

3. The rest period will be assigned when the cycling temperature is lowered from $25^{o}C$ to 0, -5, -10, $-15^{o}C$.

4. Various electrolyte will be used from LP30 and LP40 to newly created electrolyte (Table 5-2 in Chapter 5, section 5.8) with FEC additive.

- All data sets will be extracted from the MACCOR battery tester because it allows the battery to cycle freely with temperature change in single procedure.

- Once the battery cycle is finished, the artificial graphite anode will be extracted separately for further investigation using experimental techniques in Chapter 6; EIS, ATR-FTIR, and AFM. These data are important to understand the characteristics of the SEI layer.

    1. EIS is used to find out the possible resistance of the SEI layer (R_{sei}) and gain quantitative information.

    2. Using ATR-FTIR, the possible SEI components such as $(CH_2OCO_2Li)_2$, Li_2CO_3, and ROLi are expected because mainly EC-based electrolyte is used throughout this study. When an FEC additive is added to electrolyte, possibly more LiF is into to the SEI component observed.

    3. AFM analysis gives further insight into the SEI layer formed on the graphite electrode to visualises the scanned surface of the sample in 3D image.

The data from both sets will be synthesised to establish the key factor that affects the relationship between the low temperature and the characteristics of the SEI layer. The chemical composition that dominates the most in the SEI layer will be classified separately based on the number of cycles, temperature, and battery electrolyte.

Chapter 2 – Literature Review

This chapter focuses on types of batteries and their historical background. The Li-ion battery is the key in this project and therefore, its chemistry and fundamental components are contained. In addition, it delves into how solid electrolyte interphase (SEI) forms on graphite anode and various factors that affect its formation. Finally, the chapter concludes by discussing the low-temperature system of Li-ion batteries.

2.1 Battery fundamentals

Energy storage started to take an important role in human life in the 20th century as lifestyle needed more electricity. The term energy storage can be defined as the store or capture of energy that can be used at a later time. This stored energy will be available when needed. To create energy that is reliable and secure, people make more interest in the use of renewable energy resources rather than fossil fuels to seek for greener life that is more environmentally friendly and safe to use. One of the main advantages of energy storage is valued for its rapid response. For example, batteries can discharge power very quickly while fossil fuels take longer. Another advantage is renewable energies are cost-effective and more environmentally friendly than oils and gases. Currently, lifestyle is depending on electronic devices and seeking a greener life. Prices of renewable energy are relatively cheaper than fossil fuels. The battery is a good example of an energy storage device that converts the chemical energy contained in its active materials directly into electrical energy through an electrochemical oxidation-reduction (redox) reaction [2]. At present, a rechargeable battery is widely used and became an essential device in electronic applications. The battery can be recharged by a reversal of the process involved by the electrons transfer through an electric circuit.

The fundamental of battery in general is consist of five components; anode, cathode, separator, electrolyte, and current collectors. The battery can charge or discharge when anode and cathodes have connected each other with electric wire. During the charging process, oxidation (losing electrons) occurs at the cathode. Produced electrons and lithium ions transfer to anode and energy is produced due to the reduction process. The longer the charging time, the more energy can be saved. Since higher energy is stored at the anode, the driving force is acted towards the cathode and hence, oxidation occurs at the anode and reduction occurs at the cathode. Therefore, electrical energy is produced by a redox reaction between electrodes.

Li-ion batteries work on the principle of reversible insertion and extraction of lithium ions from host insertion materials. Generally, anodes are based on carbonaceous materials whereas cathodes use various transition metals compounds such as layered oxides ($LiCoO_2$), olivine type phosphates ($LiFePO_4$) or spinel-type oxides ($LiMn_2O_4$).

During charging/discharging processes, lithium-ions intercalate between electrodes and energy storage can be achieved by reversible chemical reaction through Li-ion diffusion. Different energy is driven depending on the electric potential between anode and cathode. 1C charge rate means charging nominal battery capacity for 1 hour. A typical example of a Li-ion battery is a Lithium Nickel Manganese Cobalt Oxide (NMC) - graphite battery established in commercial batteries. It consists of graphite as anode and NMC ($LiNi_{1/3}Mn_{1/3}Co_{1/3}O_2$) as a cathode.

2.1.1 Fundamental components of battery

Fundamentally, a battery is a redox reaction that takes place by electrons flowing externally to the battery. A disconnected battery prevents electron flow and the redox reaction is prevented from taking place, and so the stored chemical energy remains. Over time the reaction takes place, electrons flow externally, the cell reaction approaches equilibrium, and eventually, the cell voltage approaches zero. The redox reaction has reached equilibrium, there is no thermodynamic "push" to generate a voltage, and hence, zero current.

A battery consists of three major components; the anode, cathode, and electrolyte. The anode is the negative electrode that provides electrons to the external circuit and during the electrochemical reaction, it is oxidised. In discharge state, intercalated ions are released into the electrolyte and the electrons flow into the external circuit. Anode material should have high good conductivity, stability, be cost-effective and be easy to manufacture, and crucially, have high capacity. Capacity is defined as the measure of the amount of charge per gram stored by the battery. Since it is the measure of the amount of charge per gram stored by the battery, the unit is Ah/g and represent the charge per unit mass. As this value is normalised by mass, the capacity (as expressed in Ah/g) represents the performance of the material and not the size of the battery. The value Ah is the total discharge current a battery can deliver over time, and there is linked to both battery size and materials performance.
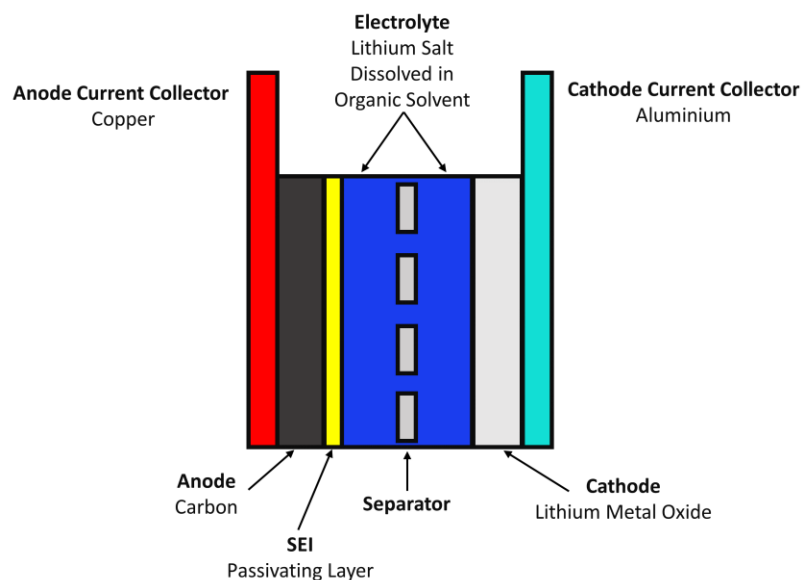
Figure 2-1: Schematic diagram of common Li-ion battery created by the autor.

6

The cathode is a positive electrode that can accept from the external circuit and the ions from the electrolyte. It is reduced during the electrochemical reaction or discharging of the battery. Ions are intercalated into the cathode material during the discharge state. An example of cathode materials are metallic oxides because it should be stable and efficient oxidising agent especially in contact with the electrolyte [2].

The electrolyte is an ionic conductor between the anode and cathode which behaves as a medium for the transfer of charge in the form of ions. Most of the electrolyte are liquids with dissolved salts and have good ionic conductivity but are chemically un-reactive with the electrodes, and the ions it contains. In addition, it should have low reactivity with the electrodes and its characteristics should be much the same with temperature change.

Finally, the separator is used to separate two electrodes but is permeable to the electrolyte. The role of the separator is to maintain ionic conductivity and prevent physical contact between the anode and cathode. When a battery is properly sealed, two electrodes are physically isolated but surrounded by the electrolyte.

The size and shape of the battery depending on the configurations of these components; button, cylindrical, and flat. Batteries are fully sealed to prevent leakage of the electrolyte and gases from air exposure.

2.1.2 Battery function

The battery operates based on two states; discharge and charge. By connecting the battery to an external load, such as an electric circuit, the discharge reaction takes place allowing electron flow from the anode to the cathode. Anode loses electrons which mean oxidation takes place and a cathode gains electrons from the anode which mean reduction takes place. At the same time, anions (negative ions) flow from cathode to anode and cations (positive ions) flow vice versa.

In a rechargeable battery, the current flow is reversed when it needs to be recharged. Unlike discharge state, reduction occurs at the anode and oxidation takes place at the cathode. Also, anions flow from anode to cathode and cations flow in opposite direction as well as the electrons.

2.1.3 Classification of batteries

There are mainly two groups of batteries in the electrochemical system; primary and secondary. Table 1 below indicates the difference between the two batteries, but the main difference is simply being either rechargeable or not rechargeable.

Primary batteries are a non-rechargeable system designed to be used (discharged) once only and discarded. Also, they are called 'dry cells' because there is no liquid electrolyte. They are low cost and small batteries widely used in toys and electronic applications which require small power. Most of the primary batteries are in cylindrical and flat button shapes such as Zinc-carbon and alkaline cells.

Secondary batteries can recharge the system electrically unlike primary batteries. Also, they are known as 'storage batteries' because they can store the energy and use them anytime the system wants [2]. The battery charges when the current flows in the opposite direction of the discharge current. They are not discarded but used multiple times because they can restore the energy to its original condition. The main applications of secondary batteries are automotive, aircraft, electric vehicles, and portable electronics. A lithium-ion battery is a typical example of the secondary battery.

Table 2-1: Primary vs Secondary Batteries [2]

	Primary	Secondary
Chemical Reaction	Non-reversible	Reversible
No of usage	Once	Re-usable
Battery life	Short	Long
Applications	Small electronics (watches, radios)	Automotive, aircraft, laptops
Examples	Zinc-carbon, alkaline cells	Lithium ion, Nickel-Cadmium cells

2.1.4 Types of Secondary Batteries

There are different types of secondary batteries such as lead-acid, nickel-based, and lithium-ion batteries based on their usage and history. Images of three batteries are shown in Figure 2-2 below.

a) b) c)
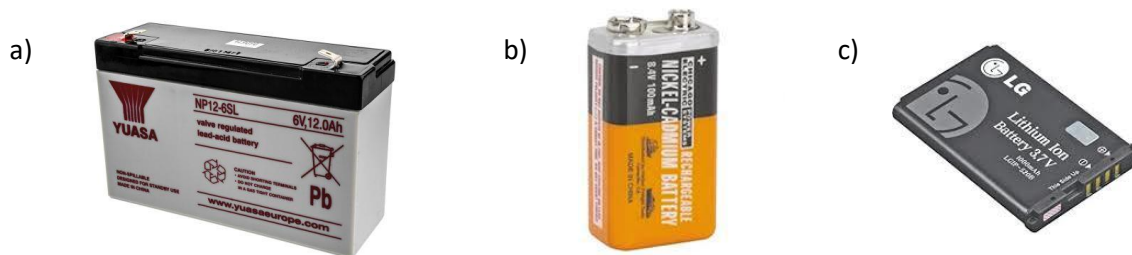
Figure 2-2: An example of a) Lead-acid battery, b) Nickel-cadmium battery, and c) Lithium-ion battery

The lead-acid battery was the first rechargeable battery for commercial use and was introduced by the French physician Gaston Planté in 1859. Grid structure was made from a lead alloy because by adding small quantities of other metals, better electrical properties can be achieved unlike pure lead is too soft. Its main application is used in automobiles because they provide high current with low cost. It has low self-discharge and good low and high temperature performance, unlike Li-ion batteries. However, it takes a long time to charge the battery.

There are different types of nickel-based batteries such as nickel-cadmium (Ni-Cd), nickel-metal-hydride (NiMH), and nickel with zinc and iron. Ni-Cd battery was the most commonly used amongst them which was invented by Waldemar Jungner in 1899. It was widely used in portable electronic devices and power tools, and emergency tools. However, its use is limited to special needs due to the high cost of material and low cell voltage although it had several advantages over the lead-acid battery.

Currently, the Li-ion battery is the most famous and commonly used rechargeable battery in electronics. Its cycle life is long, produces high voltage up to 3.6V, and has low self-discharge which is less than other batteries. However, the high cost of battery production including safe protection of a battery is needed and ageing issues are crucial factors of Li-ion batteries.

Batteries are still developing within the goal to build an ideal battery that is safe, low cost, high performance and environmentally friendly. The use of Li-ion battery has been boosted over the past 20 years and rapid research have been done to find out the science inside the battery. The crucial issue of the battery failure is the degradation process with increasing cycle number. Many factors affect the degradation process such as solid electrolyte interphase (SEI) formation on anode, temperature, and graphite exfoliation. Although their influences have been studied by researchers, more SEI investigation needs to be done because it is the main reason that occurs degradation process of Li-ion battery.

2.2 Lithium-ion battery fundamentals

In the Li-ion battery system, an anode is a negative material, and a cathode is a positive material which was explained in section 1.1.1. They are isolated by a separator. It is moistened with electrolytes and forms a catalyst which aids the ions moving from anode to cathode and vice versa. The battery can charge or discharge when anode and cathode have connected with an electric wire. During the charging process, oxidation (losing electrons) occurs at the cathode. Produced electrons and lithium ions transfer to anode and energy is produced due to the reduction process. During the discharge process, a vice versa reaction takes place; oxidation at anode and reduction at the cathode. Therefore, electrical energy is produced by a redox reaction between electrodes. As shown in Figure 2-3 below, lithium ions intercalate between electrodes and energy is produced by reversible chemical reaction through Li-ion diffusion during the charging/discharging processes. Depending on the electric potential between anode and cathode, higher or lower energy is produced. 1C charge rate means charging nominal battery capacity for 1 hour.
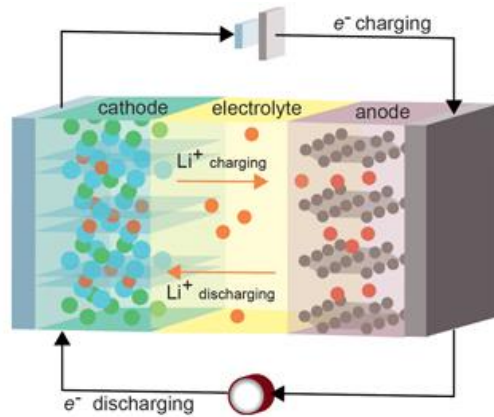
Figure 2-3: Schematic diagram of how Li-ion battery works [3]

2.2.1 Cathode

In a Lithium-ion battery system, most of the positive electrodes (cathode) are lithiated metal oxide. There are a few requirements for cathode can be used for Lithium-ion battery. For example, positive electrode materials must be cost-efficient, require good electronic conductivity, high lithium-ion diffusivity, and incorporate large quantities of lithium. Since the Li-ion battery is a rechargeable battery, it discharges by electrons transfer from anode to the cathode and charges by electrons removed from the anode. The material should have high Li-ion mobility and electronic conductivity. There must be a small structure change of material so that high efficiency and long cycle life can be achieved. Typical examples of cathodes in the Li-ion battery system are lithium cobalt oxide ($LiCoO_2$), and lithium manganese oxide ($LiMn_2O_4$) which are widely used and commercially available.

Most of the battery producing companies use $LiMn_2O_4$ as a cathode material due to its outstanding advantages such as being environmentally safe, cheap, and high cycling capacity (148 mAh/g). However, disadvantages already addressed about this material that lithium-ion rechargeable battery based on this particular material suffer poor cycling performance and storage at elevated temperatures [4] and suffers instability problem because of the capacity fade on cycling even at an ambient temperature [5].

LiCoO2 is the earliest found lithium metal oxide and one of the most widely used positive electrode materials in lithium battery technology due to the reversible nature of lithium-ion extraction/insertion. Research already addressed that in commercial Li-ion batteries, $LiCoO_2$ is the most common cathode material having long cycle life, high working voltage, and structural stability [6]. It generates very high voltages with open-circuit voltage (OCV) from 3.9 to 4.7 V. However, Ramadass et al [7] stated a disadvantage of $LiCoO_2$ cathode is the capacity fade. They used Sony 18650 Li-ion cell with $LiCoO_2$ as the positive electrode material to study the capacity fade with an increase in cycling temperature. The

reason why the capacity fading occurred is due to a repeated film formation over the surface of an anode.

Another cathode material having a great interest for secondary lithium batteries is Lithium Nickel Oxide ($LiNiO_2$). This material is a promising and cheaper alternative to $LiCoO_2$ although it is isostructural. Ohzuku et al [8] stated that it is attractive in nonaqueous lithium cells when the electrochemical reactivity is shown. However, such a material has not been commercialized due to poor structural stability on electrochemical cycling, challenging synthesis conditions, and poor thermal stability in the delighted process [8-10]. Edström et al [5] stated that these drawbacks can be avoided by partial substitution of Ni by other cations such as Co.

The final list of cathode materials in Li-ion batteries is $LiFePO_4$ having a lower voltage but similar capacity (170 mAh/g) as $LiCoO_2$. Due to low voltage, a battery is safer to use. On the other hand, extremely low electronic conductivity was a major issue of $LiFePO_4$. Literature investigated that using nanocrystalline carbon coating of the particle surface, low electronic conductivity of $LiFePO_4$ can be avoided [11].

2.2.2 Anode

The negative electrode for secondary lithium battery was lithium metal until the 1970s because of the high theoretical specific capacity of the metal 3860 mAh/g. Since it is the lightest and most electropositive metal, the main usage of this metal is in small coin cells because it is easier to handle than the other alkali metals. However, lithium metal anodes have a critical limitation with dendrites formation on the electrode surface related to persistent safety problems [2, 12]. As the cycle number increases, the lithium is plated and stripped continuously during charging/discharging. In addition, dendrite formation makes it difficult to maintain the surface area of the lithium anode that resulting in low battery efficiency and battery failure because it can pierce or damage the separator. In a Li-ion battery system, anode materials are necessary because lithium metal forms dendrites. This can cause a fire that makes the battery explode, and short-circuit [13]. To make the battery system stable, lithium must be intercalated using graphite or carbonaceous material for the anode. General types of anodes used in Li-ion batteries are graphitic (carbon), lithium titanium oxide ($Li_4Ti_5O_{12}$/LTO) and conversion materials.

2.2.2.1 Carbonaceous

The carbon material is the most commonly used as an anode in lithium-ion batteries because of the safety issues with lithium metal anode although it was developed and commercially used as a negative material until the early 1980s. This caused the industry to use intercalation of lithium into carbon anodes [14, 15]. When the battery cycles, Li-ions intercalate between layers of graphite during charge

state and a reversible process occur during discharge state. They reversibly accept and donate Li-ions during the battery cycle not affecting their mechanical and electrical properties. Carbon anode is the most commonly used in Li-ion batteries because electrochemical activity in carbon originates from the Li intercalation that occurred in between the graphene planes. Carbon owns various properties such as good electrical conductivity, low cost, moderate energy density and cycle life, and low volume change during the lithiation/delithiation process. Carbon anodes can be divided into two types commercially; Graphitic carbons and hard carbons. Graphitic carbons have large graphite grains whereas hard carbons have small graphitic grains with disordered orientation. Although graphitic carbon can achieve enough theoretical charge capacity, it does not combine well with a PC based electrolyte used for fast Li transport and low melting point [13]. Aurbach et al [16] discussed the electrochemical behaviour of lithiated graphite electrodes. An intercalation process when lithium is inserted between graphene planes is called the lithiation of graphite. They explained the capacity fading mechanism and exfoliation of graphite electrodes as an increase in the electrode's impedance at potentials above 0.5 V Li/Li$^+$[16]. To obtain a long cycle life of the graphite, surface stabilisation is needed.

There are two types of carbon material based on the manufacturing process and processing parameters (refer to Figure 2-4); soft and hard carbons. Soft carbons are stacked graphene layer materials treated at high temperature from 2000°C – 3000^{0}C whereas hard carbons are non-graphitic materials because they cannot be graphitised at high temperature [2]. Since hard carbons are highly disordered structures, more lithium can be inserted and produce a higher capacity than graphite, over 1000 mAh/g. However, they are not much accepted as anode materials due to their greater irreversible capacity and the highly disorganised structure [17]. More surface area of hard carbons being exposed to more SEI layer formation [18].

Graphite   Soft (disordered,   Hard (disordered,
                            graphitizable) carbon   nongraphitizable) carbon
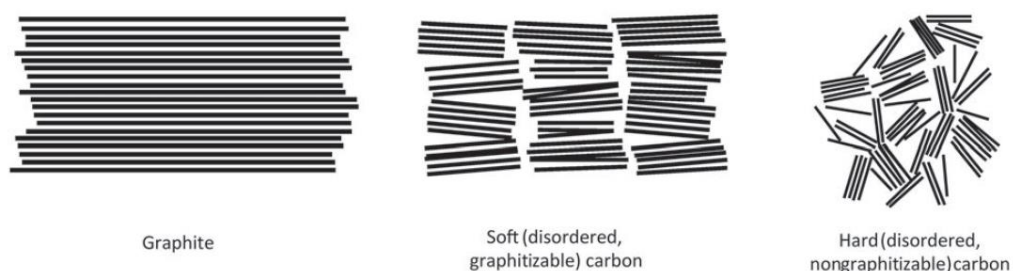
Figure 2-4: Schematic of different types of carbons referred from [19] (originally from [20])

Carbonaceous materials are available with different structure of carbon that influences their electrochemical properties. Three types are industrially available; coke, mesocarbon microbeads (MCMB), and graphite. Sony commercialised the first Li-ion batteries using petroleum coke as an anode but they were able to use it as a negative electrode with the propylene carbonate (PC) based

electrolytes although they provide good capacity, 180 mAh/g [2]. MCMB be in form of graphic spheres and was utilised as a negative material for Li-ion batteries in the 1990s because it offers a higher capacity, 300 mAh/g, than coke-based materials. Graphite (LiC_6) is the most commercially used as negative electrode material in Li-ion batteries because it generates a high theoretical capacity, 372 mAh/g, and the intercalation process occur at a very low voltage of 0.1 V vs Li^+/Li^0.

2.2.2.2 LTO

Spinel lithium titanate ($Li_4Ti_5O_{12}$, LTO) with a theoretical capacity of 175 mAh/g is one of the attractive negative electrode materials for high-performance in the lithium-ion battery system. Wang et al [21] explained LTO prevents lithium plating because of a high redox potential around 1.5 V vs. Li^+/Li. On graphite, SEI forms during the initial intercalation of lithium at 0.8 V which means a zero-strain of LTO anode owns excellent safety because thermal stability of the SEI is important in a battery system. Lan et al [22] stated that long term cycling stability can be achieved unlike graphite and other metallic oxides such as SnO_2 or Fe_3O_4 because there is no volume expansion during the lithium intercalation/deintercalation process. However, it has low electronic conductivity compared to graphite anode. To solve this problem,, Huang et al [23] introduced a synthesis procedure of thermal decomposition of $AgNO_3$ added to LTO powders to form LTO/Ag composites.

2.2.2.3 Silicon

Silicon is a more important anode compared to LTO because of its much greater theoretical capacity for lithium (4200 mAh/g) and low discharge potential. On the other hand, silicon anodes own a serious limitation which is a volume expansion by 400% upon insertion and extraction of lithium. Chan et al [24] introduced a silicon nanowire battery electrode that can circumvent because it can accommodate large strain without pulverization as shown in Figure 2-5 below. Because of the change in volume of silicon, films and particles pulverize during the cycle which leads to poor transport of electrons. However, nanowires do not break into smaller particles. Good contact with the current collector can be achieved by silicon's volume change increased the length and diameter of the nanowires [24]
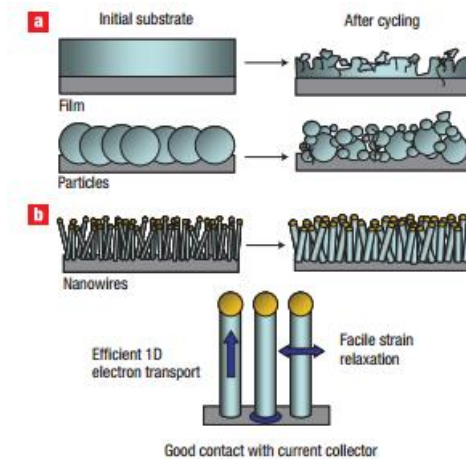
Figure 2-5: Schematic diagram of morphological changes in Si [24]

2.2.3 Electrolyte
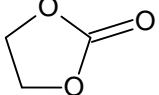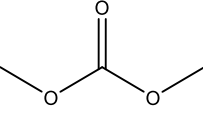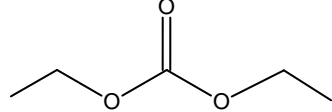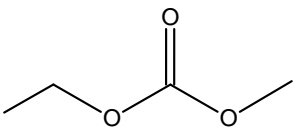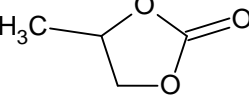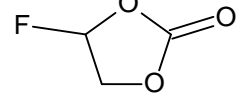
An electrolyte is another important factor besides cathode and anode in Li-ion batteries and the choice of electrolyte is critical. Since the role of the electrolyte is to allow fluent intercalation of Li-ions and exist as a medium in between cathode and anode, the characteristic of electrolyte should be compatible with various battery components, high thermal stability, and good ionic conductivity. There are various types of electrolytes suitable in Li-ion batteries, but the liquid electrolyte is the most commonly used. It is a solution of lithium salt in organic carbonate solvents. Other electrolytes can be used in Li-ion batteries such as gel, polymer, and ceramic electrolytes [2]. Liquid electrolyte is widely used in typical Li-ion batteries because it is almost fully absorbed into the electrodes and the separator that leading to no leakage from a battery.

Two types of salts are commonly used in Li-ion batteries; Lithium hexafluorophosphate (LiPF$_6$) and Lithium tetrafluoroborate (LiBF$_4$). LiPF$_6$ owns high conductivity and currently, it is the most common salts used in Li-ion batteries. However, it must be treated in a dry environment because it is hygroscopic meaning it can react with water by producing hydrofluoric acid (HF) [2]. LiBF$_4$ is less hygroscopic than LiPF$_6$ and showed improved battery performance at low temperatures as well as at elevated temperatures 50°C although it had lower ionic conductivity [25].

There are five main organic solvents typically used in industry for Li-ion batteries; ethylene carbonate (EC), dimethyl carbonate (DMC), diethyl carbonate (DEC), propylene carbonate (PC), and ethyl methyl carbonate (EMC). These carbonate solvents dominate battery solvents because they are compatible with battery electrode materials and offer good safety properties. Table 2-2 represents the physical properties and the chemical structures of five common organic carbonate solvents that can mix with lithium salts and behaves as common electrolyte solutions in the Li-ion battery system.

An additive can be used to overcome the limitation of certain electrolytes. The battery using an EC based electrolyte has a low initial coulombic efficiency due to the SEI formation occurring. An additive can solve this problem because it has a comparatively higher breakdown voltage than the electrolytes which means it will decompose first instead of the electrolyte. Fluoroethylene carbonate (FEC) is a good example of the commonly used additive because it not only allows to have less capacity loss but also maintains good cell efficiency with long cycle life [26]. In addition, FEC showed improvement not only in the capacity and the coulombic efficiency compared to the EC based electrolyte [27] but also the stability and the elasticity of the SEI layer forms in Si/Li cells [28, 29]. Hence, FEC is used in this thesis to compare the experimental results with different types of electrolytes with or without the FEC.

Table 2-2: Physical properties and chemical structures of organic carbonate solvents and additive [2, 30]

Electrolytes	Melting Point (°C)	Boiling Point (°C)	Density (g/ml)	Breakdown voltage	Chemical Formula	Chemical structure
Ethylene carbonate (EC)	38	243	1.321	1.36 [31]	$C_3H_4O_3$	
Dimethyl carbonate (DMC)	3	90	1.069	1.32 [31]	$C_3H_6O_3$	
Diethyl carbonate (DEC)	-43	127	0.975	1.32 [31]	$C_5H_{10}O_3$	
Ethyl methyl carbonate (EMC)	-55	109	1.0		$C_4H_8O_3$	
Propylene carbonate (PC)	-48	242	1.21	1.0-1.6 [31]	$C_4H_6O_3$	
Fluoroethylene carbonate (FEC)	18 - 23	212	1.454	0.9-2.25 [32, 33]	$C_3H_3FO_3$	

2.2.4 Lithium-ion battery failure

There are a few typical problems that can occur inside the lithium-ion batteries such as structural disordering, particle cracking, SEI formation and build-up, SEI decomposition and re-precipitation, dendrite formation, and lithium plating on a separator. Battery degradation takes place due to these reasons. Amongst various problems that occur, the most important point is the dendrite formation, lithium plating on the separator, and SEI formation. In a battery system, a separator is very important because it separates the gap between anode and cathode. Also, it prevents not only moving electrons in between electrodes but also adheres to cathode and anode materials. Preventing the growth of dendrite formation on the insulating separator is a key challenge because when dendrites pierce through the separator, this short circuit the cell, the temperature increases, and the battery gets discharged automatically. This energy can cause the battery to explode because the battery contains electrolyte, a combustive material. However, it is not easy to approach and understand such a complex system especially due to complex degradation processes happening inside the battery. In addition, these problems do not occur when investigating parts of cells or isolated components. They occur when all parts are assembled and charge/discharge them.

2.3 Solid Electrolyte Interface (SEI)

2.3.1 What is SEI?

There is a passive layer formed on the electrode after the first charging cycle due to the electrolyte undergoing reduction at the anode surface during the first charge in the Li-ion battery. This layer has been named as sold electrolyte interface (SEI). Peled [34] described SEI as an instantly formed layer by the contact of the active metal (anode) with the battery electrolyte. This interface allows Li-ions to pass through but does not allow electron transport. Due to the existence of a layer in between the anode and the electrolyte, Li-ion batteries own low self-discharge characteristics. An example of an SEI layer covered around a lithiated graphite electrode is shown in Figure 2-6 below; Dark grey represents mainly inorganic SEI components whereas lighter grey is organic components. It is comprised of organic and inorganic electrolyte decomposition mostly lithium salts.
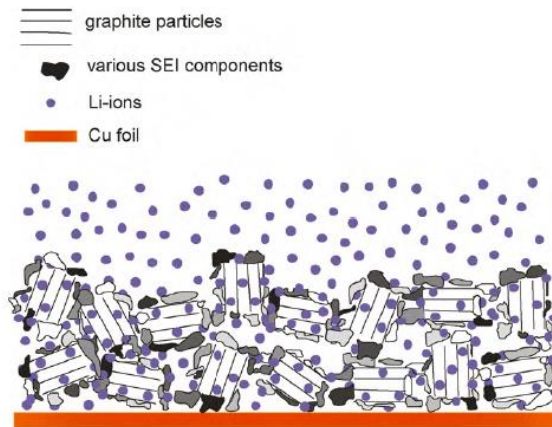
Figure 2-6: Inhomogeneous SEI formed around a lithiated graphite electrode [35]

It is well understood that SEI is essential to operate a Li-ion battery successfully. Previous studies [35-37] explained about SEI layer formed on graphite anode in Li-ion battery. There is a reason why the research was focused on the SEI layer rather than the performance and development of the Li-ion battery. This inhomogeneous layer is the most important factor in the Li-ion battery system which determines not only the performance of the battery but also safety. An ideal SEI must be physically flexible and stable so that a safe and efficient Li-ion battery can be made. Hence, it is very important to know the characteristics of SEI. The formation of SEI on graphite anode depends on the type of carbon (coke and graphite powders), the type and concentration of electrolytes, and the temperature [35, 37]. The composition and thickness of SEI keep changing throughout battery cycles so it is not easy to determine them precisely. Also, it is difficult to address which factor affects the SEI because they are associated with each other.

2.3.2 Factors affecting the formation of SEI

Properties of the active material (anode) are very important to determine the contents of the SEI layer because it is an interphase between the anode and the electrolyte. As mentioned in section 1.2.2, there are various types of carbon which was used as anode; graphite, coke, and mesocarbon microbeads (MCMB). Zheng et al [38] showed that instability of the SEI layer formed on MCMB anode leads to the capacity loss in battery and stated that it occurs in any type of lithium intercalation carbon. From this, it determines that the crystallographic structure of the carbon is important for SEI formation. Also, Verma et al [35] stated that more vulnerable exfoliation of carbon occurs in highly ordered carbons. This will lead to a faster degradation mechanism of a battery because it can damage the electrode and SEI layer.

At elevated temperature, two reactions; transformation of SEI and the reaction of active material, SEI, and electrolyte occur which was explained by Verma et al [35]. They said stable SEI components such as Li_2CO_3 is formed that is converted from lithium alkyl carbonates and semicarbonates [35]. When

the temperature reaches 120 – 140°C, the transformed SEI allows the electrons to pass through the SEI which was not supposed to occur. Because an electrolyte, inhomogeneous SEI layer, and graphite active material are assembled in order, the reaction takes place each other; electrolyte with SEI, SEI with graphite, and electrolyte with graphite [39]. One role of the SEI layer is to stop the electrons from passing through it. Du Pasquier et al [40] stated that more exothermic reactions are likely to happen than of lithiated carbon with binders at a temperature higher than 300°C. Therefore, these exothermic processes are crucial for the safety issue and the performance of the battery.

At low temperatures below 0°C, the poor performance of the Li-ion battery is achieved because it is difficult to acquire reversible capacity. Literature explained three factors; organic electrolytes, carbon electrodes, and SEI layer, as the main causes that lead to poor battery performance at low temperatures [41-43]. Battery electrolytes have different ionic conductivity that is a solution that owns the ability of anions and cations to deliver electric current in between electrodes. It determines whether a solution conducts electricity well or not. At low temperature, reduced ionic conductivity of the electrolyte is achieved which leads to poor battery performance [30, 44, 45]. Thus, the temperature is an important factor that affects the SEI and it needs to be investigated further.

2.3.3 Components of SEI

The chemical components of the SEI layer are associated with the concentration and type of electrolyte. Based on Sigma-Aldrich, there are some commonly used battery-grade solvents; EC, DMC, DEC, PC, and EMC. By mixing battery-grade solvents with LiPF6 salt, it becomes an appropriate Li-ion battery electrolyte. Different SEI layers will be formed when batteries are assembled with different types of electrolytes. In addition, a diverse SEI layer will be formed by varying the concentration of salt and the volume ratio of solvents. Some identified contents of the SEI are listed in Table 3 below.

The formation of solid products and the uniformity of the SEI layer will differ depending on various factors such as the composition of electrolytes and electrodes. For example, Lithium oxalate ($Li_2C_2O_4$) and polyoxyethylene are unique products of the SEI layer forming on the graphite particles due to the reduction process of EC-based electrolyte [46]. In addition, the composition of SEI film will change in a control cell and cycled cell as well as an aged electrode is washed with DMC [47]. Detailed components of SEI layer is explained in Table 2-3 below. The composition of SEI layer on uncycled cell are $Li_2C_2O_4$, lithium succinate ($C_4H_5LiO_4$), and lithium methoxide ($LiOCH_3$).

Table 2-3: Some examples of the SEI components (modified table of Verma et al [35])

Component	Notes
$(Ch_2OCO_2Li)_2$	Easily found in EC based electrolytes
$ROCO_2Li$	Mostly found in PC based electrolytes. Also present in the outer layer of the SEI
Li_2CO_3	May appear as a reaction product of semicarbonates with HF or water or CO_2
ROLi	Most commonly found in the SEI in electrolytes DMC or EMC
LiF	A major salt reduction product
LiOH	Mainly formed due to water contamination
Polycarbonates	Present in the outermost layer of the SEI

2.4 Low temperature systems

2.4.1 Lithium-ion battery

Many factors lead to Li-ion batteries failures such as dendrite formation, electrode ageing, high temperature, formation of SEI layer on electrodes, capacity fade, graphite exfoliation, and corrosion of current collector. It is well known that these failures can occur at room temperature (25^oC) when the battery achieves reversible capacity. However, when the temperature goes down to 0^oC or less, it becomes a different story. Poor performance of Li-ion battery is achieved because it is difficult to acquire reversible capacity when the temperature goes down to below 0oC. Long cycle life and low self-discharge are the two main reasons why Li-ion batteries are used. On the other hand, these promising batteries lose their characteristics at low temperatures due to three factors that were addressed by previous researchers [30, 42, 44, 48-52]. They are organic electrolytes, Solid Electrolyte Interphase (SEI) layer, and carbon electrodes (anode). In a battery system, ionic mobility is very important because it determines the performance of a battery. As explained above, previous studies were focusing on the performance of the battery and its different causes. If these causes are studied further, it will be easier to understand the truth of failure of Li-ion battery at low temperature.

2.4.2 Electrolyte

Although SEI layer and electrolyte are not the main causes for the limitations of low-temperature Li-ion battery performance, they still need to be investigated in more detail to understand their behaviour at low temperatures. It is difficult to judge whether the SEI layer is necessary or unnecessary in a Li-ion battery system. The SEI layer components are determined based on types of electrodes and electrolytes. They are lithium salts formed on negative carbon electrodes (anode) based on the chemical reaction in between a graphite electrode and an electrolyte. Hence, the condition of electrolytes is very important because it determines the motion of molecules in liquids that can affect lithium intercalation, especially in low-temperature conditions.

The condition of electrolyte changes from solid to liquid state and vice versa depending on the environmental temperature. Most of the battery electrolyte freezes at a temperature below 0°C which occur low ionic mobility in between electrodes and poor battery performance is achieved. SEI layer and graphite anode are closely related to the condition of electrolyte because the components and the thickness of the SEI layer as well as the diffusivity of Li-ions in graphite can be determined. Previous studies were focused on the development of battery electrolytes having high ionic conductivities and low melting points to improve the low-temperature battery performance [30, 44, 49, 51, 52]. On the other hand, the low diffusivity of Li-ions in graphite is the real limitation of low-temperature battery performance which was addressed by Huang et al [48].

As shown in previous Table 2-2, some organic solvents based electrolytes will be in a solid state at low temperature because their melting points are higher than 0°C. Therefore, by comparing with the capacity of Li-ion battery at room temperature, it will not be able to achieve the same capacity when the temperature goes down below 0°C or more. It shows that EC and DMC are not suitable for low-temperature analysis because they own high melting points except DEC. On the other hand, this drawback can be solved by mixing with other battery solutions such as PC and EMC. The melting points of newly formed electrolytes have gone down and most of them are in a liquid state at a temperature below -35°C as shown in Figure 2-7.

Figure 2-7: Different electrolyte phases at low temperature [48]

Label	Composition	−30°C	−35°C	−40°C	−42.5°C
1	EC:DEC:DMC (1:1:1)/1.0 M LiPF$_6$	Liquid 100%	Liquid and solid coexist	Liquid and solid coexist	Solid 100%
2	EC:DEC:DMC:PC (3:3:3:1)/0.9 M LiPF$_6$	Liquid 100%	Liquid and solid coexist	Solid 100%	Solid 100%
3	EC:DEC:DMC:EMC (3:5:4:1)/0.8 M LiPF$_6$	Liquid 100%	Liquid 100%	Liquid 100%	Liquid 100%
4	EC:DEC:DMC:EMC (3:5:4:2)/0.8 M LiPF$_6$	Liquid 100%	Liquid 100%	Liquid and solid coexist	Liquid and solid coexist

There are various mixing ratios of organic carbonic solvents to create a well-functioned electrolyte, especially for low-temperature battery systems. As explained in section 2.2.3, there are five organic carbonate solvents; EC, DMC, DEC, EMC, and PC. With a combination of either LiPF$_6$ or LiBF$_4$, these battery electrolytes are widely used not only for room and high temperature battery systems but also low-temperature batteries. However, it is difficult to say which is the best solvent mixing ratio, especially for low-temperature cases. This is due to the restricted choice of electrolyte and electrode (anode/cathode) in the Li-ion battery system. For example, graphite anode and 1M of LiPF$_6$ in EC/DMC 1/1 electrolyte is the most common combination in Li-ion battery system at atmospheric temperature. Previous studies showed that if the temperature goes down to 0°C or below, 1M of LiPF$_6$ in EC/DMC/EMC 1/1/1 [53] or 1M of LiPF$_6$ dissolved in EC/EMC 3:7 [42] are introduced as suitable for the low-temperature battery. Although they tested different battery types (full cell and button cell),

graphite was used as an anode. It is hard to say which electrolyte is better for a low-temperature system because both of them were tested that battery was operable at temperatures down to -20°C[42] and -40°C [53] respectively. However, the component of solvent can be possibly estimated if the list of electrolyte ratio with types of electrodes is available which was tested by previous researchers. Table 2-4 below is an example of battery electrolytes and types of electrodes for low-temperature systems tested by previous researchers.

Table 2-4: List of electrode and electrolyte ratio for low temperature battery system on the literatures

Anode	Cathode	Salt	EC	DMC	DEC	EMC	PC	Additive	Operable Temp
Graphite	Li	1M LiPF$_6$	3	7					-20°C [30]
Graphite	Li	1M LiPF$_6$	3		7				-20°C [30, 42]
Graphite	Li	1M LiPF$_6$	1	1	1				-20°C [30]
Graphite	LiCoO$_2$	1M LiPF$_6$	1	1		1			-40°C [53]
MCMB	LiCoO$_2$	1M LiPF$_6$	1			3			-40°C [54]
Graphite	Li nickel-based mixed oxide	1M LiPF$_6$	1			3	1	VC	-30°C [41, 55]
		1M LiBF$_4$	1			3	1	VC	-40 ~ -60°C [41]
MCMB, Coke	LiCo$_{0.2}$Ni$_{0.8}$O$_2$	1M LiPF$_6$	1	1	1				-30 ~ -40°C [48]
		0.9M LiPF$_6$	3	3	3		1		-30 ~ -40°C [48]
		0.8M LiPF$_6$	3	4	5	2			-30 ~ -40°C [48]
		0.8M LiPF$_6$	3	4	5	1			-42.5°C [48]

It can be estimated that EMC is a suitable solvent for battery performance at a temperature of -30°C or below. In addition, it shows that although different types of electrodes are used, the battery can function at low temperatures if the relevant choice of solvent with various mixing ratios is in the right condition. Still, there is no perfect electrolyte that makes no capacity loss at low temperature by comparing with generated capacity in atmospheric temperature because 1M LiBF$_4$ PC/EC/EMC 1:1:3 electrolyte retained only 20% of relative capacity (capacity at 20°C) [41]. From this, it can be stated that it is only possible to say which is the best electrolyte for a low-temperature battery only if every mixing ratio of organic solvent and same electrode condition are used to build an identical battery. There is still a lot of research that needs to be done in the future related to electrolytes suitable for a low-temperature battery system.

2.5 Conclusion

This chapter was introduced to understand the fundamentals of Li-ion batteries and their development until the present day. It consists of four components; cathode, anode, electrolyte and separator and the low-temperature system was addressed to find out not only the behaviour of battery but also the formation of SEI layer on graphite anode. Since the formation of the SEI layer and low temperature is a good reason for Li-ion battery failure, it needs to be studied further. It can be hypothesised that it is not clear which factor affects the low-temperature battery performance the most. Therefore, the behaviour of the SEI layer at low temperature must be done. Aims and objectives are introduced to understand and explain qualitative and quantitative results to develop knowledge about the Li-ion battery system, low-temperature behaviour, and SEI layer. In this thesis specific experiment, I attempt to clarify these proposals by observing the behaviour of the SEI layer in the low-temperature range (down to -15°C).

Chapter 3 - Experimental

The following chapter describes the experimental technique employed throughout this study and coin cell fabrication techniques to help further understand the SEI layer structure and its relationship with temperature. Each technique discusses separately in both theoretical and practical terms.

3.1 Battery production and cycling

3.1.1 Chronopotentiometry

The performance of a battery can be measured by using an electrochemical technique called chronopotentiometry which is commonly used to understand the mechanism of chemical reactions of a battery. It measures the produced capacity which is caused by a controlled current flow between two electrodes [56]. For example, the potential of the graphite electrode is monitored as a function of time to a Lithium metal reference electrode. The controlled current is usually kept as a constant current. This technique operates in a galvanostatic mode so that it can measure voltage in controlled current (constant). It is a common method to measure the charge/discharge curves of tested batteries in C-rates which indicates the time taken to charge or discharge a cell and owns the inverse proportional relationship. To explain, a 1C rate battery means that the charge/discharge current will take 1 hour to fully charge/discharge the entire battery. Similarly, a 2C rate battery takes 30 minutes to fully charge/discharge the entire battery. Choosing a suitable C-rate is important to analyse the SEI layer formation. As mentioned in previous paragraphs, a C-rate is inversely proportional to the time taken of charging/discharging a battery. A high C-rate will have a fast charge/discharge cycle, but this might potentially make an inefficient battery due to an increase in temperature from the higher current. To acquire as close to the theoretical capacity of a graphite anode (372 mAhg^{-1}) [57], slow C-rate (0.1C) has been assigned in this experiment unless stated otherwise. The battery will have 10 hours to charge/discharge the battery which is more than enough of Li can intercalate to the graphite anode. This nearly perfect layered structure will accept good amount of Li to produce high capacity which allows to be a desirable anode material. More detailed experimental setup is mentioned in next section.

3.1.2 Thesis specific experimental considerations

In this experiment, the CS2016 half coin cell is used as the test battery so that the anode surface and its behaviour for temperature change can be studied only. CS2032 is another type of coin cell which is slightly bigger than CS2016 physically, but this is not used in this experiment because the battery will have too much free space in CS2032 since the size of the punched electrode will be 1.44 cm2. They have the same diameter (20mm) but different thicknesses; CR2016 – 1.6 mm, CR2032 – 3.2 mm. Since CS2032 is bigger, it produces a larger capacity and will have more total capacity and a higher maximum current, but it is not suitable for low-temperature analysis because low total capacity is achieved. The ideal coin cell for this experiment will be C6 |LP30 ‖ LP30 | Li 2016 coin cell (Cambridge energy solutions). To start with, graphite anode must be prepared. Artificial graphite was made from 90% artificial graphite (Timcal), 5% carbon black (Cabot), 2.5% carboxymethyl cellulose (CMC, MTI corp.), and 2.5% Styrene-butadiene rubber (SBR, MTI corp.) that is a method outlined by Marks et al

[58]. They are added into a Thinky container, and it is placed in a Thinky mixer for 5 minutes at 2000 rpm. Once they are well mixed, it is poured on the carbon-coated copper foil, and they are placed on the automatic fil coater. Then, graphite electrodes were punched and dried in a hot vacuum chamber for 48 hours.

The completely dried artificial graphite anode was carefully weighed on a precise analytical balance and recorded separately. A recorded electrode was carefully placed inside a Thinky container and transferred into an argon filled glovebox. Lithium (0.75 x 45mm, 99.9%, Sigma Aldrich) were scrapped and then punched having a 6mm diameter disk. Next, a glass fibre separator (Whatman Schleicher & Schuell) was placed on top of a punched lithium disk. On top of the separator, an artificial graphite electrode (anode) was placed. For battery electrolyte, 1.0M of $LiPF_6$ in EC / DMC = 50/50 (v/v) (Sigma Aldrich) (LP30) is used unless stated otherwise. These coin cells were fully sealed in a crimping machine and any electrolyte leaks were wiped off. Entire battery fabrication was done in an argon filled glovebox with H_2O and O_2 both below 0.1 ppm.

Li-graphite half cells were placed in the MACCOR series 4000M temperature chamber to investigate the behaviour of the SEI layer based on the change in temperature starting from ambient temperature to -15°C. Using a MACCOR battery tester, all batteries were at rest for 8 hours. The cell was assigned as 0.1 C-rate (10 hours charge/discharge). Normally, the battery starts the charging cycle first but since this experiment uses Li-graphite half-cell, discharge cycle is assigned first. There is no need to release the Li-ions to the Lithium electrode that is counter and reference electrode. The discharge cycle is assigned until voltage drops to 0.01 V and the charge cycle is assigned up to 2.5 V at constant current. The batteries will have different constant current C-rate (in Amps) that is mostly determined by the weight of artificial graphite electrode. This value specifies how much constant current is applied for each C-rate in discharge/charge cycles of tested cell. It can be calculated based on the equation 3.1 below;

$$\left(\begin{array}{c} Weight\ of \\ artificial\ graphite \\ electrode \end{array} - 0.0102 \right) \times 0.9 \times 0.372 = C-rate\ [in\ Amps] \qquad \text{(Eq 3.1)}$$

Independently measured a weight of artificial graphite electrode is addressed separately in Chapter 4 and 5. The three values represent as; the weight of Cu foil is 0.0102 g, 0.9 (90 wt%) is the percentage of artificial graphite itself, theoretical capacity of artificial graphite in Amps is 0.372 Ah/g. It helps to run multiple channels of the batteries with same procedure but with different constant current settings. This particular C-rate [in Amps] is input at the 'start test setup' stage which is the last stage before the actual test begins. C-rate for every tests are separately presented in following Chapters 4 and 5.

The first cycle was carried at 25°C to allow the formation of SEI layer on graphite anode. For the low-temperature analyses, the temperature is altered after a certain number of cycles to allow SEI formation at room temperature. At low temperature, the same C-rate and cycle were used as room temperature setup. After the procedures were completed, these batteries were disassembled in a decrimping machine. Artificial graphite electrodes were washed with DMC then dried in a big ante-chamber for a few days. A detailed experimental setup is mentioned in each section respectively. The cycling number and temperature can be changed, and this will be mentioned individually.

3.2 In-Situ and Ex-Situ experimental testing

Numerous investigations tried to understand the SEI layer by using various analytical techniques such as microscopy and spectroscopy. These measurements aid to study the nature of the SEI in operating conditions such as growth, components, and thickness. Researchers have been used various techniques to analyse the SEI layer. The most frequent techniques used were Fourier- Transform Infrared Spectroscopy (FTIR) and Electrochemical Impedance Spectroscopy (EIS) since they are suitable for surface analysis like SEI. To produce an image of the surface film, Scanning Electron Microscope (SEM) and Atomic Force Microscopy (AFM) was used. However, there are a few limitations to characterising the SEI layer. First, analysing SEI is a challenging task because it is not only difficult to show the correct boundary between the beginning of the electrolyte and end of the solid electrolyte layer but also hard to identify the thickness of the surface layer from the carbon surface. Second, there is an uncertainty in the methods which measure the SEI after washing with solvents of the electrolyte or along with the electrolyte [35].

In this project, four experimental techniques will be used; ionic conductivity, AFM, FTIR, and EIS. To study the behaviour of the SEI layer at different low temperatures from 25°C to -15°C, these techniques are necessary due to a few reasons. First, it is important to know and reaffirm that there is an SEI layer formed on graphite anode after battery cycles. This result can be compared with a pure graphite electrode. To do this, AFM will visualise the graphite anode surface before and after SEI layer formation and identify the change in roughness and thickness of the scanned area. AFM can obtain high quality 3D images of the electrode surface and therefore, it overcomes the drawbacks of SEM which produces 2D images, limited scanned area, and takes a long time to scan a single image. EIS is a good technique to find out the impedance of the battery and evaluate its temperature dependence. FTIR is used because it scans the surface of electrodes and identifies the chemical bonds of molecules in a material. Experimental data can be compared with literature data and can evaluate its temperature dependence. The type and concentration of the electrolyte are crucial that determines

the content of SEI and therefore, ionic conductivities of common battery electrolytes are calculated. These techniques will confidently aid this project to achieve the following aims and objectives.

3.2.1 Ionic conductivity

3.2.1.1 Theory

The motion of ions in the electrolyte is important to understand the condition of electrolyte at various temperatures in a Li-ion battery. When ions can move freely amongst anode and lithium metal, it turns out to be an efficient battery because of the potential difference between them. Considering the good performance of a battery, the nature of molecular motion becomes a key factor. If they lose their role, the battery might fail because their charging/discharging cycle is inefficient. The condition of battery electrolytes based on the temperature change, can be analysed by measuring their ionic conductivity.

Conductivity, a solution owns the ability of anions and cations that deliver electric current in between electrodes, determines whether a solution conducts electricity well or not. By knowing the ionic conductivities of various electrolytes, the information about ionic mobility in liquids can be understood. It can be calculated as shown in the equations below.

$$G = \frac{1}{R} \qquad\qquad K = \frac{l \ or \ d}{A} \qquad\qquad\qquad \text{(Eq. 3.2)}$$

$$\kappa = \frac{1}{R} \times \frac{l}{A} = \frac{G \times l}{A} \qquad\qquad\qquad \text{(Eq. 3.3)}$$

where K is the ionic conductivity. G, the conductance of the electrolyte (Ω^{-1}), is calculated from the inverse of its resistance R. However, the designation has been changed to the siemens (S) [59]. L is the distance between the electrodes and A is the cross-sectional area of the electrode. By taking the ratio of the length to the area, cell constant, K, can be determined. Therefore, conductivity (Scm^{-1}), κ, can be calculated with a conductance and a cell constant. These equations result in an increase in conductivity with its conductance and length but decrease with the area. Ionic conductivity of the battery electrolyte can be measured using an ionic conductivity cell shown in Figure 3-1 below.
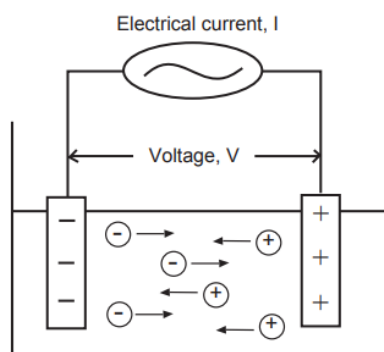
Figure 3-1: A schematic diagram of ionic conductivity cell [60]

Electrolytes mixed with one or multiple solvents can provide different cell performance, conductivity, and temperature range depending on electrolyte formulations and these results can be better than a single solvent electrolyte. For example, most of the battery electrolytes are formulated with EC solvents because Li-ion batteries with a graphite anode, produces low capacity fade and irreversible capacity [2]. However, EC solvent on its own is not a good choice as an electrolyte because it is a solid at room temperature. To solve this problem, electrolytes are formulated with EC and other solvents such as DEC and DMC to lower the melting point of the solution.

3.2.1.2 Thesis specific experimental considerations

To find the ionic conductivities of a solution, the cell constant of an ionic conductivity cell needs to be calculated. Cell constant was calculated by dividing the area of the electrodes by the distance of the electrodes. Since it is difficult to measure the length between the electrodes accurately, this method is not used. Potassium chloride (KCl) solution is prepared because its conductivities for temperatures are already known. 0.01 M of KCl solution was used to test the ionic conductivity at 25°C. The ionic conductivity of its solution is 1.413 mS/cm at room temperature. From this, the cell constant can be obtained by measuring the resistance of its solution and the distance between the electrodes of the ionic conductivity cell which were 713.623 Ω and 0.55 cm respectively. Once the cell constant is found, two battery electrolytes (1M of LiPF$_6$ in EC/DMC=50/50 (v/v), known as LP30, and 1M of LiPF$_6$ in EC/DEC=50/50 (v/v), known as LP40, battery grade, Sigma Aldrich) were used to obtain its ionic conductivities because they are the most common Li-ion battery electrolytes. Solutions were poured into the ionic conductivity cell until the electrodes are fully soaked. After fully sealing the cell, it was tested with a range of temperatures from -10°C to 60°C in the MACCOR series 4000M temperature chamber with Solartron 2101A AMETEK. When the procedure is ended, the electrolyte is poured into the solution waste and the ionic conductivity cell is cleaned with Isopropyl Alcohol (IPA) and kept safe so that it can be dried overnight. MIMS software (MACCOR) was used to generate data from the MACCOR battery tester.

3.2.2 Atomic Force Microscopy

3.2.2.1 Theory

Atomic Force Microscopy (AFM) is an amazing technique that measures the height of the surfaces and visualises the image showing the structure and morphology of a surface sample. The key advantage of AFM is it can produce three-dimensional images because it magnifies X, Y, and Z axes whereas other microscopes such as SEM and TEM produce two-dimensional images of the surface sample without height information. They produce images by focusing light or electrons onto a surface whereas AFM physically touches and scans the surface of the sample using a sharp probe.

The basic principle of AFM is based on the close separation of interaction forces acted in between the surface of the sample and the probe tip [61]. These forces are measured using a laser and a detector, which detects the motion of the cantilever that moves up and down based on the surface morphology of the sample as the tip moves across the surface. Since the cantilever moves up and down (Z-direction), the scanned surface can be visualised into a 3D image based on the X and Y position of the sample from measuring the deflection of the cantilever [62].
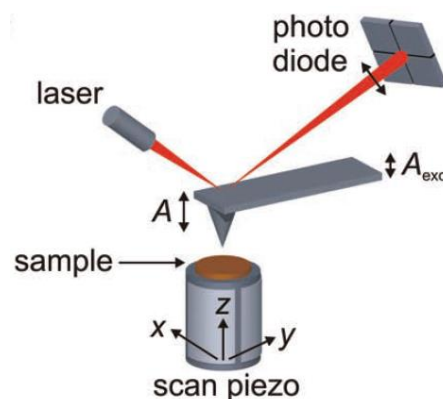
Figure 3-2: An example of AFM mechanism [63]

AFM can be operated in three modes; contact, tapping, and non-contact mode. In contact mode, the tip is in contact with the surface and dragged across the surface of the sample. Then, the surface topographic image of the sample is visualised into a 3D image based on the information of vertical movement of the cantilever that is monitored by a photo diode (refer to Figure 3-2 above). However, this mode might damage the sample and the tip because there are having physical contact with each other during scanning the surface of the sample.

To overcome the drawbacks of contact mode operation, tapping mode has been introduced that the tip is brought close to the surface of the sample but with less applied forces. The important principle of this mode is to maintain close to its resonance frequency as the cantilever oscillates during the

surface scan. It has less possibility of damaging the tip and the surface of the sample because the morphological image is produced based on the change in oscillation characteristics that is equivalent to interaction forces that occurred in between them [61]. Since the tip is in contact with the surface for a very short time in each oscillation cycle [62], tapping mode is suitable to image soft materials.

Non-contact is another mode to solve the drawbacks of both contact and tapping mode. A tip breaks or becomes blunt during or after the surface scan because they are physically contacted to each other in both operation modes that resulting in low atomic resolution images. However, the non-contact mode does not have physical contact between tip and sample because the oscillation amplitude is kept constant at small values (few nanometres) so that shape of the tip will remain as it is [61]. In non-contact mode, the force sensor that consists of typically a cantilever with a sharp tip is oscillated at its resonance frequency and lowered down close to the surface of the sample.

AFM has been used as a useful experimental technique for studying morphology, thickness, and characteristics of the thin surface because it can measure differences in depth at Angstrom resolution. Previous literature used AFM to investigate SEI formation on various types of electrodes such as $Li_4Ti_5O_{12}$ and MnO anodes [21, 64], and $LiFePO_4$ cathode [65]. In addition, it has been used to directly measure the morphological changes on the surface of the Li-ion battery cathodes during cell cycling [66]. Therefore, it is an ideal technique to investigate the SEI layer formed on graphite anode because it is a thin surface film. To explain, AFM has previously been used to study the SEI formation on HOPG anode after the first lithiation cycle [67]. To investigate any sample like hard and soft material such as the surface of a ceramic material or individual molecules of DNA [68], AFM is a good choice because it provides not only a high atomic resolution image that represents morphological information of the surface of the sample but also it functions well scanning solid and liquid surface.

Even though AFM owns various advantages, it has a few limitations. For example, it is restricted to a large scanning area not greater than 100 μm [68]. Since it mechanically scans over the surface of the sample using a probe, it takes a long time to scan and measure the large area. Another disadvantage of AFM is greater X and Y resolution compared with Z resolution because of the sharp probe. When the surface of the sample is measured, the scanning process should be treated carefully. If not, the probe might damage the sample. Therefore, much sharper probes need to be handled carefully which results in much higher X and Y resolution [68].

3.2.2.2 Thesis specific experimental considerations

For this particular experiment, AFM is used to study the morphology of the SEI layer formed on artificial graphite anode based on the temperature change from ambient to low temperature at -15°C. It is made by the Bruker dimension icon. This ex-situ AFM is located outside the glovebox, so the

artificial graphite electrode needs to be fully dried. After completion of the battery cycle, the coin cells were disassembled inside an argon filled glovebox and the electrode was gently washed with DMC to remove $LiPF_6$ from the sample. Electrodes were kept and leftover few days inside the glovebox. Then, they were individually placed inside a small THINKY container and left outside the glovebox for a few days to allow the electrodes to completely dry. They must be fully dried so that chance of a blunt tip or breaking the tip will minimise. In addition, it prevents from not producing a low atomic resolution image of the surface. All dried electrodes were attached on double-sided tape and placed on sample mount individually. Graphite anode is scanned in ScanAsyst mode developed from Bruker that is suitable to visualise the thin surface film and monitor the integrity of the imaging process at the same time causing less damage to the sample and the tip [69]. Obtained 3D images are analysed with Bruker software and a free AFM software called Gwyddion.

3.3.2 Fourier Transform Infrared Spectroscopy

3.3.2.1 Theory

Fourier Transform Infrared (FTIR) Spectroscopy is another analytical technique that is suitable for the investigation of the surface of material because it provides diverse information of molecular structure by a frequency spectrum. It is an optical approach to measure the absorbance from a sample in the wavelength range of $500 - 4000$ cm^{-1}. These energies correspond to the atomic bond vibrations and bending of specific bonds and so can be used to determine the chemical bonding present in a surface sample. When infrared radiation passes through a sample, some IR radiations are absorbed by the sample, and some are passed through and transmitted to the detector. This information results in a frequency spectrum that represents the molecular absorption and transmission of the sample [70].

The basic principle of the FTIR is using infrared radiation that passes through the sample and the detector measures the amount of energy at each frequency. Old infrared instruments were either dispersive or filter type by using an infrared prism or grating methods. A prism separates the individual frequencies of energy emitted from the infrared source which is the same as a visible prism that also separates visible light into its colours [70]. The grating method has been used as a more modern dispersive type because it has a detector that measures the emitted energy at each frequency passed through the sample and results into a spectrum. Currently, FTIR is more preferred than the other two methods because this non-destructive technique provides a precise measurement with a fast scanning rate and high sensitivity.
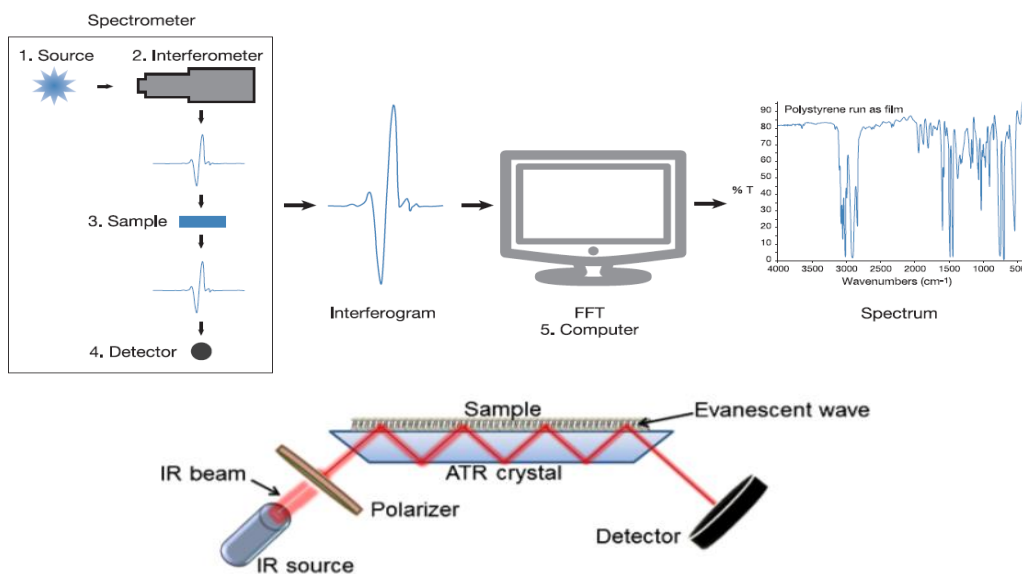
Figure 3-3: Top) How FTIR works [70, 71], bottom) A schematic diagram of how ATR-FTIR works [72]

The components of FTIR consist of five different parts as shown in Figure 3-3 above; the source, an interferometer, a detector, a computer, and the sample compartment [70, 71]. From the source, infrared light passes through an aperture so that the energy of the light can be adjusted to present to the tested sample. Next, the adjusted beam enters to interferometer which is suitable for precise measurement of the sample by creating an interference pattern. FTIR can measure all infrared frequencies simultaneously by using an interferometer which is an optical device producing a unique signal having all encoded infrared frequencies. An interferometer has a beamsplitter that splits the beam from the infrared source into two optical beams which are reflected by the mirror. It is an interferogram that is the result of these signals that unite and exit the beamsplitter. The resulting signal strikes the sample and passes into the detector. When the signal strikes the sample, it gets absorbed by the sample and transmitted through the sample. Finally, the detector delivers data to the computer, and the resulting information is represented into a frequency spectrum with multiple peaks that indicates the wavelength of respective chemical bonding of the sample's surface which is analysed by a computer using a mathematical method called Fourier transformation.

Instead of using the obtained results by the FTIR, there is a standard technique called the Attenuated Total Reflection (ATR)-FTIR that is a sampling method analysing the material of the surface sample and producing independent FTIR spectra. It only requires an Infrared source, a detector, and the ATR crystal (consists of diamond, germanium, or zinc selenide) that has a higher refractive index than the sample so that the infrared can be reflected in the detector because the sample is placed on the ATR crystal [73]. In addition, it produces high quality of data even with a small amount of sample [73]. Hence, this technique is ideal for the experiment interested in the material composition of the surface of the sample.

This technique is commonly used in battery studies because it scans the surface of electrodes and identifies chemical bonds of molecules in a material. Previous studies used FTIR as an investigation technique to find out the electrolyte decomposition process on battery electrodes [74] and the electrochemical reduction of the electrolytes on graphite electrodes [46]. Also, FTIR has been used to investigate the nature of the surface passive film formed on Li-doped spinel $Li_{1.05}Mn_{1.96}O_4$ cathode [75] and graphite anodes at high temperature (55°C) [47] and low temperature (-30 or -50°C) [76]. The literature widely used the FTIR to find out the environment of the surface electrode and the electrolyte. Hence, the SEI components of the graphite anode can be determined by using this promising technique.

Although it is a promising analytical technique in Li-ion battery electrode investigation, it shows few limitations. First, the obtained spectrum might show inaccurate results because they measure Fourier transformed interferometer signal. Second, the spectrum can contain a lot of noise since FTIR takes measurement simultaneously and produce a related spectrum having many peaks. If high noise occurs, it will be hard to differentiate the peaks whether it represents chemical bonding or not. In addition, it is possible to have all frequencies shift by a small (10cm-1) constant due to the linear background correction of the experimental data.

3.3.2.2 Thesis specific experimental considerations

In this experiment, FTIR is used to investigate the nature of the SEI layer formed on graphite anode based on temperatures. Tested samples were treated separately since in-situ FTIR (Bruker) was located inside an argon filled glovebox. Detailed coin cell preparation was mentioned in Section 3.1.2. Similar to AFM sample preparation, graphite anode was separated and gently washed with DMC to remove miscellaneous contaminants and hazardous compounds, $LiPF_6$. A background scan was measured before a graphite anode scan which is a measurement with no sample in the beam. This process is done only once because a single background measurement is used for many sample measurements [70]. This result is compared with the measurement with the sample which will result in a spectrum. It has pure transmitted data of the sample without instrumental data. After a background scan, pure graphite anode was tested first to have a comparative model of data for further analysis. Later, other graphite anodes with SEI layer formation were scanned on FTIR as well. There is a major difference between a graphite anode and a graphite anode with an SEI layer. Detailed information about battery cycling conditions is mentioned individually from the next chapter onwards.

All experimental measurements were set to resolution as 4cm-1 because it is the normal setting for the spectral resolution of the instrument. If the resolution value increases to 8 or 16 cm-1, data collection time will be faster than the normal setting but some peak information can be lost [77]. In

addition, a low resolution value will have an increased noise at the spectrum showing too many unwanted peaks which results in difficulty of data analysis. Generally, the default value of background and sample scan time is set to 16 scans. Similar to the resolution value, the scan time can be altered depending on which scan spectra show clear and best results. The background and sample scan value were fixed to 96 scans for the entire FTIR experiment after a few alterations (8 – 256 scans) of scan time to compare their results.

Data acquisition was done with OPUS (Bruker) and Origin software. First, FTIR spectra were shown in OPUS because all results are directly sent and analysed via wireless in the laptop that is connected with Bruker FTIR spectroscopy. All spectra will have various peaks and slopes based on the nature of surface samples. Hence, they are implemented with a function called a baseline correction which makes the randomly sloped baselines of a particular tested sample's spectrum is levelled out. This will alter the sloped baselines uniformly so that all spectra can be compared accordingly. Once all functions are applied to the spectra, all data were transferred to the Origin software for further analysis.

3.4.2 Electrochemical Impedance Spectroscopy
3.4.2.1 Theory

To study the impedance of the Li-ion battery, Electrochemical Impedance Spectroscopy (EIS) is a good choice because it provides information about electrochemical reactions, the behaviour of the battery system, and the electron transfer rate of reaction. Using Faraday's Law, this frequency-dependent technique takes not only the electrical measurements such as resistance and impedance but also the response of a battery. Before resistance and impedance are introduced, the general concept of electrical resistance needs to be addressed which can be explained from Ohm's law ($V = IR$). From this equation, resistance is defined in terms of the ratio between voltage and current. Resistance in a circuit is the ability to resist the flow of electrical current which is limited to the ideal resistor only. In addition, it is independent of frequency which is determined by the current and voltage from Ohm's law [78]. Impedance is similar to resistance but has different factors that as the ability to resist the flow of electrical current. However, it is frequency-dependent resistance and the conditions are not limited to the resistance does [78].

EIS produce the data by applying a sinusoidal current to measure the response of the battery and computes the impedance at each frequency. It uses an alternating current (AC) potential that is a sinusoidal potential and measures the current that periodically changes the direction of flow. Direct current (DC) is not suitable for the electrochemical systems because the direction of the current is limited to one direction only. The input is a small AC signal (1 – 10 mV) that is generally applied to the

cell and produce a high frequency that has a short period. Then this responsive AC signal is treated logarithmically, and it is reduced to its lowest frequency which means high impedance is achieved.
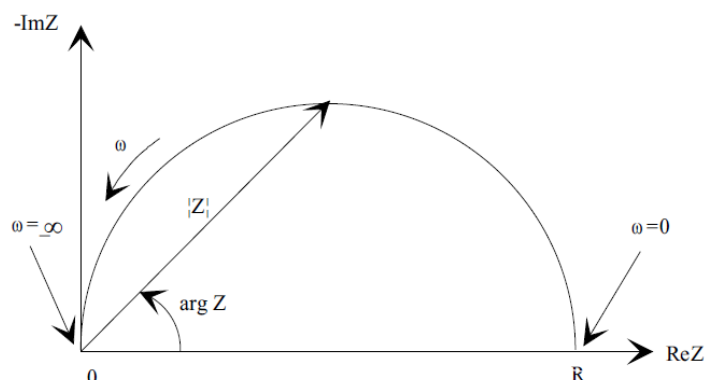

Figure 3-4: Nyquist plot with an impedance vector [48]

As shown in Figure 3-4 above, the output is plotted as a semicircle called 'Nyquist Plot' that indicates a real and an imaginary part of an impedance of the cell. The left side of the plot represents high-frequency data, and the right side is low-frequency data. The data is plotted as a semicircle by considering the measurement of real and imaginary impedance and the phase change or shift that is the time delay between the input and output of a sinusoid frequency. The EIS data can be analysed by fitting it to the common electrical circuit model such as capacitor, inductor, and resistors. The real impedance is equal to the resistance in a DC measurement because the resistor has the current which is in phase with the voltage and has no imaginary component. However, the imaginary impedance is dependent on the capacitance in the system that is available in the AC system only. An EIS data of a battery can be fitted to a capacitor model because they are similar electrochemical systems. The impedance of a capacitor decreases as the frequency increases and owns the current that is phase-shifted 90 degrees for the voltage [78]. The semicircle represents the characteristic of one time constant but a semicircle is often seen partially [78]. The electrochemical impedance of a battery system will have multiple semicircles of electrochemical impedance plots.

3.4.2.2 Li-ion battery considerations and circuit models

In a Li-ion battery system, the SEI layer and battery electrolyte are two parameters that affect the impedance of the battery. Since it is built with various components, Li-ions and electrons pass through resistive and capacitive components during electrochemical reactions [79]. An example of the common electrical circuit model is the simplified Randles cell that consists of a solution resistance (R_s), a double layer capacitor (C_{dl}), and a charge transfer (R_{ct}). As shown in Figure 3-5 below, the solution resistance is on the left and the double layer capacitor is in parallel with the resistance of the charge transfer. R_s is the inherent resistance of the cell because an electrolyte is not a conductor, and it has its resistance that represents the resistible characteristic of chemical compounds. The resistance

of an ionic solution can be directly measured from an ionic conductivity, κ, that depends on the temperature, types, and concentration of ions. An electrochemical system of Li-ion battery is more complicated than simplified Randles cell, but few additional components are added to its fundamental model.
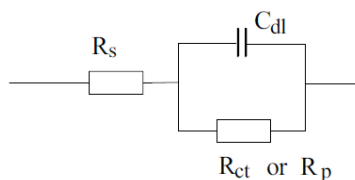
Figure 3-5: Schematic diagram of a simplified Randles cell [78]

SEI layer is the interface that firstly involves the electron transfer after the electrolyte resistance. It is a resistor-capacitor circuit (RC circuit) because it has both a resistive and capacitive component. Two additional elements in the Li-ion battery system are the constant phase element (CPE) and Warburg impedance (W). CPE is determined as the non-deal behaviour of the double layer such as surface roughness, leakage capacitance and non-uniform distribution [78, 79]. W is described as an impedance formed by the lithium diffusion process and is characterised as a straight line on a Nyquist plot that has a constant phase change of 45° [80].

The equivalent circuit model of an entire Li-ion battery can be determined but in a complicated model rather than a simplified Randels cell. There are various components in the Li-ion battery system such as anode and cathode with copper and aluminium foils, electrolyte, SEI layer, and separator. These variables are minimised for the ease of impedance analysis and the counter electrode model is not considered since the EIS spectra are from the contribution of the working electrode in half-cell conditions [79]. In addition, various resistance such as electrolyte, separator and current collector is recognised as the single factor that is the bulk resistance, R_b. Since the capacitance components such as SEI and electrodes are not ideal values in the Li-ion battery system, they can be replaced with a CPE. Hence, some components are adjusted from the simplified Randles cell, and the most fundamental equivalent circuit model of Li/graphite half-cell is shown in Figure 3-6 below. R_{sei} represents the resistance of the SEI layer that is the first semicircle in the Nyquist plot. SEI is the layer interface between the electrode and electrolyte that is mostly formed on graphite anode as mentioned in Section 2.3. From the R_{sei} value, the electrochemical characteristic, and the formation of the SEI layer can be observed.

It is important to understand the fundamental equivalent circuit model of the cell because a diverse circuit model is representing the Li-ion battery system. There is no single equivalent EIS circuit model

that can fit all Li-ion battery systems [81] and they are customised based on the characteristics of tested electrochemical cells by adding or subtracting necessary elements.
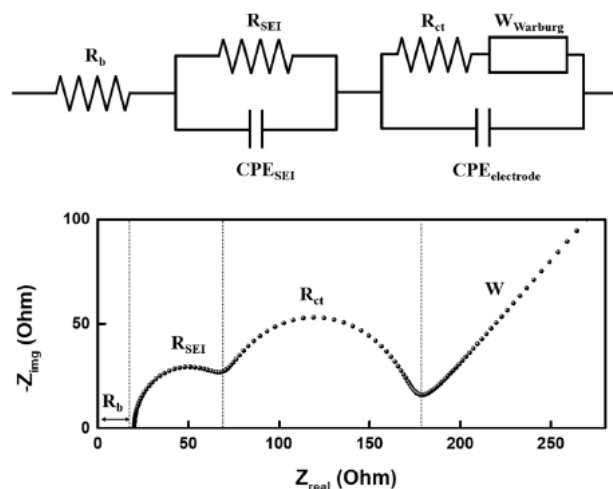

Figure 3-6: An example of equivalent circuit model for Li-ion half-cell [79]

Literatures already used EIS to investigate the electrochemical characteristics and the cycling performance of Li-ion cells. For example, EIS has been used to understand the dynamic models of Li-ion batteries [82] and to determine the resistance and diffusional effect of the SEI layer in different battery electrolytes [83]. Various studies use EIS as an experimental technique to understand the performance and characteristics of Li-ion battery at low temperature such as the study of graphite anode [42], and the battery system such as charging of a fully discharged battery [43], low temperature Li-ion battery [55], and analysis of its AC impedance [84].

Although this promising non-destructive technique is widely used to analyse the battery system, it has certain disadvantages. The interpretation of the data depends on the equivalent hypothesised circuit model since the experimental data are measured from it. Also, data analysis is a complicated process because it deals with the real and imaginary number that leads to complex computation. If an equivalent circuit does not match the tested model, then poor data accuracy can be achieved.

3.4.2.3 Thesis specific experimental considerations

In this experiment, EIS is used to analyse the formation of the SEI layer based on the temperature change from 0 to -15°C. Unlike other experimental techniques such as AFM and FTIR, there is no separate sample preparation for the EIS experiment. The Li-graphite half-cell is built inside the glovebox and the cell is cycled inside a MACCOR temperature chamber as mentioned in section 3.1.2. The impedance test was done using a Solartron Modulab 1260A impedance analyser that is connected to the MACCOR system. The impedance test can be assigned in the MACCOR test procedure because the system is flexible and automatically connects the MACCOR and Solartron impedance

analyser and vice versa. Since the impedance analyser is connected to the MACCOR test system, the impedance tests can be programmed during the battery cycle. To analyse the formation of the SEI layer based on temperature, the impedance test can be implemented before and after the battery cycle.

Chapter 4 - Cell cycling at ambient temperature

The following chapter describes the quantitative data of Li/graphite half-cells to understand its battery performance and to compare the data from various experimental conditions in atmospheric temperature. Individually, it covers most of the important experimental criteria in each section and the use of the experimental technique.

4.1 Introduction

This chapter is to understand the general battery performance at room temperature and to present its quantitative values such as capacity and coulombic efficiency (CE). There is a need for some room temperature experiments before low-temperature experiments because it is necessary to preview the effects of the increasing number of battery cycles on the battery performance without changing the environment temperature. There are various criteria to consider the battery performance, but the key experimental condition of this chapter is battery cycling environment temperature is fixed to 25°C. From this, it is easier to understand exactly which factor affected the battery performance at room temperature by changing types of electrolytes and the number of battery cycles. In addition, it is expected to know the battery efficiency and the capacity loss.

4.2 The effects of battery cycle

4.2.1 Experimental setup

In this experiment, the galvanostatic Li-graphite half-cells are built with a graphite anode and Lithium metal as a reference and counter electrode. Galvanostatic means an electrode is maintained at a constant current to directly observe anodic behaviour and measure its electrochemical reactions. Half-cells were built rather than full cells because the fabrication process is fast, easier, and cost-effective. Results are compared to the formation of the SEI layer by varying cycling numbers because the SEI layer directly forms on graphite anode. As an electrolytic solution, 1.0M of $LiPF_6$ in EC / DMC = 50/50 (v/v) (Sigma Aldrich) (LP30), was used which is the most commonly used electrolyte in the fabrication of Li-ion batteries. Other fabrication processes such as glass fibre separators and crimping the half coin cells were explained in Section 3.1.2. All input values remain constant, and the 100 cycles were assigned. The charge rate of all built batteries was kept constant as 0.1C (C/10) because it is a common value to provide enough capacity to the battery as a function of time. This means it takes 10 hours to discharge the battery and vice versa.

To understand the role of the SEI layer formed on graphite anode, the typical galvanostatic Li-graphite half-cell was built to make the graphite anode is maintained at a constant current throughout 100 cycles in LP30 electrolyte at room temperature. Since it is a half-cell, the battery was discharged first because Lithium foil is used as a counter and reference electrode. It is necessary to discharge the battery first rather than charge cycle so that Lithium is ionised, and Li-ions intercalate from bulk metallic Lithium to Carbon graphite anode. At this stage, Li-ions get inserted into the anode and form an SEI layer on the carbonaceous anode that consist of inorganic and organic components. The theoretical capacity of graphite is around 372 mAh/g in general.

4.2.2 Results

4.2.2.1 20 cycles

Since the battery is Li-graphite half-cell using Lithium as reference and counter electrode, the battery must discharge first so that Lithium ionises and get inserted into the graphite anode. In the Li-ion half-cell discharge cycle, the Li-ions are intercalated to the graphite anode and the Li-ions are deintercalated to the metallic Lithium. The discharge capacity data set actually represents a charge capacity in a full cell and vice versa. Hence, the discharge capacity data sets are called charge capacity (full-cell point of view) which were used for data analysis because the capacity of the anode is the main focus of this thesis.

Figure 4-1: Discharge capacity (data) vs Voltage at different cycling numbers; 1, 5, 10, and 20th. Battery 1 is a Li/graphite half-cell with LP30 electrolyte cycled 20 times at 25°C in C-rate of 0.0039 A. (weight – 0.02165 g).

Figure 4-1 shows the discharge capacities of a Li-graphite half-cell at various cycling numbers (1st, 5th, 10th, and 20th). It is visible that when the capacity is at 0, the starting voltage at the 1st cycle is less than 0.5 V which is significantly lower than other cycles. This is due to more SEI layer formation has taken place as an intact SEI layer forms during 8 hours of ageing time (rest) was given before the cell starts to discharge. The ageing time provides the carbon and the electrolyte interphase to stabilise because the graphite surface will be fully wetted with the LP30 electrolyte. However, at this stage, an unstable

intact SEI layer is formed because there is no load connected to the cell and is in OCV state which is the difference of electrical potential between positive and negative terminals to identify the capability of the electrical potential of a cell. The practical value of onset voltage of SEI formation is 0.8 V vs Li/Li$^+$ [35, 36, 85] but the intact SEI layer is desired to be formed before Li intercalation begins (> 0.3 V) and graphite stabilisation taking place [86]. Hence, the formation of the SEI layer has deeply involved in 1st cycle because the potential is significantly lower than other cycles. Other graphs look like identical graphs meaning the amount of Lithium interaction from bulk metallic Lithium to graphite anode is similar to each other. Their capacity start to increase as the voltage drops from 0.8-0.9 range in which is close to the onset voltage of SEI formation (0.8 V) until it reaches close to 0.01 V.

The discharge capacity of Battery 1 for each cycle were as follows; 1st - 320.617 mAh/g, 5th – 314.959 mAh/g, 10th – 305.745 mAh/g, 20th – 304.794 mAh/g. This is an expected result because the graphite anode should show a decrease in capacity as the Li-ions are consumed more as cycle number increase. It was close to theoretical value of 372 mAh/g, but it was not close enough possibly due to less weight of graphite electrode.
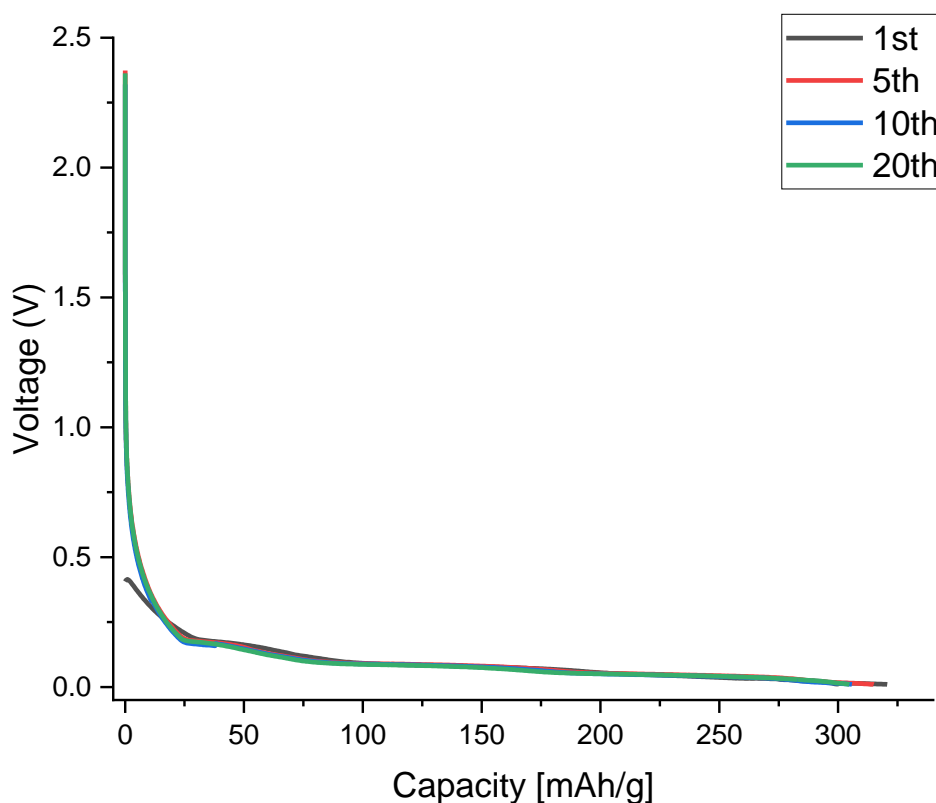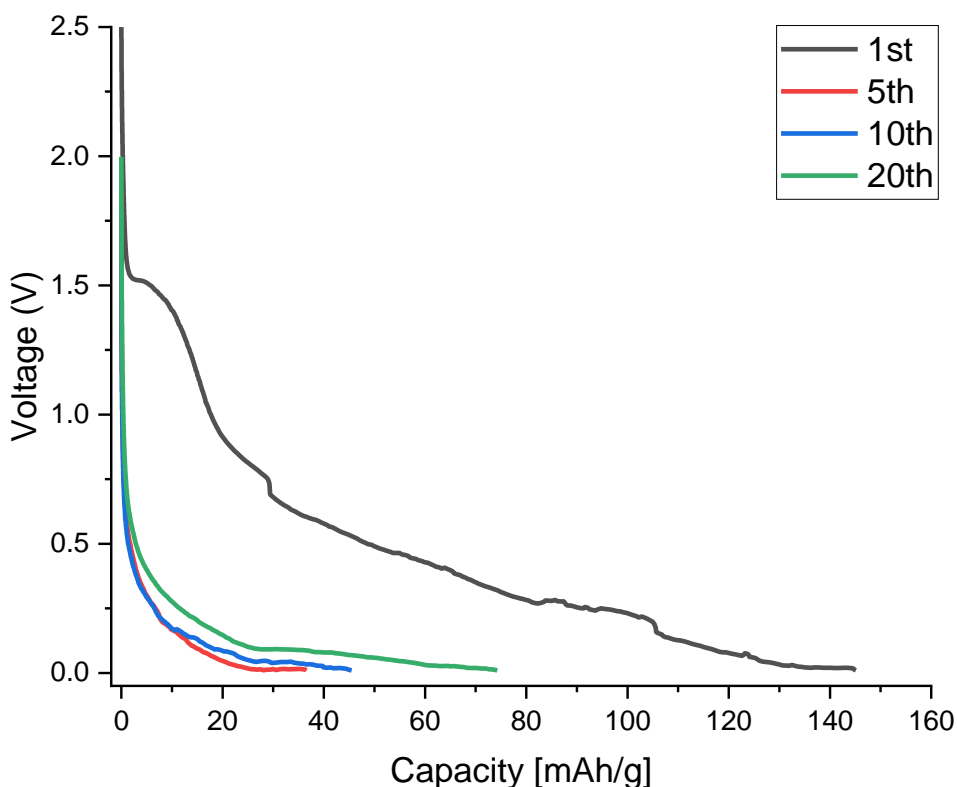

Figure 4-2: Discharge capacity (data) vs Voltage at different cycling numbers; 1, 5, 10, and 20th. Battery 2 is a Li/graphite half-cell with LP30 electrolyte cycled 20 times at 25°C in C-rate of 0.00321 A. (weight – 0.01958 g).

Similarly, Figure 4-2 shows the discharge capacities of a Battery 2 that is similar to Battery 1 in previous Figure 4-1. However, there are some clear differences in between. Two cells were fabricated with identical conditions such as the same types of an artificial graphite anode, electrolyte, and Lithium foil. It is well understood that after 8 hours of ageing time, the Li-graphite half-cell must discharge first to allow Lithium intercalation to take place from Lithium foil to graphite anode that leads to the formation of an intact SEI layer possibly.

Unlike previous data, the potential starts to drop from 1.5 V below and discharge capacities starts to increase up to 150 mAh/g. Battery 1 had a starting voltage of less than 0.5 V and it started to drop slowly as an increase in discharge capacities up to 320 mAh/g. In addition, other cycles (5th,10th, and 20th) had significantly lower discharge capacities and voltages than Battery 1. Their capacities are significantly low until the 20th cycle by comparing with Battery 1. From this, it can be hypothesised as due to poor intact SEI layer formation during 8 hours of ageing time as well as an electrode was not fully wetted in the initial cycles. Theoretically, the capacity cannot be increased as the cycle number increase because more Li-ions are consumed. The 1st cycle had significantly higher capacity than others; 1st - 145.103 mAh/g, 5th – 36.566 mAh/g, 10th – 45.494 mAh/g, 20th – 74.261 mAh/g. After 1st cycle, the capacity dropped massively then started to increase until the end which showed opposite to the theoretical idea. Literature showed that graphite stabilisation occur above the onset of Li intercalation (> 0.3 V) and lead to precipitation of SEI layer [86]. At 1st cycle, it can be assumed that the electrolyte and the electrode were not yet stabilised. From 1.5 V, the capacity started to increase as the voltage drops which is not close to the practical value of onset voltage of SEI formation is 0.8 V vs Li/Li$^+$ [35, 36, 85]. Having less capacity can also be explained by less weight of artificial graphite anode and C-rate than Battery 1.

Another possibility of improper behaviour can be assumed as the coin cell compressed the electrode too much. This might have negative effect on the SEI formation as the excess force acting towards the Li and artificial graphite electrode that leads to faster graphite exfoliation and multiple cracks (SEI, Li foil, separator, electrode).
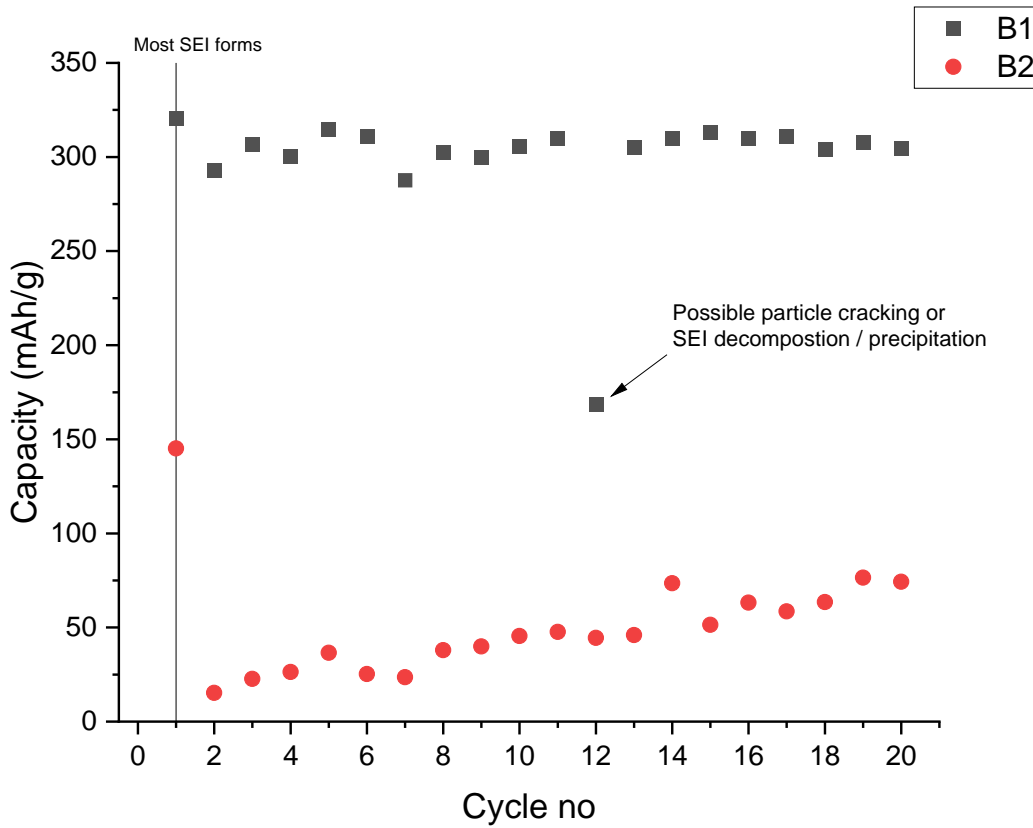
Figure 4-3: Discharge capacities of the same 20 cycled Li/graphite half-cells at 25°C in Figure 4-1 and 4-2; Battery 1: weight – 0.02165 g, C-rate – 0.0039 A, Battery 2: weight – 0.01958 g, C-rate – 0.00321 A

Figure 4-3 represents the obtained discharge capacities of two cells up to 20 cycles at 25°C. Battery 1 had a good intact SEI formation during the ageing time so that after 1st cycle, the capacity gradually decrease until the 20th cycle except the 12th cycle where there was approximately 45.6% capacity loss compared to the 11th cycle. Capacity loss indicates the capacity loss in between two battery cycles (refer to Equation 4.1). It is crucial to keep the capacity loss as minimum as possible because it affects the battery life.

$$\text{Capacity loss} = \frac{Capacity\;_{initial} - Capacity\;_{final}}{Capacity\;_{initial}} \times 100 \qquad \text{(Eq. 4.1)}$$

If the dropped capacity from the 13th cycle onwards was similar to the capacity value from the 12th cycle, it can be explained as general battery failures such as graphite exfoliation or electrolyte decomposition that leads to low Li-ionic diffusivity. However, the possibility is low because the capacity is back to the normal range of values from the 13th cycle onwards. Hence, it can be hypothesised that either particle cracking on anode or some part of SEI decomposition and

precipitation was occurred. Overall, the capacity of Battery 1 was close to theoretical idea because it showed decrease in capacity over cycles.

Unlike Battery 1, Battery 2 had significantly less capacities overall except the 1st cycle where most of SEI layer forms. This is due to the less weight of anode with C-rate of Battery 2. C-rate correlated with the weight of the electrode which was explained in Section 3.1.2. The weight of the electrode can be crucial to determine the capacity because less weight of the artificial graphite anode means limited amount of artificial graphite to react with Lithium and the electrolyte physically and chemically. Another key point is that the capacities were gradually increased throughout the end of the battery cycle. As explained in Figure 4-2 previously, this can be hypothesised as the artificial graphite anode not fully wetted in ageing time. The capacity should decrease over cycle as more Li-ions are consumed more and more due to the Lithium intercalation/deintercalation process.
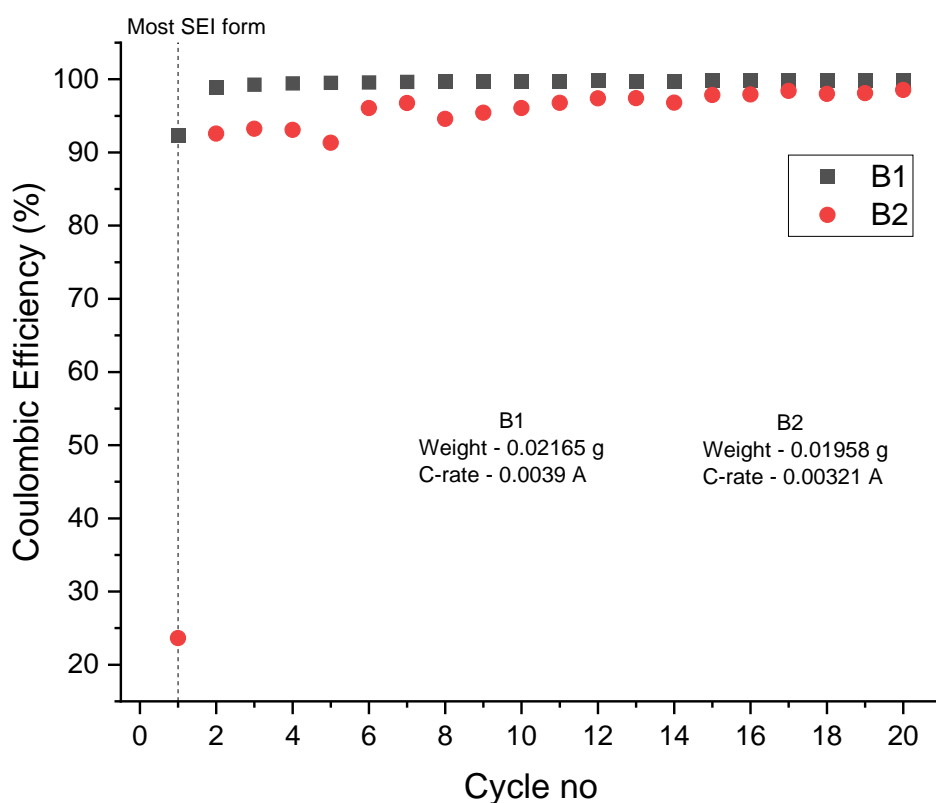

Figure 4-4: Coulombic efficiency of the same Li/graphite half-cells from Figure 4-3. Battery 1 and 2 are a Li/graphite half-cell with LP30 electrolyte cycled 20 times at 25°C. They had C-rate of 0.0039 A and 0.00321 A respectively (weight – 0.02165g and 0.01958 g).

Figure 4-4 represents the coulombic efficiency of two cells which are the same as all previous Figures (4-1, 4-2, and 4-3). The efficiency of the cell can be calculated by finding the difference between the charge and discharge capacity of a battery (refer to Equation 4-2 below). Coulombic efficiency cannot be greater than unity and in general, its value is greater than 99%. The coulombic efficiency of the 1st cycle of Battery 1 is less than 99% because the parasitic reaction occurred mostly due to SEI formation. Glazier et al [87] explained the parasitic reactions as electrochemical reaction processes that occur at the interfaces between the high voltage positive electrode or low voltage negative electrode and the electrolyte by consuming electrolyte species and/or active lithium. When these reactions occur, it leads to disturbance of chemical processes because it is extremely difficult to analyse such complex electrode-electrolyte interfaces. This proves the conclusion that most of SEI layer is formed in the 1st cycle because, from the 2nd cycle onwards, the efficiency is greater than 99%. In addition, it justifies in the previous data Figure 4-3 where the capacity in the 12th cycle was significantly lower than the others. When this phenomenon is explained in terms of the coulombic efficiency, there is no problem in the 12th cycle because there is not much difference in Lithium intercalation during lithiation/delithiation. If there was a decrease in the efficiency from 12th cycle onwards, it can be assumed that something happened at an artificial graphite anode because less amount of Li-ions will intercalate to the reference/counter electrode compared to the anode. Since this was not the case, the conclusion can be more supportive to the partial crack of SEI decomposition/precipitation. In addition, it can be hypothesised that SEI formation can still occur although some partial SEI crack exist on the graphite anode. Lastly, it is possible due to an experimental error, so it is explained in section 4.3.

$$\text{Coulombic Efficiency} = \frac{Q_{discharge}}{Q_{charge}} = \frac{Delithiation\ to\ metallic\ Li}{Lithiation\ to\ graphite\ anode} = 100\% \qquad \text{(Eq. 4.2)}$$

The 1st cycle of Battery 2 had only 23.6 % of coulombic efficiency which is not even close to 90 %. This means there was a small amount of lithiation taken place to graphite anode compared to the amount of the intercalated Lithium reverted to metallic Lithium. Then, the efficiency starts to gradually increase up to 92.5 % from the 2nd cycle onwards. From this, it can be explained that an unstable SEI layer is formed during 1st cycle although there was a parasitic reaction that occurred mostly due to an intact SEI formation. Although Battery 2 had such a low capacities as shown in previous Figure 4-3, its coulombic efficiencies were well achieved over 90% from the 2nd cycle onwards. Another possibility is that more SEI formation occurred in Battery 2 than Battery 1 because the efficiencies were still below the 99% until 15th cycle and it was getting closer from 16th cycle onwards. When the efficiency is less than 90%, it can be assumed that more Li-ions are intercalated to the graphite anode than the delithiation to metallic Lithium due to Li-ions are involved in SEI formation. As explained in Figure 4-2

and 4-3, it can be possibly due to the electrode not fully wetted in initial cycles and it shows increase in capacity and efficiency as they soak over cycle.

These results are very interesting because the data sets were obtained from two cells fabricated in identical conditions. It can be concluded that if an imperfect, but stable SEI layer is formed in 1st cycle similar as Battery 1, the capacity and coulombic efficiency will be similar to the theoretical and literature values. If an unstable intact SEI layer is formed in ageing time, most of SEI layer is still formed in 1st cycle but there is an increase in capacity over cycle and as the battery cycle is repeated, a more stabilised SEI layer can be formed. This is not supposed to happen theoretically because the capacity cannot be increased over cycle as Li-ions are consumed more and more. This phenomenon occurs due to multiple reasons but possibly due to the electrode not fully wetted in initial cycles, less weight of the electrode with C-rate, or better SEI layer needs to be formed. These graphs aid the previous hypothesis where it is possible to have a good SEI layer formed on the graphite anode during 1st cycle but sometimes, it needs more than 1 cycle to have complete SEI formation.
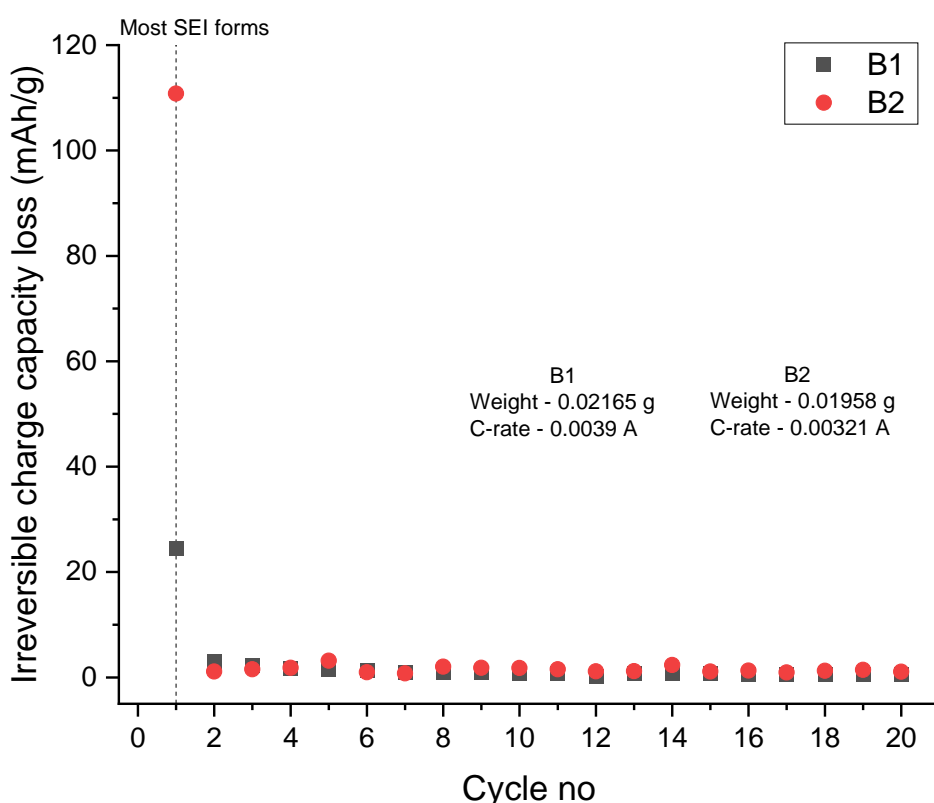

Figure 4-5: Irreversible charge capacity loss of same Li/graphite half-cells with LP30 electrolyte cycled 20 times at 25°C. They had C-rate of 0.0039 A and 0.00321 A respectively (weight – 0.02165g and 0.01958 g).

Figure 4-5 represents the irreversible charge capacity loss of same batteries as all previous Figures. It showed an expected results which charge capacity is higher than discharge capacity because some binding of lithium ions are not taking part in further discharge process because they are involved in SEI formation on graphite anode, Lithium plating and stripping at bulk metallic Lithium [88]. It is visible that charge capacity is higher than discharge capacity because, in 1st cycle, irreversible charge capacity loss (refer to equation 4-3 below) was high enough to differentiate amongst others. Battery 1 had significantly less charge capacity loss than Battery 2 which can be explained as a better SEI layer was formed during the initial cycles (ageing time). If high irreversible charge capacity loss is obtained, this means larger amount of Li-ions are not intercalated back to metallic Lithium and stayed in or around graphite anode to help more SEI formation or Lithium plating/stripping in the electrode-electrolyte interface area. The individual amount of charge/discharge capacity is not important because the charge capacity of Battery 2 was 145.1 mAh/g which was almost half of Battery 1 capacity, 320.6 mAh/g but Battery 2 had comparably much higher irreversible charge capacity loss than Battery 1. After 1st cycle, both batteries had a small irreversible charge capacity loss which was lower than 5 mAh/g until the end. This means an almost similar amount of Lithium intercalation/deintercalation took place during the charge/discharge state, but still higher charge capacity was seen in each cycle. To explain, there were some amounts of Li-ions not deintercalated to metallic Lithium foil but reacted as SEI formation/stabilisation or Lithium plating/stripping on graphite anode in every cycle. Battery 1 had decrease in irreversible charge capacity loss over cycle whereas Batter 2 showed unstable relationship.

$$Q_{ir} = Q_{charge} - Q_{discharge} \hspace{2cm} \text{(Eq. 4.3)}$$

To conclude, Battery 1 had better SEI formation than Battery 2 because it showed decrease in irreversible charge capacity loss over cycle which means the difference in between the amount of Li-ions intercalated during discharge/charge decreased until 20th cycle. It means that a decent intact SEI layer is formed in initial cycles and addition to that, good SEI formation was occurred in 1st cycle. On the other hand, Battery 2 had unstable irreversible charge capacity loss because the amount of Li-ions intercalated during discharge/charge differ over cycle. It can be hypothesised that poor SEI was formed in ageing time, and it needed more time to build a decent quality of SEI layer over cycle as the graphite anode of Battery 2 was not fully wetted.

4.2.2.2 100 cycles

Similar to the previous 20 cycles experimental conditions, Li/graphite half-cell was used with the same battery fabrication conditions as mentioned in section 3.1.2 and 4.2.1 except cycle number has increased to 100. The idea of increasing the cycle number is to understand how Li/graphite half-cell

performs up to 100 cycles because the battery life of Li-ion battery is 100 cycles in general. Unfortunately, the analysed data in this section is limited to only one data although multiple cells were tested, and this will be explained in section 4.3 more detail.
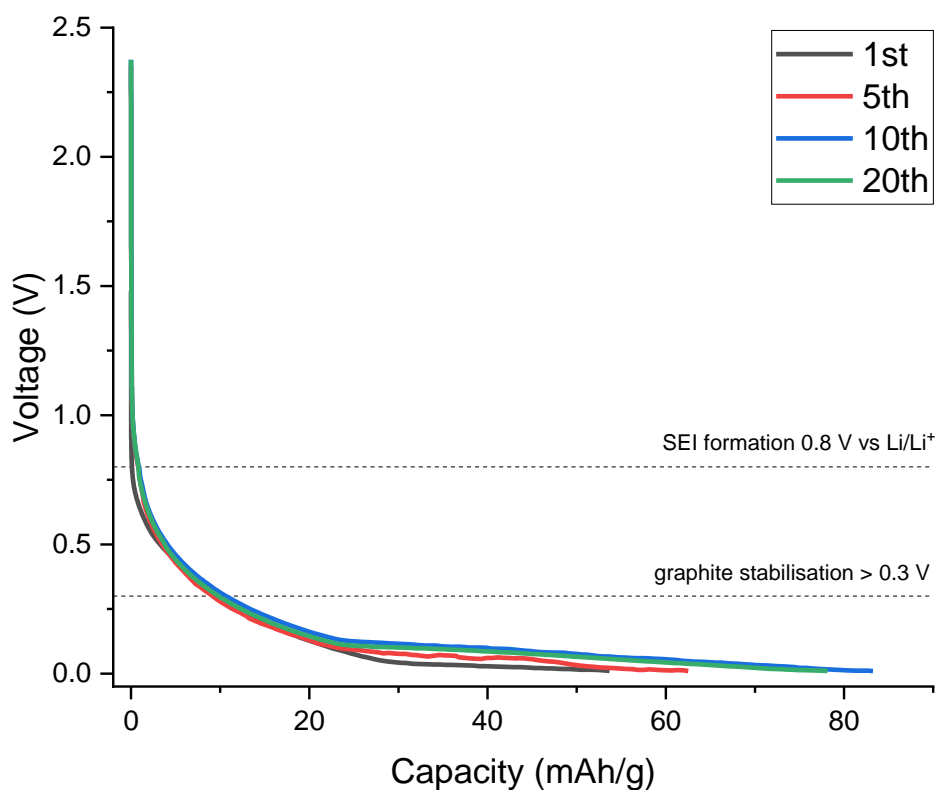

Figure 4-6: Discharge capacity (data) vs Voltage at different cycling numbers; 1, 5, 10, and 20th. It is a Li/graphite half-cell with LP30 electrolyte cycled 100 times at 25ºC in C-rate of 0.00461 A. (weight – 0.02376 g).

Figure 4-6 represents the discharge capacities of a Li-graphite half-cell at relative cycle numbers (1, 5, 10, and 20th). Similar to Figure 4-1 in previous section 4.2.1.1, the starting voltage of the 1st cycle is 1.5 V which is lower than other cycles. Previously in Figure 4-1, the capacity started to increase until 320 mAh/g as the voltage started to drop from 0.4 V until 0.01 V. However, Figure 4-6 showed a much smoother inversely proportional graph than other previous Figure 4-1 and 4-2. The discharge capacity of a battery for each cycle were as follows; 1st – 53.692 mAh/g, 5th – 62.515 mAh/g, 10th – 83.246 mAh/g, 20th – 78.148 mAh/g. They were not even close to the theoretical capacity of graphite, 372 mAh/g. The starting voltage of 1st cycle differs depending on the condition of an unstable SEI layer formed during 8 hours of ageing time, carbon, and electrolyte stabilisation because they had diverse starting voltages based on Figures 4-1, 4-2, and 4-6. Li-ions of this cell were heavily involved in SEI formation at 1st cycle because a very smooth inversely curved gradient is visible around the voltage range of 0.2 - 0.8 V. This is the range where the practical value of onset voltage of SEI formation is 0.8

V vs Li/Li$^+$ [35, 36, 85] and intact SEI layer is desired to be formed before Li intercalation begins (> 0.3 V) and graphite stabilisation taking place [86]. In addition, this inversely curved gradient was shown in all four cycles unlike previous Figures 4-1 and 4-2. In conclusion, a smooth inversely curved gradient in the 0.2 – 0.8 range of potential was shown in 1st cycle, and it can be hypothesised that a Li-ions are heavily involved in good SEI formation on graphite anode. As the cycle number increases, it helps to stabilise and improve the quality of the SEI layer because other graphs look identical graphs meaning the amount of Lithium interaction from bulk metallic lithium to graphite anode is similar to each other.

However, it is possible that this is not the case because theoretically, the capacity cannot increase as Li-ions are consumed more and more over cycle. It was supposed to have similar look as Figure 4-1 as the highest capacity achieved at 1st cycle and decrease over cycle. Figure 4-6 was more similar to Figure 4-2 which can be assumed as the electrode was not fully wetted so poor intact SEI layer was formed in ageing time. This particular Li/graphite half-cell was expected to have better performance than previous Battery 1 and 2 because it had higher weight and C-rate. Since this is not the case, it can be concluded that the weight of anode and C-rate is not dependent on the battery performance but the condition of the electrode whether it is fully wetted or not is crucial determining the battery performance.
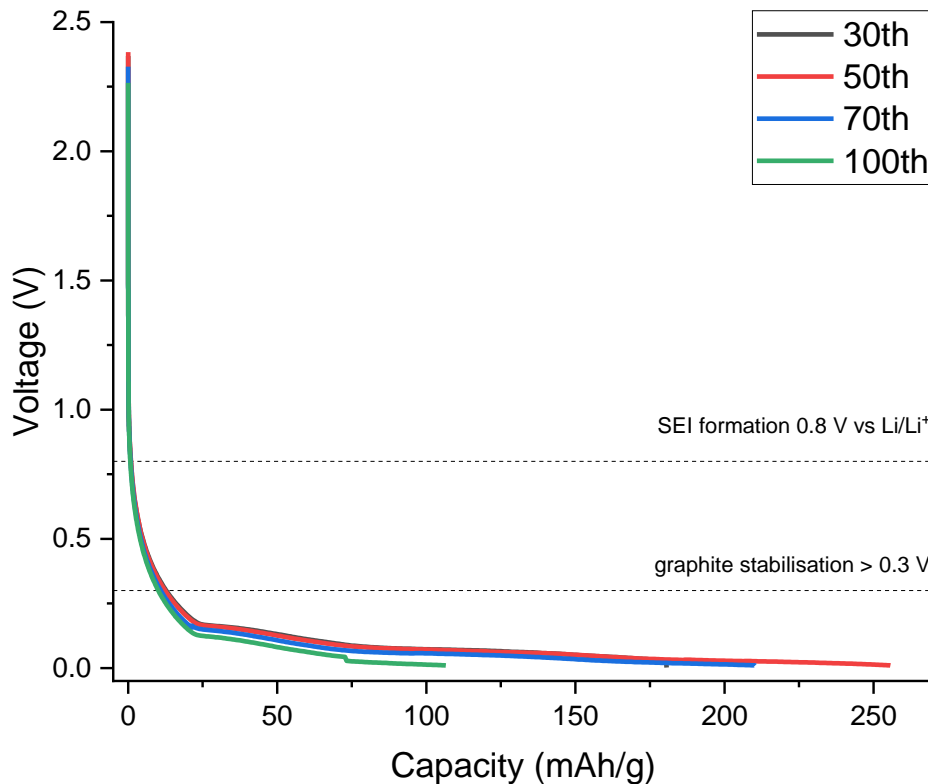
Figure 4-7: Discharge capacity (data) vs Voltage at different cycling numbers; 30, 50, 70, and 100th. It is same Li/graphite half-cell with LP30 electrolyte cycled 100 times at 25°C in C-rate of 0.00461 A. (weight – 0.02376 g).

Figure 4-7 is showed to understand how discharge capacity changes at 30, 50, 70, and 100th cycles. The discharge capacity of a battery for each cycle were as follows; 30th – 180.606 mAh/g, 50th – 255.650 mAh/g, 70th – 210.286 mAh/g, 100th – 106.527 mAh/g. It is clear that the capacity has increased until the 50th cycle and it dropped as the battery cycle reaches the end. The gradient of the graphs at a voltage range of 0.2 – 0.8 V was not smooth as the previous Figure 4-6, and the curve is more relaxed towards the end of the battery cycle that is similar to linear. This is possibly due to the existence of a decent SEI layer formed on graphite anode. The amount of Li-ions intercalation during charge state will decrease as the cycle number increase because the poor condition of the SEI layer will allow a limited amount of Li intercalation to graphite surface that leads to possibly a shortage of battery life and failure [35]. The capacity fade occur when the Li/graphite half-cell reaches 100th cycle as it cannot maintain its capacity long enough that results in battery limitations. There are various reasons for the degradation mechanism of Li-ion battery such as SEI decomposition and precipitation, graphite exfoliation, Lithium plating and dendrite formation [89]. Hypothetically, the capacity was

increased by comparing with Figure 4-6 because the electrode had more time to cover with the electrolyte.

In addition, the smooth curved gradient in 0.2 – 0.8 V is relaxed as the Li-graphite half-cell cycles (100 times) because of a stabilised SEI layer is damaged by multiple reasons such as SEI decomposition, graphite exfoliation, and dendrite formation. This can occur poor condition of SEI layer which allow a limited amount of Li-ion to intercalate towards the active material surface that results shortage of battery life due to loss in capacity and performance.

Figure 4-8: Capacity (data) vs Voltage at different cycling numbers; 1, 2, 5, 7, and 10th. It is same Li/graphite half-cell with LP30 electrolyte cycled 100 times at 25ºC in C-rate of 0.00461 A. (weight – 0.02376 g).

Figure 4-8 represents the generated capacity at the voltaic range from lowest 0.01 V to maximum of 2.5 V. It is the same Li/graphite half-cell as Figure 4-6 and 4-7 but with different data analysis. The left side of the graph represents the discharge capacity, and the right side is the charge capacity of the half-cell. As the Li-graphite half-cell was fully built and started to discharge, Li-ions intercalate and diffuse to the carbonaceous anode. As mentioned in 4.2.2.1, the discharging in half-cell means it produces charge capacity because Li-ions intercalate to graphite anode and vice versa. At the same time, the electrolyte decomposes to form a stable SEI layer that only allows Li-ions to pass through

but completely blocks the electrons. Hence, discharge/charge in half-cell can be explained as charge/discharge in full-cell.

The graph represents five different battery cycles to show the change in discharge/charge capacity to voltage. It clearly shows that as the cycle number increases, the graph shifts to the right which means both capacity values increase. This is due to the graphite anode not fully wetted in ageing time and needed to be wet over cycle. It can be assumed that poor SEI layer is formed as electrolyte stabilisation was not stable in initial cycle so it needs more cycle to allow the graphite anode is well covered with the electrolyte as well as more SEI formation can occur. Providing more time for the electrolyte decomposition and diffusion of Li-ions that assists the improvement of the SEI formation. It was supposed to have highest capacity at 1st cycle close to the theoretical value of 372 mAh/g and the graph should shift to left because decrease in capacity over cycle is what is expected theoretically.
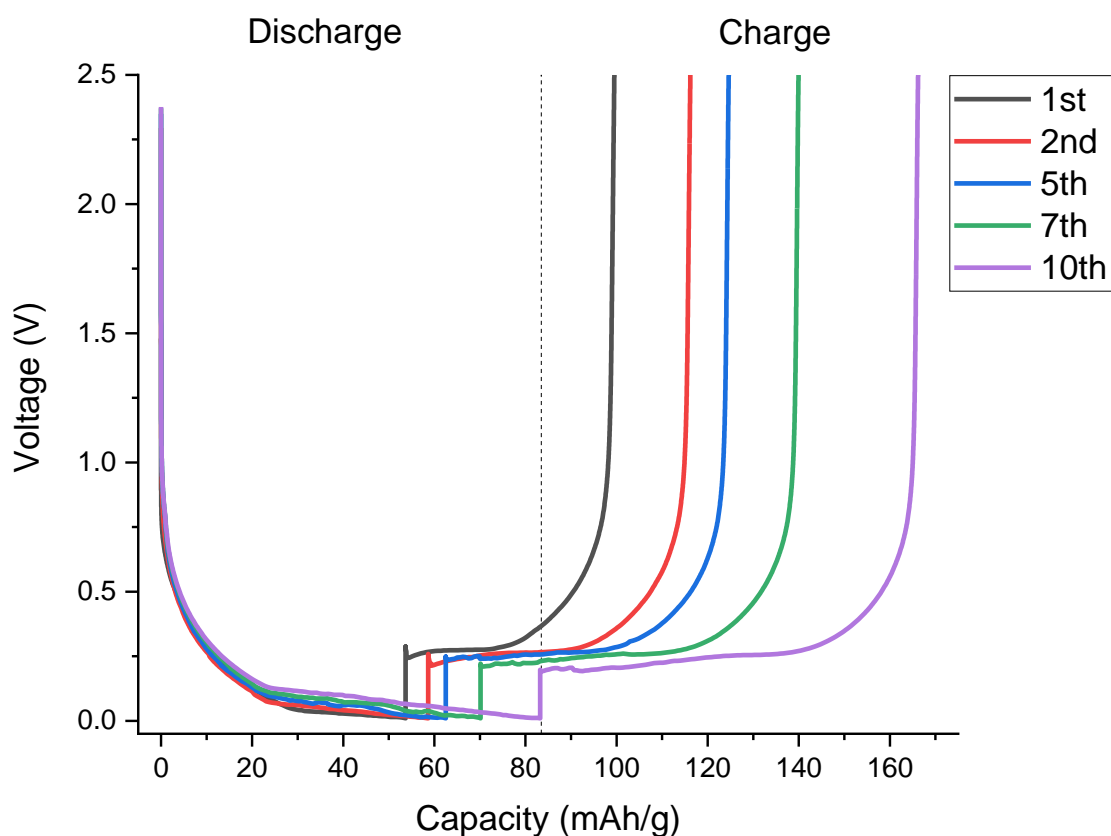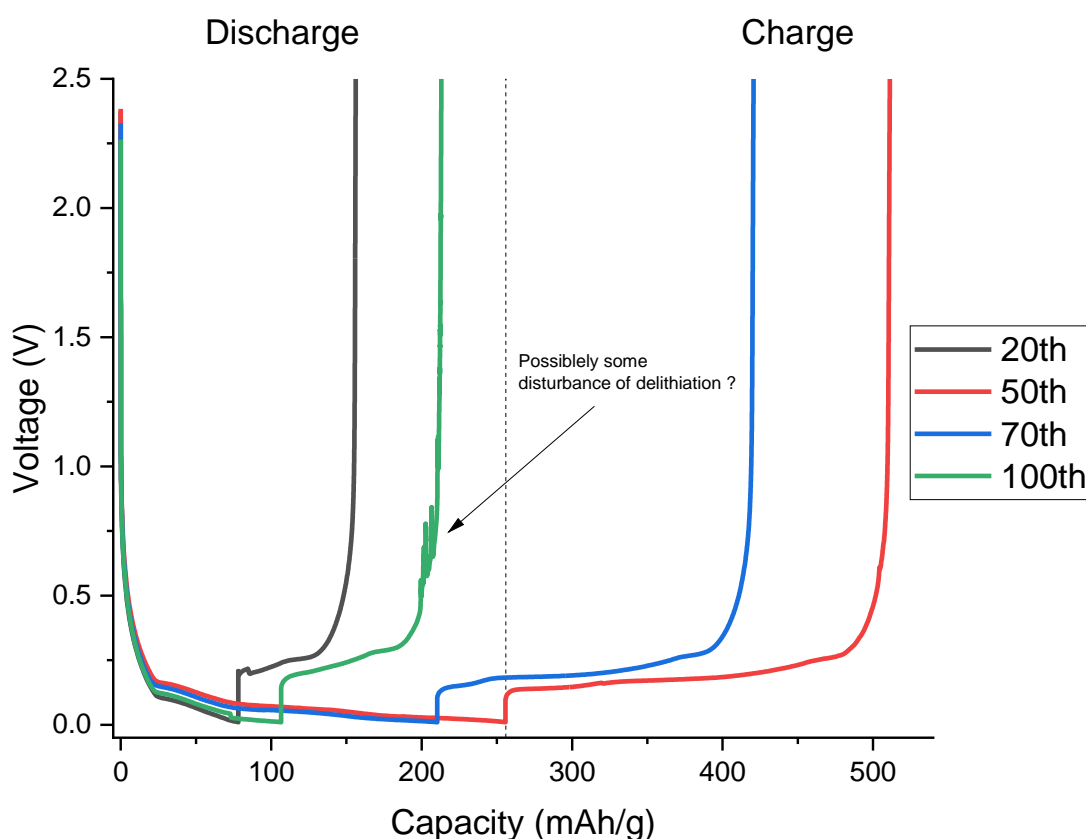

Figure 4-9: Capacity (data) vs Voltage at different cycling numbers; 20, 50, 70, and 100th. It is same Li/graphite half-cell with LP30 electrolyte cycled 100 times at 25°C in C-rate of 0.00461 A. (weight – 0.02376 g).

Figure 4-9 shows the similar graphs as previous Figure 4-8 but with increase in cycle numbers up to the 100th cycle. The graph shifts to the right up to the 50th cycle and the graph shifts to the left from 70th cycle onwards. As shown in Figure 4-8, relatively low capacities were achieved until the 10th cycle

and even 20th cycle in Figure 4-9 was not even close to the expected value of 372 mAh/g. However, it was nearly doubled at the 50th cycle which can be assumed as decent SEI layer was formed beforehand. It is expected that capacity starts to fade roughly after 40 − 50th cycle. From this, it can be hypothesised that the good intercalation process of Li-ions taking place around 30th cycle in which mostly Li-ions are involved in SEI formation. It is clear that the capacity fade occurred after the 50th cycle because the graph is shifted to the left. This is due to battery ageing that leads to a decrease in battery efficiency. Battery ageing can occur from many failure phenomena. As the number of battery cycles increases, there are some changes at electrode/electrolyte interphase. At first few cycles, SEI layer forms on graphite anode due to electrolyte decomposition and Li-ion intercalation in between two electrodes. As the battery keeps on cycling, its layer will grow and stabilise when the thickness is reached its maximum. Then, from top to bottom, the layer starts to fall apart and dissolute. When the battery cycle is reached near the limit, lithium plating takes place at the corrosion layer. The charge capacity of the half-cell for 100th cycle showed some irregular disturbance during the charge cycle when the capacity reached 200 mAh/g. It can be hypothesised as some disturbance of delithiation occurred because the disordered voltage was showed as capacity increase. Since it was not seen in the discharge state, it is assumed that only delithiation was disturbed at 100th cycle. It can be explained as dendrite formation or particle cracking on metallic Li because it caused near the end of charge cycle not the start.
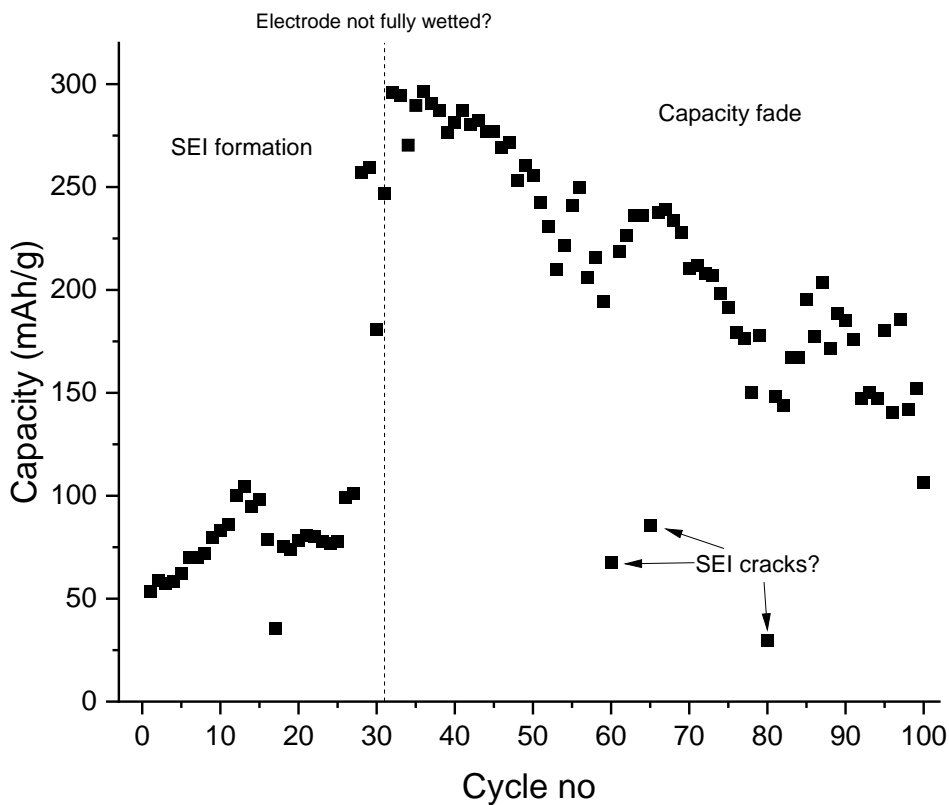
Figure 4-10: Discharge capacity (half-cell based) with cycle number of a same Li/graphite half-cell with LP30 electrolyte cycled 100 times at 25°C in C-rate of 0.00461 A. (weight – 0.02376 g).

Figure 4-10 shows various charge capacities of a same Li/graphite half-cell obtained in each cycle up to 100 cycles. The graph can be separated into two sections; left is the possible SEI formation and right is the capacity fade. The capacities until 30th cycle were relatively lower than the others because of the possible SEI formation due to the electrode not fully wetted in ageing time. The capacity until 27th cycle was relatively low which can be determined as the electrode was not fully wet because the capacity massively increased at 28th cycle. It is estimated that the electrode was fully wetted from 31st cycle onwards because the capacity was close to the theoretical value of 372 mAh/g. If the electrode was not fully covered with electrolyte, it will have negative effect on the lithiation/delithiation process during discharge/charge cycle that produce less capacity. This will result to unstable SEI formation although an intact layer is formed in ageing time and mostly in 1st cycle. In general, the SEI layer mostly forms at the 1st cycle, and it continues up to 10 to 20th cycle. Second, it can be due to low electrolyte conductivity, but the possibility is low because LP30 is a commonly used battery electrolyte that has high ionic conductivity (10 mS cm^{-1}) at room temperature. When the battery discharges, Li-ion moves from cathode to anode and vice versa reaction takes place in general Li-ion battery. Since the role of Li foil in Li-ion half-cell is a counter and reference electrode, charge capacity is slightly higher than

discharge capacity. This is due to some Li-ions being taken to bind with relevant components of electrolyte solution and graphite anode to form SEI layer at the beginning of the discharge process which can be explained as irreversible capacity losses. Based on the SEI formation region, this battery is similar to Battery 2 from previous section 4.2.2.1 because their capacity was in a similar range and the capacity tends to increase as the cycle number increases until the 20th cycle.

The capacity starts to fade roughly after the 40th cycle onwards due to the battery degradation. At this point, the discharge/charge time of the battery will increase because of battery ageing. It is difficult to address what is the main issue for battery ageing but slow Li-ion mobility in between electrodes, graphite exfoliation, electrolyte, and SEI decomposition as the number of battery cycle increase, are good example of possible issues. The Li-ions is consumed more and more over cycle, so this phenomenon was an expected result. It was supposed to happen at the beginning of the cycle because largest amount of Li-ions is available.

After the 31st cycle, it is very clear that the capacity starts to drop slowly until the 100th cycle. There were a few cycles where the capacity loss occurred in between; 60th, 65th, and 80th cycles (65.3 %, 63.7 %, and 83.3 %). This can be hypothesised as possible SEI or particle cracks, but further investigation needed. Although it is crucial to minimise the capacity loss in every cycle, the capacity gradually drops throughout the end of the battery cycle. This can be directly related to battery failure where the detrimental process can take place such as SEI starts to slowly decompose and fall out into small pieces due to precipitation roughly after the 30th cycle. In addition, exfoliation of graphite anode and dendrite can be formed in electrode-electrolyte interphase that limits the amount of Li-ion intercalated to graphite anode.
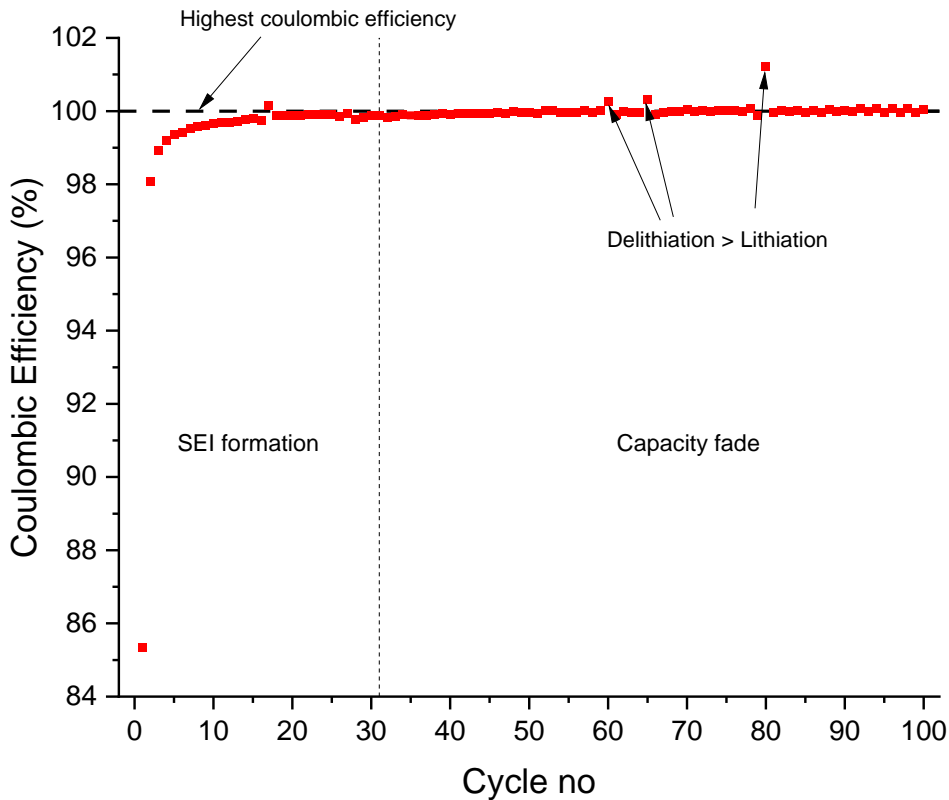
Figure 4-11: Coulombic efficiency of a same Li/graphite half-cell with LP30 electrolyte cycled 100 times at 25°C in C-rate of 0.00461 A. (weight – 0.02376 g).

Figure 4-11 represents the coulombic efficiency of the same Li/graphite half-cell in each cycle number. As mentioned in previous Equation 4-2, the efficiency of the cell can be calculated by finding the difference between the charge and discharge capacity of a battery. This cell also had 85.3 % of coulombic efficiency at 1st cycle which is relatively lower than an ideal value (99 %) because of parasitic reaction taken place to form an SEI layer which means less amount of Li-ions were intercalated to the metallic Lithium than the number of Li-ions lithiated to the graphite anode. From the 2nd cycle onwards, the efficiency starts to gradually increase, and its value is fixed to 98 – 99 % in most cycles. Based on Figure 4-10, the discharge capacity (charge in full-cell) was relatively low until 31st cycle possibly due to unstable SEI layer is formed in ageing time as graphite anode is not fully wetted with electrolyte. There was increase in capacity over cycle which was opposite to the theoretical expectation. However, the coulombic efficiencies until 31st cycle were close to the theoretical value of 99%. It is difficult to determine whether this battery is good or bad because it is good based on the efficiency, but it is bad based on the capacity. In addition, the capacity started to fade after 31st cycle but the efficiencies were close to theoretical range. This represents the discharge/charge capacity had similar values which means almost similar amount of Li-ions were delithiated/lithiated.

However, there were some cycles where the efficiency exceeds 100%. This is due to comparably more amount of Li-ions deintercalated during cell discharge than charge in which less amount of Li-ions intercalated towards the graphite anode. There will be more amount of Li ions to transport mostly during the discharge (deintercalation) process as the cycle number increases because of structural interference of anode. As shown in previous Figure 4-10, capacity starts to fade approximately after the 31st cycle because of anode structure changes by SEI decomposition, precipitation, and graphite exfoliation. In addition, Lithium plating and dendrite can be formed in electrode-electrolyte interphase. This detrimental process can have a major impact on discharge capacity higher than charge capacity, but the possibility is low. It was only occurred in 60th, 65th, and 80th cycle which was similar to Figure 4-10 where the capacity was relatively low. From this, it can be hypothesised that partial SEI or particle cracks occurred on graphite anode during that particular cycles.
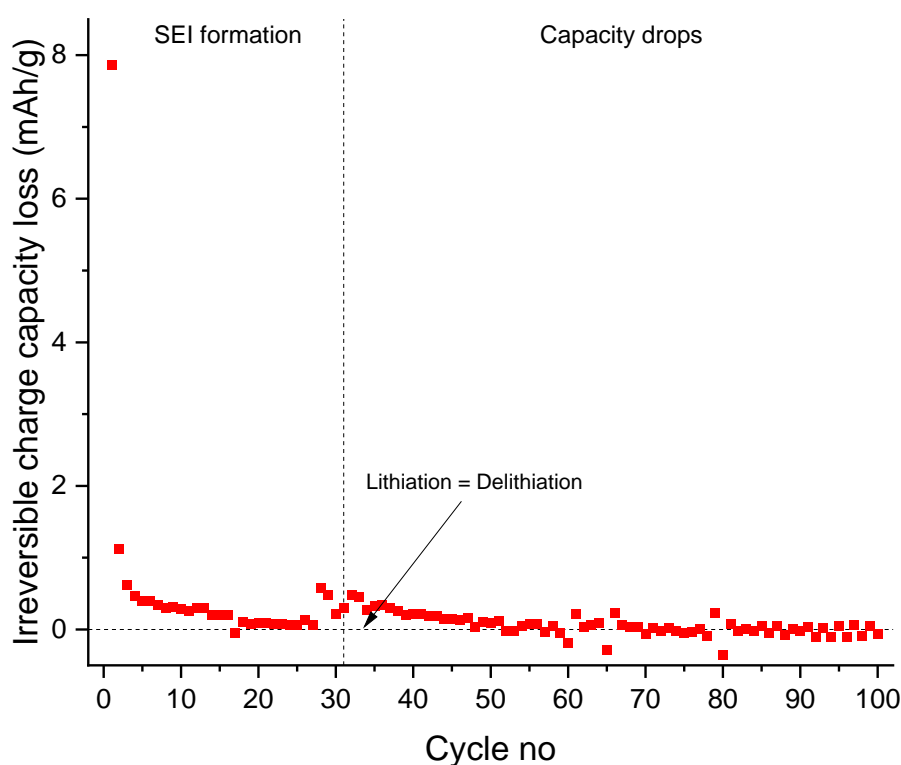
Figure 4-12: Irreversible charge capacity loss based on cycle number of a same Li/graphite half-cell with LP30 electrolyte cycled 100 times at 25°C in C-rate of 0.00461 A. (weight − 0.02376 g).

Figure 4-12 shows how the irreversible charge capacity (discharge in half-cell) loss changes over cycle. Once again, the capacity loss in 1st cycle had a significantly higher value than others mostly due to SEI formation taking place by having higher charge capacity than discharge capacity which was similar to previous Figure 4-5. It is known that a certain amount of Li-ions are not involved in the further

discharge process but used information of SEI layer, Lithium plating and stripping at bulk metallic Lithium [88]. From the 2nd cycle onwards, the irreversible charge capacity loss drastically decreased to 1.1 mAh/g and this stayed within 0.1 – 0.4 mAh/g in the most cycle. Based on the previous Figure 4-10 and 4-11, SEI formation has taken place roughly until 31st cycle and capacity started to drop gradually throughout the end of the battery cycle due to the electrode not fully wetted with the electrolyte in initial cycle and need more time to stabilise the electrolyte and the electrode. Data set in SEI formation region had relatively higher irreversible charge capacity loss than Capacity drops region. This showed that more cycles are needed to form a decent SEI layer although most of the SEI layer is formed in ageing time and 1st cycle. Roughly until the 31st cycle, the larger amount of Li-ions is not involved in the deintercalation process because they are involved in the formation of SEI layer, and Lithium plating/stripping which could result in a detrimental process later cycle.

Interestingly, there were few cycles where irreversible charge capacity loss was the negative value which means discharge capacity is slightly higher than charge capacity. This means the amount of Li-ions involved in the deintercalation process is relatively more than the intercalation process. It was mainly visible on 60th, 65th, and 80th cycles which correlates as previous Figure 4-10 and 4-11. It seems like roughly after 50th cycle, higher delithiation occurs than lithiation besides 60th, 65th, and 80th cycles.

After the 80th cycle, the irreversible charge capacity loss is randomly disordered until the 100th cycle. This means the amount of Li-ions intercalate during charge/discharge state is not constant and keeps on changing as the cycle number reaches the end that leads to capacity fade and shortage of battery life because the movement of Li-ions are heavily disturbed by structure interference of anode and metallic Lithium which is not smooth as first few cycles.

4.3 Experimental error

This section is introduced to explain some possible experimental errors that can be occurred in theoretical and practical ways. It is important to know how to minimise the experimental error low as possible. First, repeatability of the same experiment is needed because the experimental data cannot be definite in all cases. For example, two cells were fabricated in identical conditions such as the size of the coin cell (CS2016), type of electrolyte (LP30) and electrode (artificial graphite), glass fibre separator, and metallic Li foil. These Li/graphite half-cells were fully sealed in a crimping machine and connected to MACCOR channels respectively using the same procedure and CC was applied at the discharge process. Based on the data from section 4.2.2, the same experimental conditions were applied in both cells, but different experimental data were obtained such as capacity and coulombic efficiency. This is due to human error during battery fabrication. The graphite anode and Lithium are manually punched one by one. It is impossible to make all graphite anode and pieces of Lithium with

the same size of 1.44 cm^2. In addition, the size can be exactly 1.44 cm^2 but the weight of graphite anode varies. The weight of two batteries with 20 cycles are as follows: Battery 1 – 0.02165 g and Battery 2 – 0.01958 g. The weight of 100 cycled batteries was 0.02376 g. However, these cells had different experimental data quantities, but a similar scientific phenomenon is shown such as gradual charge capacity increase due to SEI formation. From this, it shows that it is nearly impossible to have multiple numbers of electrodes of the same size and weight, but a similar scientific phenomenon is discovered due to cycling temperature, the composition of electrolyte and electrodes are the same.

Another human error can occur during the fabrication of a cell especially when a few drops of the electrolyte using a pipette are added to the separator. Although the amount of electrolyte needed can be fixed by an Eppendorf pipette, the process where electrolyte added to separator cannot be the same every time in battery fabrication. It is important to maintain enough amount of electrolytes added to the separator so that a graphite anode is fully wetted in the initial cycles. If an electrode is not fully wetted due to less electrolyte solution, there will be a capacity increase as the battery cycles repeatedly until the expected value is reached somewhere around 372 mAh/g.

The internal battery components must be aligned in parallel and carefully placed. Especially, when the graphite anode and Lithium foil are not aligned correctly and they are slightly off position, it results in capacity loss and poor battery efficiency that leads to short battery life. There will be a limited area of graphite anode reacting with Lithium metal because when they are placed further apart, the intercalating area will be decreased. When they are perfectly aligned in parallel, there will be enough area for the Li-ions to intercalate/deintercalate in between graphite anode and Lithium metal because they share the same area of 1.44 cm^2. However, if either anode or metallic Lithium is slightly off the position, there will be some area where either intercalation or deintercalation can process but not the other which is represented as red colour in Figure 4-13 below. Five possible alignments can occur during coin cell fabrication.
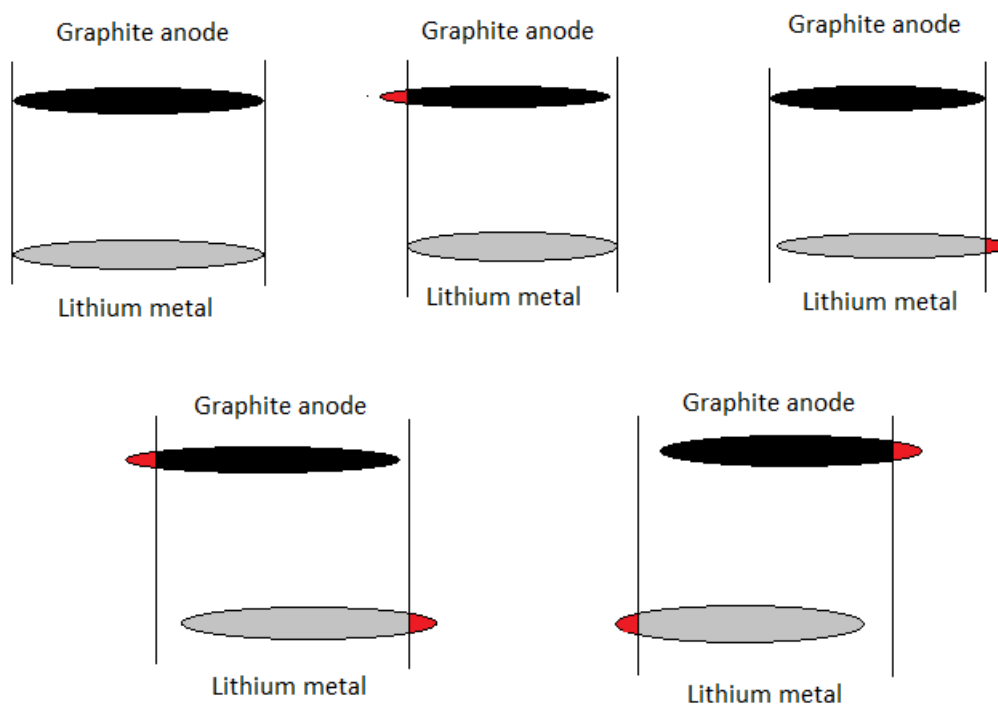
Figure 4-13: Possible alignments of graphite anode and Lithium metal during battery fabrication

Although it is necessary to repeat the same experiment a few times, it is difficult to keep doing the same experiment repeatedly because it is a time managing process. For example, if a cell needs to be tested in short battery cycles, it is possible to repeat a few times because it takes approximately a few days to get a result. However, if a cell needs to be cycled many times (50-100 cycles), it takes 2-5 weeks depending on the electrolyte and electrode composition of the cell. Hence, the experiment in this chapter was repeated 2 – 3 times but only necessary data were introduced. One of 20 cycled batteries and two of 100 cycled batteries failed on charge/discharge process because of technical issues such as temperature changing issue, a constant current cannot be applied at tested circuit channel in MACCOR system, or voltage cannot reach 2.5 V or 0.01 V.

4.4 Conclusion

This chapter was introduced to understand the general performance of Li/graphite half-cell based on cycling number at 25°C. The tested cell had 8 hours of ageing time before it starts to discharge to form an intact SEI layer on graphite anode surface. This layer will be formed once the graphite electrode surface is fully covered with LP30 electrolyte. Ageing time was needed prior to the battery cycle to stabilise in multiple positions such as electrolyte, SEI formation, and electrode-electrolyte interphase depending on the properties of electrolyte and anode material. The battery was discharged first because Lithium foil was used as a counter and reference electrode. As Li/graphite half-cell was fully

built and started to discharge, Li-ions intercalate and diffuse to the carbonaceous anode. At the same time, the electrolyte decomposes to form more SEI layer that only allows Li-ions to pass through but completely blocks the electrons. An adequate SEI layer can be formed as the battery continues more discharge/charge cycles and the capacity should be decreased as Li-ions are consumed more and more over cycle. The main focus of this experiment was to understand how Li/graphite half-cell performs at room temperature and its discharge capacity (charge in full-cell).

It proved that most of the SEI layer is formed in 1st cycle because the discharge capacity (charge in full-cell) started to increase as the potential decreased having an inversely proportional relationship. It started to increase when the practical value of onset voltage of SEI formation was reached which is 0.8 V vs Li/Li^{+} [35, 36, 85]. However, desired SEI layer is formed before Li intercalation begins (> 0.3 V) and graphite stabilisation takes place [86]. Irreversible charge capacity loss of 1st cycle also proved that most of the SEI layer is formed in the 1st cycle because significantly much higher charge capacity was obtained compared to discharge capacity which means a certain amount of Li-ions are not involved in further discharge process but used in the formation of SEI layer, Lithium plating and stripping at bulk metallic Lithium [88]. In addition, the coulombic efficiency of the 1st cycle was significantly less than 99 % which is a practical value. At the beginning of a few battery cycles, a few lithium ions are taken to form inorganic and organic lithium salt on graphite anode. Although most of the SEI layer is formed in the 1st cycle, it showed that SEI formation is still taking place roughly until the 30th cycle because of the higher charge capacity than discharge capacity based on the irreversible charge capacity.

Battery 1 in section 4.2.2.1 can be determined as close to the theoretical battery because it not only had the highest capacity (320.617 mAh/g) at 1st cycle in which most of SEI layer is formed but also had the decrease in capacity over cycle. Battery 2 (20 cycles) and a battery in section 4.2.2.2 had similar issues which had significantly less capacity that Battery 1 and increase in capacity over cycle. This was totally opposite to the theoretical expectation due to the artificial graphite anode was not fully wetted that leaded to poor intact SEI formation, electrolyte decomposition and stabilisation in initial cycle. Therefore, it needed more time for the electrode to fully soaked with the electrolyte over cycle by showing increase in capacity which theoretically it is not possible as Li-ions are consumed more and more over cycle. In addition, it was discovered that the weight of the graphite electrode and C-rate (in Amps) were not crucial determining the battery performance.

Based on the battery in section 4.2.2.2, the capacity starts to gradually fade throughout the end of the battery cycle (100th) because of the anode structure changes due to SEI decomposition, precipitation, and graphite exfoliation. In addition, Lithium plating and dendrite can be formed in electrolyte-electrolyte interphase. This detrimental process can have a major impact on discharge capacity higher

than charge capacity, but the possibility is low. It is also possible that partial SEI or particle cracks can occur in the middle of the cycle (60th, 65th, and 80th) as capacity fade over cycle based on Figure 4-10, 4-11, and 4-12.

To conclude, most of the SEI layer is formed in the 1st battery cycle but its layer can continuously form roughly until the 30th cycle if poor intact SEI layer is formed in ageing time or when the electrode need more cycles to fully wet by the electrolyte. This will allow the battery to reach the practical capacity value of graphite anode. Once a decent SEI layer is formed, the battery gradually losses the capacity and battery performance due to various detrimental processes. From this, it shows that the SEI layer is important in all aspects because it directly relates to not only the performance but also the physical and chemical phenomena of Li/graphite half-cell.

Chapter 5 - Cell cycling at low temperature

This chapter is to understand the battery performance of Li/graphite half-cell and study the effects of different battery electrolytes and various environmental temperatures below 0°C. In real life, the battery performs well at ambient and elevated temperatures but is unlikely at low temperatures and poor battery performance is achieved as discussed in Chapter 1.4. The comparative study of battery performance with SEI layer formation is done with previous results obtained in Chapter 4. From this, the effects of low environmental temperature on poor battery performance can be understood. Each section explains the used experimental technique and analyses the data based on the cell cycle in the low-temperature environment.

5.1 Introduction

Before judging the effect and the behaviour of the SEI layer formed on graphite anode to the low-temperature environment, the function of the battery at low temperature must be understood first. Previously, literature focused on the behaviour and performance of a battery [41, 54], and electrolyte [30, 44, 51, 52]. However, the choice of electrolyte and electrode to build a battery based on low-temperature conditions are too broad and vague. Although the low-temperature battery function and electrolyte behaviour were studied already, the battery performance and the electrolyte are stated based on the effect of a low-temperature environment in this chapter.

The LP30 electrolyte is consist of EC and DMC solvents where their melting points are $34^{\circ}C$ and $2^{\circ}C$ respectively. In addition, it consists of $LiPF_6$ salt having a melting point of $200^{\circ}C$. The experiments were carried out at ambient temperature so theoretically, solvents are partially in a mixed state because DMC is in a complete liquid state and EC components are partial solid and liquid state. The experiment from Chapter 4 was only introduced to understand the battery performance and behaviour of the SEI layer in ambient temperature. However, this stage is to understand the general battery performance at a temperature below $0^{\circ}C$ down to $-15^{\circ}C$ and to present its quantitative values such as capacity and coulombic efficiency (CE). It is necessary to preview the effects of the increasing number of battery cycles on the battery performance without changing the environment temperature. There are various criteria to consider the battery performance, but the key experimental condition of this chapter is the battery cycling environment temperature. With referring to the atmospheric temperature data in Chapter 4, the data can be directly analysed because the variance can be easily determined such as cycle number, and type of electrolyte to the low-temperature environment. From this, it is expected to know the battery efficiency and the capacity loss as the battery cycle increases.

5.2 Temperature change at 1st cycle

This section is introduced to address the importance of cycling temperature and SEI formation to determine the battery performance.

5.2.1 Experimental setup

The similar galvanostatic Li-graphite half-cells are built with an artificial graphite anode and Lithium metal as a reference and counter electrode. The same experimental methods and materials are used as mentioned in Chapter 3.1. As an electrolytic solution, 1.0M of $LiPF_6$ in EC / DMC = 50/50 (v/v) (Sigma Aldrich) was used which is the most commonly used in the fabrication of Li-ion batteries. Unlike previous Chapter 4, various battery electrolytes are used besides LP30 electrolytes, and a certain type of electrolyte will be clearly stated in each section throughout the end of Chapter 5. The main reason for using diverse electrolytes is to find out not only the effects of types of electrolytes on their battery

performance but also to understand their generated capacity at the discharge/charge state of a Li/graphite half-cell. The charge rate was kept constant as 0.1C (C/10) with the constant current was applied on a Maccor 4000M. Unlike previous Chapter 4, cycle number and cycling temperature were varied so they will be mentioned in every section of the results.

5.2.2 Results

Before showing low-temperature results, it is important to find out whether the cell can complete the battery cycle directly after fabrication at a temperature below ambient temperature. Figure 5-1 is a voltage vs time graph of the 1st cycle of Li/graphite half-cell at 25°C with LP30 electrolyte to provide as an example how a battery performs at room temperature. As mentioned in Chapter 4 previously, 8 hours of ageing time is given before the cell starts cycling to have stabilisation of electrolyte and graphite anode. In addition, the half-cell need to be discharged first because metallic Lithium foil was used as counter and reference electrode, unlike the full cell. This time-based graph clearly shows a good example of a well-cycled cell because the discharge/charge cycle had a smooth line with not much noise. The cell discharged/charged for approximately 2 hours/1.5 hours until the voltage was reached 0.01 V/ 2.5 V respectively.

Figure 5-1: An example of how a Li/graphite half-cell should perform at 25°C with LP30 electrolyte with constant current of C-rate – 0.00792 A. (Weight – 0.03346 g)

Figure 5-2 below represents an example of how a Li/graphite half-cell with LP30 electrolyte performs at 0°C. This was introduced to show how battery performance is affected by the cycling temperature comparing with Figure 5-1 (at 25°C). Although the same electrolyte composition and type of anode materials were used in half coin cell fabrication, it showed a completely different result. The cycling temperature was the only difference except the weight of the artificial graphite electrode with C-rate in Amps. It was also assigned at 0°C with 8 hours of ageing time and discharge/charge state to

complete 1st cycle. This cell took almost a week to complete just one cycle whereas the previous cell in Figure 5-1 only took 3.5 hours to complete 1st cycle at 25°C. Based on Figure 5-2, the cell kept on discharging for almost 87 hours and charging for 59 hours approximately. It took relatively longer to discharge the cell rather than to charge it because it takes a significantly longer time for Li-ions to intercalate into graphite anode and to form an SEI layer during half-cell discharge state. This is due to the electrolyte phase being altered from low battery cycling temperature. At ambient temperature, most of the LP30 compositions are in a liquid state based on their physical properties. The melting points of EC and DMC are 34°C and 2°C respectively. Theoretically at room temperature, EC will be in a solid state, but DMC will be in the full liquid state whereas, at 0°C, both will be in a pure solid state. It can be hypothesised that the LP30 electrolyte is not 100% in a liquid state at 0°C, and this leads to the low diffusivity of Li-ions. The role of electrolyte is to permit the transport of Li-ions in between anode and cathode. At low temperatures, this process can be disturbed massively by an unstable state of electrolyte (liquid and solid) that can interrupt the Lithium intercalation/deintercalation. Some noise was seen at the end of the graph in which can be assumed as more disturbance of delithiation from graphite anode to the metallic Li occurred possibly due to partial freezing of the electrolyte around the Li/electrolyte area. Another possibility is that the electrolyte partially frozen after the cell was kept for 145 - 155 hours in the 0°C cycling chamber. It is difficult to determine exactly when the battery started charging cycle so further investigation is needed in future.
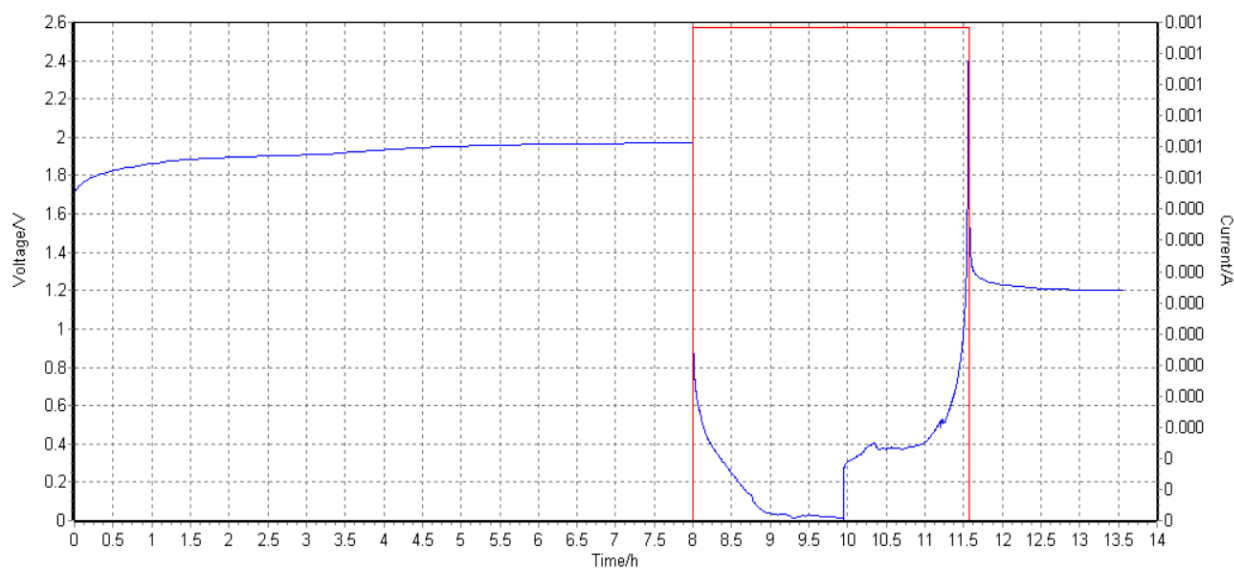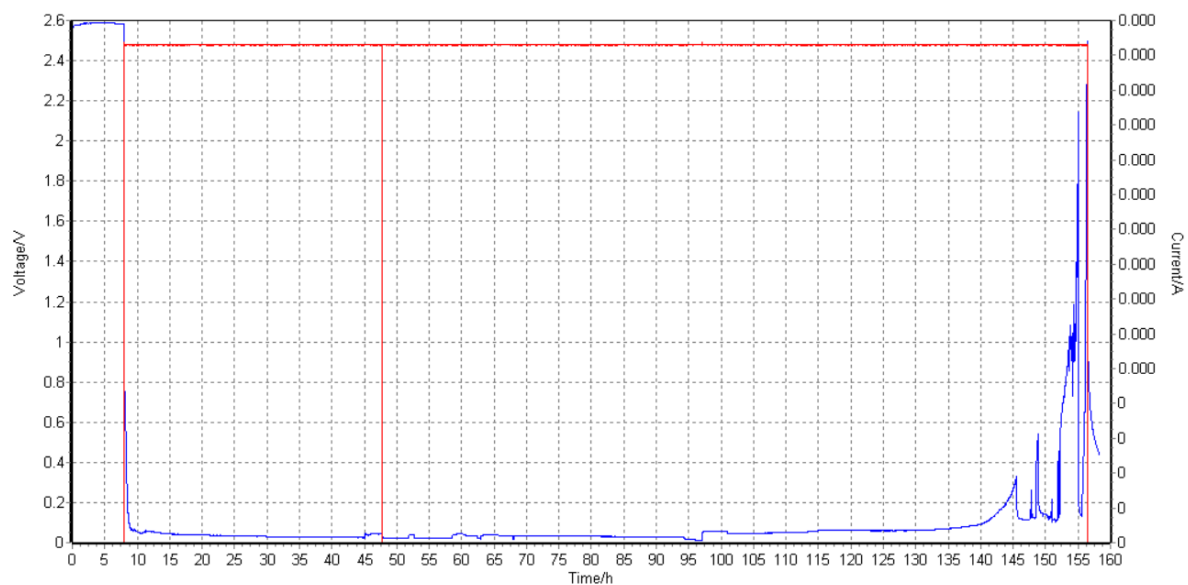

Figure 5-2: An example of how a Li/graphite half-cell performs at 0ºC with LP30 electrolyte with constant current of C-rate – 0.00286 A. (Weight – 0.01874 g).

Figure 5-3 also represents the 1st cycle of Li/graphite half-cell cycled at 0°C but with different electrolyte composition (LP30 with 10% FEC additive). This result was presented to show how battery

performs if FEC additive is added to the LP30 electrolyte at low-temperature. Although it is proposed as an effective additive [26, 28], the cell took roughly 120 hours to complete just one cycle. It cannot be determined whether the battery completed a full discharge/charge cycle or not because the shape of the graph was supposed to be similar as Figure 5-1. Figure 5-3 was not alike either Figure 5-1 or 5-2 which can be assumed that it is a failed battery although the time taken to complete 1st cycle was slightly reduced unlike the previous example shown in Figure 5-2. Interestingly, this cell produced a lot of noise throughout the end of the graph. There is a definite peak with a noise in the middle which is not easily seen in the voltage/time graph. It cannot be identified whether this peak indicates lithiation/delithiation process. There were lots of noise occurred from the start which can be assumed as there was a disturbance in lithiation during discharge cycle that can impact on SEI formation. In addition, more diverse change is seen by comparing with Figure 5-2 because of FEC component is added in battery electrolyte possibly due to its high melting point $18 - 23^oC$ (Sigma-Aldrich, Alfa Aesar). Theoretically, EC, DMC, and FEC are in full solid state at 0^oC which will have more disturbance in the electrolyte area that leads to the low diffusivity of Li-ions, unstable reversible reaction, and limited capacity. From this, it can be assumed that FEC additive only impacts on the SEI layer itself forming more LiF components to the layer [28]. It cannot solve the poor delivery of Li-ions in between metallic Lithium and graphite anode at low-temperature based on the Figure 5-3 result.
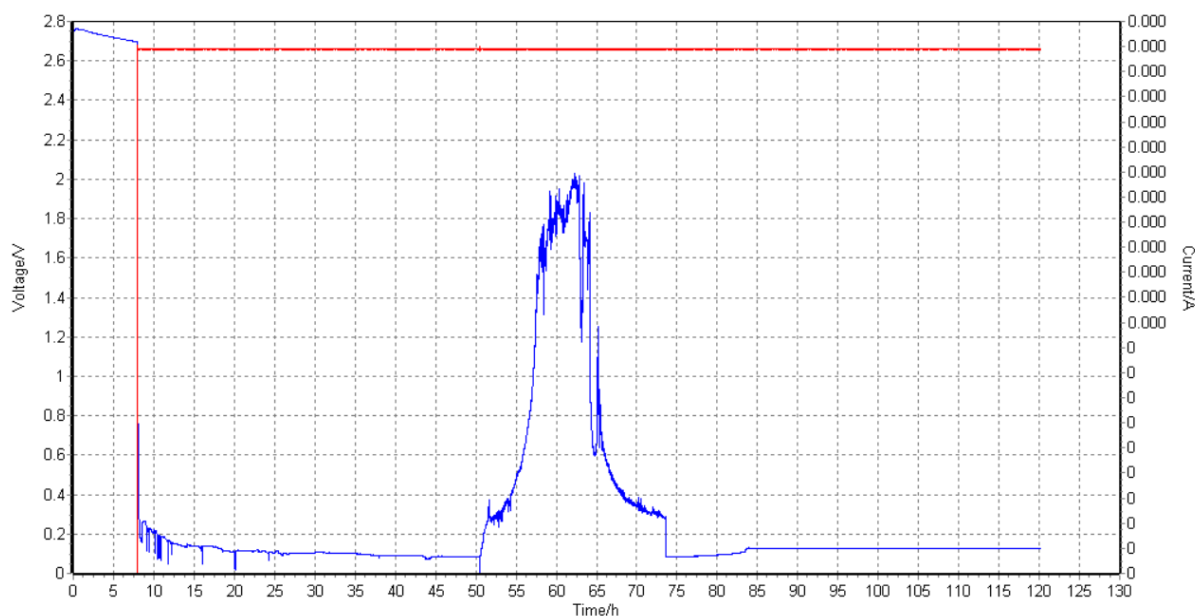

Figure 5-3: An example of how a Li/graphite half-cell performs at 0ºC using different electrolyte composition (LP30 + 10% FEC additive) with constant current of C-rate – 0.00209 A. (Weight – 0.0164 g).

5.2.3 Conclusion

The key point of this section was to express the difference in battery cycles when the cycling temperature is lowered from 25°C to 0°C by showing voltage against time graphs. It was mainly done to relate with SEI formation because it is known that most of the SEI layer is formed in 1st cycle which was shown in Chapter 4. The key variance was the low cycling temperature, 0°C and a reliable result was produced. Environment temperature is an important aspect to determine the battery life, performance, and efficiency because there is a significant disturbance in the electrolyte region. Although a certain amount of FEC additive was added, still low mobility and diffusivity of Li-ions taken place and more irreversible reaction can be seen due to uncertainty of electrolyte phase. In addition, it can be hypothesised that poor SEI formation in ageing time and 1st cycle result as poor battery cycle as shown in Figure 5-2 and 5-3. Hence, it can be concluded that temperature is a possible key factor in battery performance as well as the SEI formation.

5.3 Temperature change at 2nd cycle

Previously, the battery was cycled one time only at room temperature, and at 0°C respectively. It was mainly focused on finding out whether the battery cycle and performance will be affected by changing cycling temperature. This section introduces the experimental result of two cycled batteries, but the temperature is lowered at 2nd cycle instead. 1st cycle was carried out at ambient temperature. From this, it can be understood whether SEI layer formation before a low-temperature cycle helps to maintain better battery performance than before.

5.3.1 Experimental setup

The same experimental methods and materials are used as mentioned in Chapter 3.1. The galvanostatic Li-graphite half-cells are built with an artificial graphite anode and Lithium metal as a reference and counter electrode. Only 1.0M of $LiPF_6$ in EC / DMC = 50/50 (v/v) (Sigma Aldrich) (LP30) was used as a battery electrolyte in the fabrication of Li/graphite half-cell. The charge rate was kept constant as 0.1C (C/10) with constant current setup on a MACCOR 4000M. The cycling temperature is changed once the 1st battery cycle is completely done. Various range of low temperatures (25°C, 0°C, -5°C, -10°C, and -15°C) are used in this experiment. Once the temperature is adjusted, 2 hours of a rest period is given before 2nd battery cycle.

5.3.2 25°C results

The room temperature results are represented in this particular section so that they can be investigated further with other low-temperature data later on. The cells were assigned to have 8 hours of ageing time for an intact SEI formation, electrolyte decomposition and stabilisation. Then, two cycles were done at 25°C.
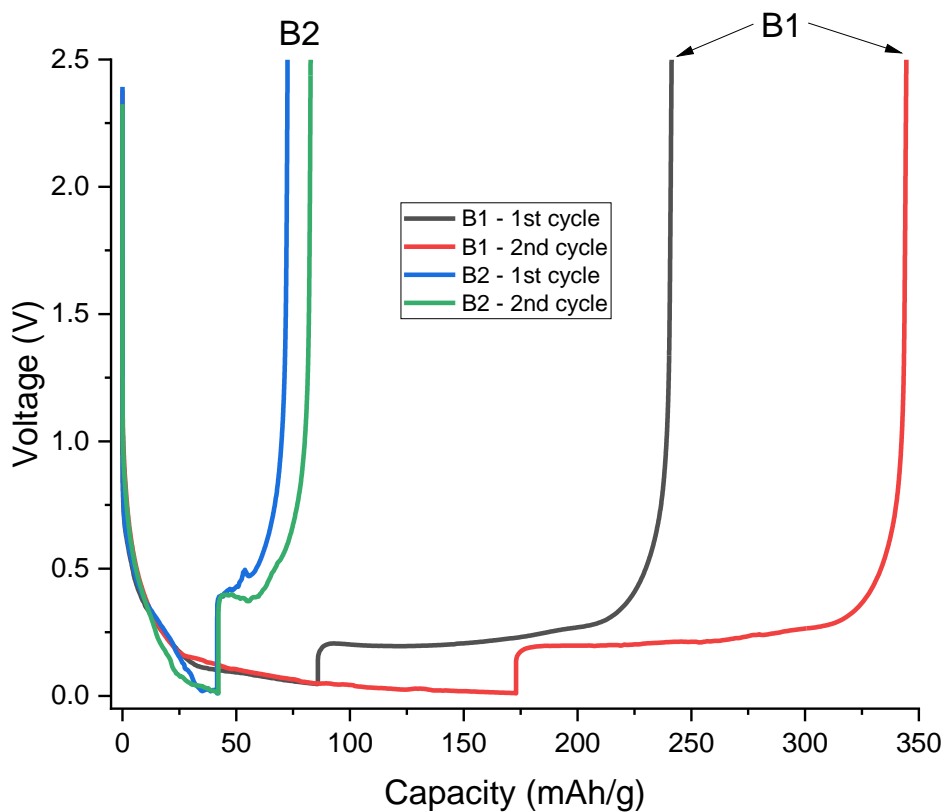
Figure 5-4: Capacity (data) vs Voltage of two Li/graphite half-cells with LP30 electrolyte cycled 2 times at 25°C. Battery 1 had C-rate of 0.0091 A. (weight – 0.03697 g), Battery 2 had a C-rate of 0.00689 A. (weight – 0.03042 g).

Figure 5-4 above represents the voltage vs capacity of two Li/graphite half-cells that had two cycles at 25°C. It was clearly shown that Battery 1 had better battery performance than Battery 2 because it had relatively higher capacity in discharge/charge state although both of them were not even close to the theoretical value (372 mAh/g). Both battery had similar results as in section 4.2.2.1 (Battery 2) and section 4.2.2.2 in which showed increase in capacity over cycle. This was mostly due to either the graphite anode is not fully wetted with the LP30 electrolyte or poor intact SEI layer is formed in ageing time. The ideal look was supposed to be similar to the Battery 1 in section 4.2.2.1. Theoretically, at 1st cycle, highest capacity is produced, and the capacity should decrease over cycle as Li-ions are consumed more and more.

Table 5-1: Coulombic efficiency and discharge capacity of Battery 1 and Battery 2. Battery 1 had C-rate of 0.0091 A. (weight – 0.03697 g), Battery 2 had a C-rate of 0.00689 A. (weight – 0.03042 g).

Battery cycle	Coulombic Efficiency (%)	Discharge Capacity (mAh/g)
B1 – 1st cyc	91.7503	169.4148
B1 – 2nd cyc	99.1805	172.9668
B2 – 1st cyc	74.2158	41.6584
B2 – 2nd cyc	95.9652	42.2057

Since room temperature data was not the main interest in this chapter, the coulombic efficiency and discharge capacity of Battery 1 and Battery 2 was separately shown in Table 5-1 above. They showed increase in capacity over cycle, but their coulombic efficiencies were close to the theoretical value (99%). This supports the previous hypothesis in section 4.2 that the battery performance should be considered by looking at both the efficiency and the capacity. Hypothetically, the capacity increase over cycle is possible only if poor SEI layer was formed in ageing time and after 1st cycle. This means the electrode was not fully covered and it needs more cycle to be fully covered with the electrolyte.

5.3.3 0°C results

At this stage of experiment, the cell cycling condition was slightly different from previous section 5.3.2. The three Li/graphite half-cells were built in same condition as section 3.1.2, but the only difference was that the cycling temperature was lowered to 0°C at the 2nd cycle. When the temperature is adjusted, the cell was kept at rest for two hours so that it can fully adapt to the environmental condition such as graphite stabilisation and further electrolyte stabilisation and decomposition as the electrolyte phase can be changed. Some parts of LP30 will be in a solid state because the temperature is below the melting point of both EC and DMC solvents. It is very difficult to judge exactly which area of LP30 is in a solid state because the battery electrolyte is covered everywhere in the cell. In this section, the effect of low-temperature (0°C) and SEI layer on battery performance can be understood.

Figure 5-5 represents the discharge/charge cycle of three Li/graphite half-cells with LP30 electrolyte over 2 cycles; 1st at 25°C and 2nd at 0°C. It is very clear that all three cells had reduced capacities in the 2nd cycle which was cycled at 0°C whereas at 1st cycle, relatively higher capacities were generated. In ageing time, an intact SEI layer forms and further SEI growth occur in 1st cycle. Hence, a graphite anode will have an improved SEI layer after 1st cycle. Since the 1st cycle was carried out at 25°C, smooth discharge/charge curve were seen for all cells due to the good diffusivity of Li-ions within graphite anode and the ionic conductivity of electrolyte.

However, 2nd cycle had significantly less capacity overall which leads to a much faster discharge/charge cycle with less voltage. The gradient of the graphs were unstable when the voltage is less than 0.5V whereas in Figure 5-4, much smoother curves were shown. This is affected by reduced ionic conductivity of electrolyte and diffusivity of Li-ions within graphite anode is decreased. It is already reported that the reduced conductivity of the electrolyte and SEI layer on the electrode affects the low-temperature performance of the battery [30, 44, 83, 90]. However, this statement might be possible for extremely low temperature conditions such as lower than -20°C because the temperature was only 0°C. In addition, Li diffusion in the SEI layer on the graphite anode may be the main reason for the limitation of discharge capability rather than conductivity and diffusivity of lithium [90]. When

the cell had only one cycle at low-temperature (0°C), the battery produced a lot of noise with significantly much longer discharge/charge cycle based on the previous section 5.2 result. From this, it can be determined that better SEI formation improves the low-temperature battery performance because the results had 1st cycle at 25°C that allows the further growth of the SEI layer. Although 2nd cycle had a faster discharge/charge cycle than 1st cycle, it was able to complete the discharge/charge cycle with significantly less noise than the previous section 5.2 data.
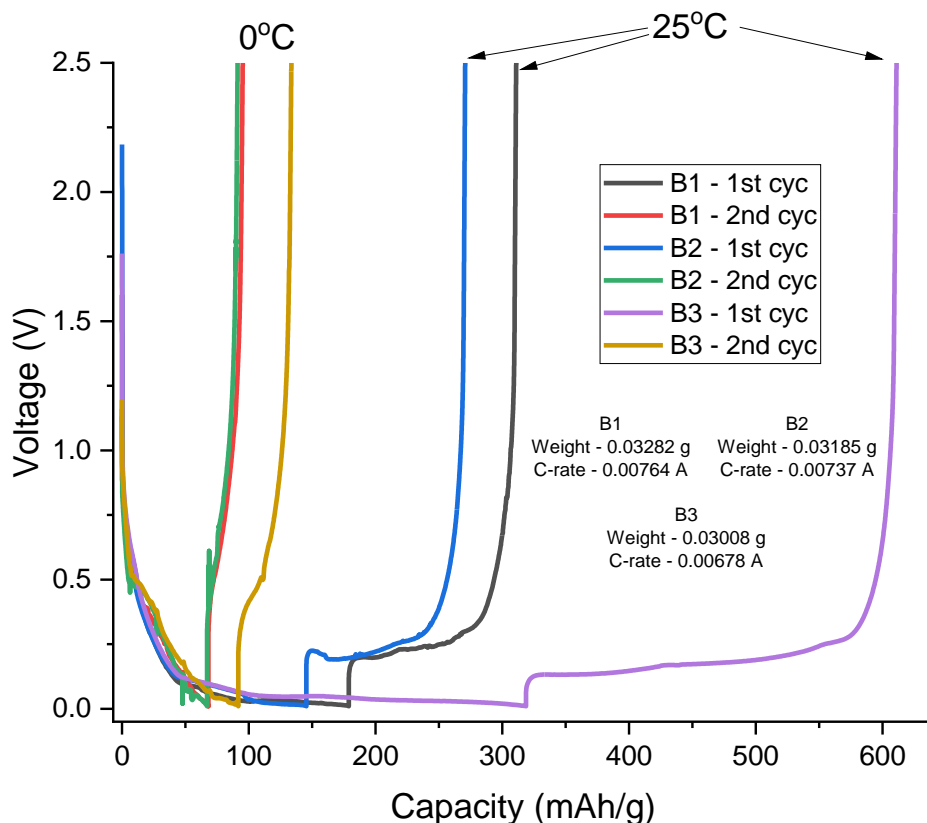

Figure 5-5: Voltage vs Capacity graphs of three Li/graphite half-cells with LP30 electrolyte cycled at different temperatures; 1st at 25°C and 2nd at 0°C. Battery 1 had C-rate of 0.00764 A. (weight – 0.03282g), Battery 2 had a C-rate of 0.00737 A. (weight – 0.03185 g), Battery 3 had a C-rate of 0.00678 A. (weight – 0.03008 g).

Figure 5-6 represents only the discharge capacity of three Li/graphite half-cell (same as Figure 5-5) as the voltage decreases over time based on cycling temperatures. It was shown to understand the Lithiation to the artificial graphite anode and effect of the SEI formation based on the low-temperature change. The 1st cycle of three cells at 25°C had a relatively smooth discharge curve inversely proportional to the voltage. It was understood that at 25°C, good SEI formation taken place from 0.8 V until 0.3 V before graphite stabilisation occurs and the capacity increase as voltage was close to 0.01 V. Overall, all three cells had suitable discharge process at 1st cycle so further SEI layer growth is expected.

However, the 2nd cycle of three cells at 0°C had much sharper gradient from 0.5 V until 0.01 V as capacity increase. The 1st cycle produced significantly longer and higher charge capacity than the 2nd cycle. In the 2nd cycle, a small capacity was produced possibly due to an unstable electrolyte state at 0°C because most of EC and DMC components will be in a solid state based on their melting points. Clearly, there are some disturbances expected on mobility and transport of ions in the electrolyte region that results in small capacity at low-temperature.

To conclude, it can be suggested that 1st cycle must be assigned at room temperature prior to the low-temperature (0°C) cycle to allow further SEI growth on graphite anode. Better SEI formation will help the battery to complete the discharge/charge cycle with a small capacity produced over time cycling at low-temperature. Although low ionic mobility is achieved at 0°C in 2nd cycle, a small SEI growth was expected because the discharge capacity started to increase as the voltage drops roughly from 0.8 V or below where this was the practical onset voltage of SEI formation, 0.8 V vs Li/Li$^+$ [35, 36, 85].
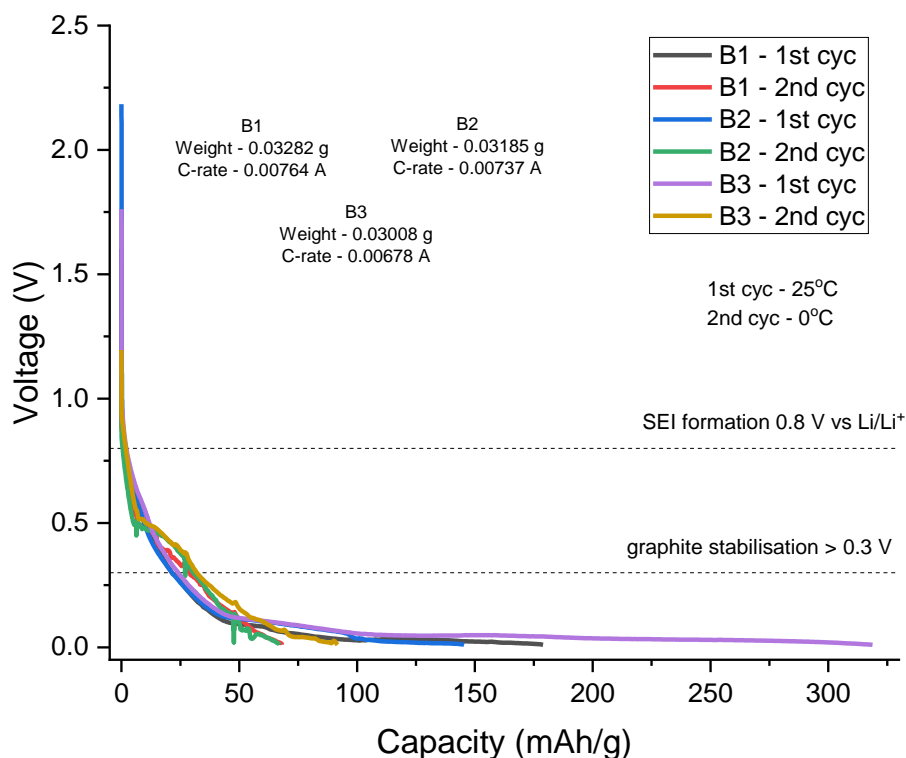
Figure 5-6: Discharge capacity (data) vs Voltage graphs of the same three Li/graphite half-cells with LP30 electrolyte cycled at different temperatures; 1st at 25°C and 2nd at 0°C. Battery 1 had C-rate of 0.00764 A. (weight – 0.03282g), Battery 2 had a C-rate of 0.00737 A. (weight – 0.03185 g), Battery 3 had a C-rate of 0.00678 A. (weight – 0.03008 g).

Figure 5-7 was shown below to represent the coulombic efficiency of the same battery (previous Figure 5-5 and 5-6) cycles based on cycling temperatures. It is very clear that the coulombic efficiency of 1st cycle is significantly higher than 2nd cycle. As the temperature drops to 0°C, the efficiency drops

to roughly below 50 %. Its value can be calculated by the previous equation 4-2 in Chapter 4 where Q_{out} / Q_{in}. The coulombic efficiency of 1st cycle was less than theoretical value of 99% due to parasitic reactions occurring mostly due to SEI formation. The amount of Lithium intercalated to graphite anode is more than the amount of delithiation to metallic Lithium because some Li-ions are involved in SEI formation, and they are not taking part in the further discharge process. When the temperature is lowered to 0°C, the efficiency is much lesser than 50 % because of a few reasons. First, the battery cannot produce a similar amount of capacity as the room temperature cycle in a low-temperature system. Low diffusivity of Li-ions are achieved due to an unstable electrolyte state that disturbs the ionic mobility in between metallic Lithium and a graphite anode. Second, SEI formation can occur even in the low-temperature system although significantly less capacity is produced. Although an intact SEI layer is formed in 8 hours of initial cycle, the further growth of the SEI layer is mostly expected to occur in 1st cycle at room temperature but as explained in previous section 4.2.2, SEI formation still can take place roughly until the 30th cycle. Although low capacity is produced, a relatively small amount of lithiation to graphite anode can take place compared to the amount of intercalated Lithium reverted to metallic Lithium.
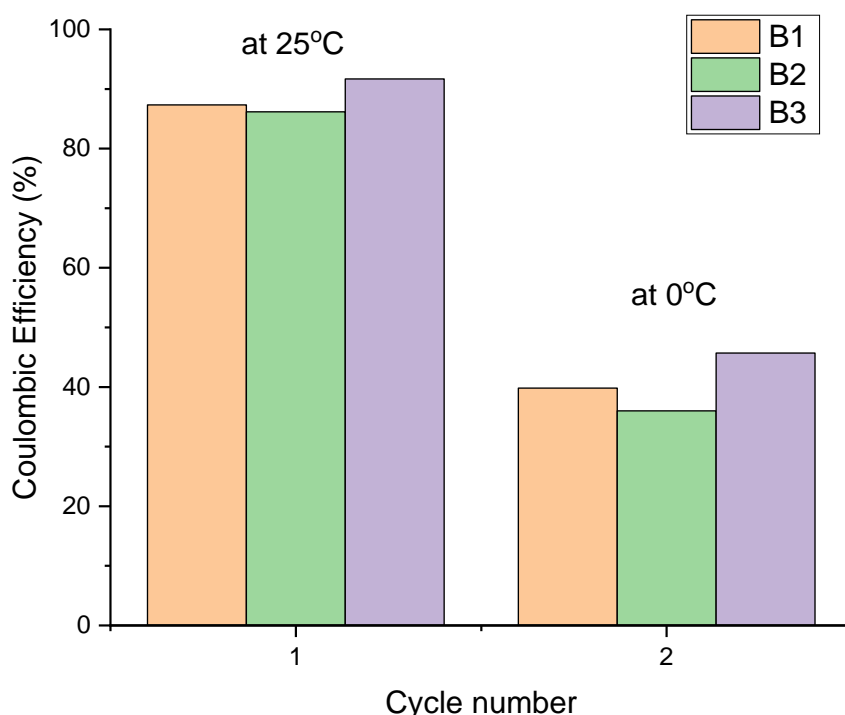

Figure 5-7: Coulombic efficiency of the same three Li/graphite half-cells with LP30 electrolyte cycled at different temperatures; 1st at 25°C and 2nd at 0°C. Battery 1 had C-rate of 0.00764 A. (weight – 0.03282g), Battery 2 had a C-rate of 0.00737 A. (weight – 0.03185 g), Battery 3 had a C-rate of 0.00678 A. (weight – 0.03008 g).

Figure 5-8 below shows the two different histograms; irreversible charge capacity loss (discharge for half-cell) and discharge capacity of the same Li/graphite half-cells cycled at different temperatures. It is very clear that comparatively higher discharge capacity was generated in ambient temperature. At 0°C, all cells had capacities of less than 100 mAh/g. They had more than 50% of capacity loss in between 1st and 2nd cycle possibly due to the uncertain solid/liquid state of EC and DMC components from LP30 electrolyte which cannot transport the Li-ions fluently at low-temperature. It is much easier to deliver Li-ions at room temperature because the state of the battery electrolyte will be mostly in a liquid state.
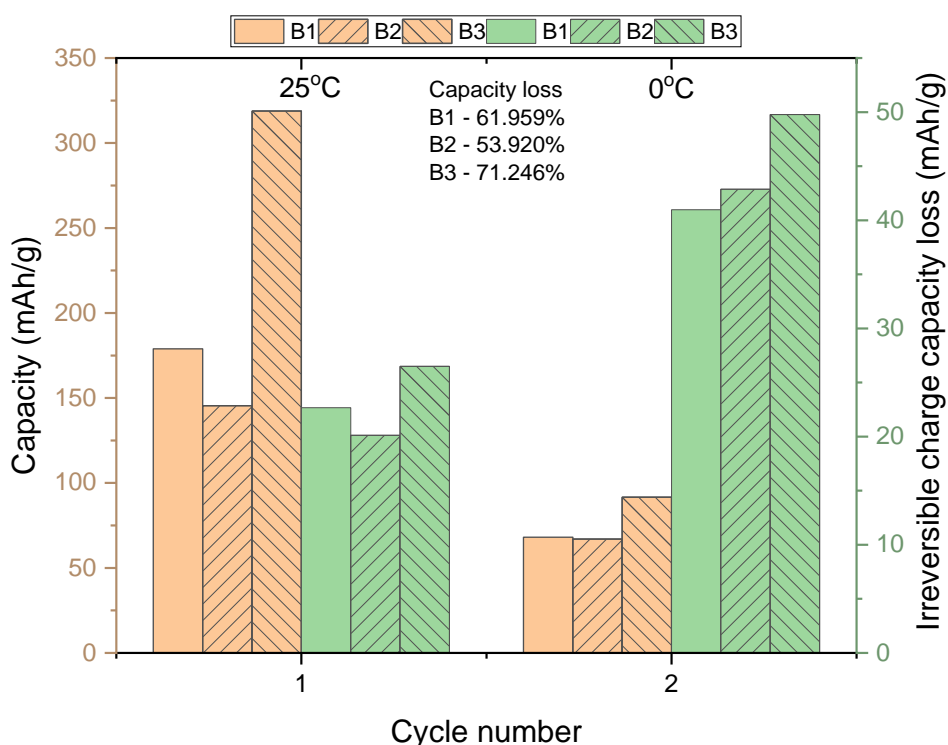

Figure 5-8: Discharge capacity and irreversible charge capacity of the same three Li/graphite half-cells with LP30 electrolyte cycled at different temperatures; 1st at 25°C and 2nd at 0°C. Battery 1 had C-rate of 0.00764 A. (weight – 0.03282g), Battery 2 had a C-rate of 0.00737 A. (weight – 0.03185 g), Battery 3 had a C-rate of 0.00678 A. (weight – 0.03008 g

Since the electrolyte is mostly in a liquid state, there is some irreversible charge capacity loss in 1st cycle because charge capacity can be slightly higher than discharge capacity due to some Li-ions being mostly involved in SEI formation. However, the irreversible charge capacity loss is almost doubled in the 2nd cycle although the capacity was reduced to nearly 1/3 of 1st cycle capacity. From this, it can be stated that some Li-ions intercalated to graphite anode will be still involved in SEI formation at 0°C even though it is reported that reduced conductivity of the electrolyte and SEI layer on the electrode affects the low-temperature performance of the battery [30, 44, 83, 90]. It is necessary to minimise the capacity loss as low as possible because it affects the battery life, but still there was 54 – 71 % of

capacity loss in between 1st cycle and 2nd cycle where cycling temperature is adjusted from room temperature to 0°C. However, the statement which SEI layer affects the low-temperature performance of the battery is possibly counterargued based on results from Figure 5-7 and section 5.2 that is without the SEI layer, the battery cannot be cycled at low temperature.

5.3.4 -5°C results

In this section, the three Li/graphite half-cells were built in same condition as section 3.1.2 but only the data of the two cells (Battery 1 and Battery 2) are represented because of Battery 3 failed the battery testing multiple times. The cycling temperature was the only difference in this section which was further lowered down to -5°C at the 2nd cycle. When the temperature is adjusted, the cell was kept at rest for two hours so that it can fully adapt to the environmental condition such as graphite stabilisation and further electrolyte stabilisation and decomposition as the electrolyte phase can be changed. Some parts of LP30 will be in a solid state because the temperature is below the melting point of both EC and DMC solvents. It is very difficult to judge exactly which area of LP30 is in a solid state because the battery electrolyte is covered everywhere in the cell. In this section, the effect of low-temperature (-5°C) and SEI layer on battery performance can be understood.
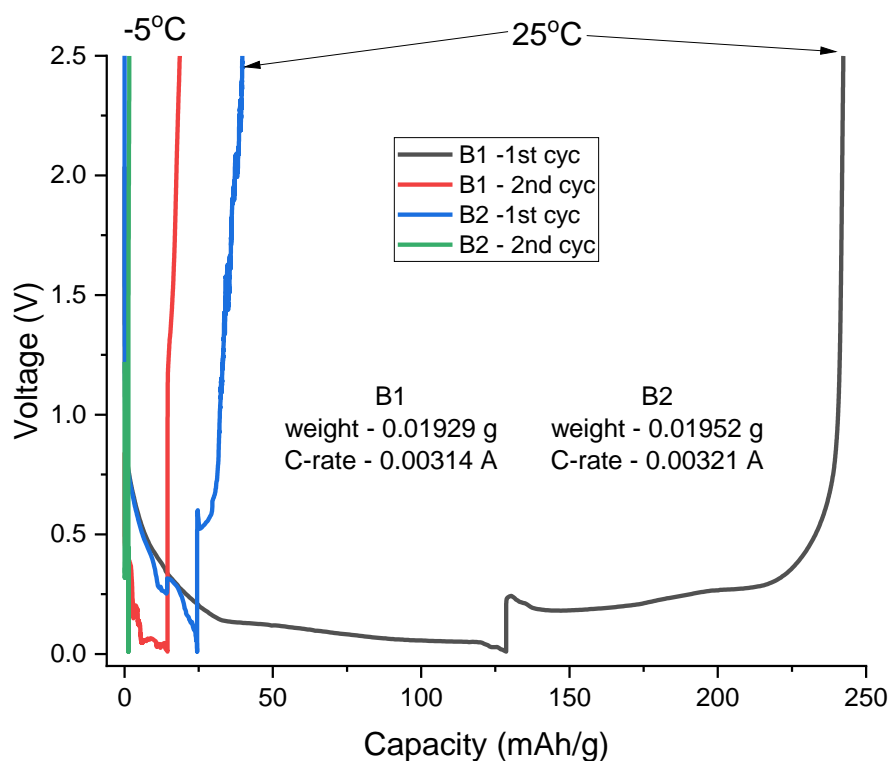

Figure 5-9: Voltage vs Capacity graphs of two Li/graphite half-cells with LP30 electrolyte cycled at different temperatures; 1st at 25°C and 2nd at -5°C. Battery 1 had C-rate of 0.00314 A. (weight – 0.01929 g), Battery 2 had a C-rate of 0.00321 A. (weight – 0.01952 g).

The discharge/charge cycle of the two Li/graphite half-cells with LP30 electrolyte at different temperatures were shown in Figure 5-9 above. Theoretically, the performance of the 1st cycle (25°C) is expected to be much longer than the 2nd cycle (-5°C) because of the different cycling temperature. Although Battery 2 had significantly shorter cycle than Batter 1, their 1st cycle were similar to the expected result. It is assumed that Battery 2 had either poor SEI formation in ageing time or the graphite anode was not fully wetted enough because its charge cycle was relatively shorter than the discharge cycle (Blue line). Overall, they showed satisfactory discharge graph in 1st cycle where SEI formation taking place from 0.8 V and the capacity started to increase as the potential drops until 0.01 V although Battery 2 was supposed to have similar discharge/charge curve as Battery 1. Since the 1st cycle is done at room temperature, good diffusivity of Li-ions within graphite anode and ionic conductivity of the electrolyte is expected.

However, the cell discharged/charged much faster in 2nd cycle because of low cycling temperature. The 2nd cycle of the two cells were shifted towards more to the left which means there were not much capacity produced from the cell. Unlike the 0°C result in section 5.3.3, the 2nd cycle in Figure 5-9 had a different shape of the graph. For example, in discharge cycle, there was some noise produced especially the potential drops from 0.5 V to 0.01 V and charge cycle was almost like a straight line. It is already known that low-temperature battery performance can be affected by reduced ionic conductivity of electrolytes and the existence of an SEI layer on the electrode [30, 44, 83, 90]. From this, it can be hypothesised that the 2nd cycle at -5°C produced a lower capacity than room temperature but still binding of Li-ions are mostly involved in SEI formation because based on previous results in section 4.2.2 and literature [35], SEI formation may continue up to few more cycles. In addition, it can be assumed that the much faster discharge/charge cycle occurs at -5°C compared to 0°C because of more partial freezing of the LP30 electrolyte is expected.
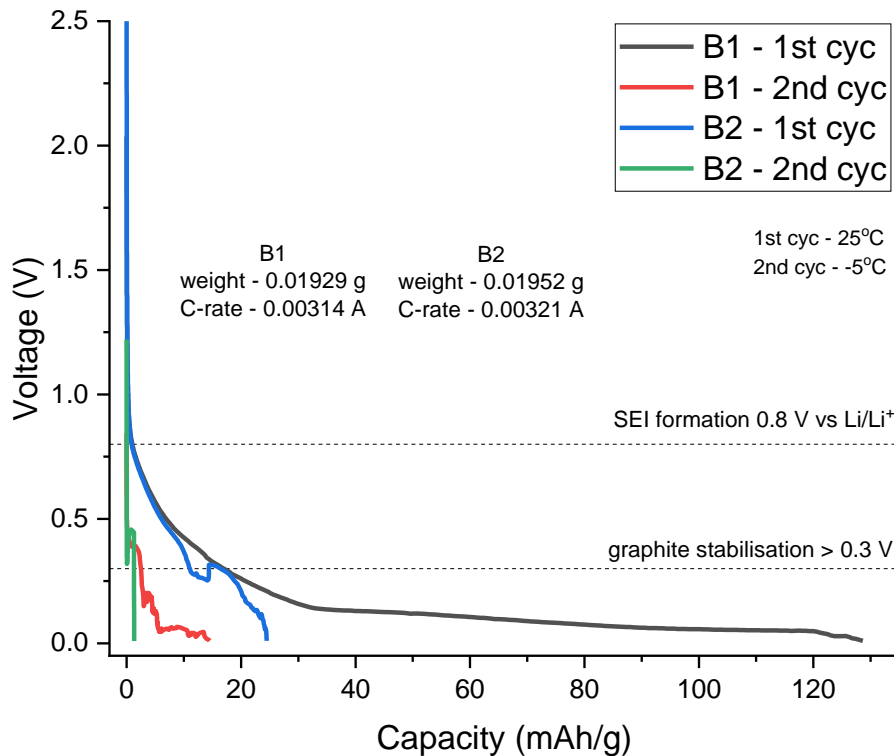
Figure 5-10: Discharge (half-cell) cycle of the two Li/graphite half-cells with LP30 electrolyte cycled at different temperatures; 1st at 25oC and 2nd at -5oC. Battery 1 had C-rate of 0.00314 A. (weight – 0.01929 g), Battery 2 had a C-rate of 0.00321 A. (weight – 0.01952 g).

Figure 5-10 is presented above to understand the lithiation (discharge in half-cell) to the graphite anode of the two Li/graphite half-cells (same as Figure 5-9) as the voltage decreases over time based on cycling temperatures. Based on the 1st cycle results, the discharge cycle of the two cells were a bit similar to the expected result except Battery 2 which had much shorter discharge curve than Battery 1. This was assumed as due to the electrode was not fully wetted in 8 hours of ageing time so relatively poor intact SEI layer was formed in Battery 2. Both 1st cycle curve had SEI formation from 0.8 V which were close to the expected results similar as previous 1st cycle results shown in sections 5.3.2 and 5.3.3. Since the 1st cycle is cycled at room temperature, the good ionic conductivity of LP30 electrolyte is achieved as it is mostly in a liquid state so that good transport of Li-ions can be expected during the cell discharge cycle.

However, the 2nd discharge cycle produced significantly less capacity in a short period compared to the 1st cycle which produced a good amount of the capacity in a much longer period. In addition, both cells showed some disordered (noise) shape on the graph because unstable lithiation takes place to the graphite anode. In -5oC, there will be more amount of solidified LP30 electrolyte than in 0oC because the cycling temperature of the 2nd cycle is further away from the melting points of EC and

DMC solvents. From this, it can be stated more disturbances in the electrolyte region affect the battery capacity that leads to more bad battery performance.
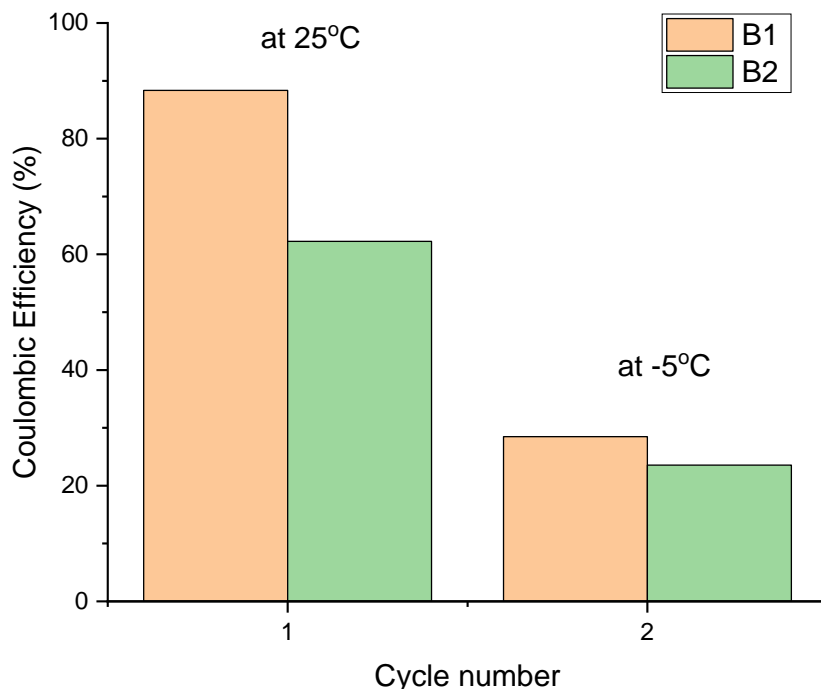

Figure 5-11: Coulombic efficiency of the same two Li/graphite half-cells with LP30 electrolyte cycled at different temperatures; 1st at 25oC and 2nd at -5oC. Battery 1 had C-rate of 0.00314 A. (weight – 0.01929 g), Battery 2 had a C-rate of 0.00321 A. (weight – 0.01952 g).

Figure 5-11 shows the coulombic efficiency of the same two tested cells with LP30 electrolyte cycled at different temperatures. Based on the previous equation 4-2 in Chapter 4, the coulombic efficiency can be calculated from Q_{out} / Q_{in}. The coulombic efficiency of 1st cycle was less than theoretical value of 99% due to parasitic reactions occurring mostly due to SEI formation. The efficiency of the 1st cycle for the two cells at 25°C represents the amount of Lithium intercalated to graphite anode is more than the amount of delithiation to metallic Lithium because some Li-ions are involved in SEI formation, and they are not taking part in the further discharge process.

On the other hand, the two cells had less than 30 % of the coulombic efficiency at -5°C. By comparing with 0°C results in section 5.3.3, relatively less coulombic efficiencies were achieved in 2nd cycle. This directly shows that there are more proportion of solidified electrolytes that exist, and this disturbs the intercalation process. It can be stated that at a lower temperature, SEI formation still takes place if an imperfect SEI layer is formed on graphite anode within the aging time and 1st cycle although low ionic mobility and diffusivity are expected to be seen. In addition, a relatively smaller amount of lithiation is expected in -5°C because either not many Li-ions can intercalate towards the anode due to

disturbance in the electrolyte region or few binding of Li-ions are used to form more SEI layers and these Li-ions will not take part in the further discharge process.
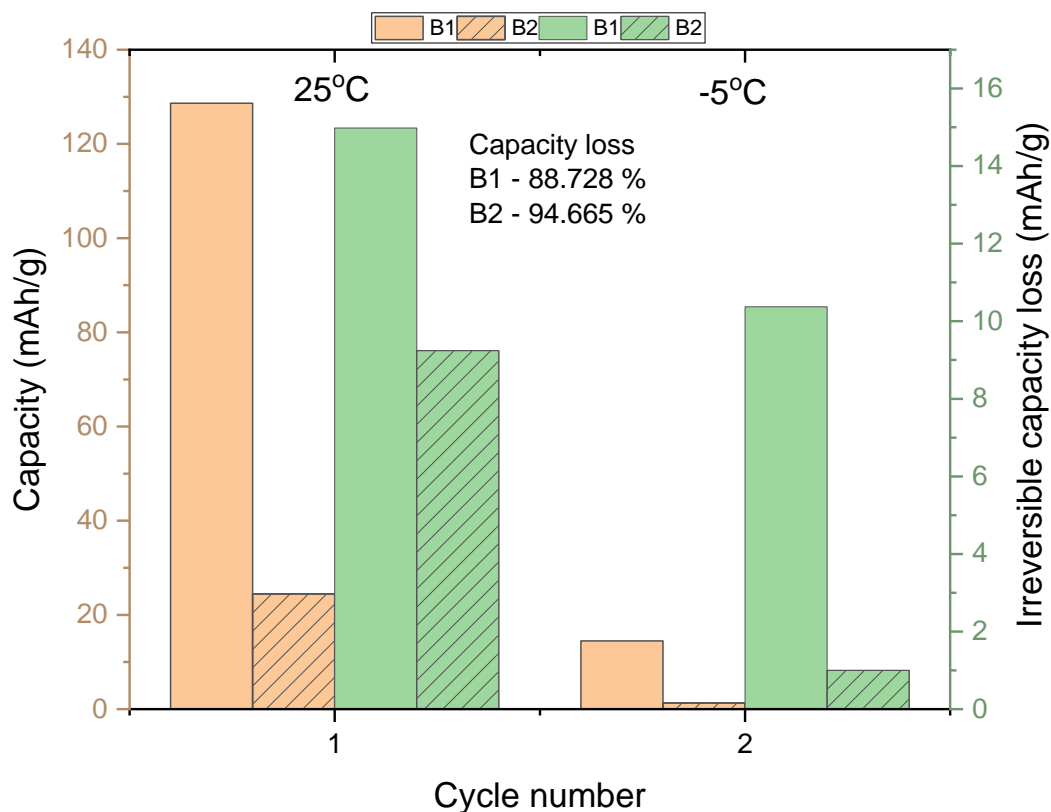

Figure 5-12: Discharge capacity (half-cell) and irreversible charge capacity of the same two Li/graphite half-cells with LP30 electrolyte cycled at different temperatures; 1st at 25°C and 2nd at -5°C. Battery 1 had C-rate of 0.00314 A. (weight – 0.01929 g), Battery 2 had a C-rate of 0.00321 A. (weight – 0.01952 g).

Figure 5-12 is shown above to understand the produced discharge capacity of the same tested cells and their respective irreversible capacity loss at 25°C and -5°C. They showed decrease in discharge capacity (charge in full-cell) over cycle which were an expected result because theoretically, low capacity is produced at -5°C as more limited amount of Li-ions will be available to intercalate between metallic Li and graphite anode. Comparing with 0°C results in section 5.3.3, the discharge capacity in 2nd cycle was expected to be lower at -5°C because of more partial freezing of the electrolyte. The tested cells had more than 89 % capacity loss in between 1st and 2nd cycle. From this, it can be estimated that the lower the cycling temperature, the more the capacity loss in between the temperature change cycles.

Since the electrolyte is mostly in a liquid state, there is some irreversible charge capacity loss in 1st cycle because charge capacity can be slightly higher than discharge capacity due to some Li-ions being mostly involved in SEI formation. However, the irreversible charge capacity loss was decreased in the

2nd cycle unlike Figure 5-8 in section 5.3.3 which had increase in the 2nd cycle. From this, it can be stated that some Li-ions intercalated to graphite anode will be still involved in SEI formation at -5°C but it depends on the condition of the electrolyte even though it is reported that reduced conductivity of the electrolyte and SEI layer on the electrode affects the low-temperature performance of the battery [30, 44, 83, 90]. If the irreversible charge capacity loss is high, it means there are more binding of Li-ions involved in SEI formation or stayed in the graphite anode surface and they are not used in the further discharge process. Since Battery 1 had a relatively higher value than Battery 2, it can be assumed that Battery 1 had more SEI layer formed in 1st cycle and produced higher discharge capacity. From this, it can be stated that the amount of capacity is not important especially when irreversible charge capacity loss is explained because it is the difference between charge and discharge capacity only. However, it is more affected by cycling temperature because in 0°C, increased irreversible capacity loss is shown whereas, in -5°C, it decreased in the 2nd cycle.

In conclusion, SEI formation still taken place in both cycling temperatures and producing decreased capacity was less affected by the SEI layer but instead more affected by the state of the battery electrolyte because at -5°C, the more solidified electrolyte can be formed which can disturb the transport of Li-ions and reduced conductivity will lead to poor low-temperature battery performance.

5.3.5 -10°C results

In this section, the three Li/graphite half-cells were built in same condition as section 3.1.2 but only the data of the two cells (Battery 1 and Battery 2) are represented because of Battery 3 failed the battery testing multiple times similar as previous section 5.3.4. The cycling temperature was adjusted to -10°C at the 2nd cycle. When the temperature is adjusted, the cell was kept at rest for two hours so that it can fully adapt to the environmental condition such as graphite stabilisation and further electrolyte stabilisation and decomposition as the electrolyte phase can be changed. It is expected that more parts of LP30 will be in a solid state because the temperature is below the melting point of both EC and DMC solvents. It is very difficult to judge exactly which area of LP30 is in a solid state because the battery electrolyte is covered everywhere in the cell. In this section, the effect of low-temperature (-10°C) and SEI layer on battery performance can be understood deeper.

The voltage vs capacity graph indicating the two discharge/charge cycle of the two tested Li/graphite half-cells with LP30 electrolyte at different temperatures was shown in Figure 5-13 below. As expected, both cells had smooth discharge/charge curve at 1st cycle where SEI formation takes place from 0.8 V and the capacity start to increase as the potential drops until 0.01 V in cell discharges. Good ionic conductivity of the electrolyte and ionic mobility is assumed in 1st cycle because it is cycled at room temperature. Battery 1 had relatively lower capacity than Battery 2 possibly due to either the

electrode was compressed too much during cell assembly or the electrode was not fully wetted in ageing time that leads to the limited intact SEI formation.

The poor ionic conductivity of the electrolyte and ionic mobility are expected when the cycling temperature is further lowered down to -10°C due to detrimental processes such as blockage of ionic mobility. The literature already showed that LP30 can perform at low temperature down to -20°C because its freezing point is at -21.9°C [91, 92] but it is not recommended for low-temperature applications due to low ionic conductivity [93]. Hence, the discharge/charge cycle of the cell is expected to be much faster in 2nd cycle at -10°C. The 2nd cycle for both cells were more shifted towards the left-hand side because of more limited capacities were produced at -10°C. In addition, more noise on the graph is shown near the end of the cell discharged cycle in the voltage region of 0.3 – 0.01 V. It can be hypothesised that very unstable discharge/charge cycle is expected when the cycling temperature is close to the freezing point of the electrolyte.

Figure 5-13: Voltage vs Capacity graphs of two Li/graphite half-cells with LP30 electrolyte cycled at different temperatures; 1st at 25°C and 2nd at -10°C. Battery 1 had C-rate of 0.00409 A. (weight – 0.02221 g), Battery 2 had a C-rate of 0.00358 A. (weight – 0.02060 g).

Figure 5-14 below shows the discharge capacity (charge in full-cell) as the potential drops until the end of the same two Li/graphite half-cells discharge. As expected, the charge capacity of the 1st cycle showed smooth discharge curve without any noise in which are similar to other 1st cycle results from

previous sections 5.3.3 and 5.3.4. From 0.8 V, the SEI formation taking place until 0.3 V where graphite stabilisation occurs and the capacity increase until 0.01 V. Battery 2 had relatively higher discharge capacity than Battery 1 which means it had better an intact SEI formation in initial cycle. The limitation of the Battery 1 can be assumed as unstable electrolyte and electrode stabilisation in ageing time, or the electrode was compressed by the coin cell too much.

However, the discharge curve of the 2nd cycle had significantly less charge capacity in the fast cell discharge period with a lot of noise especially near the end whereas, in the 1st cycle, the cell produced more and longer charge capacity. This phenomenon was similarly seen in previous low-temperature results (0°C and -5°C) in section 5.3.3 and 5.3.4. From this, it can be assumed that the low-temperature results of the two cells are inaccurate because there will be more partially freezing LP30 electrolytes than other low temperatures (0°C and -5°C). As the low cycling temperature is further away from the room temperature, there will be more unstable lithiation/delithiation can occur in between the metallic Li and the graphite anode because the temperature is close to the freezing point of LP30 electrolyte, -21.9°C [91, 92] due to significantly decreased ionic conductivity that leads to poor low-temperature battery performance.
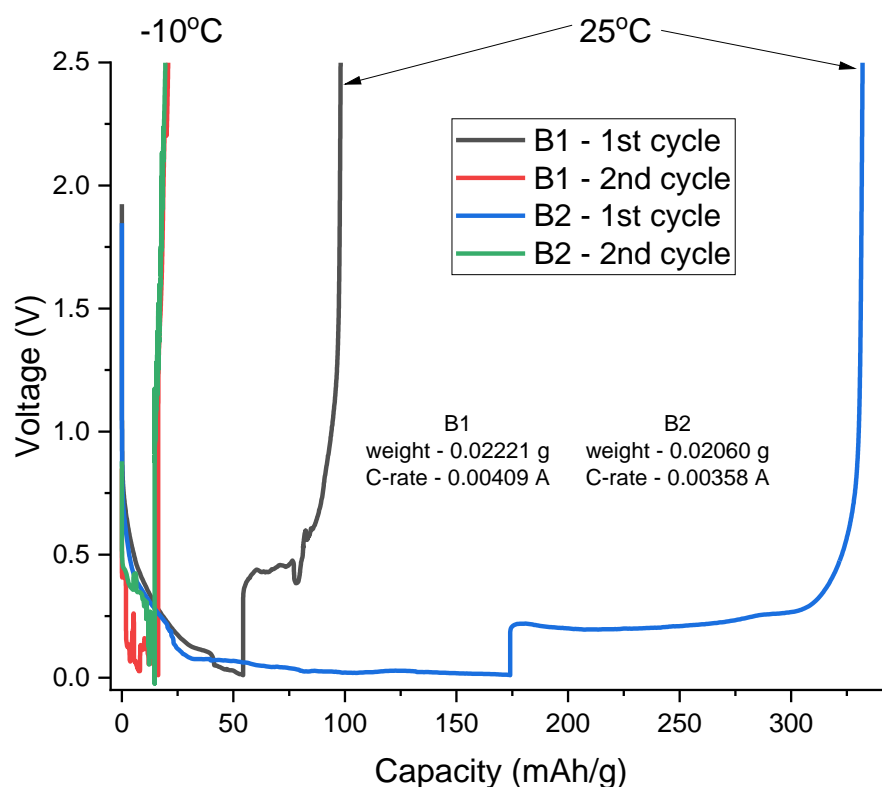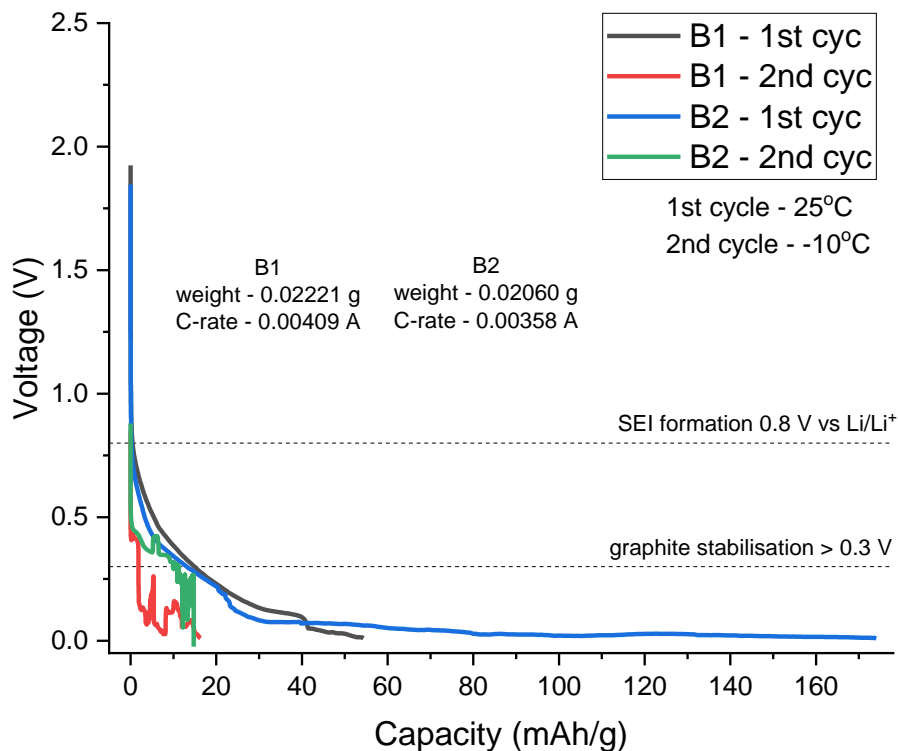

Figure 5-14: Discharge (half-cell) graphs of the same two Li/graphite half-cells with LP30 electrolyte cycled at different temperatures; 1st at 25°C and 2nd at -10°C. Battery 1 had C-rate of 0.00409 A. (weight – 0.02221 g), Battery 2 had a C-rate of 0.00358 A. (weight – 0.02060 g).

Figure 5-15 below indicates the coulombic efficiency of the same two tested cells at different temperatures. As expected, much higher coulombic efficiencies were achieved in 1st cycle than the 2nd cycle which both had less than 40 % of the efficiencies. It is known that there will be a decrease in battery performance, especially at low temperatures due to reduced ionic conductivity and low ionic diffusivity. Hence, poor coulombic efficiency was expected in the 2nd cycle compared to the 1st cycle where the coulombic efficiency will be close to its theoretical value of 99 % due to the parasitic reaction occurring mostly due to SEI formation. By comparing with previous 0°C and -5°C results, it can be stated that the cell will have more decrease in coulombic efficiency as the cycling temperature decrease but it depends on the electrolyte condition. Since cycling temperature is much lower than the previous 0°C and -5°C, there will be more partially freezing LP30 electrolyte that leads to much reduced ionic conductivity, ionic mobility, and diffusivity. In general, a relatively smaller amount of lithiation should occur in -10°C because less amount of Li-ions can intercalate towards the anode due to disturbance in the electrolyte region and some bindings of Li-ions are used to form more SEI layer in 2nd cycle which they will not take part in the further discharge process. In addition, further SEI growth is possible at low-temperature based on the efficiency of the 2nd cycle.

Figure 5-15: Coulombic efficiency of the same two Li/graphite half-cells with LP30 electrolyte cycled at different temperatures; 1st at 25°C and 2nd at -10°C. Battery 1 had C-rate of 0.00409 A. (weight – 0.02221 g), Battery 2 had a C-rate of 0.00358 A. (weight – 0.02060 g).

Figure 5-16 below represents the discharge capacity (half-cell) and irreversible charge capacity loss of the same two Li/graphite half-cells in each cycle at a certain cycling temperature. Two cells had a decrease in discharge capacity in the 2nd cycle where cycling temperature is lowered down to -10°C. In addition, the 1st cycle of Battery 1 and 2 had a big difference in discharge capacity but in the 2nd cycle, there was not much difference in between which was similar to Figure 5-12 in previous section 5.3.4. Hence, it can be stated that the capacity drop is dependent on cycling temperature because it affects the electrolyte condition. The condition of the SEI layer is not important because although Battery 2 had a better SEI layer formed in the 1st cycle, both cells produced similar discharge capacity in the 2nd cycle at -10°C. It can be hypothesised that the capacity loss is not dependent on the amount of the capacity but more dependent on the condition of the electrolyte.
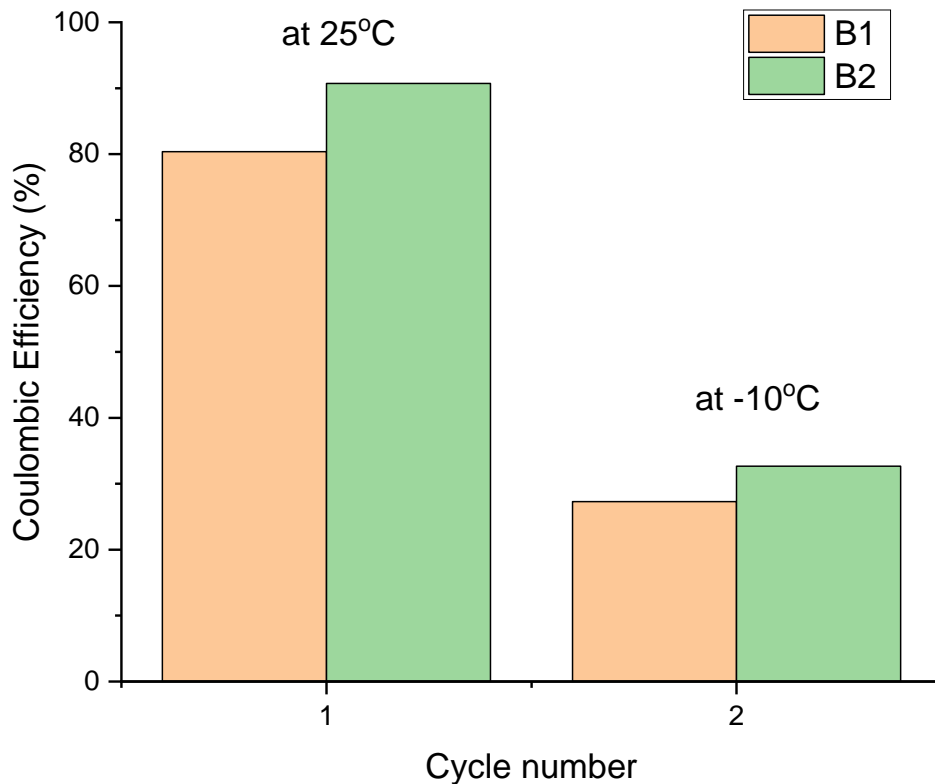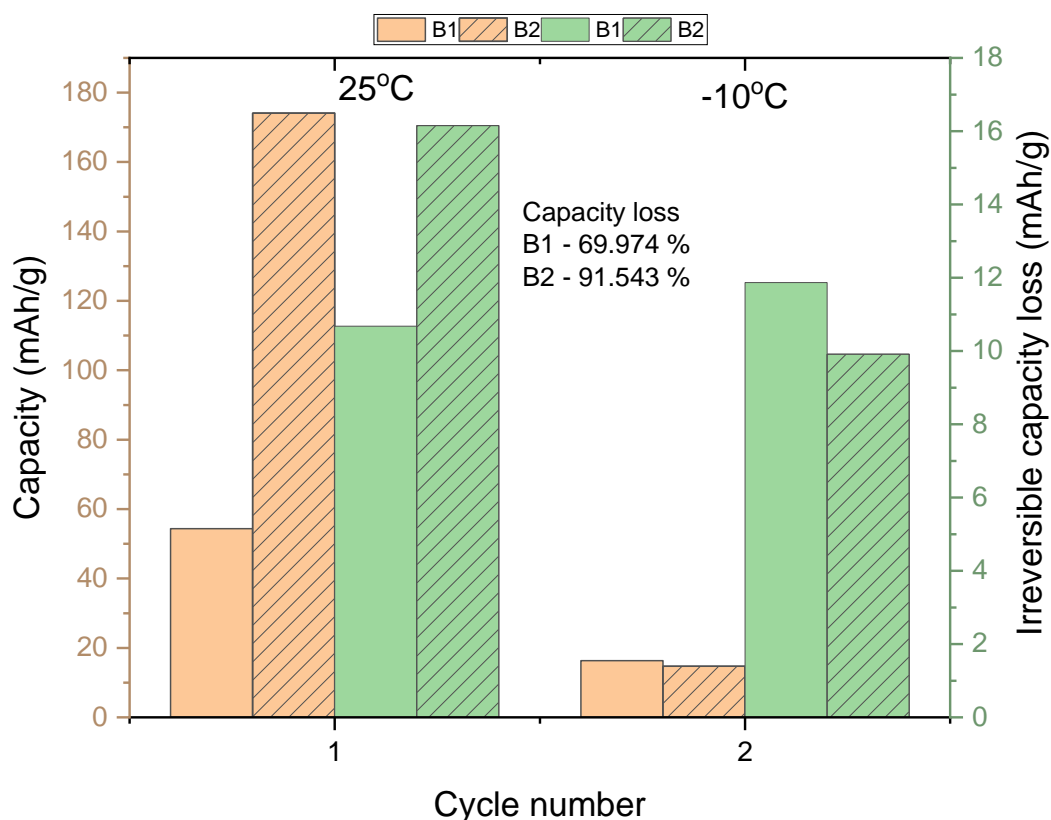
Figure 5-16: Discharge capacity (half-cell) and irreversible charge capacity of the same two Li/graphite half-cells with LP30 electrolyte cycled at different temperatures; 1st at 25ºC and 2nd at -5ºC. Battery 1 had C-rate of 0.00409 A. (weight – 0.02221 g), Battery 2 had a C-rate of 0.00358 A. (weight – 0.02060 g).

Battery 2 had higher irreversible charge capacity loss in 1st cycle because more bindings of Li-ions are used in SEI formation, and they are not used in the further discharge process. In the 2nd cycle, it had relatively less irreversible charge capacity loss than Battery 1 although the cell had better SEI formation in the 1st cycle. In conclusion, it can be stated that the cycling temperature is more important than the condition of the SEI layer for low-temperature systems. In addition, SEI layer still forms in 2nd cycle although the cycling temperature is lowered to -10ºC that is closer to the freezing point of LP30 electrolyte, -21.9ºC [91, 92]. More partially freezing of LP30 electrolyte can be expected in electrolyte region which disturbs transport of Li-ions more than other low temperatures, 0ºC and -5ºC.

5.3.6 -15ºC results

In this section, the three Li/graphite half-cells were built in same condition as section 3.1.2. Unlike previous section 5.3.4 and 5.3.5, three cell results were shown in this section. The cycling temperature was adjusted to -15ºC at the 2nd cycle which was the lowest cycling temperature that MACCOR can go down. It can go down to -20ºC but the temperature in MACCOR chamber was very unstable and

experimental issues occurred repeatedly. Therefore, the temperature was fixed to -15°C. When the temperature is adjusted, the cell was kept at rest for two hours so that it can fully adapt to the environmental condition such as graphite stabilisation and further electrolyte stabilisation and decomposition as the electrolyte phase can be changed. It is expected that most parts of LP30 will be in a solid state because the temperature is not only below the melting point of both EC and DMC solvents but also very close to the freezing point of LP30, -21.9°C [91, 92]. In this section, the effect of low-temperature (-15°C) and SEI layer on battery performance can be understood deeper.

Figure 5-17 shows the performance of the three Li/graphite half-cells with LP30 electrolyte in two different cycling temperatures; 25°C and -15°C. The 1st cycle of all three cells had smooth discharge/charge cycle because further growth of SEI formation was taking place at 25°C which were similar as previous 1st cycle results of 0°C, -5°C, and -10°C. The capacity increased as the dropped voltage are reached 0.8 V which is the typical onset potential of SEI formation [35, 36, 85] and the cell discharged long enough until the voltage reaches 0.01 V. Battery 1 and 2 produced similar capacity as theoretical value (372 mAh/g) whereas Battery 3 had comparatively less capacity possibly due to poor SEI layer was formed in ageing time. All cell had understandable discharge/charge cycle in 1st cycle due to good ionic conductivity of LP30 electrolyte in ambient temperature.

However, the graph of the 2nd cycle was even more shifted towards the left compared to the previous Figures (5-9 and 5-13). In addition, the cell discharge/charge cycle was very short compared to the 1st cycle. There will be more partially freezing LP30 electrolytes expected because the 2nd cycle is done at -15°C which is close to the complete freezing point of LP30, -21.9°C [92]. Since there will be more solidified electrolytes available in the electrolyte region, Li-ions will face more disturbance on lithiation/delithation in between metallic Lithium and graphite anode. Hence, the cell produced very small capacity and had the fastest discharge/charge cycle at -15°C because of more solidified LP30 electrolyte that leads to much reduced ionic conductivity, ionic diffusivity, and mobility.
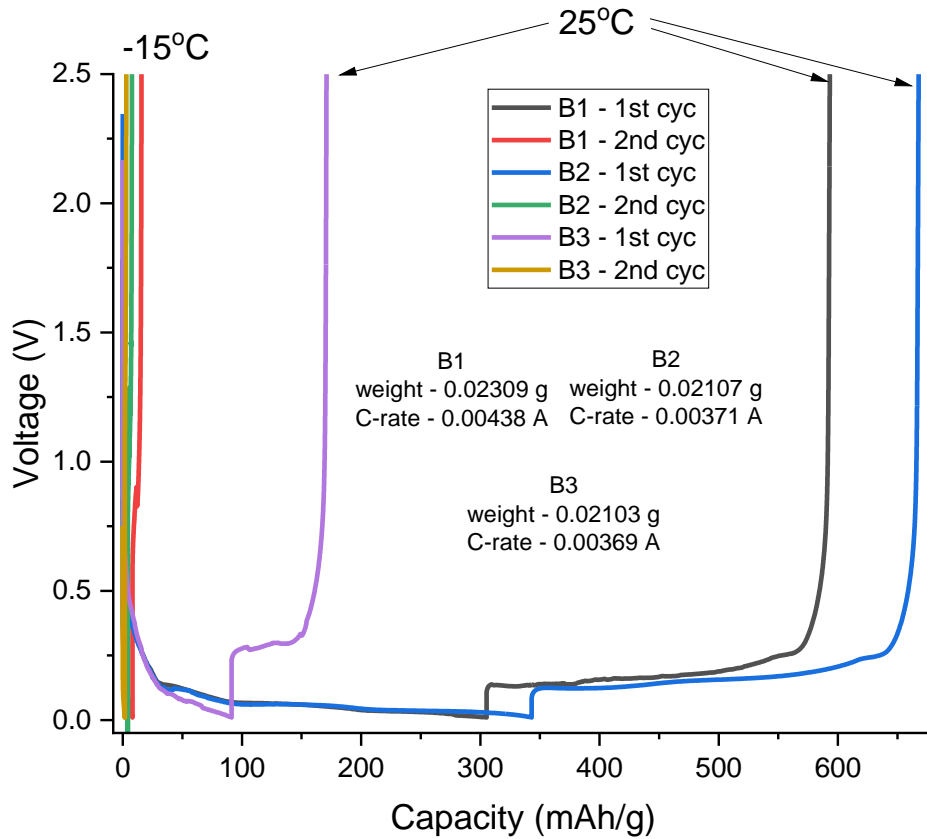
Figure 5-17: Voltage vs Capacity graphs of three Li/graphite half-cells with LP30 electrolyte cycled at different temperatures; 1st at 25ºC and 2nd at -15ºC. Battery 1 had C-rate of 0.00438 A. (weight – 0.02309 g), Battery 2 had a C-rate of 0.00371 A. (weight – 0.02107 g), Battery 3 had a C-rate of 0.00369 A. (weight – 0.02103 g)

Figure 5-18 is introduced below to show how discharge capacity (half-cell) of the same three cells changes over voltage at different cycling temperatures. As expected, the 1st cycle of three cells had good discharge capacity as voltage drops to 0.01 V without any noise of the graph. This represents smooth lithiation process occurred in discharge cycle with SEI formation which was similar as previous 1st cycle results of 0ºC, -5ºC, and -10ºC. In addition, it can be stated that the weight of the electrode with C-rate in Amps is not dependent on the capacity because Battery 1 did not produce highest capacity although it was the heaviest electrode.

However, 2nd cycle of discharge curves were extremely short for all three cells. They were close to a straight line which means very small discharge capacity was produced as the voltage massively drops in very short period. This is due to the extremely poor condition of LP30 electrolyte with more reduced ionic conductivity. Since the cycling temperature was near the complete LP30 electrolyte freezing point, most of the electrolyte region was expected to be in a solid state that leads to very poor low-temperature battery performance having a huge influence on intercalation/deintercalation process, and the role of electrolyte will be disappeared because it cannot deliver Li-ions as fluent as in room

temperature. Since the discharge graphs of three cells were close to a straight line, it can be assumed that either very small SEI formation was occurred, or no SEI formation was formed in 2nd cycle.
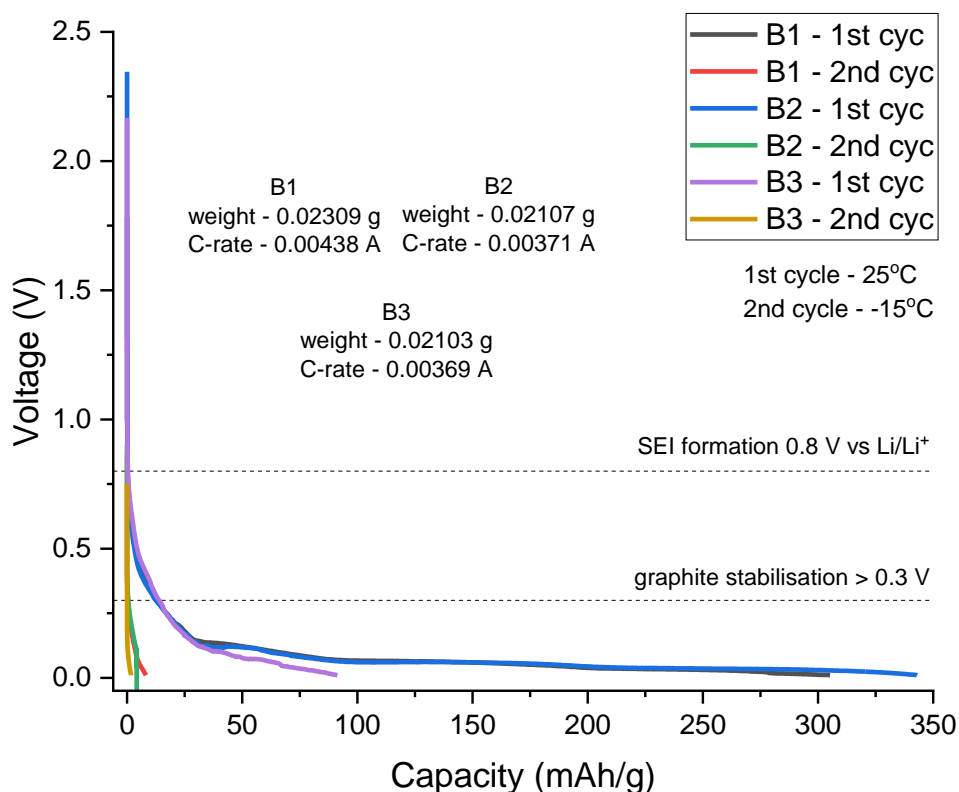

Figure 5-18: Discharge (half-cell) graphs of the same three Li/graphite half-cells with LP30 electrolyte cycled at different temperatures; 1st at 25°C and 2nd at -15°C. Battery 1 had C-rate of 0.00438 A. (weight – 0.02309 g), Battery 2 had a C-rate of 0.00371 A. (weight – 0.02107 g), Battery 3 had a C-rate of 0.00369 A. (weight – 0.02103 g).

The coulombic efficiency of the same cells at different cycling temperatures was shown in Figure 5-19 below. Similar as previous coulombic efficiency of 1st cycle results at 0°C, -5°C, and -10°C, the 1st cycle had the efficiency close to the theoretical value of 99%. This represents the similar amount of Li-ions were lithiated/delithiated which can be explained as good intact SEI layers were formed for all three cells in 8 hours of ageing time. In 1st cycle, the coulombic efficiency is normally less than 99 % due to the parasitic reaction occurring mostly due to SEI formation. Since the 1st cycle was done at 25°C, smooth intercalation/deintercalation process are expected due to stable electrolyte phase.

However, the coulombic efficiency for 2nd cycle showed very interesting results because although the cycling temperature was lowered to -15°C, significantly higher efficiency were shown unlike other low-temperature results (0°C, -5°C, -10°C) which they had relatively reduced efficiencies. Since the cycling temperature of the 2nd cycle was close to the complete electrolyte freezing point, poor efficiency was expected to be seen. Based on previous Figure 5-18, the discharge cycle of three cells were extremely

poor. It is known that poor battery performance is achieved at low temperatures due to reduced ionic conductivity and low ionic diffusivity. From this, it can be hypothesised that when the cycling temperature is lowered to -15°C, there will be not much reduction in coulombic efficiency if certain condition and quality of SEI layer is formed on graphite anode.

Figure 5-19: Coulombic efficiency of the same three Li/graphite half-cells with LP30 electrolyte cycled at different temperatures; 1st at 25°C and 2nd at -15°C. Battery 1 had C-rate of 0.00438 A. (weight – 0.02309 g), Battery 2 had a C-rate of 0.00371 A. (weight – 0.02107 g), Battery 3 had a C-rate of 0.00369 A. (weight – 0.02103 g).

Figure 5-20 below shows the discharge capacity (half-cell) and irreversible charge capacity loss of the same cells in each cycle with temperature adjustment. It was clearly seen that the discharge capacity of all three cells massively decreased as the cycling temperature is lower downed from 25°C to -15°C. Although they had different capacities in 1st cycle, three cells had similar discharge capacity in 2nd cycle. From this, it can be stated that the capacity is more affected by the cycling temperature rather than the condition of the SEI layer. Battery 3 had relatively less discharge capacity than other cells which can be assumed as comparatively an incomplete SEI layer is formed. Since the discharge capacity of two cells (Battery 1 and 2) were close to the theoretical capacity of graphite, 372 mAh/g, they formed much better SEI layer than Battery 3. However, in the 2nd cycle, their capacities were close to Battery 3 because all cells were cycled in -15°C which is near the complete freezing point of LP30 electrolyte

that will influence the transport of Li-ions to the graphite anode due to reduced ionic conductivity. To explain, all cells had more than 97 % of capacity loss in between 1st and 2nd cycle.

The irreversible charge capacity of the three cells were relatively high in 1st cycle compared to in 2nd cycle where all cells had a small irreversible charge capacity loss. This means there is not much difference between charge and discharge capacity in the 2nd cycle whereas in the 1st cycle, more charge capacity is produced rather than discharge capacity. Since Battery 1 and 2 had much higher irreversible charge capacity loss in 1st cycle, it shows that a significantly better SEI layer is formed than Battery 3. In conclusion, the cycling temperature, -15°C, has more effects on the reduced capacity produced by the cell rather than the SEI layer which results in a capacity fade, poor battery performance and short battery life because of more solidified electrolyte available that leads to reduced ionic conductivity.
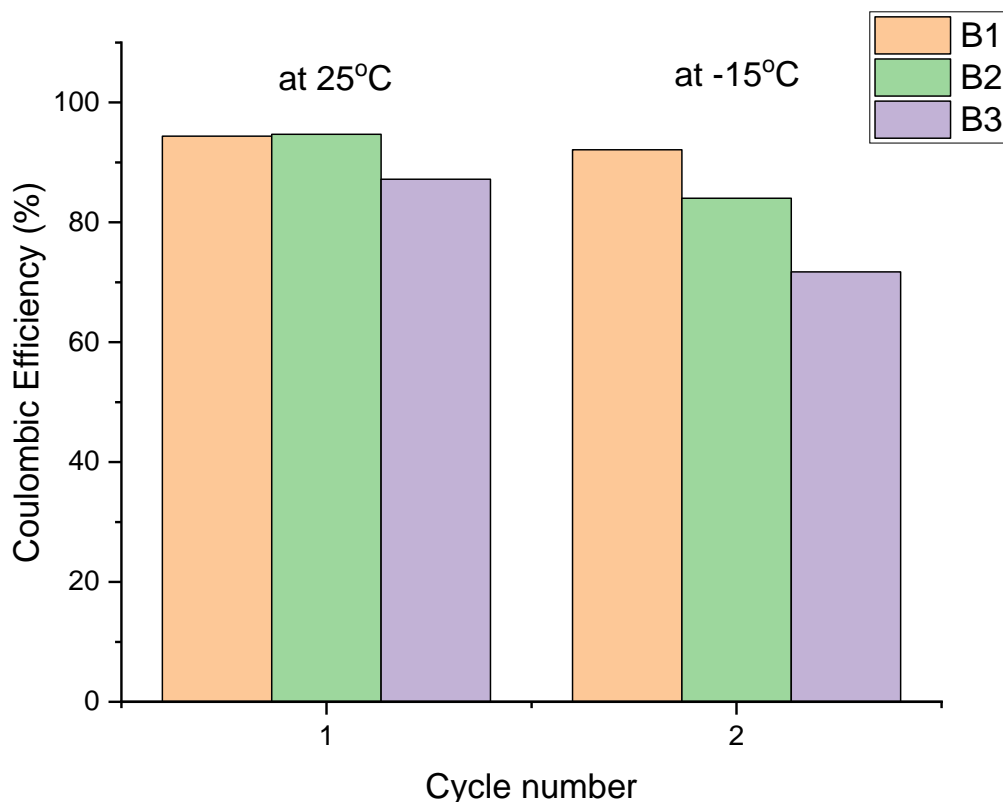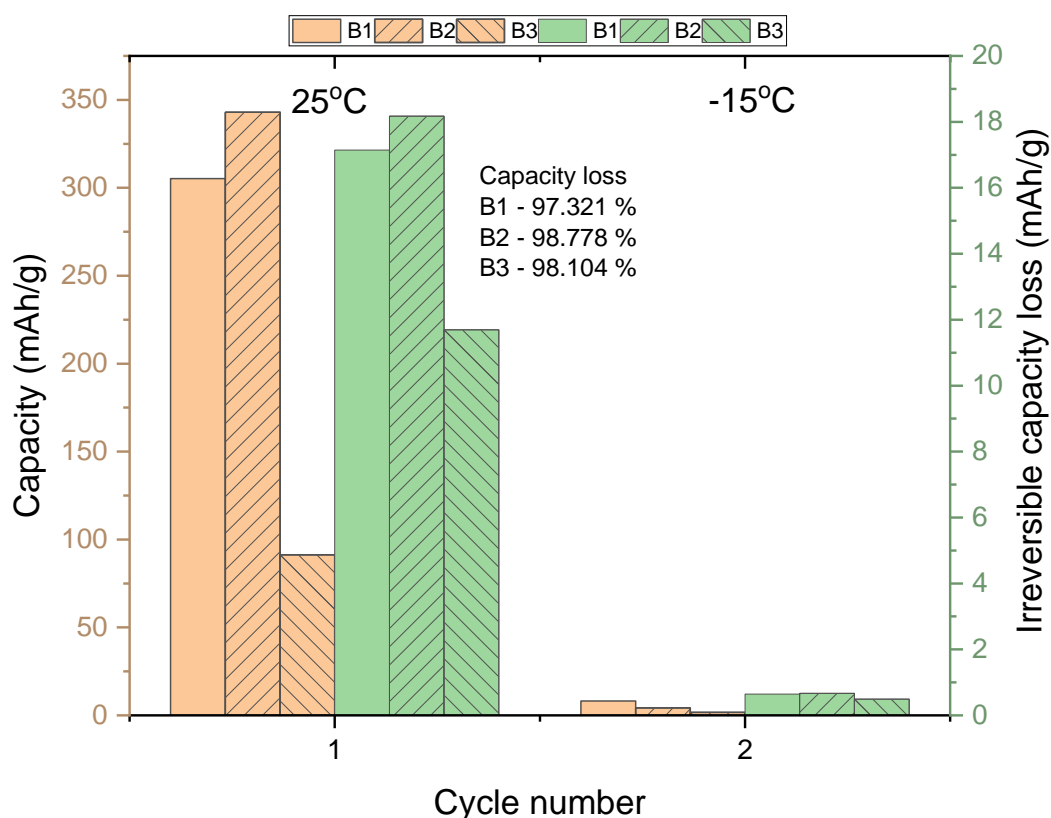

Figure 5-20 Discharge capacity (half-cell) and irreversible charge capacity of the same three Li/graphite half-cells with LP30 electrolyte cycled at different temperatures; 1st at 25°C and 2nd at -5°C. Battery 1 had C-rate of 0.00438 A. (weight – 0.02309 g), Battery 2 had a C-rate of 0.00371 A. (weight – 0.02107 g), Battery 3 had a C-rate of 0.00369 A. (weight – 0.02103 g)

5.3.7 Conclusion

This set of experiments was mainly focused on the effect of changing low cycling temperature after allowing SEI formation in 1st cycle at room temperature. All cells were fabricated in the same experimental condition such as same composition of the artificial graphite anode and LP30 electrolyte

which was already mentioned in section 3.1. It was well-proved that SEI formation is necessary before the low-temperature cycle in section 5.2. If not, the cell fails to complete the battery cycle within the time and produces a lot of noise on the voltage/time graph which means an unstable reversible reaction taking place during the cell discharge/charge state.

In 1st cycle, all tested cells showed similar result having smooth discharge/charge curve as change in potential over time. The discharge curve was the main focus in this section because the lithiation to the graphite anode explains the possible SEI formation. Having 8 hours of ageing time allows the electrolyte stabilisation and decomposition as well as an intact SEI formation on graphite anode. Since the 1st cycle was allowed to discharge/charge at 25°C, the discharge capacity started to increase as the practical value of onset voltage of SEI formation reaches 0.8 V vs Li/Li+ [35, 36, 85] until 0.01 V. At 25°C, it was expected to have good diffusivity of Li-ions as the electrolyte phase is much stable.

However, all tested cells had much faster discharge/charge cycle in 2nd cycle based on their respective low cycling temperatures (0°C to -15°C). Theoretically, poor battery performance is expected as the temperature close to the freezing point of the LP30 electrolyte (-21.9°C [92]). Figure 5-21 is shown below to represent the different coulombic efficiency and capacity loss of the 2nd cycle only at various cycling temperatures. This particular result was obtained by taking the average of all batteries at relevant cycling temperatures. It was clear that at room temperature, the highest coulombic efficiency is achieved which is close to 99 %. To explain, negative capacity retention (-1.7 %) was achieved at room temperature which means the capacity of the 2nd cycle was larger than the 1st cycle capacity. From this, it can be assumed that the graphite electrode was not fully wetted within the ageing time and the 1st cycle because theoretically, the capacity cannot be increased as Li-ions are consumed more over cycle. This is possibly due to the imperfect SEI layer being formed in 1st cycle but more battery cycle is needed to obtain an intact SEI layer [35].

As the cycling temperature of the 2nd cycle is lowered down to -15°C, there was an increase in the capacity loss. Since -15°C is close to the complete freezing point of LP30 electrolyte (-21.9°C [92]), there will be more capacity loss between 1st and 2nd cycles. In general, poor low-temperature performance is shown because of unstable reversible reactions that are affected by reduced ionic conductivity of electrolytes and diffusivity of Li-ions. It is already reported that the reduced conductivity of the electrolyte and SEI layer on the electrode affects the low-temperature performance of the battery [30, 44, 83, 90]. However, the average coulombic efficiency of cells at -15°C had a significantly higher value than other low cycling temperatures although it had the highest capacity loss from room temperature to -15°C. Hence, it can be concluded that coulombic efficiency

shows how efficient the battery is but sometimes, it cannot be fully dependent on battery performance especially at low cycling temperatures.
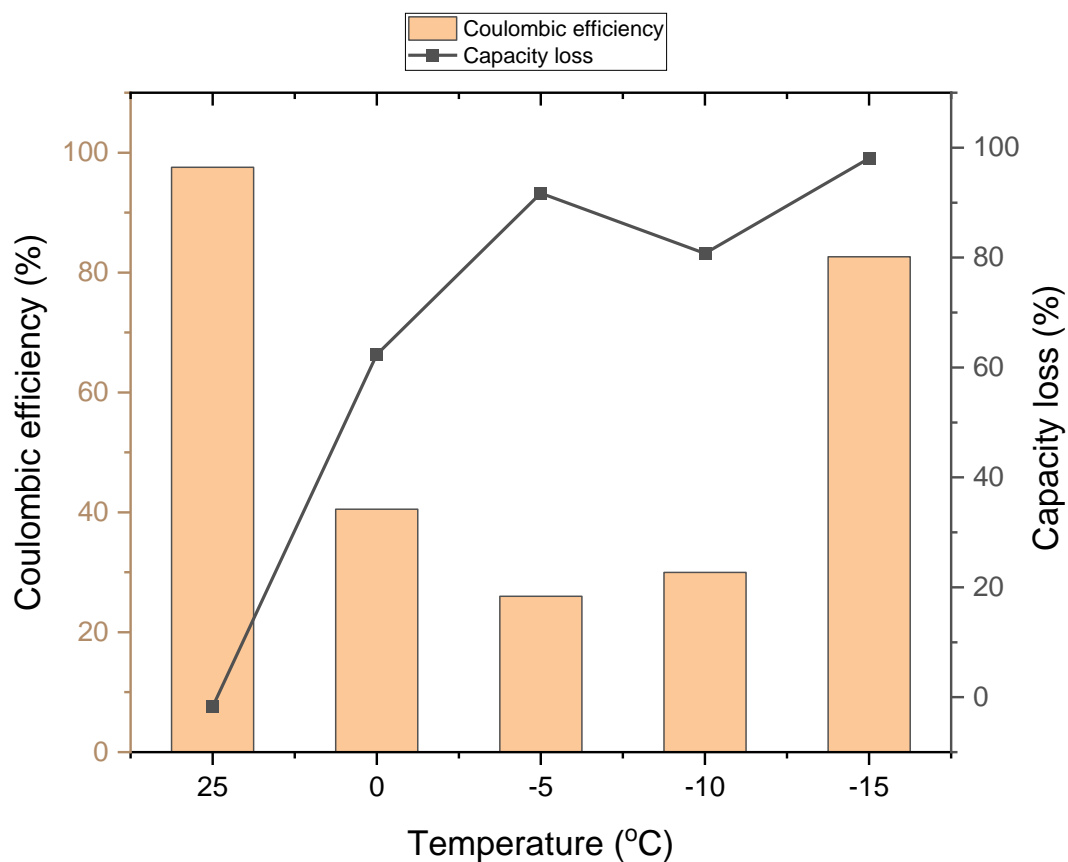
Figure 5-21: The average cell data of the coulombic efficiency and capacity loss in 2nd cycle based on cycling temperatures

5.4 Temperature change at 6th cycle with various electrolyte

This section is mainly focused on the effect of battery performance based on changing cycling temperature from the 6th cycle onwards by allowing five battery cycles at room temperature so that a better SEI layer can be formed on graphite anode. The total battery cycle is limited to ten cycles; the first five cycles are at room temperature and the last five cycles are at low cycling temperatures. In addition, three electrolytes are used for further comparison to determine the effect of the electrolyte on low-temperature performance. From this, it can be found out whether better SEI formation before the low-temperature cycle will improve the low-temperature battery performance as well as the electrolyte.

5.4.1 Experimental setup

The same experimental methods and materials are used as mentioned in section 3.1. The galvanostatic Li-graphite half-cells are built with an artificial graphite anode and Lithium metal as a reference and counter electrode. In this set of experiment, three electrolytes; 1.0 M of $LiPF_6$ in EC/DMC = 50/50 (v/v) (Sigma Aldrich) (LP30), 1.0 M of $LiPF_6$ EC/DEC = 50/50 (v/v) (Sigma Aldrich) (LP40), and 1.0 M of $LiPF_6$ EC/DEC = 50/50 (v/v) (Sigma Aldrich) (LP40) with 10% FEC (98%, Alfa Aesar) additive, are used to find out how different types of electrolytes affect the SEI formation and determine the low-temperature performance of the cells. In previous Section 5.2, FEC could not solve the poor delivery of Li-ions in between metallic Lithium and graphite anode although FEC is used to improve stability of SEI [28]. The first five cycles were carried out at 25°C to allow better SEI formation. Then, the cycling temperature is lowered to 0°C. 2 hours of a rest period is given before the 6th battery cycle so that the electrolyte stabilisation can take place due to change in temperature. The experimental data will be introduced with each type of electrolyte at 0°C. The types of battery electrolytes will be mentioned accordingly.

5.4.2 Results

5.4.2.1 LP30 electrolyte

Figure 5-22 represents the discharge/charge curve of the two Li/graphite half-cells at different cycling temperatures using LP30 electrolyte. The graphs can be separated into two temperatures; 25°C and 0°C. It is shown that the further SEI formation possibly occurred until the 5th cycle because the graph at 25°C produced more discharge/charge capacity than the 0°C results. Most of the SEI layer is formed in 1st cycle but further cycles are necessary to form better SEI layer. By having a few more repeated cycles at room temperature, a better SEI layer can be formed because of the good diffusivity of Li-ions, and the ionic conductivity of the electrolyte. Both cells showed increase in capacity from 1st to 5th cycle possibly due to poor intact SEI layer were formed in ageing time having the electrodes not fully wetted with the electrolyte. Theoretically, the highest capacity is expected at 1st cycle and lower capacity at 5th cycle because Li-ions are consumed more and more over cycle.

From the 6th cycle to the 10th cycle, the graphs were shifted towards the left because the cycling temperature was lowered to 0°C which leads to reduced ionic conductivity and low mobility of ions can be achieved due to partial freezing of electrolyte similar as previous 5.3.3. Therefore, the cell had a relatively faster discharge/charge cycle with relatively low capacity produced in a short time. In addition, both cells had better cycling state in 6th cycle than 10th cycle because not only did the cycle number increase but also the cycling process was done in 0°C. This can be assumed as either more partial freezing of the electrolyte occurred over cycle or more Li-ions were consumed over cycle.
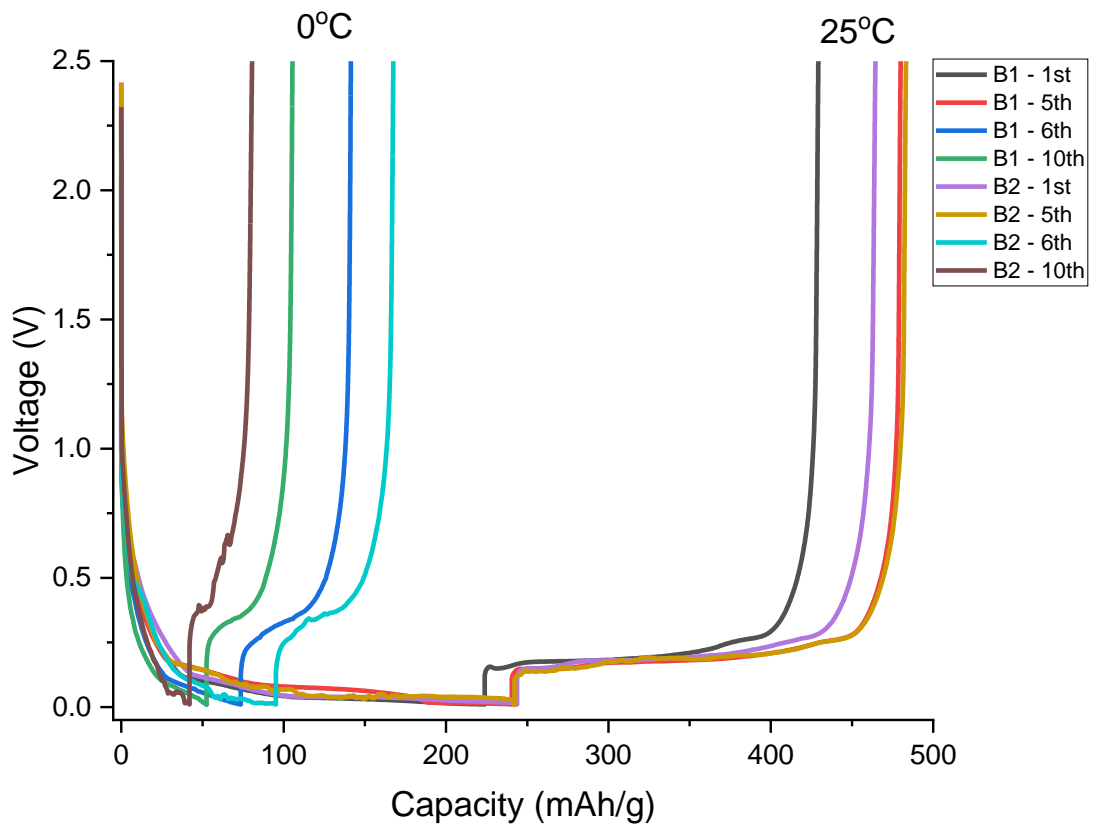
Figure 5-22: Voltage vs Capacity graphs of the two Li/graphite half-cells with LP30 electrolyte cycled at different temperatures; 1st – 5th at 25oC and 6th – 10th at 0oC. Battery 1 had C-rate of 0.006987 A. (weight – 0.03087 g), Battery 2 had a C-rate of 0.00782 A. (weight – 0.03336 g).

The coulombic efficiency of the same two cells at different cycling temperatures was shown in Figure 5-23 below. Similar as previous coulombic efficiency of 1st cycle results at 0°C, -5°C, -10°C and -15°C, the 1st cycle was less than a theoretical value of 99% because of the parasitic reaction occur mostly due to the SEI formation. Most of the efficiencies for Batter 1 were close to 99 % which represents the similar amount of Li-ions were lithiated/delithiated that can be explained as good intact SEI layers were formed in 8 hours of ageing time. Since the 1st to 5th cycle were done at 25°C, smooth intercalation/deintercalation process were expected due to stable electrolyte phase.

However, the coulombic efficiency from 6th to 10th cycle showed very interesting results because although the cycling temperature was lowered to 0°C, Battery 1 still had increase in efficiency whereas comparatively less efficiency were shown for Batter 2. Since the electrolyte phase is not stable at 0°C, poor efficiency is expected because poor battery performance is achieved at low temperatures due to reduced ionic conductivity and low ionic diffusivity. This supports the hypothesis in section 5.3.6 that when the cycling temperature is lowered to 0°C, there will be not much reduction in coulombic efficiency if certain condition and quality of SEI layer is formed on graphite anode.
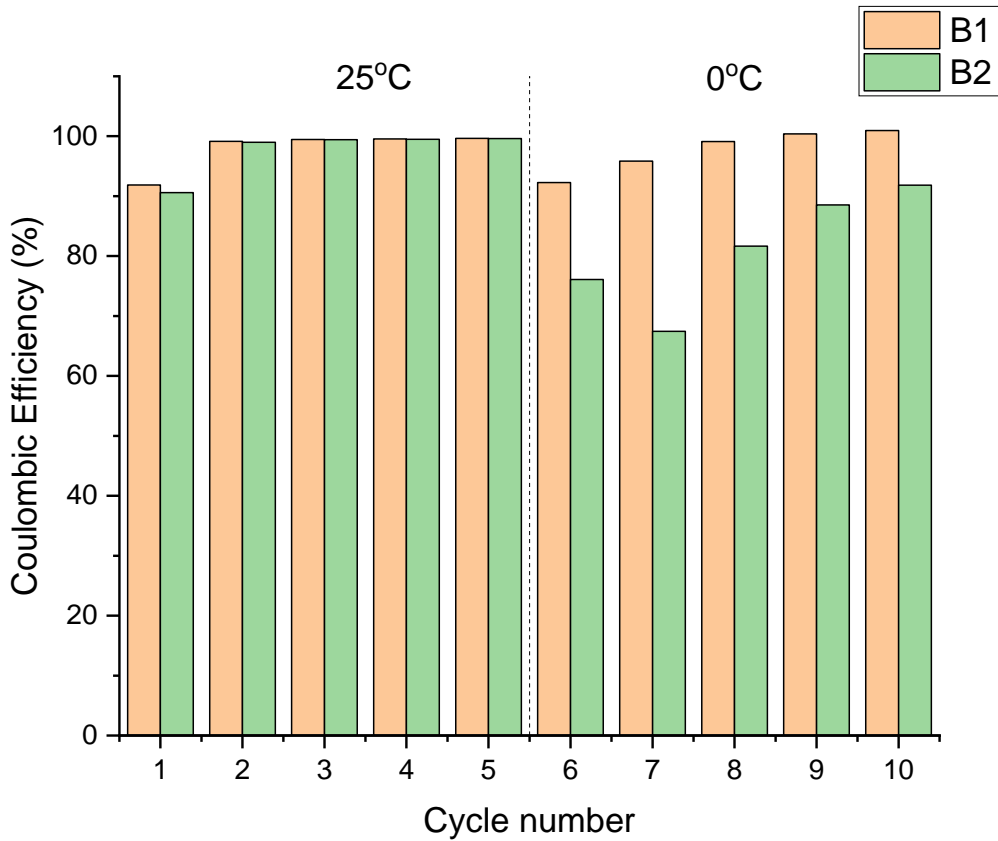
Figure 5-23: Coulombic efficiency of the same two Li/graphite half-cells with LP30 electrolyte cycled at different temperatures; 1st − 5th at 25ºC and 6th − 10th at 0ºC. Battery 1 had C-rate of 0.006987 A. (weight − 0.03087 g), Battery 2 had a C-rate of 0.00782 A. (weight − 0.03336 g).

Figure 5-24 below represents the discharge capacity (half-cell) and irreversible charge capacity loss of the same two cells in each cycle at different cycling temperatures. As expected, the discharge capacities at 25ºC for two cells were significantly higher than the 0ºC. At room temperature, LP30 electrolyte will have better ionic conductivity because most of EC and DMC components will be in the liquid state whereas, at 0ºC, partial freezing of electrolyte will have reduced ionic conductivity that leads to slow transport of ions. Both cells showed increase in capacity until 5th cycle possibly due to the electrodes not fully wetted with LP30 electrolyte that leads to less SEI formation. Theoretically, the capacity decrease as more Li-ions are consumed over cycle. From 6th cycle, the capacity decreased over cycle as partial freezing of the LP 30 electrolyte was expected at 0ºC. In between 5th and 6th cycle, both cells had 60 − 69 % capacity loss as the cycling temperature was changed to 0ºC. However, both cells had relatively higher discharge capacities than section 5.3.3 results. It can be assumed that this is due to the more SEI growth at 25ºC before the temperature change. Previous 0ºC results in section 5.3.3 had only one cycle for the SEI formation at 25ºC whereas these cells had five cycles.
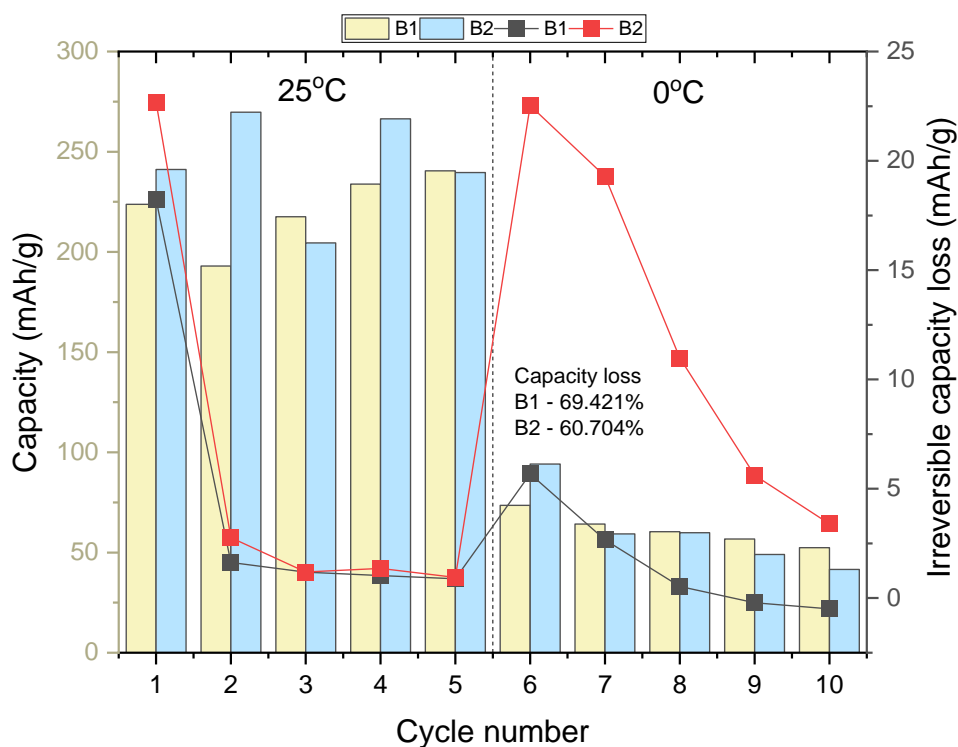
Figure 5-24: Discharge capacity (half-cell) and irreversible charge capacity of the same two Li/graphite half-cells with LP30 electrolyte cycled at different temperatures; $1^{st} - 5^{th}$ at 25°C and $6^{th} - 10^{th}$ at 0°C. Battery 1 had C-rate of 0.006987 A. (weight – 0.03087 g), Battery 2 had a C-rate of 0.00782 A. (weight – 0.03336 g).

It is known that most of the SEI layer is formed in 1st cycle because the parasitic reaction occurs mostly due to SEI formation. To explain, the highest irreversible charge capacity loss is expected in 1st cycle because relatively higher charge capacity is produced than discharge capacity. Some bindings of Li-ions are involved in SEI formation that can result in irreversible capture in graphite anode surface. Both cells had highest irreversible charge capacity loss in 1st cycle. From the 2nd to 5th cycle, the irreversible charge capacity losses were decreased although their capacities were increased. This means more SEI formation were taking place but in much slower process because small irreversible charge capacity loss means there are not much difference in between the amount of Li-ions intercalated and deintercalated. When the temperature is changed to 0°C, the irreversible charge capacity loss increased in the 6th cycle, but it started to drop until the end. This is possibly due to bindings of Li-ions are still involved in the formation and stabilisation of the SEI layer in the 6th cycle. In addition, the electrolyte stabilisation can be expected over cycle. The irreversible charge capacity loss of the Battery 1 at 9th and 10th cycle had minus value which means higher delithiation was occurred compared to the lithiation process. It can be hypothesized that decent SEI layer was formed until 8th cycle so possibly no further Li-ions need to be involved in SEI formation. Possibly, irregular captured Li-ions were added to the delithiaion process from the graphite anode to the metallic Li.

Hence, it can be concluded that having multiple battery cycles at room temperature will allow better SEI formation and this will have a positive effect on low-temperature performance where improvement in capacity and coulombic efficiency but reduced irreversible charge capacity loss can be achieved. However, capacity loss cannot be solved because this is more affected by the cycling temperature where it varies the condition of LP30 electrolyte.

5.4.2.2 LP40 electrolyte

The two cells were tested but the Battery 2 kept failing discharge/charge cycle possibly due to channel issue in MACCOR. Hence, only Battery 1 data was provided in this section. Figure 5-25 represents the discharge/charge curve of a Li/graphite half-cell at different cycling temperatures using LP40 electrolyte. Unlike previous Figure 5-22 in section 5.4.2.1, this battery had failed to discharge/charge multiple times at 25°C. Theoretically, highest discharge/charge capacity is expected close to the theoretical capacity of the graphite, 372 mAh/g and the capacity decrease as Li-ions are consumed more and more over cycle. However, this cell had very small discharge/charge curve (black) in 1st cycle and the 5th cycle (red) was nearly a straight line. It is hypothesised that the graphite electrode was not fully wetted possibly due to small amount of LP40 electrolyte in the tested cell. It cannot be estimated whether the SEI formation occurred from 1st to 5th cycle as their discharge/charge cycle were too fast due to the unforeseen experimental error.

Although the cycling temperature was 0°C, the cell had a better discharge/charge state than the 1st and 5th cycles. The 6th cycle (blue) had an irregular shape compared to 10th cycles (green) because possibly it was the first cycle after the cycling temperature is lowered to 0°C. Theoretically, discharge/charge curve of the 0°C data was supposed to be much faster than the 25°C data because of unstable LP40 electrolyte state. Low diffusivity of Li-ions and slow lithiation/delithiation process are expected due to the partial freezing of the electrolyte. The SEI formation occurred in 10th cycle because the discharge capacity started to increase as the voltage reaches 1.0 V which was slightly above the onset voltage of the SEI formation (0.8 V). From this, it can be assumed that lithiation to the graphite anode was occurred in 10th cycle at 0°C.
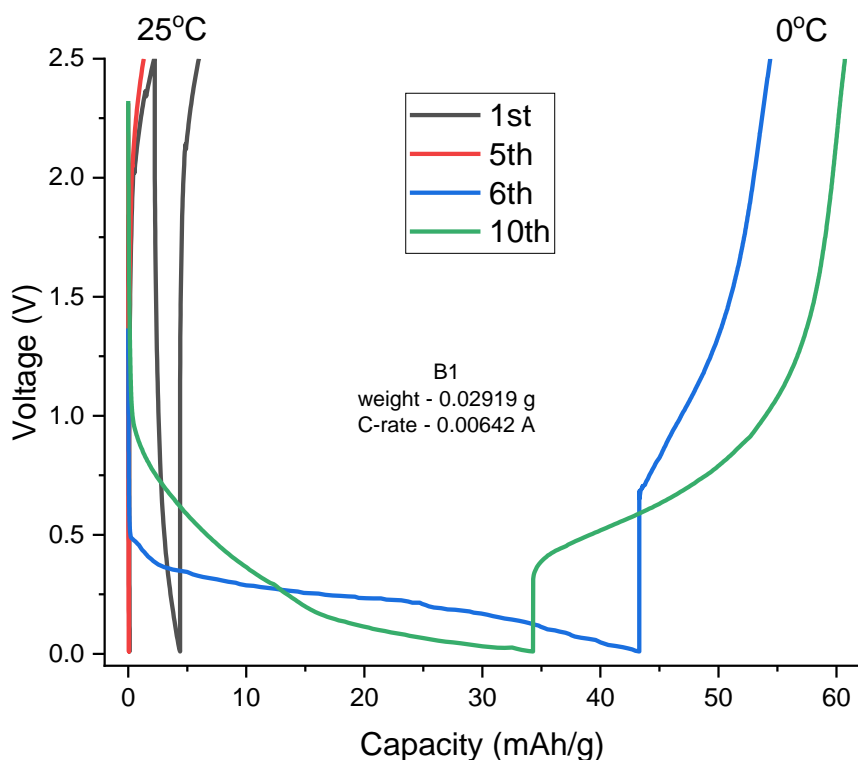
Figure 5-25: Voltage vs Capacity graphs of a Li/graphite half-cell with LP40 electrolyte cycled at different temperatures; 1st – 5th at 25°C and 6th – 10th at 0°C. Battery 1 had C-rate of 0.00642 A. (weight – 0.02919 g).

Figure 5-26 below shows the coulombic efficiency of the same Li/graphite half-cell with LP40 electrolyte based on change in temperature. This cell showed increase in coulombic efficiency over cycle until 5th cycle which was an expected result at 25°C because of smooth lithiation/delithiation process due to good ionic conductivity of the LP40 electrolyte. In addition, most of the SEI formation occurs in 1st cycle so lowest coulombic efficiency was expected which this cell had. Delithiation (charge in half-cell) will have less Li-ions for intercalation than the lithiation (discharge in half-cell) because some Li-ions are involved in SEI formation and irregular capture in graphene layers. However, this cell showed very poor discharge/charge cycle at 25°C based on previous Figure 5-25. Hence, it can be stated that the coulombic efficiency by itself cannot be a strong determinant factor in battery performance. Reduced coulombic efficiency were shown in 6th cycles and this gradually increased over cycle at 0°C. There was a strong decrease in the coulombic efficiency in 6th cycle unlike previous Figure 5-23 in section 5.4.2.1 which had similar efficiency as the 25°C cycles. This is possibly due to either the partial freezing of the electrolyte or the further SEI formation, but it cannot be fully determined because the cell had an experimental error having poor discharge/charge cycles at 25°C.
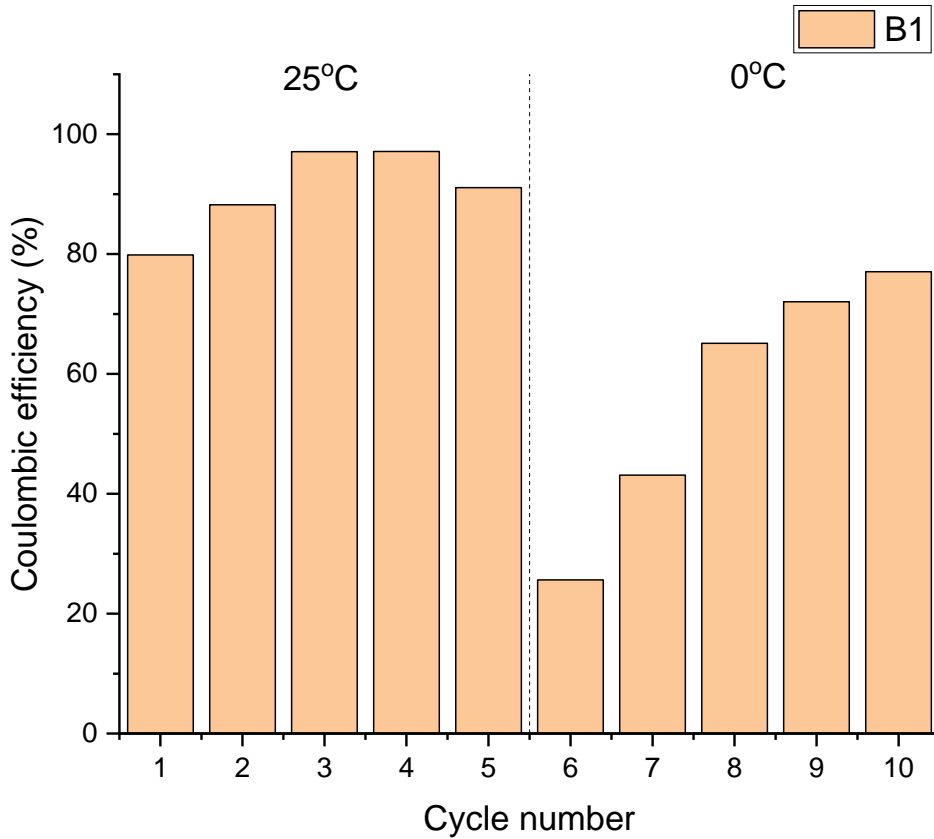
Figure 5-26: Coulombic efficiency of the same Li/graphite half-cell with LP40 electrolyte cycled at different temperatures; 1st – 5th at 25°C and 6th – 10th at 0°C. Battery 1 had C-rate of 0.00642 A. (weight – 0.02919 g).

Figure 5-27 represents the discharge capacity (half-cell) and irreversible capacity loss of the same Li/graphite half-cell with LP40 electrolyte at different cycling temperatures. Very small discharge capacity and irreversible charge capacity loss were occurred in each cycle at 25°C due to an experimental error. The discharge capacity was lower than 1 mAh/g and the irreversible charge capacity loss lower than 0.01 mAh/g which does not make sense at all based on all previous results in Chapter 5. The expected result was supposed to have capacity close to the theoretical value, 372 mAh/g and highest irreversible charge capacity loss in 1st cycle. Hence, the 25°C cannot be further analysed.

At 0°C, the discharge capacity and the irreversible charge capacity loss were decreased over cycle where a cell might have some partial freezing of LP40 electrolyte although the complete freezing point is -18.1°C [92]. Highest irreversible charge capacity loss was shown in 6th cycle because this was the first cycle after the cycling temperature was lowered to 0°C in which electrolyte stabilisation and further SEI growth possibly occur. Decrease in irreversible charge capacity loss was an expected result because the electrolyte phase will be stabilised over cycle.
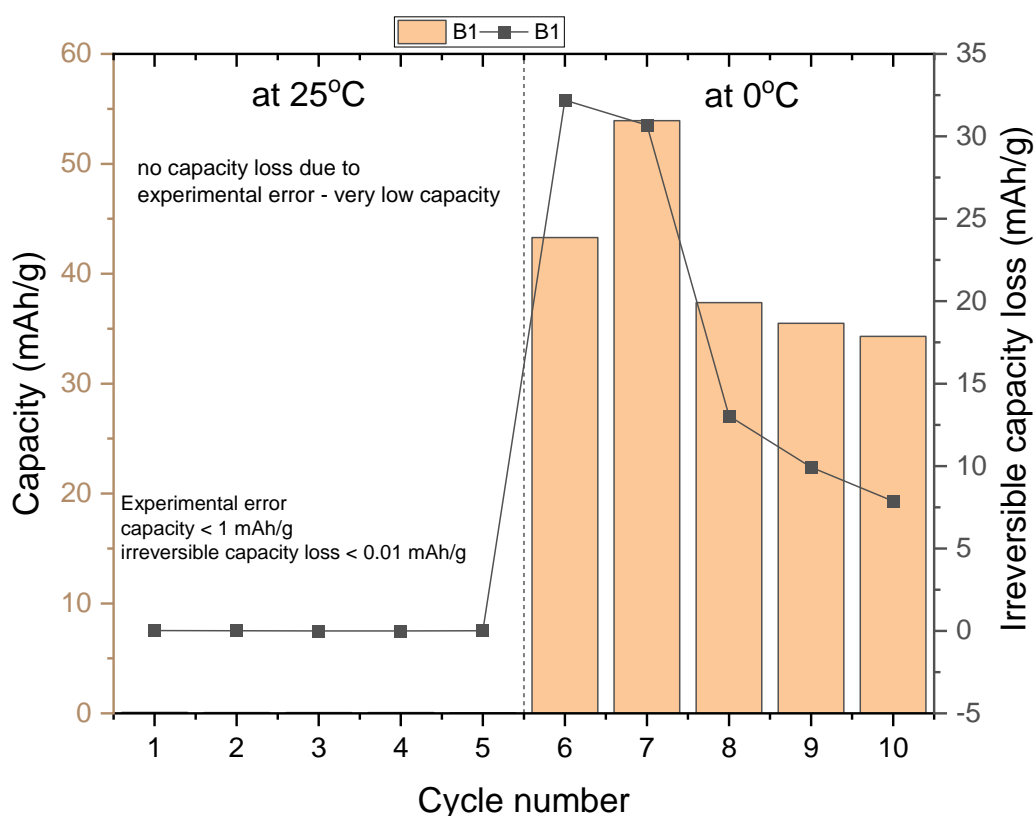
Figure 5-27: Discharge capacity (half-cell) and irreversible charge capacity of the same Li/graphite half-cell with LP40 electrolyte cycled at different temperatures; $1^{st} - 5^{th}$ at 25^oC and $6^{th} - 10^{th}$ at 0^oC. Battery 1 had C-rate of 0.00642 A. (weight – 0.02919 g)

5.4.2.3 LP40 electrolyte + 10% FEC additive

Figure 5-28 indicates the discharge/charge cycles of the two Li/graphite half-cells at different cycling temperatures using LP40 electrolyte with 10% FEC additive. In this section, FEC additive was used to find out whether the battery performance at 0°C changes or not. It is already known that FEC additive can improve the stability of the SEI layer [28] by forming more LiF components to the SEI layer. Although 10% FEC additive was added to LP40 electrolyte, the cells produced significantly fewer capacities than the previous result of Figure 5-23 in section 5.4.2.1 which had much higher capacities using LP30 electrolyte. In addition, both cells had much faster discharge/charge cycles than LP30 electrolyte. Although FEC is widely used as an electrolyte additive where it improves the stability of the SEI layer [28], it can be assumed that it does not improve the produced capacity at low cycling temperatures. Unlike other previous low-temperature results, discharge/charge cycle of the 25°C were similar to the 0°C possibly due to the better quality and the stability of the SEI layer was formed due to FEC additive.

Figure 5-28: Voltage vs Capacity graphs of the two Li/graphite half-cells with LP40 electrolyte + 10% FEC additive cycled at different temperatures; 1st – 5th at 25°C and 6th – 10th at 0°C. Battery 1 had C-rate of 0.00701 A. (weight – 0.03094 g), Battery 2 had C-rate of 0.00710 A. (weight - 0.03121 g).

Figure 5-29 below shows the coulombic efficiency of the two same Li/graphite half-cells with LP40 electrolyte + 10% FEC additive based on change in temperatures. Both cells showed the lowest coulombic efficiency in 1st cycle because most of the SEI layer is formed in 1st cycle after an intact SEI layer is formed in ageing time. Delithiation (charge in half-cell) will have less Li-ions for intercalation than the lithiation (discharge in half-cell) because some Li-ions are involved in SEI formation and irregular capture in graphene layers. From 2nd cycle onwards, both cells showed increase in the coulombic efficiency until 5th cycle close to an ideal value of 99%. From this, it can be determined that all cells had good SEI layer formed in ageing time and 1st cycle because the efficiency in 2nd cycle was suddenly increased. Smooth lithiation/delithiation process is expected at 25°C due to good ionic conductivity of the LP40 electrolyte. Unlike previous LP40 results in Figure 5-26, relatively higher coulombic efficiencies were shown at 0°C for LP40 electrolyte with 10% FEC additive results. At 0°C, relatively less coulombic efficiency was estimated due to the limitation of the LP40 electrolyte having an unstable partial freezing phase. Instead, both cells showed increase in efficiency over cycle. From

this, it can be assumed that FEC additive improved the stability and the quality of the SEI layer that helps better battery efficiency forming LiF to the SEI layer.
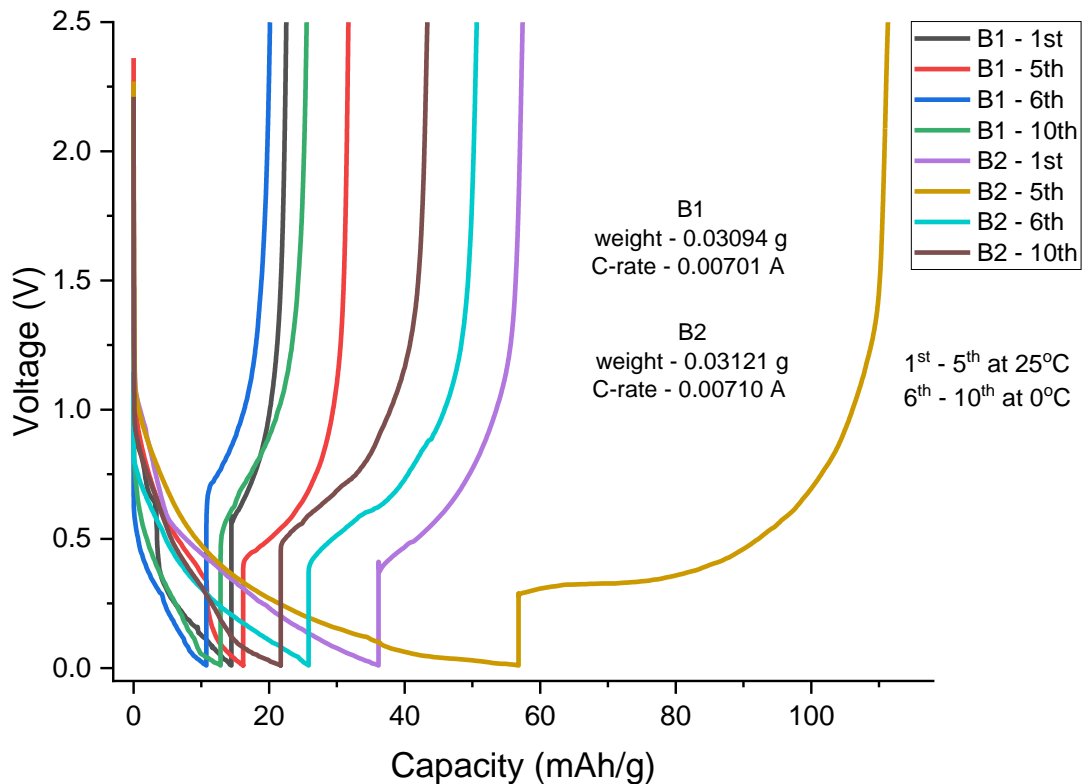

Figure 5-29: Coulombic efficiency of the two same Li/graphite half-cells with LP40 electrolyte + 10% FEC additive cycled at different temperatures; $1^{st} - 5^{th}$ at $25^{o}C$ and $6^{th} - 10^{th}$ at $0^{o}C$. Battery 1 had C-rate of 0.00701 A. (weight – 0.03094 g), Battery 2 had C-rate of 0.00710 A. (weight - 0.03121 g)

Figure 5-30 below shows the discharge capacity (half-cell) and the irreversible charge capacity loss of the same two tested cells with LP40 electrolyte and 10% FEC additive based on temperature. Overall, Battery 1 had relatively less discharge capacity than Batter 2 possibly due to either lower weight of the artificial graphite electrode or poor SEI layer was formed in Battery 1. Both cells showed increase in discharge capacity over cycle at 25°C. Theoretically, both cells should have decrease in capacity over cycle as more Li-ions are consumed over cycle. Previous hypothesis in section 5.2 and 5.3 was that if capacity increase over cycle, it is assumed as either poor SEI formation in ageing time and 1st cycle and the graphite electrode not fully wetted by electrolyte or the electrode compressed too much by the coin cell. Both cells were expected to have better SEI formation than all previous cells due to FEC additive that stabilise the SEI layer by forming LiF [28]. Hence, the hypothesis can be narrow downed to either the electrode is not fully wetted in initial cycles, or the electrode is compressed too much by the coin cell.

The irreversible charge capacity loss of the 1st cycle of the two cells clearly shows that parasitic reaction occurred mostly due to SEI formation. The highest irreversible charge capacity loss was achieved because charge capacity is relatively higher than discharge capacity since bindings of Li-ions are not used in further discharge but are involved in SEI formation and irreversible capture in graphite anode surface. Both cells had relatively higher irreversible charge capacity loss at 25°C than at 0°C. From the 7th cycle onwards, it was close to 0 which means similar amount of lithiation/delithiation occurred in half-cell discharge/charge cycle. This is possibly due to the FEC additive because it improves the stability and elasticity of the SEI layer [28] although possibly unstable LP40 electrolyte phase was expected due to the partial freezing at 0°C.
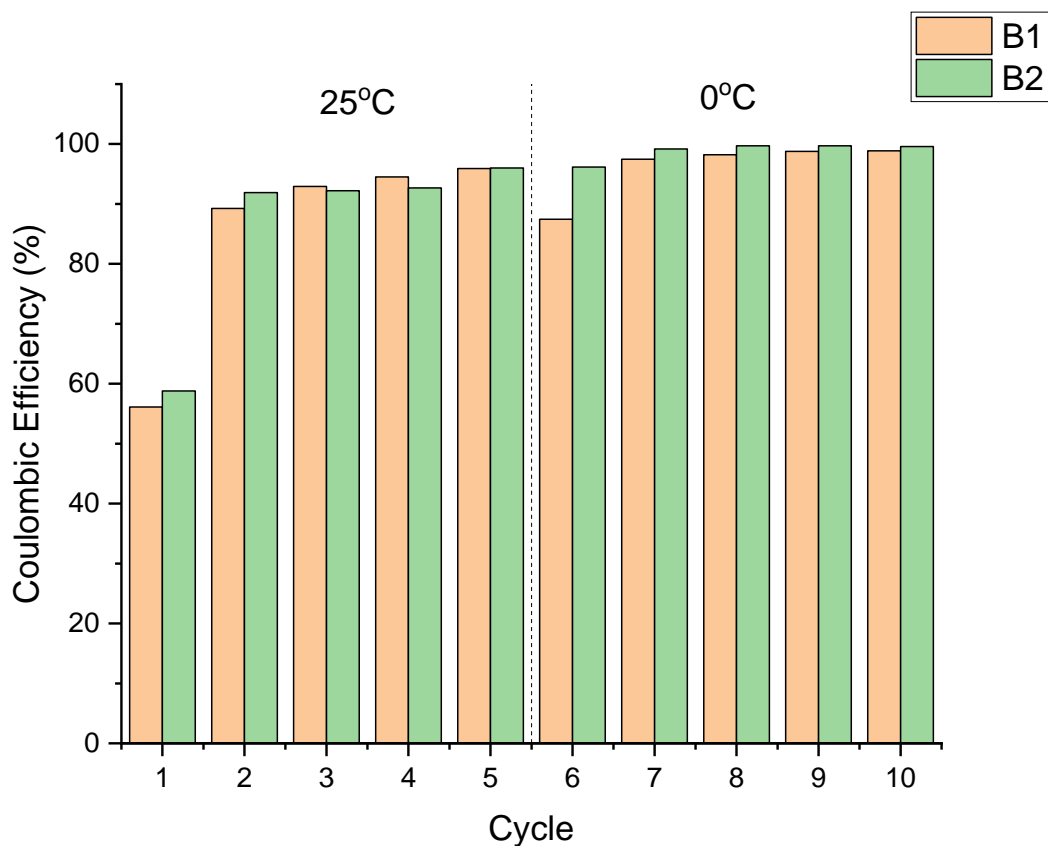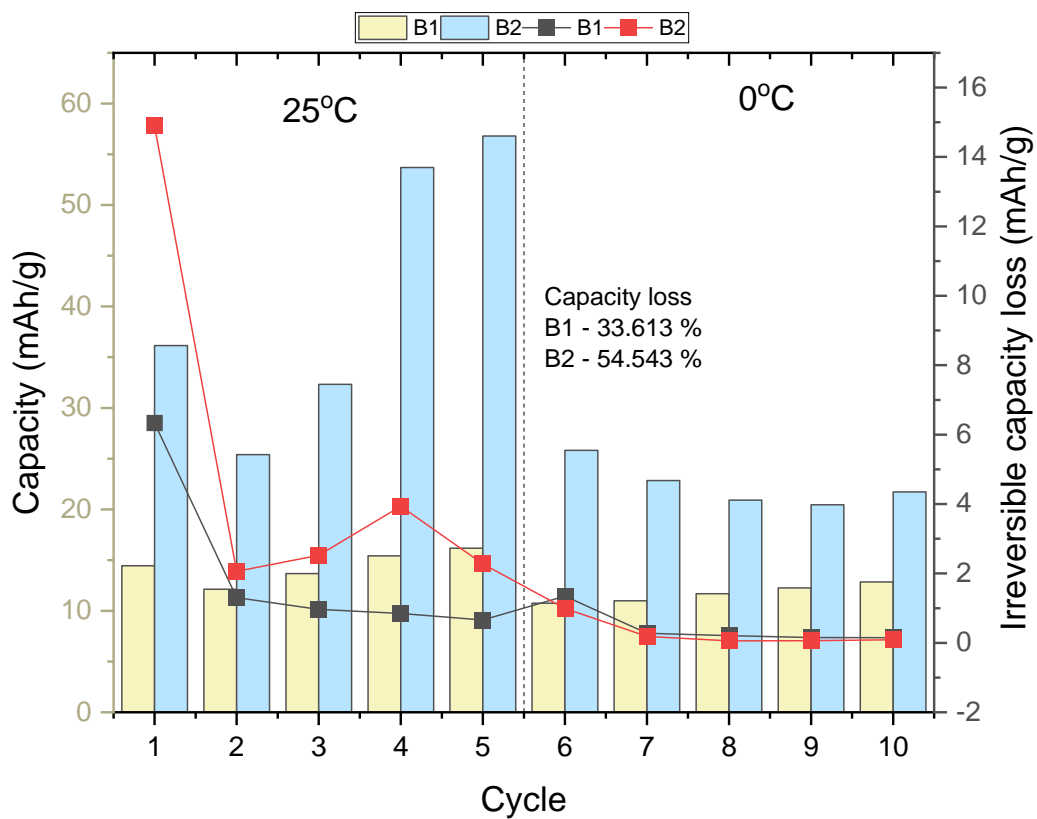

Figure 5-30: Discharge capacity (half-cell) and irreversible charge capacity of the same two Li/graphite half-cells with LP40 electrolyte + 10% FEC additive cycled at different temperatures; 1st – 5th at 25°C and 6th – 10th at 0°C. Battery 1 had C-rate of 0.00701 A. (weight – 0.03094 g), Battery 2 had C-rate of 0.00710 A. (weight - 0.03121 g)

5.4.3 Customised battery electrolyte

This stage of the experiment is similar to previous section 5.4.2 but uses different compositions of electrolytes to understand the effect of battery performance based on the temperature change in between the battery cycle. Previously, LP30, LP40, and LP40 with 10% FEC additive were used. This section introduces some customised electrolytes to understand the change in battery performance

with different compositions of the electrolyte having EC, DMC, DEC, and EMC solvent. The total battery cycle is limited to ten cycles; the first five cycles are at 25°C, and the last five cycles are at 0°C which was similar as section 5.4.2. From this, it can be found out whether better SEI formation at 25°C will improve the low-temperature battery performance or not based on the various customised battery electrolytes. These results will be compared with section 5.4 results for further analysis later on.

5.4.3.1 Experimental setup

The similar galvanostatic Li/graphite half-cells are built with a graphite anode and Lithium metal as a reference and counter electrode. Same experimental methods and materials were used as mentioned in Section 3.1.2. The main reason for using diverse electrolytes is to find out not only the effects of types of electrolytes on their low-temperature battery performance but also to understand their relationship with the SEI layer. This is the list of three electrolytes that were used to obtain the experimental data in this section. The customised electrolytes compositions are listed as a table 5-2 below.

- 1M of $LiPF_6$ in EC/DMC/EMC = 1.5/2/1.5 (v/v) (Customised)
- 1M of $LiPF_6$ in EC/DEC/EMC = 2.5/1/1.5 (v/v) (Customised)
- 1M of $LiPF_6$ in EC/DEC/DMC/EMC = 2/1/0.5/1.5 (v/v) (Customised)

Table 5-2: Detailed compositions of three customised electrolyte used for galvanostatic Li/graphite half-cells cycled 10 times at different temperatures; 25°C and 0°C

Electrolyte A	+	Electrolyte B	Customised electrolyte
1M of $LiPF_6$ in EC/EMC = 50/50 (v/v) (Sigma Aldrich) 15mL		1M of $LiPF_6$ in DMC (Sigma Aldrich) 10mL	1M of $LiPF_6$ in EC/DMC/EMC = 7.5/10/7.5 (volume) 25mL
1M of $LiPF_6$ in EC/EMC = 50/50 (v/v) (Sigma Aldrich) 15mL		1M of $LiPF_6$ in EC/DEC = 50/50 (v/v) (Sigma Aldrich) 10mL	1M of $LiPF_6$ in EC/DEC/EMC = 12.5/5/7.5 (volume) 25mL

Electrolyte A	+	Electrolyte B	+	Electrolyte C	Customised electrolyte
1M of $LiPF_6$ in EC/DEC = 50/50 (v/v) (Sigma Aldrich) 5mL		1M of $LiPF_6$ in EC/EMC = 50/50 (v/v) (Sigma Aldrich) 15mL		1M of $LiPF_6$ in DMC = (Sigma Aldrich) 5mL	1M of $LiPF_6$ in EC/DMC/DEC/EMC = (10/5/2.5/7.5) (volume) 15mL

Three customised electrolytes are used so that comparative study can be done with previous low-temperature data in Section 5.4.2. In addition, its effect in the room and low temperature on the

battery function can be stated by comparing with other previously investigated electrolytes [30, 42, 48] later on. As mentioned in section 2.4.2, electrolyte composition with EMC is more helpful to achieve better low-temperature battery function. Hence, all three customised electrolytes will contain EMC components but with different compositions based on the electrolyte available from the lab. This stage of the experiment is not finding the perfect electrolyte composition for the low-temperature system but more focused on understanding the effect of EMC added to the common battery electrolyte LP30 and LP40 and analysing its behaviour based on temperature.

Each battery grade solution is carefully measured with a syringe and Eppendorf. Since the magnetic stirrer was not available due to faulty, the solutions are added into a 58ml Thinky container (Umano UG) and it was kept for at least 48 hours or more so that the mixed solution can decompose naturally. All work was done in an argon-filled glovebox with H_2O and O_2 both below 0.1 ppm.

Other fabrication processes such as glass fibre separators and crimping the half coin cells are explained in Section 3.1.2. The charge rate of all built batteries was kept constant as 0.1C (C/10) because it is a common value to provide enough capacity to the battery as a function of time. This means it takes 10 hours to discharge the battery and vice versa. The cells were discharged first but similarly, the constant current was applied on the discharge/charge process because the main interest is the charge capacity of a battery to understand how the graphite anode can accept the Li-ions.

5.4.3.2 Results

5.4.3.2.1 EC/DMC/EMC

Figure 5-31 represents the discharge/charge curve of the two Li/graphite half-cells at different cycling temperatures using 1M of $LiPF_6$ in EC/DMC/EMC = 1.5/2/1.5 (v/v) (Customised). At 25°C, both cells showed expected result having highest discharge/charge state in 1st cycle and they decrease over cycle as Li-ions are consumed more and more. In addition, good SEI formation occurred in 1st and 5th cycle because the discharge capacity started to increase when the potential reach the onset voltage of the SEI formation 0.8 V until graphite stabilisation start taking place around 0.3 V. Then the discharge capacity increase until close to the theoretical value of 372 mAh/g at 0.01 V. By having multiple cycles at room temperature, a better SEI layer expected to be formed because of the good diffusivity of Li-ions, and the ionic conductivity of the customised electrolyte.

From the 6th cycle to the 10th cycle, the graphs were shifted towards the left because the cycling temperature was lowered to 0°C which leads to reduced ionic conductivity and low mobility of ions can be achieved due to partial freezing of customised electrolyte similar as section 5.4.2 results. Therefore, both cells had relatively faster discharge/charge cycles with relatively low capacity

produced in a short time. This can be assumed as either more partial freezing of the electrolyte occurred over cycle or more Li-ions were consumed over cycle.
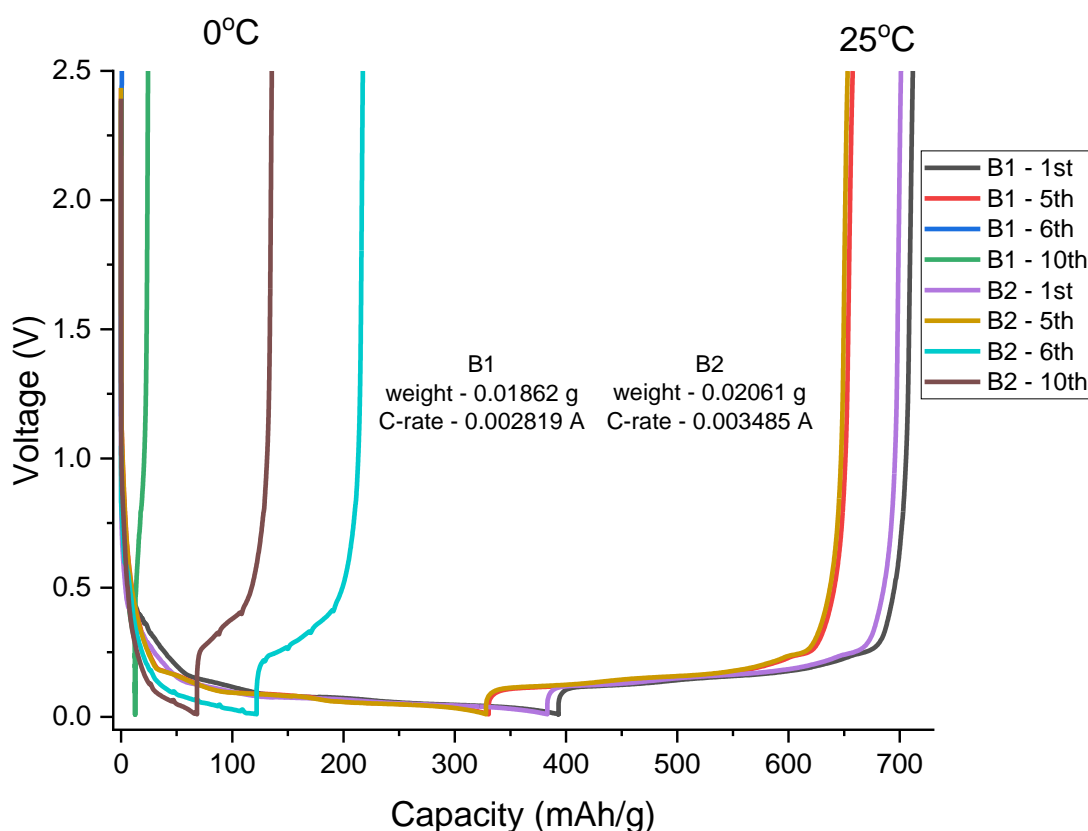

Figure 5-31: Voltage vs Capacity graphs of the two Li/graphite half-cells with 1M of LiPF$_6$ in EC/DMC/EMC = 1.5/2/1.5 (v/v) (Customised) cycled at different temperatures; 1st – 5th at 25°C and 6th – 10th at 0°C. Battery 1 had C-rate of 0.002819 A. (weight – 0.01862 g), Battery 2 had a C-rate of 0.003485 A. (weight – 0.02061 g).

Figure 5-32 below represents the coulombic efficiency of the two same Li/graphite half-cells with 1M of LiPF$_6$ in EC/DMC/EMC = 1.5/2/1.5 (v/v) (Customised) based on change in temperatures. At 25°C, both cells showed the lowest coulombic efficiency in 1st cycle because most of the SEI layer is formed in 1st cycle after an intact SEI layer is formed in ageing time. Delithiation (charge in half-cell) will have less Li-ions for intercalation than the lithiation (discharge in half-cell) because some Li-ions are involved in SEI formation and irregular capture in graphene layers. From 2nd cycle onwards, both cells showed increase in the coulombic efficiency until 5th cycle close to an ideal value of 99%. From this, it can be determined that all cells had good SEI layer formed in ageing time and 1st cycle because the efficiency in 2nd cycle was suddenly increased. Smooth lithiation/delithiation process is expected at 25°C due to good ionic conductivity of the customised electrolyte.

At 0°C, relatively less coulombic efficiency was estimated due to the possible partial freezing of customised electrolyte having an unstable phase. However, Battery 2 produced similar coulombic

efficiencies as 25°C results possibly due to the EMC solvent having lowest melting point (-55°C) among EC and DMC. There was unexpected error shown in 6th cycle for Battery 1 having 0 coulombic efficiency because there was no discharge capacity (half-cell) produced in 6th cycle. If only delithiation process was calculated as charge capacity (half-cell), it can be assumed as no Li-ions intercalated to the graphite anode but only Li-ions deintercalated to the metallic Li. These Li-ions are possibly from the irregular captured in between graphene layers in ageing time.
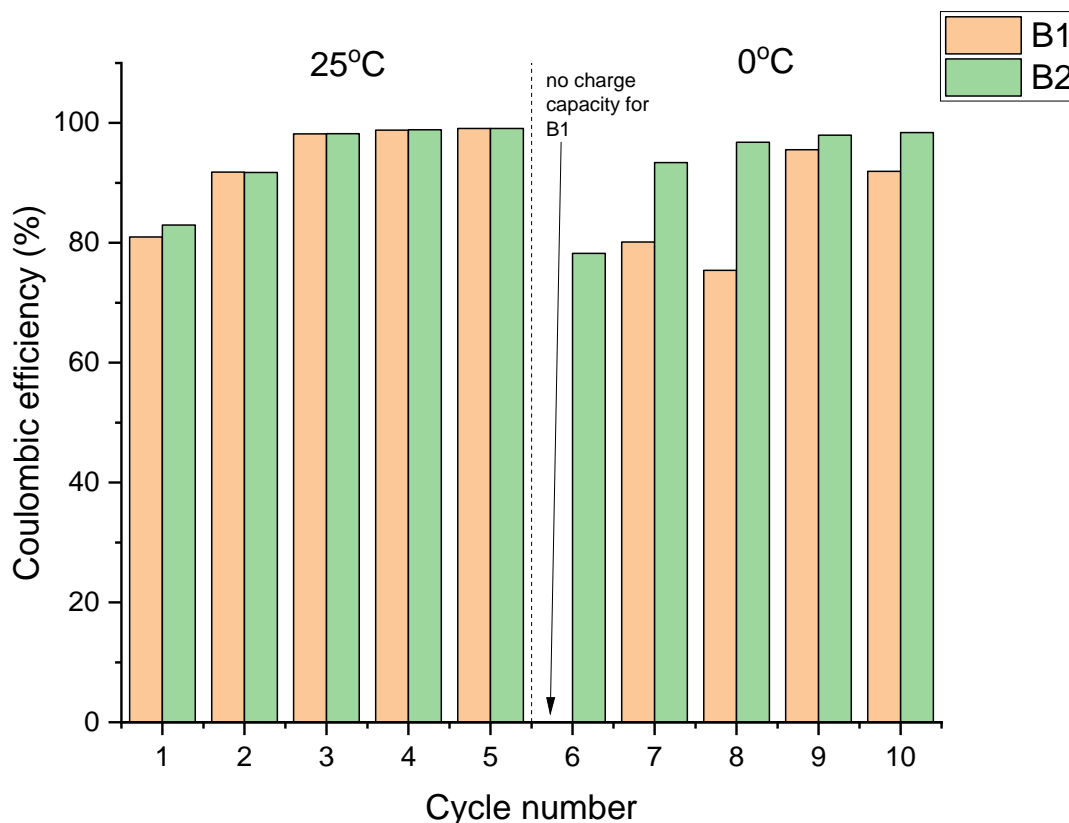
Figure 5-32: Coulombic efficiency of the two same Li/graphite half-cells with 1M of LiPF$_6$ in EC/DMC/EMC = 1.5/2/1.5 (v/v) (Customised) cycled at different temperatures; 1st – 5th at 25°C and 6th – 10th at 0°C. Battery 1 had C-rate of 0.002819 A. (weight – 0.01862 g), Battery 2 had a C-rate of 0.003485 A. (weight – 0.02061 g)

Figure 5-33 below shows the discharge capacity (half-cell) and the irreversible charge capacity loss of the same two tested cells with 1M of LiPF$_6$ in EC/DMC/EMC = 1.5/2/1.5 (v/v) (Customised) cycled at different temperatures. Overall, Battery 1 had relatively less discharge capacity than Batter 2 possibly due to poor SEI layer was formed in ageing time and in 1st cycle. At 25°C, both cells showed similar to the theoretical results having decrease in capacity over cycle as more Li-ions are consumed over cycle. In addition, both cells had highest discharge capacity due to most of the SEI formation is occurred in 1st cycle. At 0°C, they produced significantly less discharge capacity over cycle due to unstable partial freezing of the customised electrolyte. When the temperature was lowered to 0°C, there were more

than 62 % capacity was lost. The capacity loss of the Battery 1 was estimated in between 5th to 7th cycle because of an error occurred having 0 discharge capacity produced in 6th cycle. Overall, Battery 2 produced comparatively more discharge capacity than Battery 1 at 0°C possibly due to better SEI formation in Battery 2.

The irreversible charge capacity loss of the 1st cycle of the two cells clearly show that parasitic reaction occurred mostly due to SEI formation because the highest irreversible charge capacity loss was achieved. The charge capacity is relatively higher than discharge capacity since bindings of Li-ions are not used in further discharge instead are involved in SEI formation and irreversible capture in graphite anode surface. At 25°C, both cells had decrease in irreversible charge capacity loss over cycle. Highest irreversible charge capacity loss was shown in 6th cycle for Battery 2 whereas Battery 1 had an experimental error occurred at 0°C. Then, it decreased over cycle which was close to 0 meaning similar amount of lithiation/delithiation occurred in half-cell discharge/charge cycle. The irreversible charge capacity loss of the 6th and 9th cycle for Battery 1 had negative value which means higher delithiation occurred compared to the lithiation process.

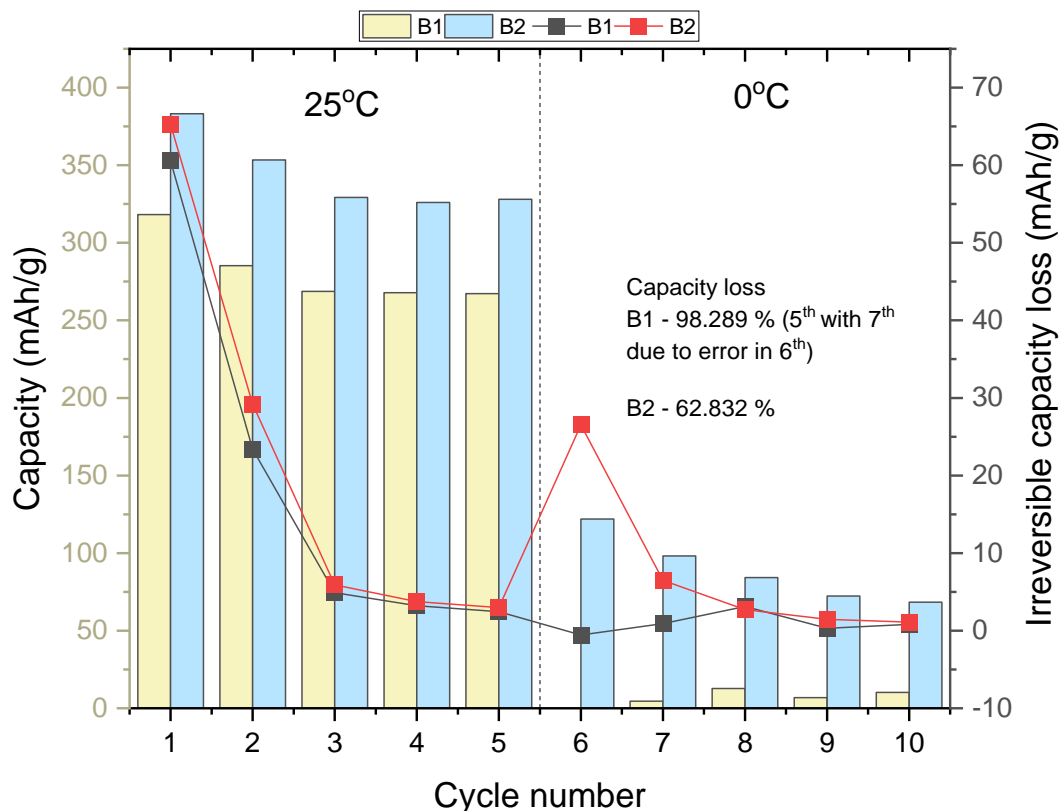*Figure 5-33: Discharge capacity (half-cell) and irreversible charge capacity of the same two Li/graphite half-cells with 1M of LiPF$_6$ in EC/DMC/EMC = 1.5/2/1.5 (v/v) (Customised) cycled at different temperatures; 1st – 5th at 25°C and 6th – 10th at 0°C. Battery 1 had C-rate of 0.002819 A. (weight – 0.01862 g), Battery 2 had a C-rate of 0.003485 A. (weight – 0.02061 g)*

Figure 5-34 represents the discharge/charge curve of the two Li/graphite half-cells at different cycling temperatures using 1M of LiPF$_6$ in EC/DEC/EMC = 2.5/1/1.5 (v/v) (customised). It is clearly divided into two sections; 1st and 5th cycle at 25°C on the right, 6th and 10th cycle at 0°C on the left. In addition, both cells showed expected result highest discharge/charge state in 1st cycle, and they decrease over cycle as Li-ions are consumed more and more. It can also be assumed that good SEI formation occurred in 1st and 5th cycle because the discharge capacity started to increase when the potential reach the onset voltage of the SEI formation 0.8 V until graphite stabilisation start taking place around 0.3 V. Then the discharge capacity increase until close to the theoretical value of 372 mAh/g at 0.01 V. By having multiple cycles at room temperature, a better SEI layer expected to be formed because of the good diffusivity of Li-ions, and the ionic conductivity of the customised electrolyte. Interestingly, both cells produced comparatively higher discharge capacity than the theoretical value, 372 mAh/g. This can be assumed as this set of electrolyte composition (EC/DEC/EMC) allows better battery performance with SEI formation compared to the other electrolyte (EC/DMC/EMC) in previous section 5.4.3.2.1.

From the 6th cycle to the 10th cycle, the graphs were shifted towards the left because the cycling temperature was lowered to 0°C which leads to reduced ionic conductivity and low mobility of ions can be achieved due to partial freezing of customised electrolyte similar as section 5.4.2 and 5.4.3.2.1 results. The 6th cycle of the Battery 1 (blue) shown fast discharge/charge cycle whereas Battery 2 had much better cycle showing smooth discharge/charge state (turquoise). The 10th cycle for Battery 1 (green) was much better than the 6th cycle which can be assumed as the electrolyte stabilisation occurred as the partial freezing will be stabilised over cycle. Battery 2 had similar discharge/charge state for both 6th and 10th which can be assumed as better SEI formation with good electrolyte stabilisation. Therefore, both cells had relatively faster discharge/charge cycles with relatively low capacity produced in a short time. This can be assumed as either more partial freezing of the electrolyte occurred over cycle or more Li-ions were consumed over cycle.
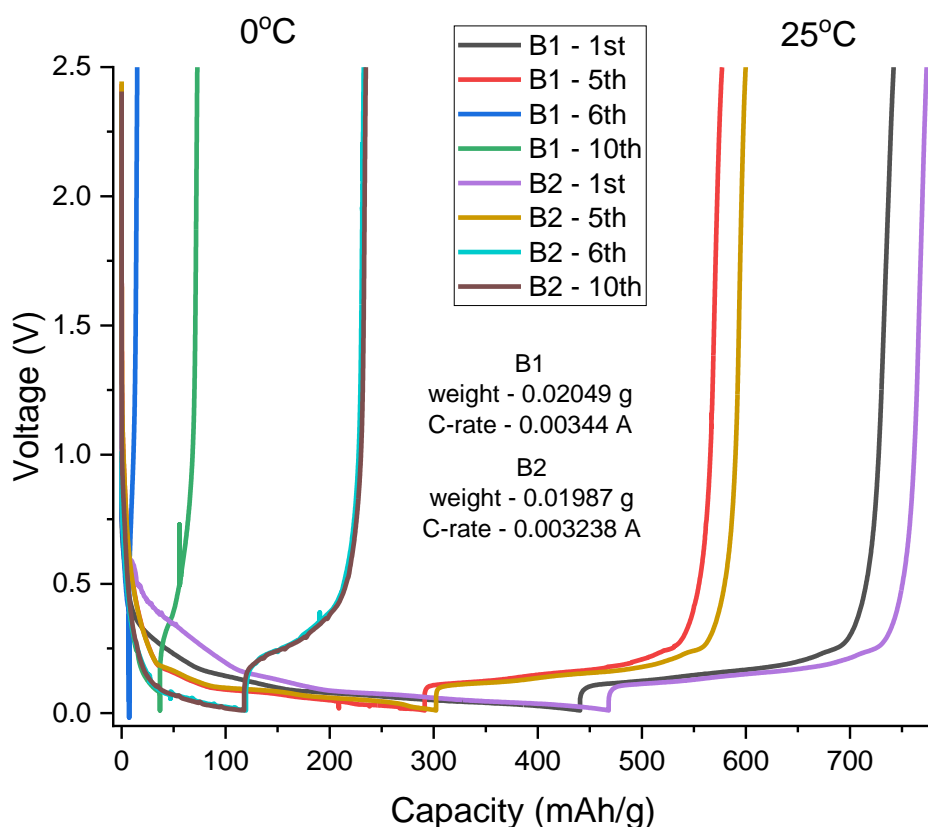
Figure 5-34: Voltage vs Capacity graphs of the two Li/graphite half-cells with 1M of LiPF$_6$ in EC/DEC/EMC = 2.5/1/1.5 (v/v) (customised) cycled at different temperatures; 1st – 5th at 25°C and 6th – 10th at 0°C. Battery 1 had C-rate of 0.00344 A. (weight – 0.02049 g), Battery 2 had a C-rate of 0.003238 A. (weight – 0.01987 g).

Figure 5-35 below represents the coulombic efficiency of the two same Li/graphite half-cells with 1M of LiPF$_6$ in EC/DEC/EMC = 2.5/1/1.5 (v/v) (Customised) based on change in temperatures. As expected, the efficiency of both cells in 1st cycle was the lowest possibly due to the parasitic reaction mostly SEI formation. Delithiation (charge in half-cell) will have less Li-ions for intercalation than the lithiation (discharge in half-cell) because some Li-ions are involved in SEI formation and irregular capture in graphene layers. The coulombic efficiency is expected to be close to 99% over cycle because more SEI layer growth is expected which means the amount of Li-ions intercalate/deintercalated will be similar over cycle. From 2nd cycle onwards, both cells showed increase in the coulombic efficiency until 5th cycle close to an ideal value of 99%. From this, it can be determined that all cells had good SEI layer formed in ageing time and 1st cycle because the efficiency in 2nd cycle was suddenly increased. Smooth lithiation/delithiation process is expected at 25°C due to good ionic conductivity of the customised electrolyte.

At 0°C, relatively less coulombic efficiency was estimated due to the possible partial freezing of customised electrolyte having an unstable phase. However, both cell had similar coulombic

efficiencies as 25°C results possibly due to the EMC solvent having lowest melting point (-55°C) as well as DEC solvent (-43°C). There was an interesting result shown in 6th cycle for Battery 1 having 108% coulombic efficiency which means higher discharge capacity than charge capacity in terms of full-cell. If delithiation is higher than the lithiation process at 0°C, this can be assumed as more Li-ions deintercalated to the metallic Li than the intercalation to the graphite anode by getting extra Li-ions from the irregular capture in between graphene layers occurred in ageing time and first few cycles at 25°C. Hence, it can be concluded that the EC/DEC/EMC composition of the electrolyte possibly showed an improvement of the low temperature performance having comparatively better efficiency than EC/DMC/EMC composition electrolyte in previous section 5.4.3.2.1.

Figure 5-35: Coulombic efficiency of the same two Li/graphite half-cells with 1M of LiPF$_6$ in EC/DEC/EMC = 2.5/1/1.5 (v/v) (customised) cycled at different temperatures; 1st – 5th at 25°C and 6th – 10th at 0°C. Battery 1 had C-rate of 0.00344 A. (weight – 0.02049 g), Battery 2 had a C-rate of 0.003238 A. (weight – 0.01987 g).

Figure 5-36 below shows the discharge capacity (half-cell) and the irreversible charge capacity loss of the same two tested cells with 1M of LiPF$_6$ in EC/DEC/EMC = 2.5/1/1.5 (v/v) (Customised) cycled at different temperatures. Overall, Battery 1 had relatively less discharge capacity than Batter 2 possibly due to poor SEI layer was formed in ageing time and in 1st cycle. At 25°C, Battery 2 showed similar to the theoretical results having decrease in capacity over cycle as more Li-ions are consumed over cycle.

Battery 1 had increase in capacity from 3rd until 5th cycle which can be assumed as due to the electrode not fully wetted in initial cycle because the capacity cannot increase over cycle theoretically. In addition, both cells had highest discharge capacity due to most of the SEI formation is occurred in 1st cycle. At 0°C, they produced significantly less discharge capacity over cycle due to unstable partial freezing of the customised electrolyte. When the temperature was lowered to 0°C, there were more than 60 - 97% capacity was lost for both cells. Overall, Battery 2 produced comparatively more discharge capacity than Battery 1 at 0°C possibly due to better SEI formation in Battery 2. It can be stated that at 0°C, the electrolyte stabilisation can be settled for few more cycles after the temperature change such as 7th cycle for Battery 2 having lowest discharge capacity in low-temperature.
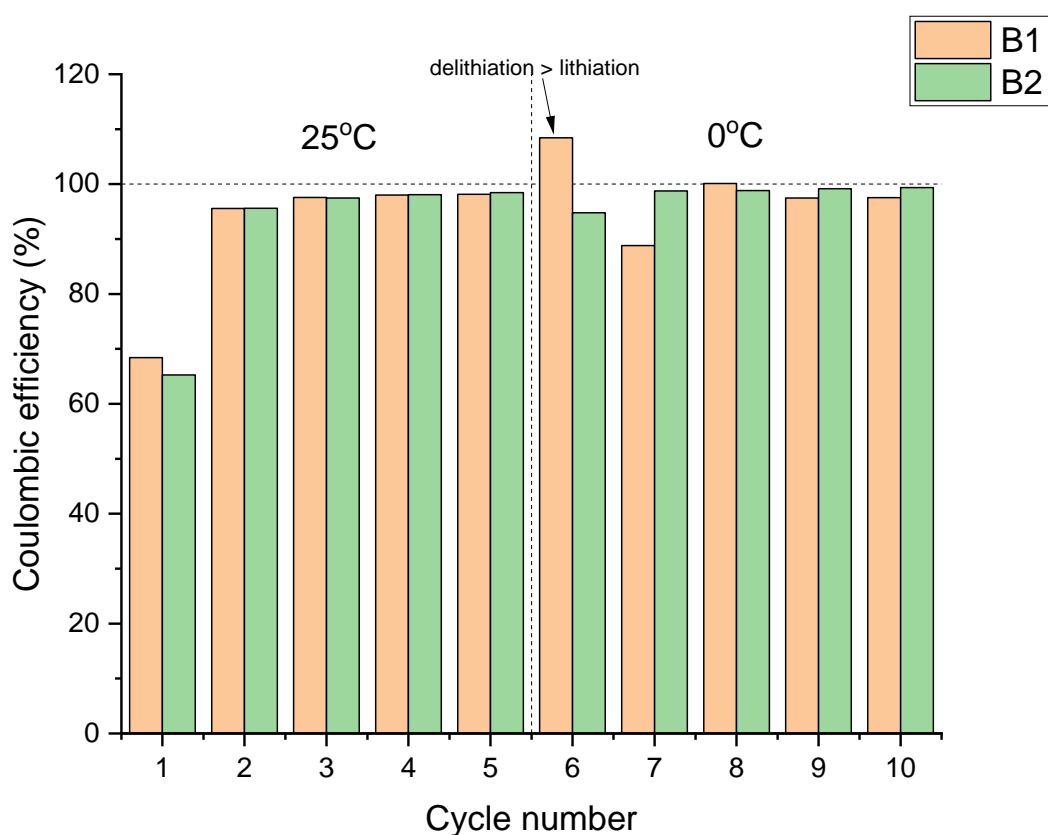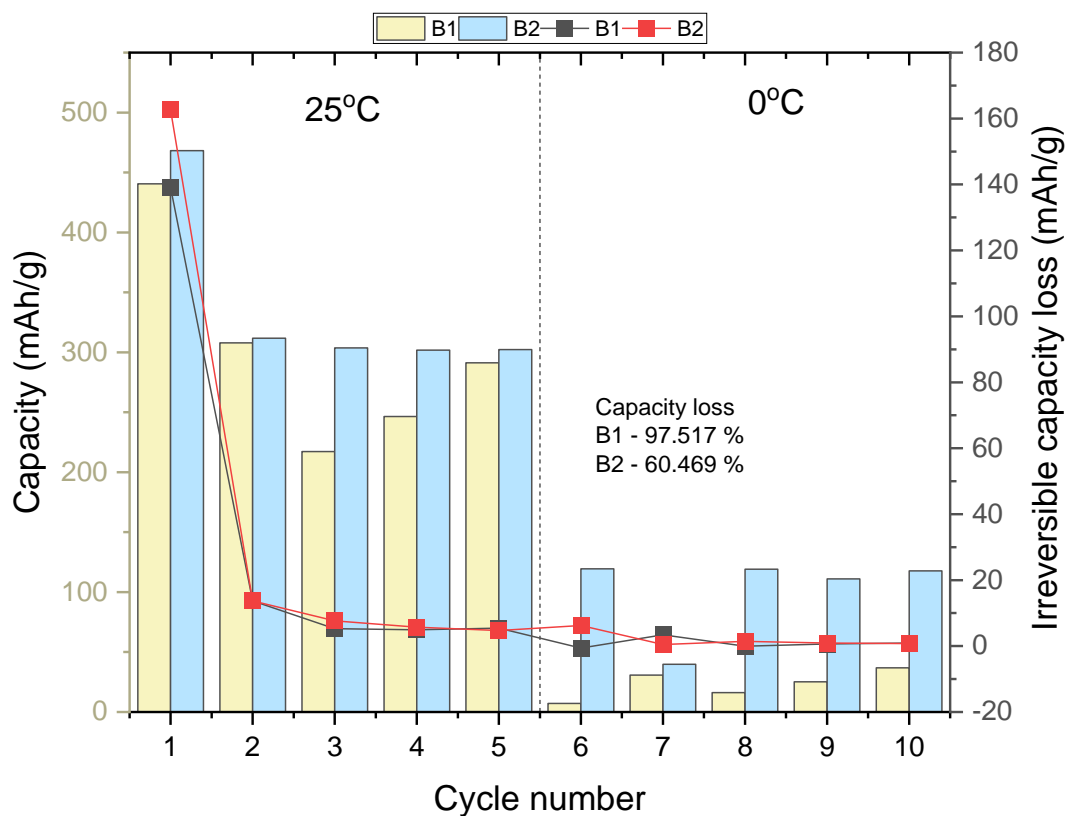

Figure 5-36: Discharge capacity (half-cell) and irreversible charge capacity of the same two Li/graphite half-cells with 1M of LiPF₆ in EC/DEC/EMC = 2.5/1/1.5 (v/v) (customised) cycled at different temperatures; 1st – 5th at 25°C and 6th – 10th at 0°C. Battery 1 had C-rate of 0.00344 A. (weight – 0.02049 g), Battery 2 had a C-rate of 0.003238 A. (weight – 0.01987 g

The irreversible charge capacity loss of the 1st cycle of the two same cells clearly show that parasitic reaction occurred mostly due to SEI formation because the highest irreversible charge capacity loss was achieved. The charge capacity (full-cell) is relatively higher than discharge capacity (full-cell) since bindings of Li-ions are not used in further discharge instead are involved in SEI formation and

irreversible capture in graphite anode surface. At 25°C, both cells had decrease in irreversible charge capacity loss over cycle which means the SEI layer was decently formed on graphite anode because similar amount of Li-ions are lithiated/delithiated. At 0°C, the irreversible charge capacity loss was decreased over cycle which can be assumed as better SEI formation for Battery 2. On the other hand, Battery 1 showed an oscillated irreversible charge capacity loss at 0°C possibly due to unstable SEI layer. Better SEI formation on graphite anode can hypothetically improve the capacity loss in low-temperature because the Battery 1 had 97% capacity loss whereas Battery 2 lost only 60%.

5.4.3.2.3 EC/DEC/DMC/EMC

Figure 5-37 represents the discharge/charge curve of the two Li/graphite half-cells at different cycling temperatures using EC/DEC/DMC/EMC = 2/1/0.5/1.5 (v/v) (customised). It is very clear that the discharge/charge curves at 25°C have smooth and longer graphs than at 0°C because of the good diffusivity of Li-ions, and the ionic conductivity of the customised electrolyte is expected at 25°C. In addition, both cells had highest discharge/charge state in 1st cycle, and they decrease over cycle as Li-ions are consumed more and more. From this, it can be assumed that good SEI formation occurred in 1st and 5th cycle because the discharge capacity started to increase when the potential reach the onset voltage of the SEI formation 0.8 V until graphite stabilisation start taking place around 0.3 V. Then the discharge capacity increase until close to the theoretical value of 372 mAh/g at 0.01 V. Better SEI layer expected to be formed having multiple cycles at 25°C because of the good diffusivity of Li-ions, and the ionic conductivity of the customised electrolyte. Once again, both cells produced comparatively higher discharge capacity than the theoretical value, 372 mAh/g which was similar as previous section 5.4.3.2.2. Hence, it can be hypothesised that the EC, DEC, and EMC solvents can improve the battery performance based on the electrolyte composition of (EC/DEC/DMC/EMC) and (EC/DEC/EMC) in section 5.4.3.2.2 This is just a simple hypothesis, so it needs further investigation in future.

From the 6th cycle to the 10th cycle, the graphs were shifted towards the left because the cycling temperature was lowered to 0°C which leads to reduced ionic conductivity and low mobility of ions can be achieved due to partial freezing of customised electrolyte similar as previous results (section 5.4.2, 5.4.3.2.1, and 5.4.3.2.2). Battery 1 had increase in discharge/charge cycle from 6th to 10th cycle possibly the electrolyte was stabilised in between the cycles. As mentioned before, the capacity cannot be increased over cycle because of limited Li-ions are available in a fully sealed battery. However, the discharge/charge state of the Battery 2 decreased over cycle even at 0°C. Hence, it can be assumed that Battery 2 is close to the theoretically expected battery.
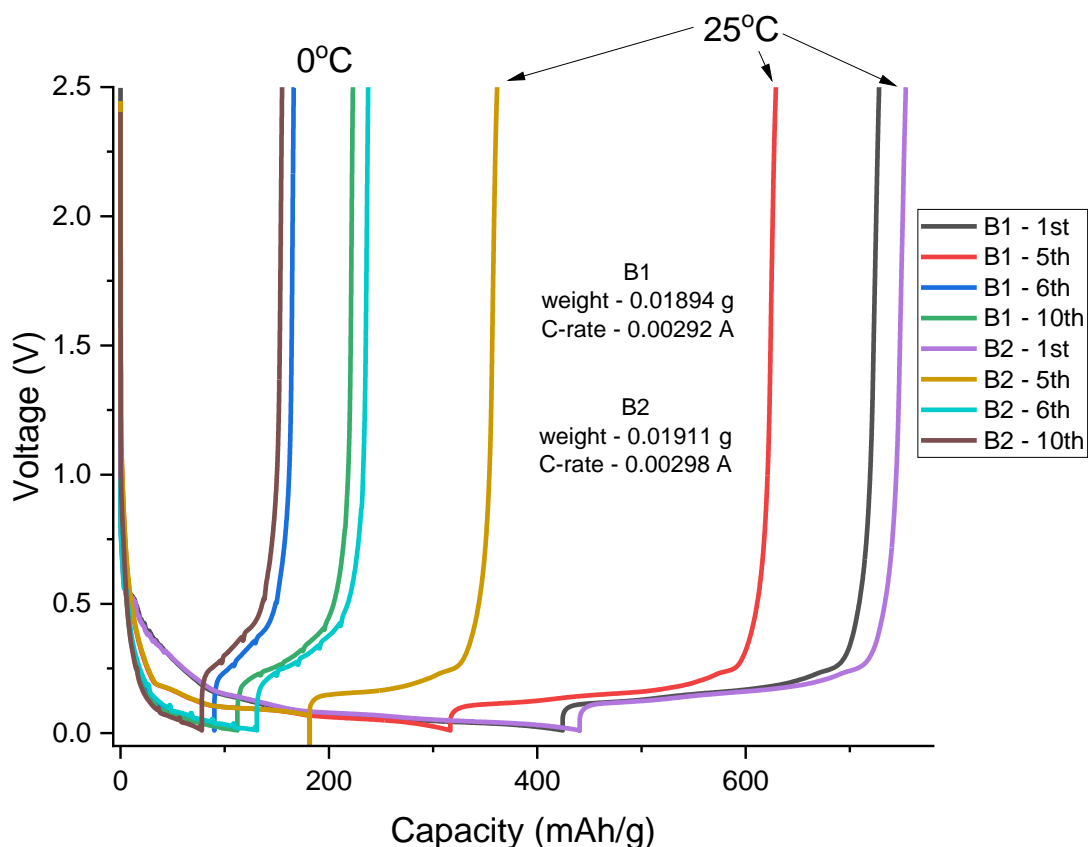
Figure 5-37: Voltage vs Capacity graphs of the two Li/graphite half-cells with 1M of LiPF$_6$ in EC/DEC/DMC/EMC = 2/1/0.5/1.5 (v/v) (Customised) cycled at different temperatures; $1^{st} - 5^{th}$ at 25^oC and $6^{th} - 10^{th}$ at 0^oC. Battery 1 had C-rate of 0.00292 A. (weight – 0.01894 g), Battery 2 had a C-rate of 0.00298 A. (weight – 0.01911 g).

Figure 5-38 below represents the coulombic efficiency of the two same Li/graphite half-cells with 1M of LiPF$_6$ in EC/DEC/DMC/EMC = 2/1/0.5/1.5 (v/v) (Customised) based on change in temperatures. As expected, the efficiency of both cells in 1st cycle was the lowest possibly due to the parasitic reaction mostly SEI formation. Delithiation (charge in half-cell) will have less Li-ions for intercalation than the lithiation (discharge in half-cell) because some Li-ions are involved in SEI formation and irregular capture in graphene layers. The coulombic efficiency of the two cells gradually increased close to the 99% over cycle because similar amount of Li-ions will be intercalated/deintercalated as further SEI layer formation over cycle. From this, it can be estimated that all cells had good SEI layer formed in ageing time and 1st cycle because the efficiency in 2nd cycle was suddenly increased. Smooth lithiation/delithiation process is expected at 25^oC due to good ionic conductivity of the customised electrolyte.

At 0^oC, relatively less coulombic efficiency was estimated in 6th cycle due to the possible partial freezing of customised electrolyte having an unstable phase. Both cells had the lowest efficiencies in 6th cycle, and it increased over cycle which was close to the theoretical expectations. Lowest coulombic

efficiency is expected in 6th cycle because it is the first cycle after the temperature changed to 0°C so highest resistance in electrolyte region is expected due to unstable electrolyte phase. The electrolyte stabilisation will occur over cycle, and this will be relaxed as much smoother lithiation/delithiation process can be expected over cycle. This set of electrolyte composition (EC/DEC/DMC/EMC) can be assumed as the best suitable mix of the electrolyte among section 5.4.3.2.1 and 5.4.3.2.2 results because it produced the most similar expected result as the theoretical expectation.

Figure 5-38: Coulombic efficiency of the same two Li/graphite half-cells with 1M of LiPF$_6$ in EC/DEC/DMC/EMC = 2/1/0.5/1.5 (v/v) (Customised) cycled at different temperatures; 1st – 5th at 25°C and 6th – 10th at 0°C. Battery 1 had C-rate of 0.00292 A. (weight – 0.01894 g), Battery 2 had a C-rate of 0.00298 A. (weight – 0.01911 g).

Figure 5-39 below represents the discharge capacity (half-cell) and the irreversible charge capacity loss of the same two tested cells with 1M of LiPF$_6$ in EC/DEC/DMC/EMC = 2/1/0.5/1.5 (Customised) cycled at different temperatures. Both cells showed an expected results having highest discharge capacity (half-cell) in 1st cycle and decrease over cycle at 25°C because the capacity should be decreased over cycle as Li-ions are consumed more and more. Both cells produced comparatively higher discharge capacity than the theoretical value, 372 mAh/g which was similar as previous section 5.4.3.2.2. Battery 1 produced more than 300 mAh/g until 5th cycle as well as Battery 2 except relatively small discharge capacity in 5th cycle. From this, it can be assumed that partial graphite exfoliation or

SEI cracks occurred because the discharge capacity decreased over cycle although there was a temperature changed to 0°C in 6th cycle. Battery 1 also showed a decrease in capacity from 6th cycle but not stable as Battery 2. Both cells had some capacity loss during temperature change but the capacity loss for Battery 2 was comparatively less than Battery 1.

Overall, Battery 2 had higher irreversible charge capacity loss than Battery 2 at 25°C and 0°C. In addition, both cells had highest irreversible charge capacity loss in 1st cycle due to parasitic reaction occur mostly SEI formation. It can be estimated that Battery 2 had better SEI formation than Battery 1 because it not only produced higher discharge capacity (half-cell) but also higher irreversible charge capacity loss was shown. More lithiation was occurred in discharging cell than delithation which the cell charges. At 0°C, relatively less irreversible charge capacity loss was obtained due to less capacity produced by the cell having unstable partial freezing of the electrolyte. Interestingly, both cells had highest irreversible charge capacity loss at 0°C in 6th cycle which means more lithiation occurred than delithiation process. From this, it can be hypothesised that the SEI formation takes place in the first cycle after the temperature change.

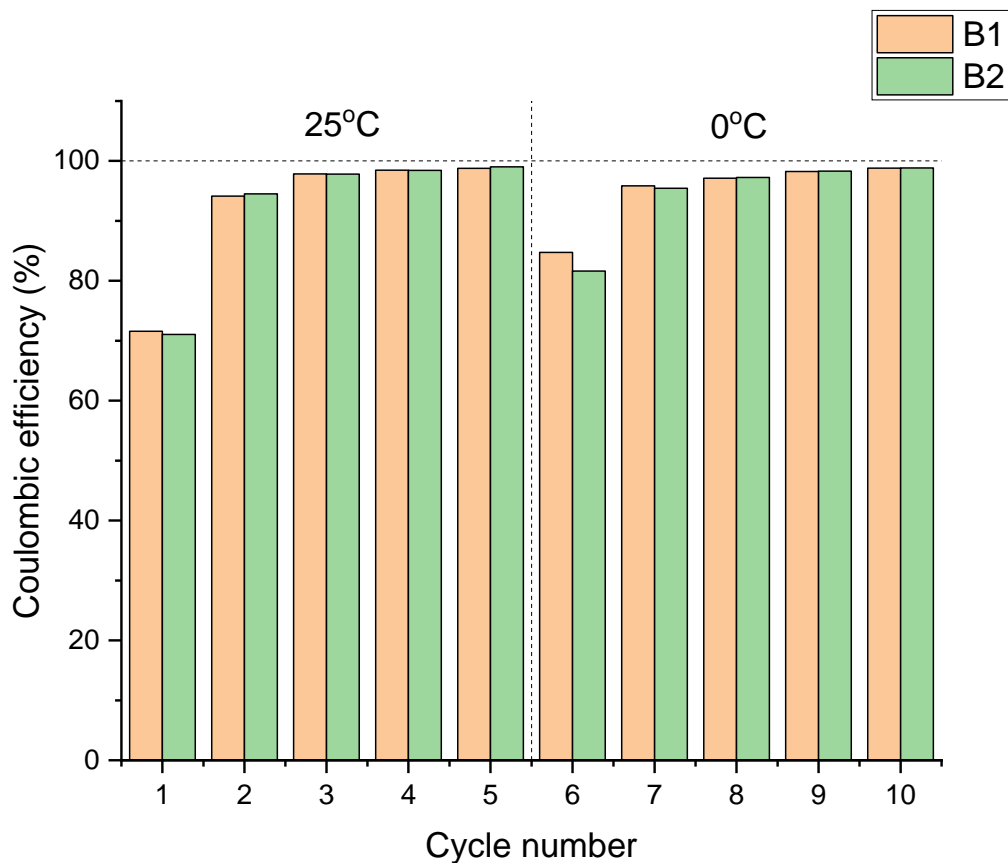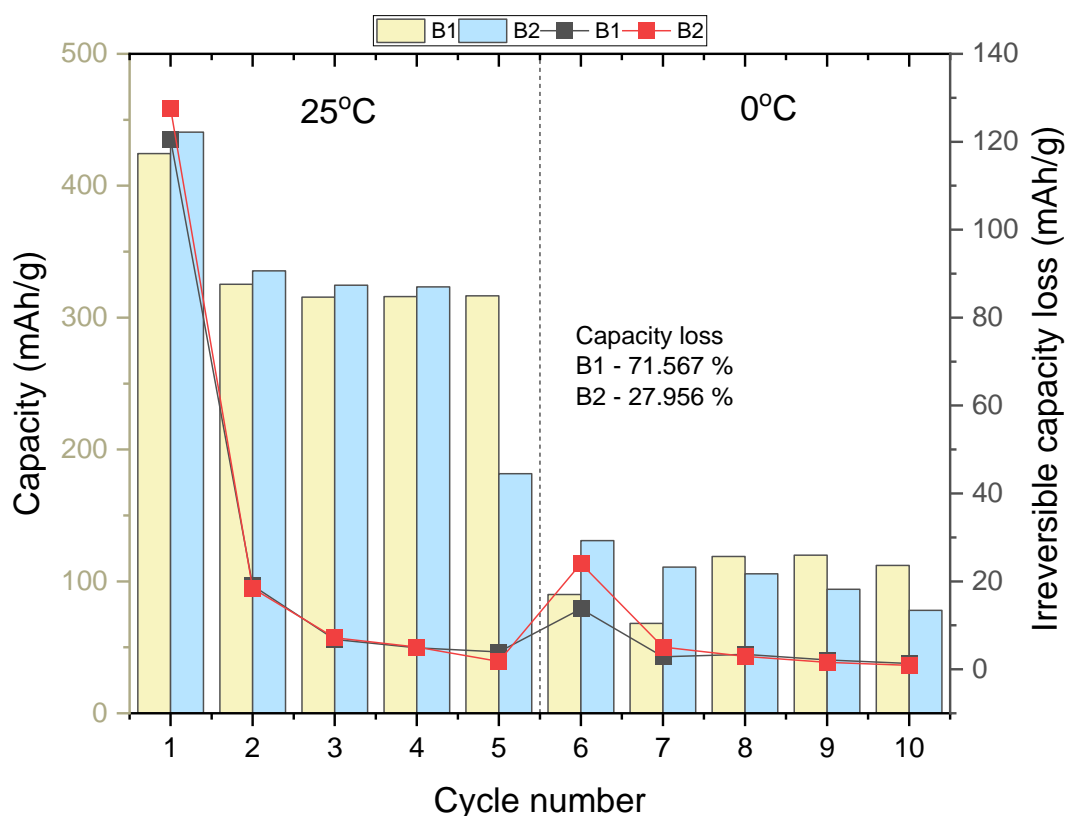*Figure 5-39: Discharge capacity (half-cell) and irreversible charge capacity of the same two Li/graphite half-cells with 1M of LiPF$_6$ in EC/DEC/DMC/EMC = 2/1/0.5/1.5 (v/v) (Customised) cycled at different temperatures; 1st – 5th at 25°C and 6th – 10th at 0°C. Battery 1 had C-rate of 0.00292 A. (weight – 0.01894 g), Battery 2 had a C-rate of 0.00298 A. (weight – 0.01911 g).*

5.4.4 Conclusion

The focus of this experiment was to understand how the performance of the Li/graphite half-cell change at 0°C with better SEI formation having five more cycles at 25°C using various electrolytes; LP30, LP40, LP40 + 10% FEC additive, and three customised electrolytes (refer section 5.4.3) which was shown below.

- 1M of $LiPF_6$ in EC/ DMC = 50/50 (v/v) (Sigma Aldrich) (LP30)

- 1M of $LiPF_6$ EC/DEC = 50/50 (v/v) (Sigma Aldrich) (LP40)

- 1M of $LiPF_6$ EC/DEC = 50/50 (v/v) (Sigma Aldrich) (LP40) with 10% FEC (98%, Alfa Aesar) additive

- 1M of $LiPF_6$ in EC/DMC/EMC = 1.5/2/1.5 (v/v) (Customised)

- 1M of $LiPF_6$ in EC/DEC/EMC = 2.5/1/1.5 (v/v) (Customised)

- 1M of $LiPF_6$ in EC/DEC/DMC/EMC = 2/1/0.5/1.5 (v/v) (Customised)
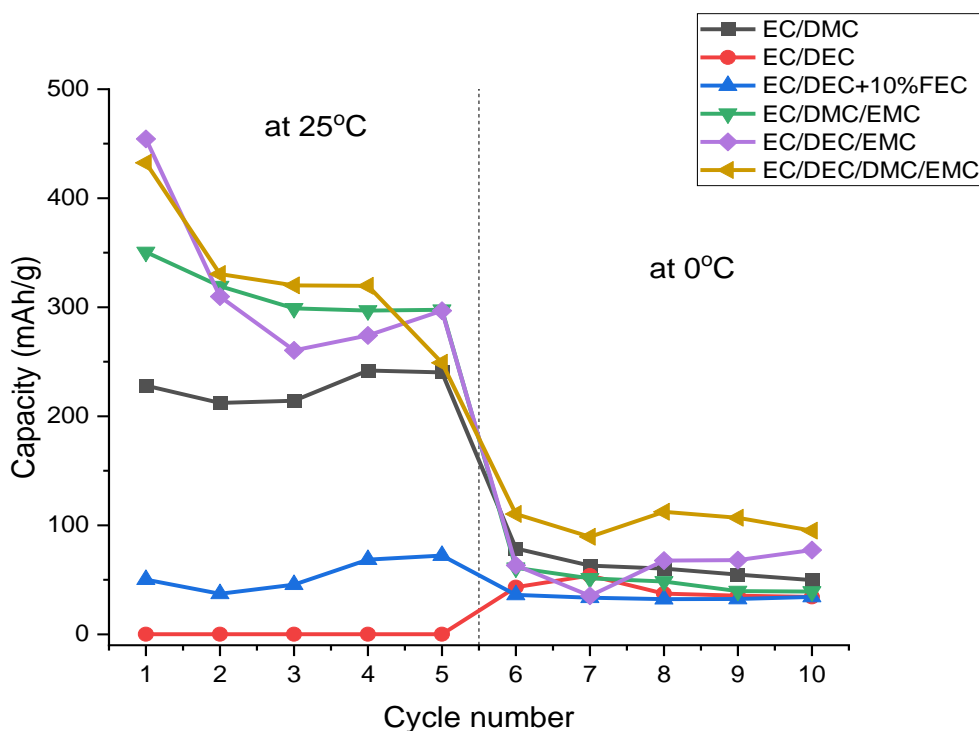
Figure 5-40: Discharge capacity of various electrolytes in each cycle based on temperatures; 1st to 5th – 25°C, 6th to 10th – 0°C. The data were obtained from taking average values of each section (5.4.2 and 5.4.3). The detailed composition of electrolytes are shown with bullet point above.

The average discharge capacity of the tested cells using various electrolytes based on temperature was shown in Figure 5-40 above. The data was obtained from the average discharge capacity of the tested cells in each section (5.4.2 and 5.4.3). The 25°C data of EC/DEC (LP40) for Figure 5-40 had an unforeseen error having capacities less than 1 mAh/g possibly due to the channel issue in MACCOR

chamber. In addition, the capacity loss for EC/DEC (LP40) was not shown because the 25°C data were error based so the capacity loss could not be estimated.
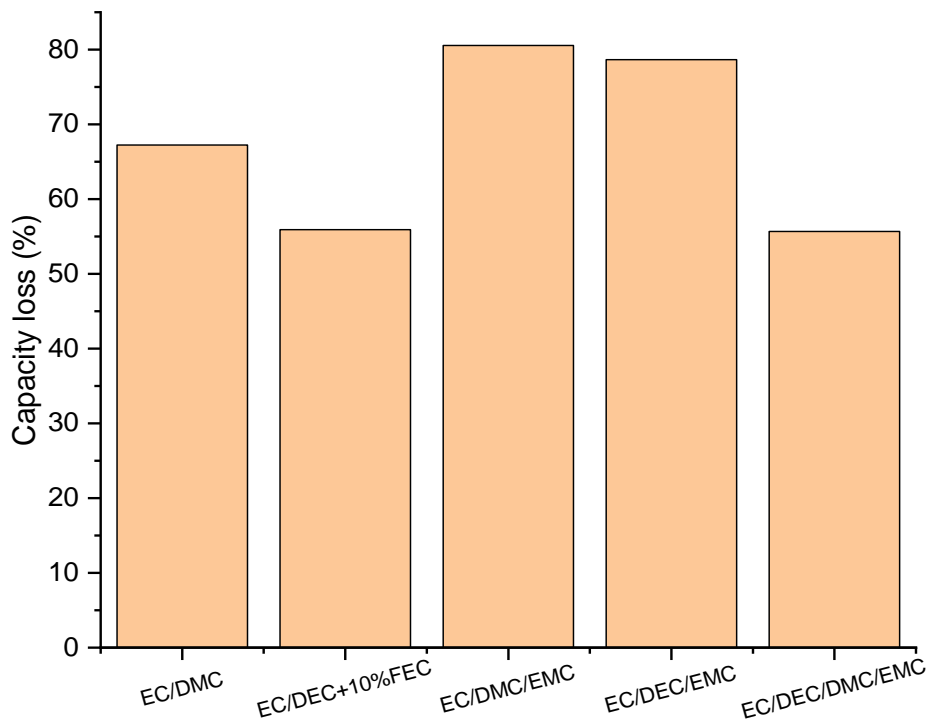
Figure 5-41: Capacity loss of the average tested cells using various electrolytes after temperature change from 25°C to 0°C. The data were obtained from taking average values of each section (5.4.2 and 5.4.3). The detailed composition of electrolytes are shown with bullet point above.

It can be concluded that relatively higher discharge capacities were produced at 25°C compared to the 0°C because of the unstable electrolyte phase mostly due to partial freezing. This section was focused to understand the effect of different types of electrolytes on battery performance based on the temperature change. Some customised electrolytes were addressed besides LP30 and LP40 with 10% FEC additive. The main reason was to understand the possible effects of the EMC solvent on the SEI formation and the low-temperature half-cell performance. An electrolyte composition with EC,DEC, and EMC can improve the low-temperature battery performance because both electrolytes (purple, orange) had relatively higher capacity than others. In addition, it was found that the more solvent is mixed, the better capacity was produced. However, EMC solvent could not solve the capacity loss at low temperatures as shown in Figure 5-41 below. FEC additive helped to reduce the capacity loss at low-temperature by having better SEI formation due to LiF components added to the SEI whereas other electrolytes still had significant capacity loss in between 5th and 6th cycle. However, FEC additive can only improve the capacity loss not the actual battery performance because the generated

capacities were comparatively less than other five electrolytes. To conclude, better SEI formation by having multiple discharge/charge cycles at 25℃ will improve the low-temperature battery performance having better capacity, coulombic efficiency with less capacity loss over cycle.

5.5 The importance of rest period

This stage of the experiment is focused on having no rest period during temperature change from 25℃ to 0℃. Previously, all tested cells had 2 hours rest period in between temperature change whereas, in this experiment, no rest period is given. This means after some room temperature cycles were done to form the SEI layer, the cycling temperature is lowered, and the cell instantly starts to discharge and charge. From this, it is expected to understand the importance of rest period during low cycling temperature change and to find out whether it affects the battery performance or not.

5.5.1 Experimental setup

The galvanostatic Li-graphite half-cells are built with an artificial graphite anode and Lithium metal as a reference and counter electrode which is same as section 3.1.2. In this experiment, only two types of electrolytes are used; 1.0 M of LiPF$_6$ in EC/DMC = 50/50 (v/v) (LP30) and 1.0 M of LiPF$_6$ EC/DEC = 50/50 (v/v) (LP40) (Both Sigma Aldrich). The constant charge rate was fixed to 0.1C (C/10) with constant current setup on a MACCOR 4000M. The first five cycles were carried out at 25℃ to allow better SEI formation. Then, the temperature is lowered to 0℃ only. Unlike the previous setup, no rest period is given which means the cell instantly starts to discharge as soon as the cycling temperature is lowered to 0℃. The types of battery electrolytes will be mentioned accordingly.

5.5.2 Results

Figure 5-42 represents the discharge/charge cycle of the two Li/graphite half-cells with LP30 and LP40 electrolytes at different temperatures. The first five cycles were done at 25℃ to allow decent SEI layer formation on graphite anode. At 25℃, both cells showed an expected results having highest discharge/charge state in 1st cycle, and it shifts to the left in 5th cycle as Li-ions are consumed more and more over cycle. At 0℃, a cell with LP30 had fast discharge/charge state in 6th cycle which can be assumed as very fast and inefficient battery cycle was seen because of the highly unstable electrolyte phase. Since no rest period was given before 6th cycle, it can be expected that the electrolyte started partial freezing as the battery discharge/charge. On the other hand, a cell with LP40 showed a decrease in discharge/charge state but much better than the LP30 result. From this, it can be explained as LP40 has lower melting point because of DEC solvent that leads to better electrolyte stability at 0℃. In the rest period, the electrolyte decomposition and stabilisation can occur to form a more stable SEI layer. Since no rest period is given to these cells, the electrolyte will start to decompose during the

cell discharge as soon as the temperature is lowered to 0°C, and the decomposition and stabilisation process can be influenced by the electrolyte partial freezing.
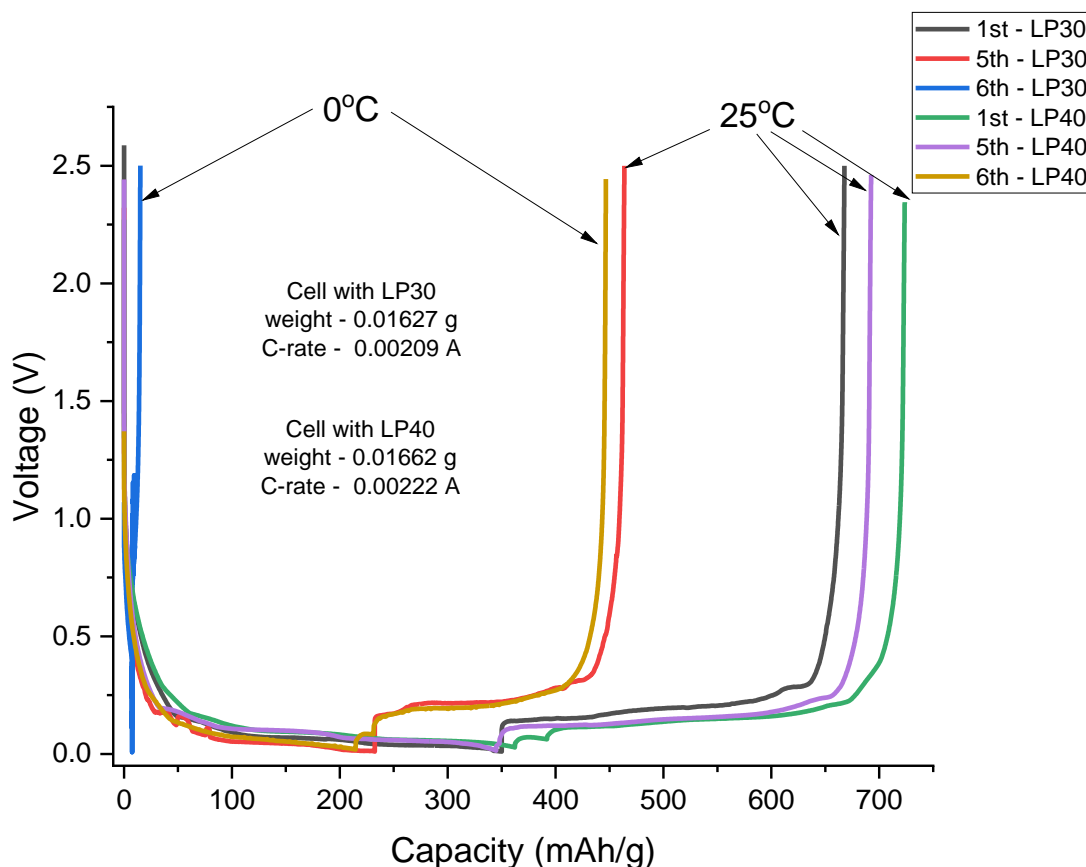
Figure 5-42: Voltage vs Capacity graphs of the two Li/graphite half-cells with 1.0 M of LiPF$_6$ in EC/DMC = 50/50 (v/v) (LP30) and 1.0 M of LiPF$_6$ EC/DEC = 50/50 (v/v) (LP40) (Both Sigma Aldrich); 1st – 5th at 25°C and 6th at 0°C. LP30 cell had C-rate of 0.00209 A. (weight – 0.01627 g), LP40 cell had C-rate of 0.00222 A. (weight – 0.01662 g).

Figure 5-43 below shows coulombic efficiencies of the same two Li/graphite half-cells with LP30 and LP40 electrolytes based on temperature without no rest period. Both cells had lowest coulombic efficiency in 1st cycle which were expected because of parasitic reaction occurs after 8 hours of ageing time mostly SEI formation. Then the efficiency of both cells gradually increased until 5th cycle because further SEI growth is expected as the difference between delithiation and lithiation in each cycle is minimised over cycle. In addition, good electrolyte decomposition and stabilisation is expected at 25°C. At 0°C, it was expected to have some decrease in coulombic efficiency for both cells due to partial freezing of the LP30/LP40 electrolyte. However, the efficiency of LP30 cell showed more than 100 % which means more Li-ions were delithiated to the metallic Li compared to lithiation to the graphite anode. This can be assumed as some Li-ions were involved in delithiation from the irregular capture in between graphene layers during ageing time and 1st cycle at 25°C. Although no rest period was given for both cells in 6th cycle, they showed similar coulombic efficiencies as 1st – 5th cycles which can be

hypothesised as the further electrolyte stabilisation and decomposition were not occurred because both cells started discharging as the temperature was lowered to 0°C.

Figure 5-43: Coulombic efficiency of the same two Li/graphite half-cells with 1.0 M of LiPF$_6$ in EC/DMC = 50/50 (v/v) (LP30) and 1.0 M of LiPF$_6$ EC/DEC = 50/50 (v/v) (LP40) (Both Sigma Aldrich); 1st – 5th at 25°C and 6th at 0°C. LP30 cell had C-rate of 0.00209 A. (weight – 0.01627 g), LP40 cell had C-rate of 0.00222 A. (weight – 0.01662 g).

Figure 5-44 indicates the discharge capacity (half-cell) and irreversible charge capacity loss of the same two cells with LP30 and LP40 electrolytes in each cycle at different temperatures. The highest irreversible charge capacity loss and charge capacity were achieved in 1st cycle for both cells because parasitic reactions occur mostly due to SEI formation. More lithiated Li-ions are expected to be intercalated to the graphite anode compared to the delithiated Li-ions to the metallic Li because some bindings of Li-ions are used in SEI formation, and they are not used in the further discharge process. In addition, both cells showed decrease in capacity and irreversible charge capacity loss which are expected results as Li-ions are consumed over cycle so less Li-ions will be available for lithiation/delithiation over cycle.

When the cycling temperature is lowered to 0°C after the 5th cycle, the 6th cycle is started instantly. Interestingly, there was very low discharge capacity (half-cell) produced but a negative irreversible charge capacity loss was achieved in the 6th cycle for LP30 cell. This means more Li-ions are delithiated

124

to metallic Li compared to lithiated Li-ions to the graphite anode. Hence, the possibility of SEI formation will be low because only 7.5 mAh/g of capacity is produced. LP40 electrolyte had significantly much higher charge capacity produced in 6th cycle although the 2 hours of a rest period is not given at 0°C. In 6th cycle, it can be stated that more SEI formation occurred because more Li-ions are intercalated to the graphite anode than deintercalation to the metallic Li. This can also represent further irregular capture in between graphene layer. LP40 cell had comparatively less capacity loss than LP30 possibly due to lower melting point due to DEC solvent. Since the temperature is adjusted instantly after the 5th cycle at 25°C, the electrolyte decomposition and stabilisation can still continuously occur to form a more stable SEI layer although an unstable state of electrolyte is achieved at 0°C.

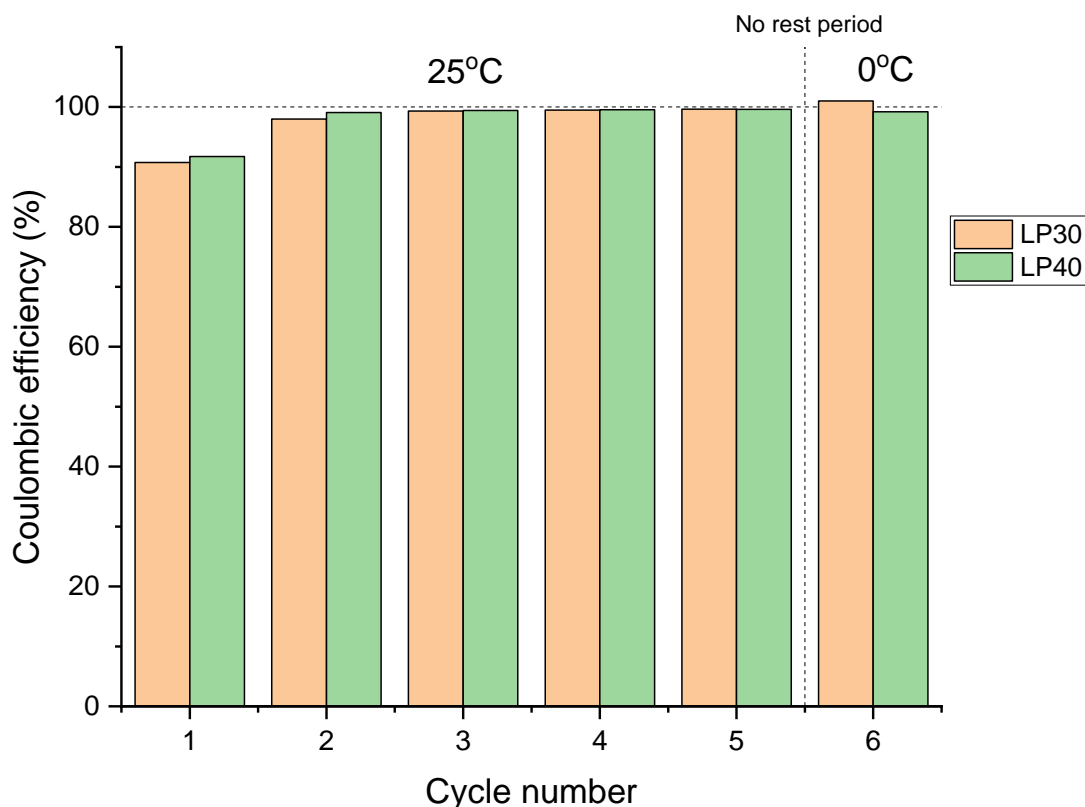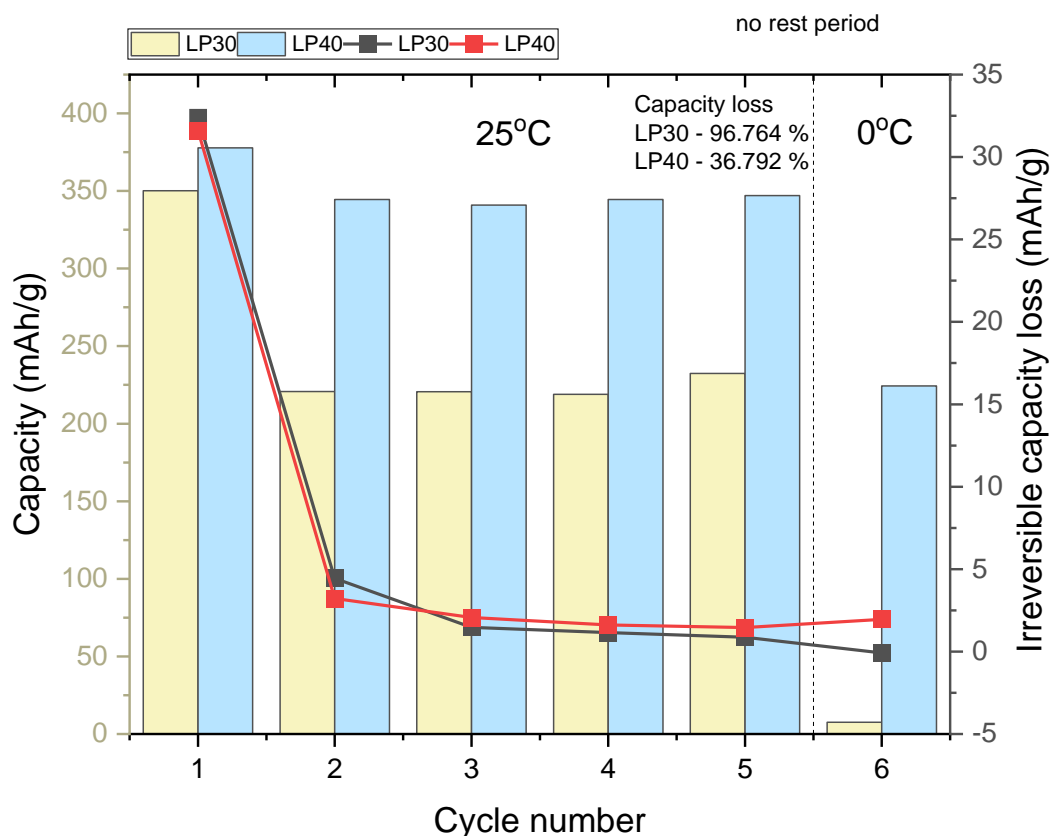Figure 5-44: Discharge capacity (half-cell) and irreversible charge capacity of the same two Li/graphite half-cells with 1.0 M of LiPF$_6$ in EC/DMC = 50/50 (v/v) (LP30) and 1.0 M of LiPF$_6$ EC/DEC = 50/50 (v/v) (LP40) (Both Sigma Aldrich); 1st − 5th at 25°C and 6th at 0°C. LP30 cell had C-rate of 0.00209 A. (weight − 0.01627 g), LP40 cell had C-rate of 0.00222 A. (weight − 0.01662 g).

5.5.3 Conclusion

This section was introduced to find out the effect of the rest period based on the temperature change. Two electrolytes; LP30 and LP40, were used in this experiment because they were commonly used battery electrolytes. LP40 performed significantly better by having significantly less capacity loss but producing much better capacity than LP30 at 0°C without a rest period given. The 2 hours rest period was necessary especially for low-temperature change because it provides enough time for the electrolyte to decompose and stabilise its condition based on the temperature. Since the battery cycles were less than ten cycles, SEI formation might still occur until the 10th cycle if an unstable layer is formed in the ageing time and the 1st cycle at 25°C. If the battery starts discharging without a rest period, the electrolyte can disturb more on the transport of ions because the state of the electrolyte will change during the discharge process whereas, in 2 hours of a rest period, the state of electrolyte will be more stabilised before the cell discharge process. Hence, it can be concluded that a rest period must be given especially for low-temperature change before the battery starts discharging because it provides enough time for the electrolyte to decompose and stabilise the condition of the electrolyte by having partial freezing.

5.6 Temperature change at 6th and 11th cycle

This stage of the experiment is similar to Chapter 5.4 which was to find out the effect of battery performance based on cycling temperature change, but more cycles were given at low temperatures. Total battery cycles were fixed to 15 cycles and the cycling temperature was lowered every five cycles starting from 25°C, 0°C, and -5°C. From this, it can be found out whether SEI formation improves low-temperature performance or not by having ten cycles at low cycling temperatures, 0°C and -5°C.

5.6.1 Experimental setup

The same galvanostatic Li-graphite half-cells are built with an artificial graphite anode and Lithium metal as a reference and counter electrode same as section 3.1.2. Two types of electrolytes were used in this case; 1.0M of LiPF$_6$ in EC/DMC = 50/50 (v/v) (Sigma Aldrich), and 1.0 M of LiPF$_6$ EC/DEC = 50/50 (v/v) (Sigma Aldrich) + 10% FEC (98%, Alfa Aesar) additive, are used. LP40 electrolyte was also used but due to unforeseen human and experimental error, multiple batteries failed cycling and therefore, obtained results were not introduced in this section. In this experiment, FEC additive is used because to find out the effect of improved stability of SEI layer [28] on low-temperature battery performance where cycling number at low temperature is increased to ten cycles. The charge rate was kept constant as 0.1C (C/10) with constant current, constant voltage setup on a MACCOR 4000M. To allow good SEI formation, the first five cycles were done at room temperature. At first, the low cycling temperature is altered to 0°C then the battery had five cycles. Then, the temperature is lowered to -5°C and the

battery had another five cycles. During every temperature change, the 2 hours rest period was assigned to have stabilised electrolyte condition. The types of battery electrolytes will be mentioned accordingly.

5.6.2 Results

Figure 5-45 represents the discharge/charge cycle of Li/graphite half-cell with LP30 electrolyte based on change in temperatures. It clearly shows that the 1st and 5th cycles (black and red) in room temperature have produced relatively more and longer capacities than other low-temperature cycles. At 25°C, both cycles showed a good cell discharge state because the capacity started to increase as the potential drops from 0.8 V which is the practical value of onset voltage of SEI formation [35, 36, 85]. From the 6th cycle (blue) onwards the graph shifted towards the left and it shifted more to the left over cycle. The 10th cycle had a relatively smaller capacity in a short period than the 6th cycle. When the temperature is lowered to -5°C, the graph shifted even more to the left which means more reduced capacities produced in much short time. This matches expected results because there will be more partial freezing of LP30 electrolyte that leads to reduced ionic conductivity at -5°C compared to 0°C and room temperatures.
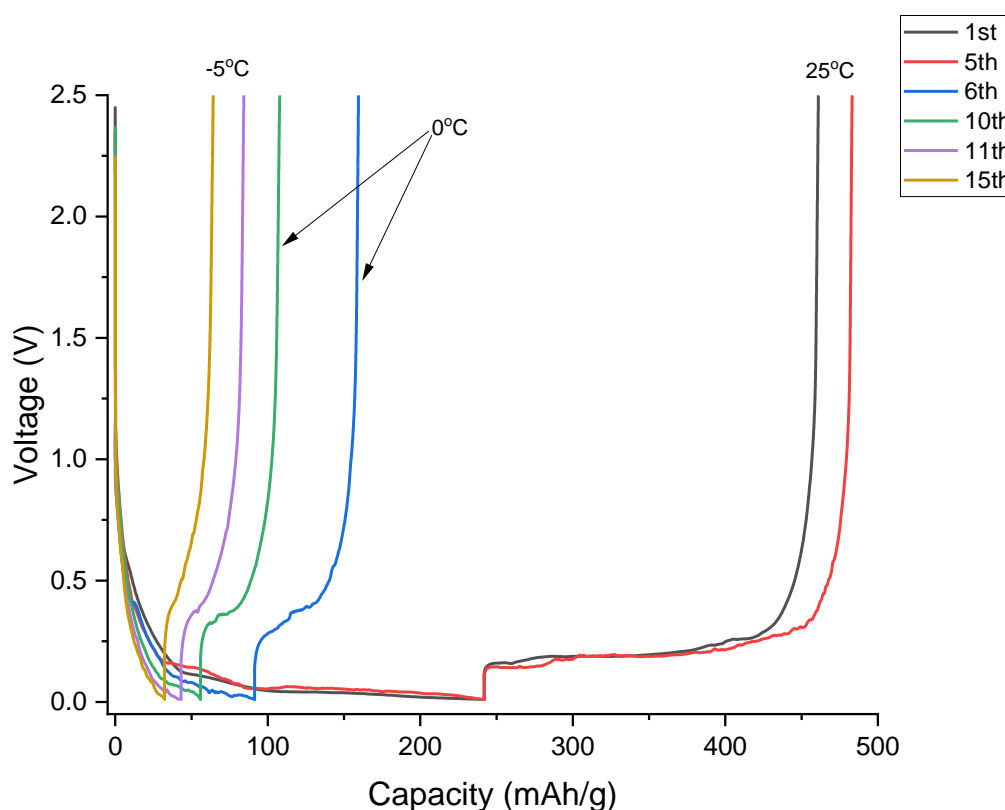

Figure 5-45: Voltage vs Capacity graphs of the Li/graphite half-cell with 1.0 M of LiPF$_6$ in EC/DMC = 50/50 (v/v) (LP30) (Sigma Aldrich); 1st − 5th at 25°C, 6th − 10th at 0°C, and 11th − 15th at-5°C. A cell had C-rate of 0.00745 A. (weight − 0.03225 g).

Figure 5-46 represents similar data with previous Figure 5-45 but LP40 electrolyte with 10% FEC additive is used instead. The 1st cycle (black) shows the highest and longer capacity produced by the cells than the 5th cycle (red) which the graph shifts to the left due to capacity fade as more Li-ions are consumed over cycle. The discharge cycle of the cell in 1st cycle had a relatively better shape of graph as the smooth curve was seen within roughly 0.8 V – 0.22 V compared to the 5th cycle graph which a more steep curve was seen. This means SEI formation has occurred more and better in the 1st cycle than 5th cycle. Overall, 1st and 5th cycles at 25°C have produced longer and higher charge/discharge capacity than low-temperature cycles. Similar to the previous Figure 5-45, the graph shifts towards to the left at low cycling temperatures 0°C and -5°C. When the temperature was lowered to 0°C and -5°C, the cell showed decrease in charge/discharge capacity, but all low-temperature cycles produced relatively decent discharge curve which means SEI formation still occurred at low-temperature. This is possibly due to the FEC additive because it enhances the stability and elasticity of the SEI layer [28].
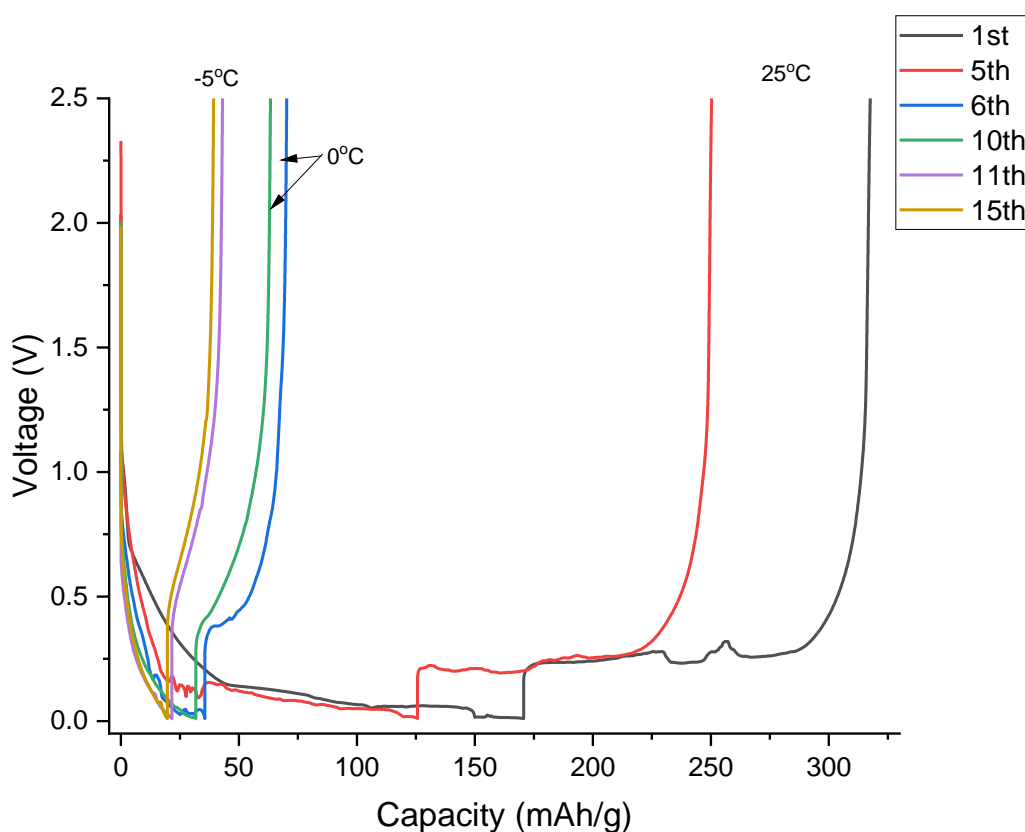

Figure 5-46: Voltage vs Capacity graphs of the Li/graphite half-cell with 1.0 M of LiPF$_6$ in EC/DEC= 50/50 (v/v) (Sigma Aldrich) (LP40) + 10% FEC (98%, Alfa Aesar); 1st – 5th at 25°C, 6th – 10th at 0°C, and 11th – 15th at-5°C. A cell had C-rate of 0.00638 A. (weight – 0.02906 g).

Figure 5-47 below represents the coulombic efficiency of the two same Li/graphite half-cells in each cycle based on change in temperature using two different electrolytes; LP30 and LP40 + 10% FEC. In 1st cycle at 25°C, both cells showed expected results having small coulombic efficiency due to parasitic reaction mostly due to SEI formation. Then, the efficiencies were close to an ideal value, 99 % over cycle. When the temperature was lowered to 0°C, the coulombic efficiency of the LP30 cell decreased until 7th cycle which can be assumed as unstable electrolyte decomposition and stabilisation occurred due to partial freezing of the LP30 electrolyte that leads to low diffusivity of Li-ions. It started to increase from 8th cycle until 15th cycle although the temperature was further lowered to -5°C after 10th cycle. However, A cell with LP40 with 10% FEC had comparatively much higher efficiency at 0°C and -5°C. In addition, the efficiency in 13th cycle was greater than 100 % which means more delithiation occurred compared to lithiation to the graphite anode. Overall, they were possible to occur due to relatively much better SEI layer was formed in LP40 with 10% FEC cell due to FEC additive adding more LiF components to the SEI layer.

Figure 5-47: Coulombic efficiency of the same two Li/graphite half-cells with 1.0 M of LiPF$_6$ in EC/DMC = 50/50 (v/v) (LP30) (Sigma Aldrich) and 1.0 M of LiPF$_6$ in EC/DEC= 50/50 (v/v) (Sigma Aldrich) (LP40) + 10% FEC (98%, Alfa Aesar); 1st – 5th at 25°C, 6th – 10th at 0°C, and 11th – 15th at-5°C. LP30 cell had C-rate of 0.00745 A. (weight – 0.03225 g). LP40 + 10% FEC cell had a C-rate of 0.00638 A. (weight – 0.02906 g).

Figure 5-48 indicates the discharge capacity (half-cell) and irreversible charge capacity loss of the same two cells with LP30 and LP40 +10% FEC electrolytes in each cycle at different temperatures. The highest irreversible charge capacity loss were achieved in 1st cycle for both cells because parasitic reactions occur mostly due to SEI formation. This means more lithiated Li-ions are expected to be intercalated to the graphite anode compared to the delithiated Li-ions to the metallic Li because some bindings of Li-ions are used in SEI formation, and they are not used in the further discharge process. Theoretically, highest capacity was expected in 1st cycle and the capacity decrease over cycle, but the cells showed both decrease and increase in capacity until 5th cycle. Since more Li-ions are consumed over cycle, decrease in capacity was expected. Further SEI formation was occurred for LP30 cell because it had more irreversible charge capacity loss than LP40 + 10% FEC cell until 5th cycle at 25°C.
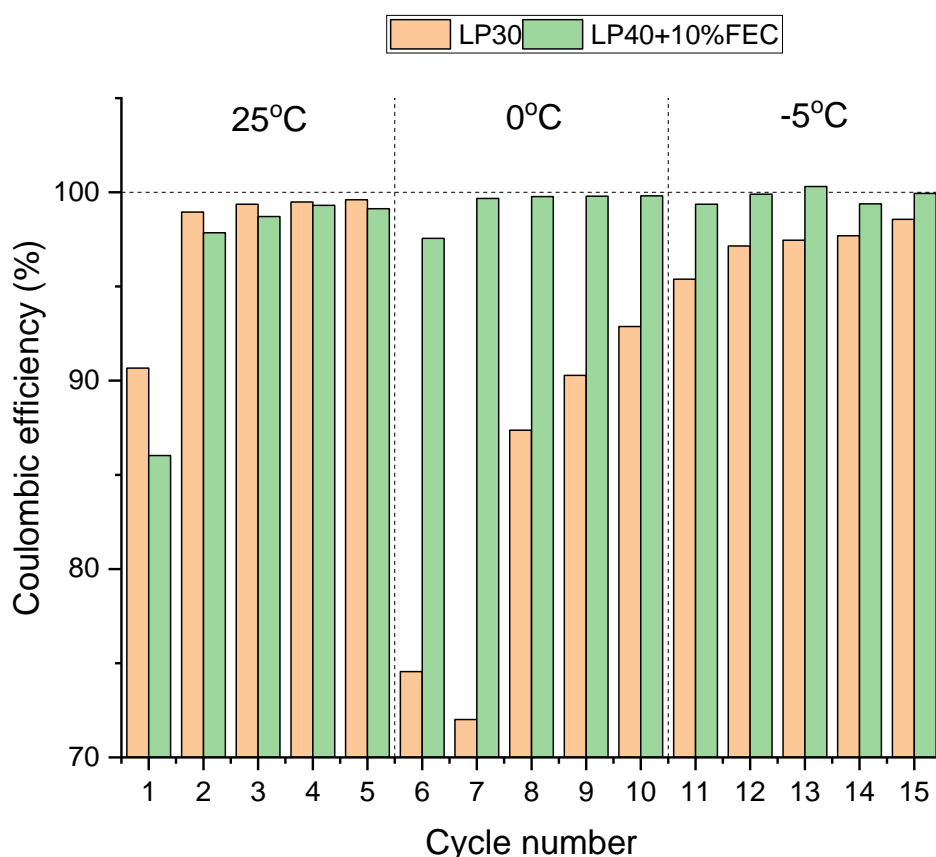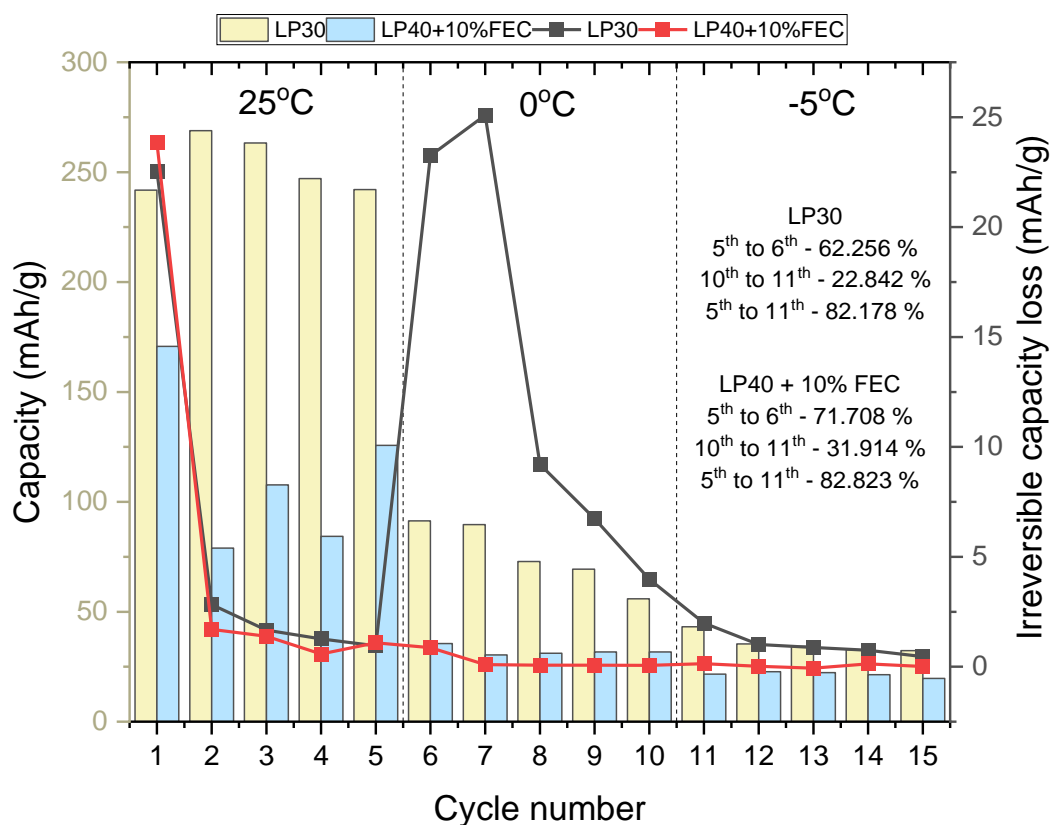

Figure 5-48: Discharge capacity (half-cell) and irreversible charge capacity loss of the same two Li/graphite half-cells with 1.0 M of $LiPF_6$ in EC/DMC = 50/50 (v/v) (LP30) (Sigma Aldrich) and 1.0 M of $LiPF_6$ in EC/DEC= 50/50 (v/v) (Sigma Aldrich) (LP40) + 10% FEC (98%, Alfa Aesar); 1st – 5th at 25°C, 6th – 10th at 0°C, and 11th – 15th at-5°C. LP30 cell had C-rate of 0.00745 A. (weight – 0.03225 g). LP40 + 10% FEC cell had a C-rate of 0.00638 A. (weight – 0.02906 g).

From 0°C, both cells showed relatively less capacity than 25°C and the capacity gradually dropped until the end of the cycle because of the reduced ionic conductivity of the LP30 and LP40 + 10% FEC electrolytes due to its unstable state (partial freezing). For LP30 cell, irreversible charge capacity loss increased in the 6th and 7th cycles unlike capacity. This is possibly due to either SEI formation still

occurred because of unstable SEI layer is formed in ageing time and first five cycles, or some Li-ions were not deintercalated back to metallic Lithium. Possibly, they can stick in electrolyte-electrolyte interphase to form a bulk because the ionic mobility is interrupted by partial freezing of electrolyte. From the 8th cycle onwards, irreversible charge capacity loss was decreased until the end possibly due to no more Li-ions are involved in SEI formation during lithiation process. The capacity of the LP40 +10 % FEC cell from 6th to 15th cycle showed similar decrease as LP30 cell which was an expected result. However, there was relatively less irreversible charge capacity loss than LP30 cell at low-temperatures. To explain, FEC additive improved the stability and elasticity of the SEI layer that leading to minimising capacity fade and irreversible charge capacity loss. It seems that FEC additive protects the SEI layer and minimise more SEI formation taking place in a more repeated cycle. However, it cannot produce a similar capacity as LP30 electrolyte on its own.

Hence, it can be concluded that LP30 electrolyte produced much higher capacities, but more capacity fade occurred over cycle as a decrease in cycling temperature. FEC additive cannot improve the produced capacity of the cell but possibly improves the overall condition of the SEI layer because, at low temperatures, the capacity fade was minimised in each cycle.

5.6.3 Conclusion

This section was introduced to find out whether SEI formation improves low-temperature battery performance over cycle until -5°C. The battery cycles were fixed to 15 cycles and the cycling temperature was lowered every five cycles starting from room temperature, 0°C, and -5°C. Two types of electrolytes were used; LP30 and LP40 with 10% FEC additive. LP40 electrolyte results were not introduced due to unforeseen human and experimental error because of multiple batteries failed cycling possibly due to channel or chamber issue of the MACCOR.

LP30 electrolyte produced relatively higher capacity and less capacity loss occurred especially on low -temperature cycles (0°C and -5°C) than LP40 electrolyte + 10% FEC additive. Since FEC additive improves the stability and elasticity of the SEI layer, the irreversible charge capacity loss were minimised especially on low cycling temperatures. However, FEC additive had a relatively lower capacity than LP30 electrolyte. Hence, FEC is not an additive that improves the produced capacity but improves the overall condition of the SEI layer because, at low temperatures, the capacity fade is minimised in each cycle.

Only LP30 electrolyte data can be compared with section 5.3.4 result which had only two cycled data of the LP30 electrolyte (1 cycle at room temperature and 1 cycle at -5°C). The capacity loss of LP30 electrolyte in this experiment was 82.178 % whereas section 5.3.4 result had 88.728 %. This is mostly due to the better condition of the SEI layer existing on graphite anode. In this experiment, not only

five cycles at room temperature was given but also another five cycles were given at 0°C which means it had ten cycles where SEI formation can occur in each cycle even at low cycling temperature. Section 5.3.4 result had only one cycle available to form SEI layer at room temperature. It is possible that a robust SEI layer can form on 1st charge cycle but the it cannot be guaranteed as SEI formation may continue in multiple cycles [35]. In conclusion, good SEI formation improves the battery performance by having multiple cycles at 25°C and at low-temperatures but to minimise the capacity fade and the capacity loss at low-temperature, FEC additive can be considered rather than using LP30 or LP40 electrolyte on its own.

5.7 Temperature change at 6th, 11th, and 16th cycle

This stage of the experiment is similar to previous section 5.6 to find out the relationship between SEI formation and battery performance based on cycling temperature change, but with five more cycles on low temperature at -10°C. The entire cycle was fixed to 20 cycles and the cycling temperature was lowered every five cycles starting from room temperature, 0°C, -5°C, and -10°C. From this, it can be understood the effect of SEI formation on low-temperature battery performance by having 15 cycles at low cycling temperatures, 0°C, -5°C, and -10°C.

5.7.1 Experimental setup

In this experiment, a similar experimental setup was used as in previous section 5.6.1 except for the cycling temperatures. The galvanostatic Li-graphite half-cells were fabricated with an artificial graphite anode and Lithium metal as a reference and counter electrode same as previous section 3.1.2. Three types of electrolytes were used in this case; 1.0M of $LiPF_6$ in EC/DMC = 50/50 (v/v) (Sigma Aldrich) (LP30), 1.0 M of $LiPF_6$ EC/DEC = 50/50 (v/v) (Sigma Aldrich) (LP40), and 1.0 M of $LiPF_6$ EC/DEC = 50/50 (v/v) (Sigma Aldrich) (LP40) + 10% FEC (98%, Alfa Aesar) additive, are used. Once again, FEC was used as an additive to allow more stabilised SEI formation. The charge rate was kept constant as 0.1C (C/10) with constant current setup on a MACCOR 4000M. After 8 hours of rest period, the first 5 cycles were assigned at room temperature to obtain a decent SEI layer. Then, the cycling temperature is lowered in every 5 cycles each from 0°C, -5°C and -10°C respectively. As soon as the temperature is lowered, 2 hours of rest period was given to allow electrolyte stabilisation. Obtained results will be shown based on the average data from multiple cells at low cycling temperatures with various electrolytes.

5.7.2 Results

Figure 5-49 below indicates the coulombic efficiency of the three tested cells with different electrolytes based on decrease in cycling temperature over cycle. At 25°C, all cells had relatively lower coulombic efficiency in 1st cycle, and it increased until 5th cycle. This was an expected result because after an intact SEI layer was formed in 8 hours of ageing time, further parasitic reaction occurs mostly

SEI formation. In addition, some Li-ions are possible to have irregular capture within graphene layers and they are not involved in further discharging process. When the temperature was lowered to 0°C, LP30 had lowest coulombic efficiency in 6th cycle but it gradually increased over cycle until the end. From this, it can be assumed that the LP30 needed more electrolyte stabilisation and decomposition in 6th cycle beside 2 hours of ageing time to settle the partial freezing of the electrolyte. LP40 and LP40 with 10% FEC electrolytes had relatively higher coulombic efficiency than LP30 possibly due to the characteristic of DEC solvent having low melting point (-43°C) than DMC (3°C) based on Table 2-2 in section 2.2.3. LP40 with 10% FEC additive electrolyte had few cycles more than LP40 in which coulombic efficiency was higher than 100 % which means more Li-ions are delithiated to the metallic Li than lithiation to the graphite anode. This possibly occurs due to no further SEI formation is needed as enough SEI layer already exists on the graphite anode surface because FEC additive improves the stability of the SEI layer forming LiF component to the SEI. Similarly in 14th cycle, LP40 electrolyte had more than 100 % of the coulombic efficiency but this is possibly due to some Li-ions were added from the irregular capture within graphene layers for the deintercalation process from the graphite anode to the metallic Li.
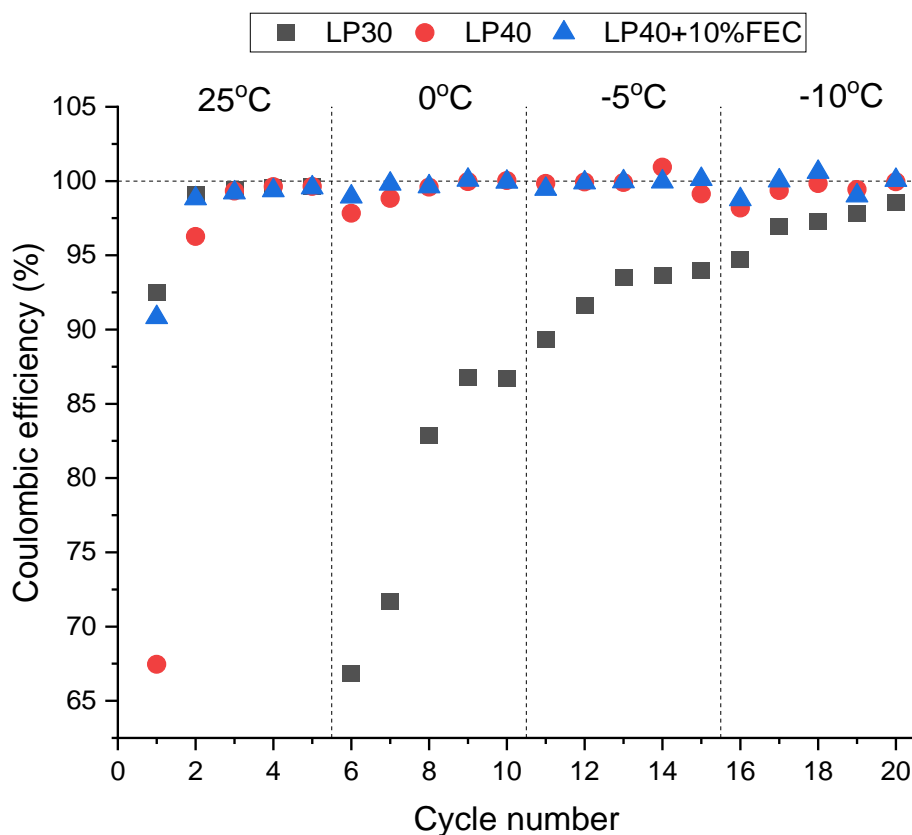
Figure 5-49: Coulombic efficiency of the three average Li/graphite half-cells with 1.0 M of LiPF₆ in EC/DMC = 50/50 (v/v) (LP30) (Sigma Aldrich), 1.0 M of LiPF₆ in EC/DEC= 50/50 (v/v) (Sigma Aldrich) (LP40), and 1.0 M of LiPF₆ in EC/DEC= 50/50 (v/v) (Sigma Aldrich) + 10% FEC (98%, Alfa Aesar); 1st − 5th at 25°C, 6th − 10th at 0°C, 11th − 15th at -5°C, and 16th − 20th at -10°C. The weight and the C-rate cannot be determined as these data are based on the average data of each electrolytes.

Figure 5-50 below shows the average discharge capacity (half-cell) of the same three Li/graphite half-cells with three electrolytes based on temperature over cycle. At 25°C, LP30 electrolyte had highest capacity in 1st cycle and showed increase in capacity from 2nd to 5th cycle. It was expected to have highest capacity in 1st cycle, and it decrease over cycle as limited Li-ions are available as they are consumed more and more over cycle. LP40 electrolyte was also expected to have similar theoretical result as LP30 electrolyte but instead, lowest discharge capacity was produced in 1st cycle. For LP40, highest discharge capacity was shown in 2nd cycle, and it decreased over cycle. From this, it can be assumed that the electrode was not fully wetted in ageing time and 1st cycle. LP40 with 10% FEC electrolyte produced expected capacity over cycle at 25°C similar as theoretical result. This is possibly due to the FEC additive that improves stability of the SEI layer by adding LiF components to the SEI [28].

Figure 5-50: Discharge capacity (half-cell) of the same average three Li/graphite half-cells with 1.0 M of LiPF$_6$ in EC/DMC = 50/50 (v/v) (LP30) (Sigma Aldrich), 1.0 M of LiPF$_6$ in EC/DEC= 50/50 (v/v) (Sigma Aldrich) (LP40), and 1.0 M of LiPF$_6$ in EC/DEC= 50/50 (v/v) (Sigma Aldrich) + 10% FEC (98%, Alfa Aesar); 1st − 5th at 25°C, 6th − 10th at 0°C, 11th − 15th at -5°C, and 16th − 20th at -10°C. The weight and the C-rate cannot be determined as these data are based on the average data of each electrolytes.

From 0°C to -10°C, the average data of all three electrolytes had decrease in capacity over cycle. As the temperature lowers in every five cycles, the capacity decreased over every five cycle as well. The average data of LP30 electrolyte had highest discharge capacities at low-temperature cycles among

LP40 and LP40 with 10% FEC electrolytes. LP40 electrolyte had lowest discharge capacities overall (6th to 20th cycle). Theoretically, LP40 electrolyte was expected to produce more capacity than LP30 because of its lower melting point due to DEC solvent (-43°C) compared to DMC (3°C). Although better SEI formation was expected in LP40 with 10% FEC electrolyte, the average data showed that the low-temperature capacities were similar as LP30 electrolyte. To discuss what was happening in battery furthermore, more data were shown in below.
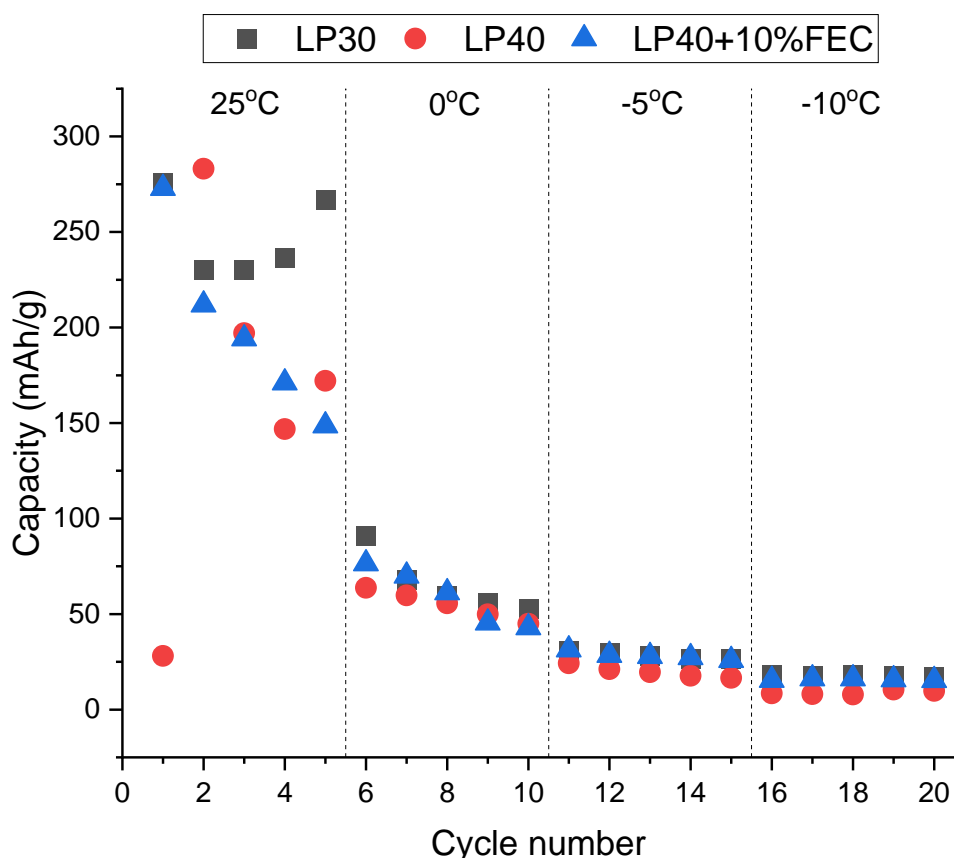

Figure 5-51: Irreversible charge capacity loss of the same three Li/graphite half-cells with 1.0 M of LiPF$_6$ in EC/DMC = 50/50 (v/v) (LP30) (Sigma Aldrich), 1.0 M of LiPF$_6$ in EC/DEC= 50/50 (v/v) (Sigma Aldrich) (LP40), and 1.0 M of LiPF$_6$ in EC/DEC= 50/50 (v/v) (Sigma Aldrich) + 10% FEC (98%, Alfa Aesar); 1st − 5th at 25°C, 6th − 10th at 0°C, 11th − 15th at -5°C, and 16th − 20th at -10°C. The weight and the C-rate cannot be determined as these data are based on the average data of each electrolytes.

Figure 5-51 above represents the average data of the irreversible charge capacity loss of the same three cells with three electrolytes based on temperature over cycle. It clearly shows that comparatively much better SEI was formed using LP40 with 10% FEC additive than LP30 and LP40 electrolytes based on the 1st cycle at 25°C because it showed highest irreversible charge capacity loss. It was known that most of the SEI formation occurs in 1st cycle so higher irreversible charge capacity loss can be understood as more lithiation to the graphite anode is expected compared to the delithiation to the metallic Li. In addition, some Li-ions can be involved in irregular capture within

135

graphene layers, so they are not involved in further discharge process. It can be estimated that the average data of LP30 electrolyte had better SEI formation than LP40 because the irreversible charge capacity loss decreased over cycle whereas LP40 electrolyte decreased from 2nd cycle onwards. LP40 electrolyte had less irreversible charge capacity loss in 1st cycle than 2nd cycle which can be assumed as more SEI formation was occurred in 2nd cycle.

It can be estimated that LP40 and LP40 with 10% FEC electrolytes had suitable SEI layer formed within five cycles at 25°C because their irreversible charge capacity loss decreased over cycle at low-temperatures (0°C, -5°C, and -10°C). If good SEI formation was not the reason, then it can be assumed as due to low diffusivity of Li-ions due to partial freezing that leads to unstable electrolyte decomposition and stabilisation in low-temperature regions. However, the average data of LP30 electrolyte showed highest irreversible capacity loss in 6th cycle at 0°C. It can be hypothesised that most SEI formation possibly occurred in 6th cycle although the temperature was at 0°C compared to 1st and 5th cycle at 25°C. It can also be more irregular capture of Li-ions around graphite anode or electrolyte-electrolyte interphase because high irreversible charge capacity loss represents more Li-ions are lithiated to the anode compared to delithiation process. Having high irreversible charge capacity loss does not always represent the SEI formation so this phenomenon needs further investigation in future.
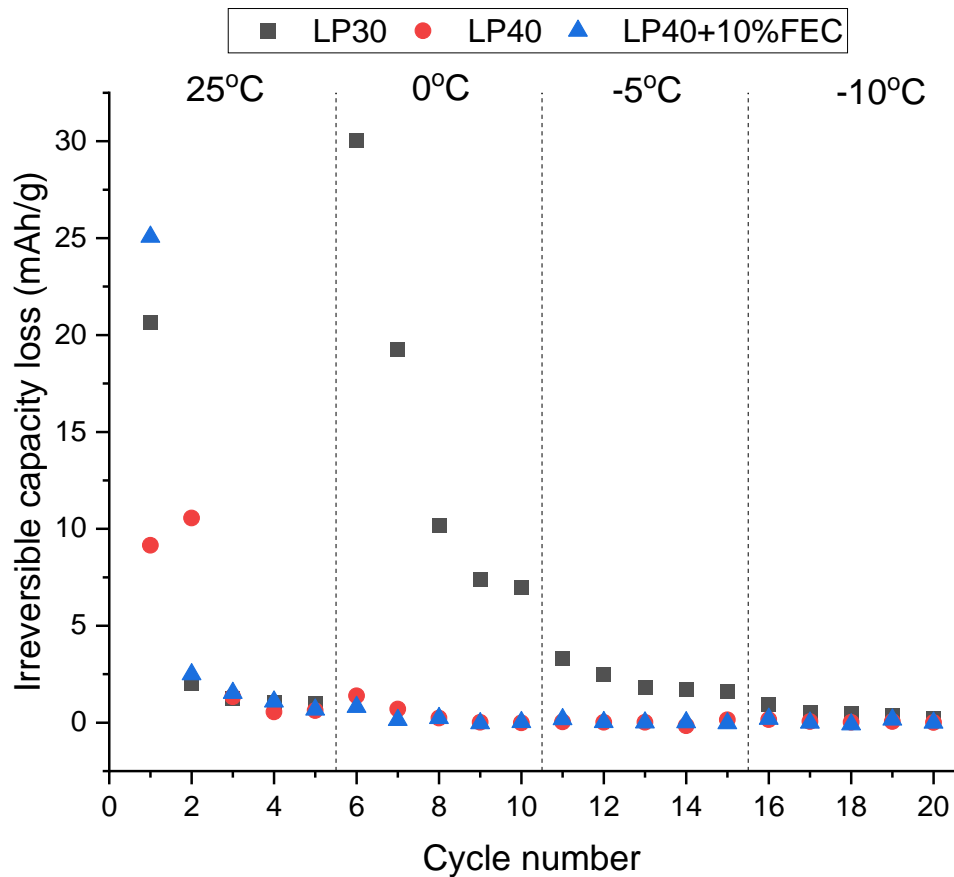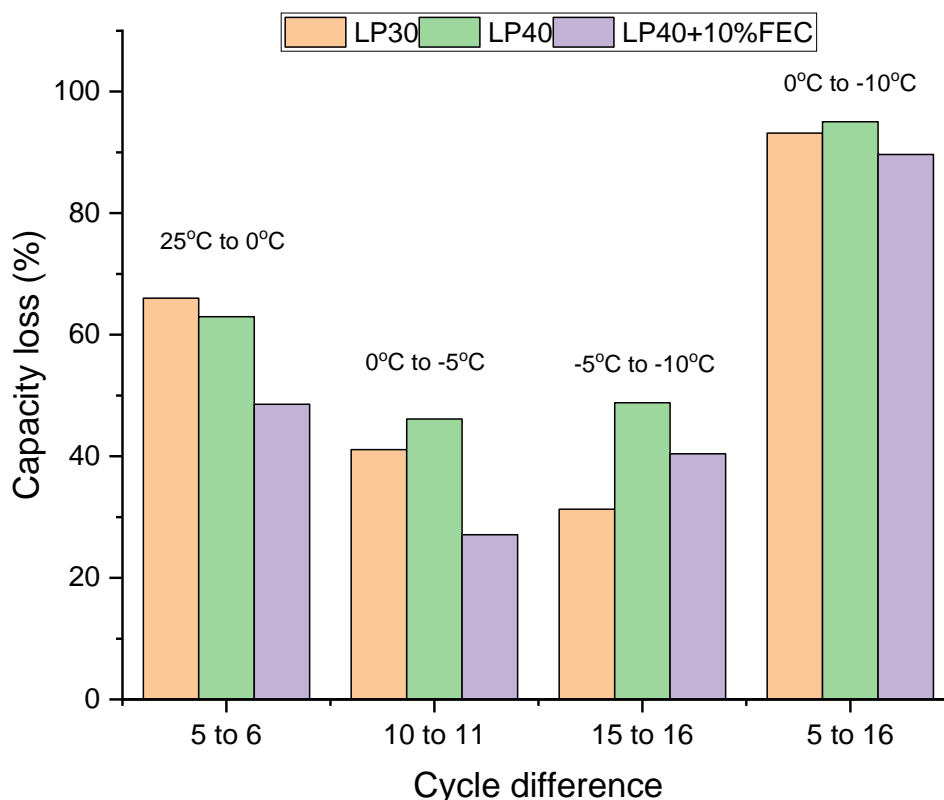
Figure 5-52: Capacity loss of the same three Li/graphite half-cells with 1.0 M of LiPF$_6$ in EC/DMC = 50/50 (v/v) (LP30) (Sigma Aldrich), 1.0 M of LiPF$_6$ in EC/DEC= 50/50 (v/v) (Sigma Aldrich) (LP40), and 1.0 M of LiPF$_6$ in EC/DEC= 50/50 (v/v) (Sigma Aldrich) + 10% FEC (98%, Alfa Aesar) based on the cycle difference. The weight and the C-rate cannot be determined as these data are based on the average data of each electrolytes.

Figure 5-52 represents the average capacity loss of the same cells with three electrolytes in between two cycles which the temperature was changed. In between 5th and 6th cycle, the temperature was lowered from 25°C to 0°C expecting some capacity loss for all electrolytes due to their unstable phase at 0°C. LP30 electrolyte had the highest capacity loss compared to LP40 and LP40 with 10% FEC electrolytes possibly due to more partial freezing occurred or comparably less SEI layer was formed for LP30 electrolyte. LP40 with 10% FEC electrolyte had small capacity loss possibly due to better SEI formation having FEC additive that forms LiF components to the SEI layer. The capacity loss of the three electrolytes at low-temperatures (0°C, -5°C, and -10°C) were relatively less than the capacity loss from 25°C to 0°C possibly due to adequate thickness of SEI layer was formed on graphite anode within 10th cycle. This includes an intact SEI formation in 8 hours of ageing time and five cycles each at 25°C and 0°C. Another possibility is that the electrolyte phase is comparably more stabilised when the temperature is lowered from 0° to -5°C or -5°C to -10°C. This is due to the partial freezing of the electrolyte began at 0°C. The electrolyte stabilisation from 25°C to 0°C will be more difficult because

its phase is changing from full liquid to partial freezing. It will be relatively easier from 0° to -5°C or -5°C to -10°C as the electrolyte phase is stabilised from partial freezing to more partial freezing.

The capacity difference in between 5th cycle and 16th cycle were presented to clarify the effect of cycling temperature to the capacity produced by the battery. The average data of the LP40 with 10% FEC electrolyte had the lowest capacity loss compared to LP30 and LP40. This can be hypothesised as due to FEC additive develops relatively better SEI layer by forming LiF components to SEI layer. LP40 electrolyte had the highest capacity loss in between 5th and 16th cycle although it had less discharge capacity than LP30 electrolyte. Further experimental study is needed to understand more about capacity loss in between 25°C and low-temperature cycle.

5.7.3 Conclusion

This section was introduced to find out whether adequate SEI formation had positive effect on low-temperature battery performance based on types of electrolytes as the cycling temperature; 25°C, 0°C, -5°C, and -10°C which was lowered in every 5 cycles. Three types of electrolytes were used; LP30, LP40, and LP40 with 10% FEC additive.

Once again, LP30 electrolyte produced relatively higher capacity than other electrolytes possibly due to better ionic conductivity than LP40 electrolyte which had the lowest capacity produced overall. LP40 with 10% FEC additive produced better capacity than LP40 electrolyte possibly due to FEC additive by forming LiF components to the SEI layer. Hence, it can be concluded that FEC additive can slightly improve the capacity of the cell which can be related to the stability and elasticity of the SEI layer that minimises the capacity loss especially at low temperature which counterargues the previous conclusion in section 5.6.3. It was also found that the electrolyte phase can be more stabilised when the temperature is changed from 0°C to -5°C or -5°C to -10°C due to the partial freezing of the electrolyte began at 0°C. It can be hypothesised that the electrolyte phase is more easier to stabilise from partial freezing to more partial freezing.

Chapter 6 – Observing anode surfaces using experimental techniques

This chapter is focused on having a close look at the SEI layer to observe its physical and chemical changes using EIS, AFM, and FTIR. The composition and morphological change of the SEI layer based on temperatures and types of electrolytes can be investigated based on experimental results from previous Chapter 5. This will be enough to show the SEI layer is a temperature-dependent layer. Each section explains the used experimental techniques and analysis of artificial graphite anode based on battery cycles from previous Chapter 5.

6.1 Introduction

There are limited studies of the SEI layer since it is a very complicated and sensitive layer because its thickness varies from a few Å to hundreds of Å [35, 36, 94] that making it more difficult to investigate the layer as it may damage the layer. Therefore, it is necessary to use both in-situ and ex-situ techniques to understand the behaviour of the SEI layer based on low temperatures. EIS is a non-destructive technique that provides the information of the SEI layer without affecting the battery cycles and performances. AFM is an effective technique that can visualise the scanned surface of the graphite anode and produce a 3D image. FTIR is another technique that can provide a composition of SEI layer by scanning the graphite electrode and reflected data will have various peaks which represent the possible functional groups of the SEI components. Previous chapters were based on a quantitative analysis of the relationship between the SEI layer and the low-temperature battery performance. This chapter is more focused on both qualitative and quantitative analyses of the SEI layer on artificial graphite anode, and this will be comparatively analysed based mainly on temperatures. Other possible variances such as types of electrolytes and cycle numbers are mentioned respectively.

6.2 Conductivity

In this stage of the experiment, only conductivities of LP30 and LP40 electrolytes were shown because they are the two most commonly used battery electrolytes and most of the coin cells were fabricated with LP30 and LP40 electrolytes in this thesis. This experiment was done only to understand the ability to transport the ions based on temperatures so that this information can help the understanding of the SEI formation related to change in temperatures. The detailed experimental setup was already mentioned in section 3.2.1.2.

Figure 6-1 on the left represents the data plotted as a function of temperature that was analysed separately in Excel and Origin software. It shows that the LP30 showed higher conductivity values than the LP40. This shows that the Li-ion battery assembled with LP30 performs better than LP40 because the ions own more ionic mobility between the electrodes that resulting in higher capacity produced. In addition, it shows that both conductivities increase gradually from 0°C throughout the end. The gradient of LP30 and LP40 were 0.153 and 0.114 respectively. From this, it can be understood that as temperature increases, LP30 achieves a higher lithium intercalation process than LP40 because of the higher gradient. Figure 6-1 on the right indicates the conductivities of three types of battery electrolytes analysed by Plichta and Behl [44]. LP30 (circle) showed the best conductivities overall whereas EMC (triangle) on its own was not suitable for the Li-ion battery electrolyte due to relatively low ionic conductivities. On the other hand, it produced higher conductivities by mixing with other solvents such as EC and DMC. There are two reasons why the conductivities of LP30 are slightly

different between the experimental data and Plichta and Behl's work [44]. First, the cell constant and resistance can be different. It can be determined by the resistance, length between the electrodes, and effective area of the electrodes. In general, the cell constant is 1 but it varies by the condition of the ionic conductivity cell because the length and the area of the electrodes change throughout multiple uses of the cell. Electrodes can be damaged and oxidised by battery electrolytes because they are highly acidic. This will affect the ionic conductivity measurement because higher resistance can be achieved which means lower conductance. If high resistance and low cell constant are obtained, low ionic conductivity is achieved. Although they are cleaned with IPA, there is a limitation of usage of cell life. To prevent this uncertainty, cell constant can be measured frequently so that hopefully it fills the unwanted gap between the experimental and published data. Second, there is a limitation of temperature variance in the experimental technique. MACCOR temperature chamber can lower down the temperature to -20°C whereas literature data [44] were obtained from the temperature -40°C. Hence, it can be concluded that LP30 performs better than LP40 electrolyte at the temperature range from -10°C to 60°C because of relatively higher ionic conductivities. This explains the reason why the coin cells with LP30 electrolyte produced more capacity and performed better at room and low temperatures than LP40 electrolyte which was already shown in previous Chapter 5.
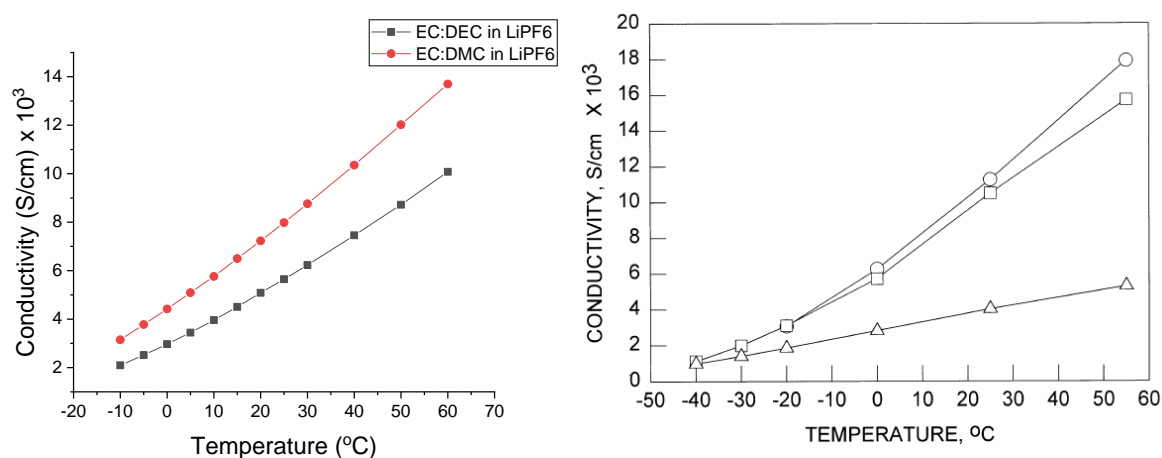

Figure 6-1: Left) Obtained ionic conductivities of 1M of LiPF$_6$ in EC/DMC=50/50 (v/v) (LP30), and 1M of LiPF$_6$ in EC/DEC=50/50 (v/v) (LP40) battery grade, Sigma Aldrich. Right) Conductivities of 1M of LiPF$_6$ in EMC (triangle), 1:1 EC/DMC (circle), and 1:1:1 EC/DMC/EMC (square) tested and determined by E.J Plichta, and W.K Behl [44].

6.3 EIS

This section introduces some important EIS data to understand the resistance change of the cells mostly based on the change in temperatures, cycle numbers, and types of electrolytes.

6.3.1 Experimental setup

The Li/graphite half-cells were fabricated as described earlier in section 3.1.2. Once the cells completed the battery cycles, the EIS was recorded between 100 kHz and 0.01 Hz using a Solartron Modulab 1260A impedance analyser that is connected to the MACCOR system. Instead of recording the EIS after each cell discharge and charge cycle, the EIS was recorded after the cell completed the cycle because the main focus is to find the effect of temperature in this thesis. After the battery cycle has completed, the temperature was changed back to 25°C, and the cell was kept for a few hours to stabilise the condition of the cell such as the electrolyte and the artificial graphite anode. Then, the EIS was performed accordingly.

6.3.2 Results

6.3.2.1 Cycle numbers

Figure 6-2 on top represents the tested EIS data of the average Li/graphite half-cells cycled at room temperature with LP30 electrolyte based on different cycle numbers; 2, 20, and 100 cycles. Their quantitative data were already introduced from previous Chapter 4 and Chapter 5.3.2. It showed expected result having increase in resistance of the cell over cycle. Figure 6-2 on the bottom is an example of typical EIS data of LI-ion cells from the literature [43]. An ideal Nyquist plot of the EIS is expected to have two semicircles that represent R_{sei} (resistance of the SEI layer) and R_{ct} (resistance of the charge transfer). Since the main interest is the R_{sei} in this thesis, other resistances were not deeply discussed.

The R_{sei} of the 2 cycled data was easily visible whereas 20 and 100 cycled data did not have clear semicircle of the R_{sei}. It is hypothesised that R_{sei} is difficult to analyse in 100 cycled data due to the graphite exfoliation or SEI crack on the graphite anode which is expected to occur around $40 - 50^{th}$ cycle. 20 cycled data was more difficult to determine the R_{se} because theoretically, it was expected to have the best semicircle of R_{sei}. Comparatively, 20 cycled data is expected to have better SEI formation than 2 cycled data because it can have better electrolyte stabilisation with adequate SEI layer over cycle. In addition, the charge transfer (R_{ct}) was not clearly seen in Figure 6-2 on top possibly due to the voltage of the cell is not suitable for the chare transfer reaction to occur possibly having either too high or too low voltage. Therefore, the possible best fit equivalent circuit was fitted with some adjustment of parameters based on the experimental data and R_{sei}. Detailed R_{sei} were shown in Table 6-1 below.

Figure 6-2: Top) Average Nyquist plot of Li/graphite half-cells at 25ºC using LP30 electrolyte based on cycle numbers - 2, 20, and 100 cycles. Bottom) An example of typical EIS of Li-ion cell with the fitted equivalent circuit [43].

Based on previous Chapter 4, it was already addressed that most of the SEI formation takes place in 1st cycle, and it continuously forms over cycle (roughly up to 30 cycles) if needed. The R_{sei} from the table 6-1 showed that higher resistance was produced in 20 cycle data compared to 2 cycled data. However, the less resistance was produced in 100 cycle data. This is possibly due to the multiple

parasitic reactions that occur after the 40-50th cycle that leads to capacity fade and limited battery performance which was already mentioned in previous Chapter 4. The possible reactions that affected the resistance of SEI of 100 cycled cells can be graphite exfoliation, SEI crack and precipitation.
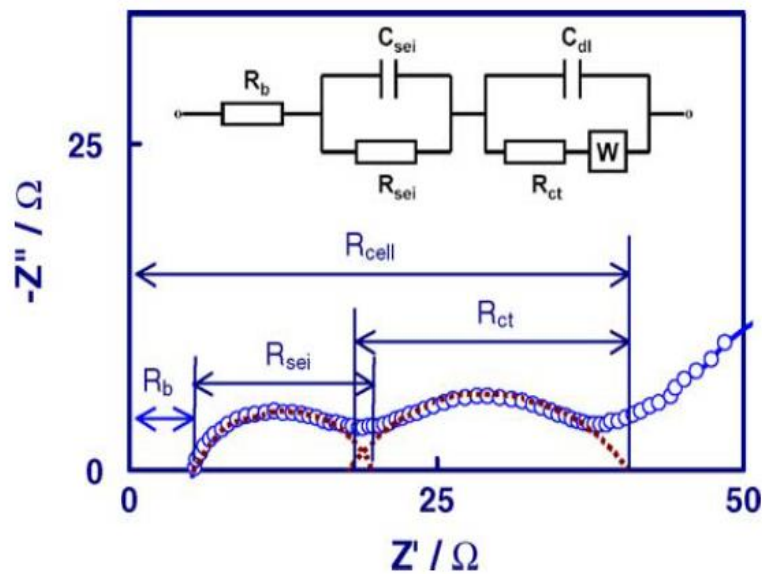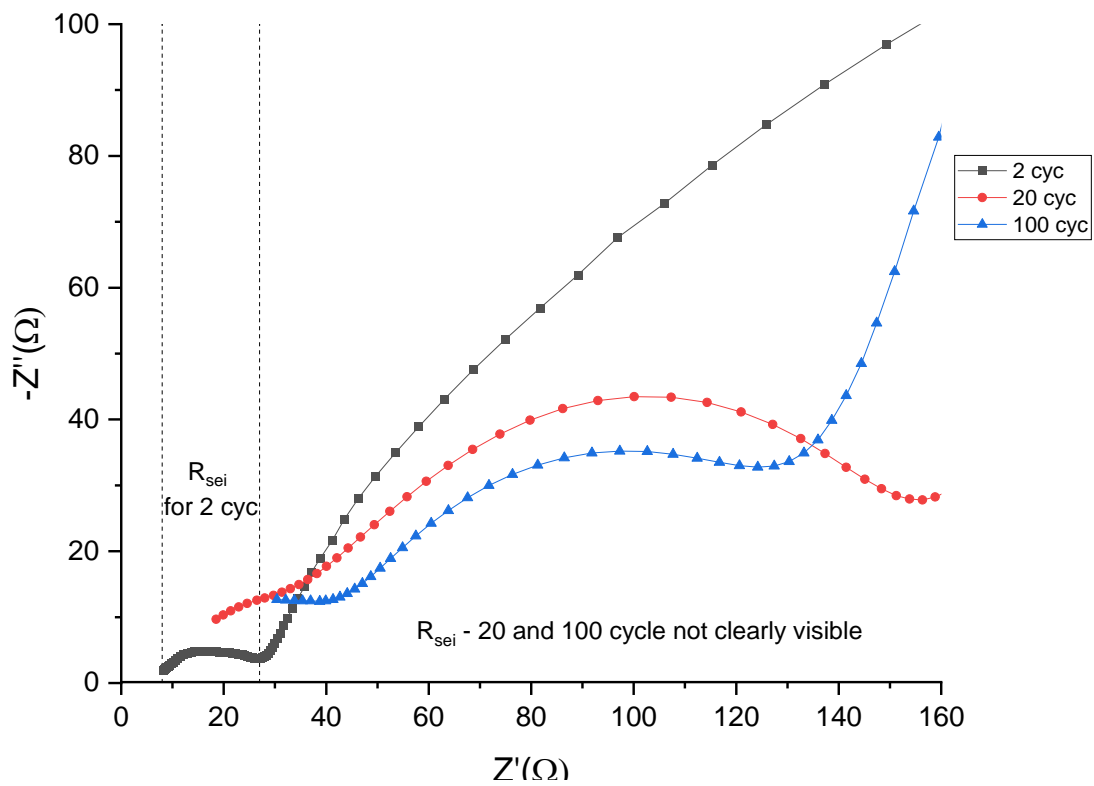
Table 6-1: Average R_{sei} data of Li/graphite half-cells at 25°C using LP30 electrolyte based on cycle numbers - 2, 20, and 100 cycles.

Cycle number	Estimated R_{sei} from equivalent circuit fitting (Ω)
2	26.86
20	156.32
100	124.26

6.3.2.2 Temperature change at 2nd cycle

Figure 6-3 represents the average Nyquist plot of the 2 cycled Li/graphite half-cells based on temperatures with LP30 electrolyte. The quantitative results including the capacities and efficiencies were already shown in Chapter 5.3. The EIS data of 0°C was not shown because of experimental error possibly due to poor cell fabrication having the graphite anode not fully wetted with LP30 electrolyte or the respective channel issue of the Solartron.
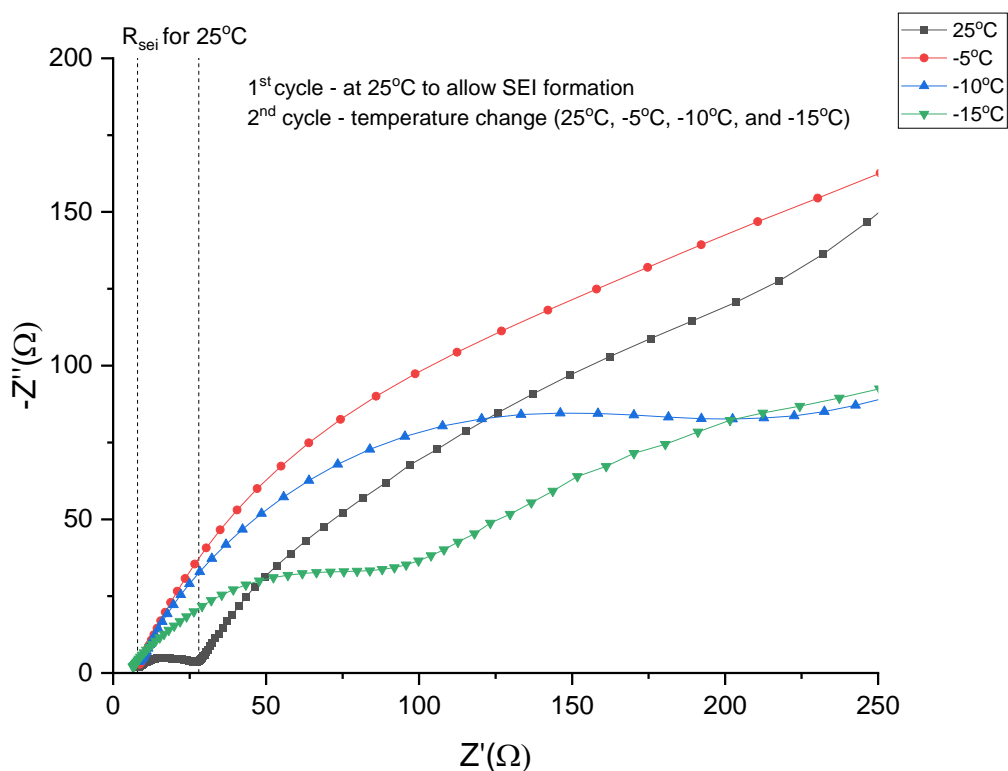

Figure 6-3: Average Nyquist plot of 2 cycled Li/graphite half-cells using LP30 electrolyte based on temperatures; 1st cycle was done at 25°C to allow some SEI formation. The temperature was changed before 2nd cycle at 25°C, -5°C, -10°C, and -15°C respectively. 0°C data was not shown because of data error (obtained data from Solartron).

Theoretically, it was expected to have relatively higher resistance at low-temperature because of low diffusivity of Li-ions possibly occurred by partial freezing of the LP30 electrolyte. Overall, the low-temperature EIS data had relatively higher resistance than the 25°C EIS data, but it cannot be distinguished in Figure 6-3. The X and Y axis were adjusted to have better R_{sei} comparison as 25°C produced significantly small R_{sei}.

Similar to previous Figure 6-2, two semicircles (R_{sei} and R_{ct}) were not appeared on all EIS data. The R_{sei} was expected to increase over decrease in temperature but at -15°C, it decreased as shown in Table 6-2 below. It was difficult to observe the correct R_{sei} for the -5°C as the semicircle was similar to a straight line. In general, the R_{sei} is dependent on temperature [43] because it is affected by the ionic conductivity of electrolyte [48]. Hence, it can be assumed that the expected result was obtained by -10°C data but at -15°C, the R_{sei} was decreased although it was supposed to be increased since more reduced ionic conductivity occur at -15°C that is close to a complete freezing point of LP30 (-21.9°C) [92].

Table 6-2: Average R_{sei} data of 2 cycled Li/graphite half-cells using LP30 electrolyte based on temperatures; 25°C, -5°C, -10°C, and -15°C. ; 0°C data was not shown because of data error (obtained data from Solartron).

Temperature (°C)	Estimated R_{sei} from equivalent circuit fitting (Ω)
25	26.86
-5	134.51
-10	202.48
-15	81.82

In conclusion, it can be stated that the EIS is highly affected by the cycling temperature because the R_{sei} and R_{ct} are obtained based on the electrolyte. If more partial freezing of the electrolyte occurs, higher R_{sei} and R_{ct} can be expected. Another possibility is that hypothetically, R_{sei} can be decreased over temperature decrease if it is affected by the electrolyte stabilisation. Further EIS experiment with repeatability is recommended especially for low-temperature analysis in future.

6.3.2.3. Electrolyte at 0°C from 6th cycle with better SEI formation

Figure 6-4 indicates the average EIS data of the 10 cycled Li/graphite half-cells with three electrolytes used; LP30, LP40, and LP40 + 10% FEC additive. The temperature was changed to 0°C before 6th cycle. From 1st to 5th cycle was done at 25°C to allow an adequate SEI formation. Their quantitative data were analysed in more detail at Chapter 5.4. Although quantitative values of LP40 data were not introduced in Chapter 5.4, the EIS data was shown possibly to understand the reason why the battery failed cycling.
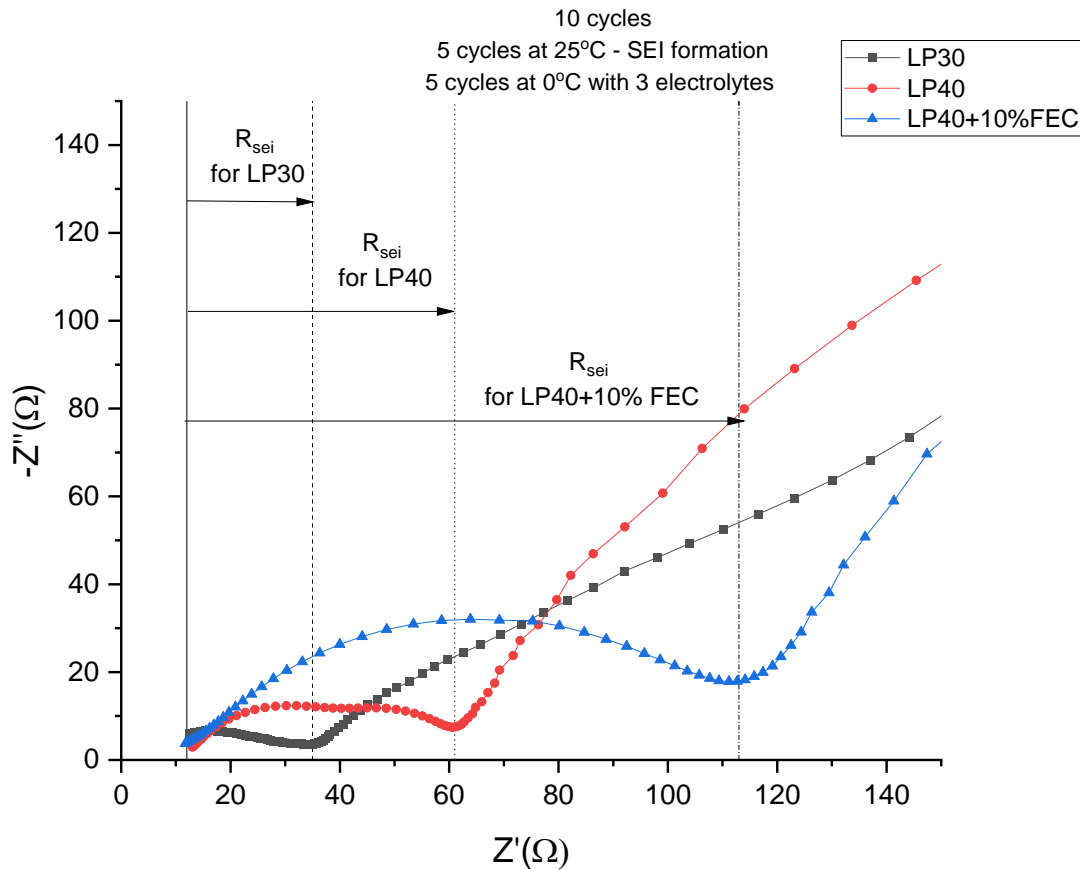
Figure 6-4: Average Nyquist plot of 10 cycled Li/graphite half-cells based on the electrolyte; $1^{st} - 5^{th}$ cycle at 25°C and $6^{th} - 10^{th}$ cycle at 0°C. Used electrolytes are as follows; 1.0 M of $LiPF_6$ in EC/DMC = 50/50 (v/v) (LP30) (Sigma Aldrich), 1.0 M of $LiPF_6$ in EC/DEC= 50/50 (v/v) (Sigma Aldrich) (LP40), and 1.0 M of $LiPF_6$ in EC/DEC= 50/50 (v/v) (Sigma Aldrich) + 10% FEC (98%, Alfa Aesar)

Overall, it can be determined that the semicircle of R_{sei} was more clearly visible than previous Figure 6-3. This is possibly due to better SEI formation because five cycles were assigned at 25°C whereas Figure 6-3 data had only one cycle. Although most of the SEI layer is formed in 1st cycle and possibly a good SEI layer can be formed in ageing time, it can be stated that multiple battery cycles at room temperature must be done before the low-temperature cycles.

Based on Figure 6-4, the semicircle of R_{sei} was more clearly visible having a more stable SEI layer on graphite anode since more battery cycles at room temperature were given. At room temperature, better SEI with less R_{sei} can be formed because relatively good ionic conductivity of the liquid electrolyte is achieved compared to 0°C since R_{sei} is dependent on temperature [48]. Based on Table 6-3 below, LP40 with 10% FEC additive had the highest R_{sei} compared to the other two electrolytes because FEC improves the stability and elasticity of the SEI layer [28] by formation of LiF that improves the ionic conductivity [95] since LiF is ionically conductive. LP40 electrolyte had higher resistance than LP30 electrolyte possibly due to comparatively more diverse SEI components can be formed. DEC has lower melting point so it might behave much better than DMC in LP30 electrolyte at 0°C.

Table 6-3: Average R_{sei} of 10 cycled Li/graphite half-cells based on the electrolyte; 1st – 5th cycle at $25^{o}C$ and 6th – 10th cycle at $0^{o}C$. Used electrolytes were LP30, LP40, and LP40 with 10 % FEC additive

Type of electrolyte	Estimated R_{sei} from equivalent circuit fitting (Ω)
LP30	34.43
LP40	60.53
LP40 + 10% FEC	111.18

6.3.2.4 Temperature change based on the electrolyte

Figure 6-5 also represents the average EIS data of 15 cycled Li/graphite half-cells based on temperature with electrolyte. The temperature was changed from $25^{o}C$ to $-5^{o}C$ in every five cycles; 1st to 5th cycle was at $25^{o}C$, 6th to 10th was at $0^{o}C$, and 11th to 15th was at -5C. The R_{sei} of the same tested cells were shown in Table 6-4 below from equivalent circuit fitting. Only two types of electrolytes were shown; LP30 and LP40 with 10% FEC and their quantitative data were already addressed in previous section 5.6.2. Similar experimental error occurred in previous section 6.3.2.3 because only LP40 electrolyte was not able to present.
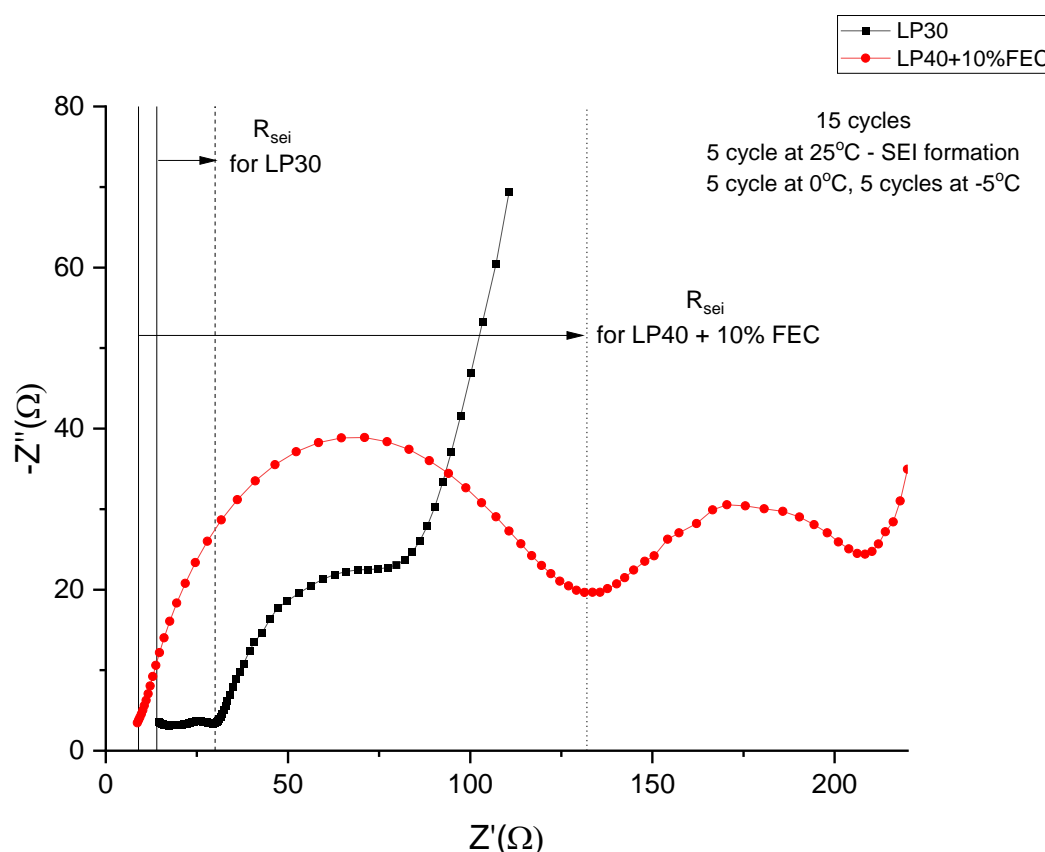
Figure 6-5: Average Nyquist plot of 15 cycled Li/graphite half-cells based on the electrolyte; 1st – 5th cycle at $25^{o}C$, 6th – 10th cycle at $0^{o}C$, and 11th – 15th cycle at -5°C. Used electrolytes are as follows; 1.0 M of $LiPF_6$ in EC/DMC = 50/50 (v/v) (LP30) (Sigma Aldrich), and 1.0 M of $LiPF_6$ in EC/DEC= 50/50 (v/v) (Sigma Aldrich) + 10% FEC (98%, Alfa Aesar). LP40 result was not shown due to experimental error.

In Figure 6-5, this set of data were close to the expected results by showing two semicircles (R_{sei} and R_{ct}) with the overall resistance of the cell, R_{cell}. LP30 data had comparatively less resistance than LP40 with 10% FEC electrolyte. It is known that FEC can improve not only the stability and elasticity of the SEI layer [28] but also the ionic conductivity of electrolytes by forming LiF components to the SEI layer [95]. Although both data had 10 cycles at 0°C and -5°C respectively, FEC additive took crucial role of improvement of the SEI layer at low-temperature. It can be hypothesised that good SEI layer possibly prevent smaller capacity loss at low-temperature because the quantitative data of LP40 electrolyte with 10% FEC could not improve the battery performance. It produced relatively less capacities than LP30 and LP40 electrolyte which was already mentioned in previous section 5.6.2. Hence, it can be stated that LP40 with 10% FEC cells had higher R_{sei} because of much better SEI layer was formed on graphite anode.

Table 6-4: Average R_{sei} of 15 cycled Li/graphite half-cells based on the electrolyte; $1^{st} - 5^{th}$ cycle at 25°C, $6^{th} - 10^{th}$ cycle at 0°C, and $11^{th} - 15^{th}$ cycle at -5°C. Used electrolytes were LP30 and LP40 with 10 % FEC additive. LP40 not shown due to experimental error.

Type of electrolyte	Estimated R_{sei} from equivalent circuit fitting (Ω)
LP30	29.33
LP40 + 10% FEC	132.48

6.3.3 Conclusion

The average Li/graphite half-cells of EIS data were shown in this section to understand whether the SEI layer is a temperature-dependent layer that possibly affects the low-temperature battery performance or not. It showed that the total resistance of the battery was increased over increase in cycle. However, the resistance might increase or decrease in temperature possibly depends on the condition of the SEI layer and the electrolyte. When the voltage of the cell is either too high or too low, the charge transfer reaction will not occur and the semicircle of R_{ct} will not be visible on the EIS data. At room temperature, better SEI with less R_{sei} can be formed because relatively good ionic conductivity of the liquid electrolyte is achieved compared to 0°C since R_{sei} is dependent on temperature [48]. The R_{sei} increased as the cycle number increased. When the R_{sei} dominates, there will be less capacity produced by the battery whereas more capacity can be produced if R_{sei} is low because more Li-ions can be accepted during intercalation by the anode. It was understood that FEC improves the ionic conductivity [95] since an ionically conductive LiF is formed and added to the SEI components. Other LP30 and LP40 electrolytes did not show the semicircle of R_{sei} on the EIS data but LP40 with 10% FEC data had it clear. It can be concluded that the SEI is a sensitive temperature-dependent layer but also follows the ionic conductivity based on cycling temperatures because it determines the condition of the battery electrolytes.

6.4 FTIR

In this section, the ATR-FTIR data of the artificial graphite anode from the Li/graphite half-cell after the completion of cycles is introduced. Estimated SEI components can be found out based on the FTIR spectra and their peaks are compared with literature values. From this, the temperature effect on the change in the composition of the SEI layer can be found.

6.4.1 Experimental setup

Once the Li/graphite half-cell finished cycling, the coin cell was disassembled in an argon-filled glovebox. The artificial graphite anode was carefully separated and gently washed with DMC to remove $LiPF_6$. This was kept in the glovebox for a few days to fully dry. Then, the electrode was scanned at in-situ ATR-FTIR (Bruker) with the parameters of 4cm^{-1} resolution and 96 scan rates once a background scan is completed. The more detailed experimental setup was explained in Section 3.3.2. The tested data was implemented on OPUS software and for further analysis, Origin software was used.

6.4.2 Results

6.4.2.1 No cycle, 1 cycle, and 2 cycle at 25°C

Figure 6-6 represents the average FTIR data from the three Li/graphite half-cells with LP30 electrolyte at room temperature based on cycle numbers; 0, 1, and 2 cycles. 0 cycle means it is a fresh artificial graphite electrode which did not use in cell fabrication. There are 8 noticeable peaks shown on the FTIR spectra which were compared with literature values. Overall, the higher peaks were shown over cycle possibly due to SEI formation as various SEI components are added to the SEI surface over cycle. No cycle data indicates the pure artificial graphite anode surface without SEI layer. 1 cycle and 2 cycle data definitely have SEI layer, but it cannot be definite. 1 cycle cell might have better SEI layer than 2 cycle cell because it was known that most of the SEI formation occurs in 1st cycle after an intact SEI layer formed in ageing time. Table 6-5 was introduced below to show some possible SEI components from literature so that they can be referred with the experimental FTIR spectra.

There was a small peak at 544 cm^{-1} which can be a ROLi component in no cycle FTIR spectrum. It is the most commonly found in SEI layer. Since LP30 electrolyte was used in cell assembly, it can be an expected SEI component on all results. This peak decreased over cycle due to further reactions might occurred as it is soluble [16]. The average data of the no cycle FTIR spectrum had a dominant peak at 831 cm^{-1}, but this peak also decreased over cycle. It represents either $(CH_2OCO_2Li)_2$ or $ROCO_2Li$ component. $(CH_2OCO_2Li)_2$ is another possible SEI component which is mostly found in the EC-based electrolytes because it is formed by a two electron reduction product of EC [35]. $ROCO_2Li$ component is mostly formed in the outer layer of the SEI. If this peak decreased over cycle, it can be assumed as

these SEI components were covered with other SEI components as newly layer will be added to the SEI surface over cycle. The peak at 1073 cm^{-1}, similar as previous three SEI components, were mainly seen in no cycle and 2 cycle FTIR spectra compared to 1 cycle result. There was a clear peak at 1200 cm^{-1} that represents the non-SEI component PVDF [35, 96]. It is a binder used to create the artificial graphite anode. The possible SEI component is RCOOLi where the peak is visible at vibration in between 1500 – 1700 [35, 47]. All three FTIR spectra had uncertain peak at 1760 cm^{-1}. It is uncertain to determine the possible SEI component because it needs more investigation in future using other experimental technique. There was another unknown peak at 2100cm^{-1} which was not found in the literature. This peak increased as the cycle number increased. The peak at 2905 cm^{-1} was mostly seen in 2 cycle result which can be either another functional group of ROCO$_2$Li or ROLi based on literatures [35, 97, 98].

Figure 6-6: Average FTIR spectra of artificial graphite anodes from Li/graphite half-cells using LP30 electrolyte based on cycle numbers. They are the average data of the cells.

Based on Table 6-5, some peaks had the same SEI components but, in more detail, their functional group was different in every range of wavenumbers. Since this is going too deep, only possible SEI components were introduced because only the composition of the SEI layer based on temperature is the main focus in this thesis.

Wavenumber (cm^{-1})	Possible SEI components
544	ROLi [98]
831	$(CH_2OCO_2Li)_2$, $ROCO_2Li$ [99]
1073	$(CH_2OCO_2Li)_2$ [99], $ROCO_2Li$ [98, 100], ROLi [98]
1200	PVDF [35, 96]
1400	$(CH_2OCO_2Li)_2$ [100, 101], $ROCO_2Li$ [97, 100], Li_2CO_3 [47]
2905	$ROCO_2Li$ [97, 100], ROLi [98]
1760, 2100	Unknown

6.4.2.2 Temperature (25°C, 0°C, -5°C, -10°C and -15°C) change before 2nd cycle

Figure 6-7 indicates the average FTIR data of the two cycled Li/graphite half-cells with LP30 electrolytes based on temperatures. The 1st cycle was done at 25°C to allow SEI formation and the cycling temperature was changed before 2nd cycle. The FTIR data were plotted based on only 2nd cycle temperatures at 25°C, 0°C, -5°C, -10°C, and -15°C. From this, the effect of temperature on SEI formation can be understood. Similar to previous Figure 6-6, 8 noticeable peaks were aligned so that possible SEI components can be referred from literature values as shown in Table 6-6 below.
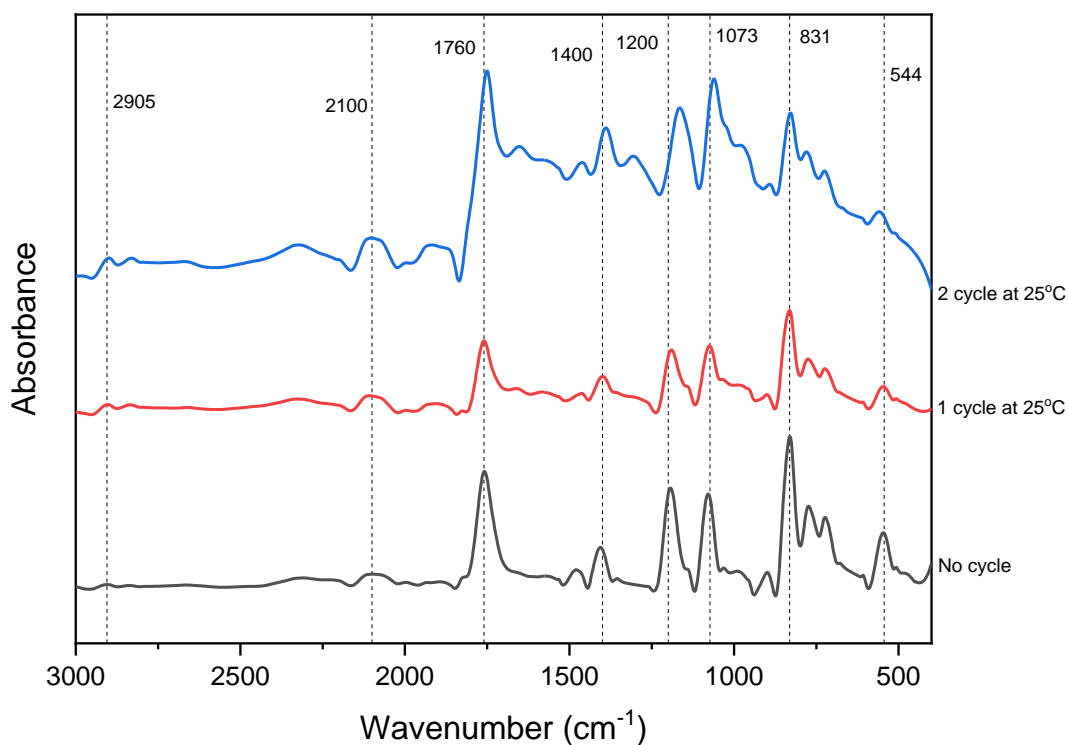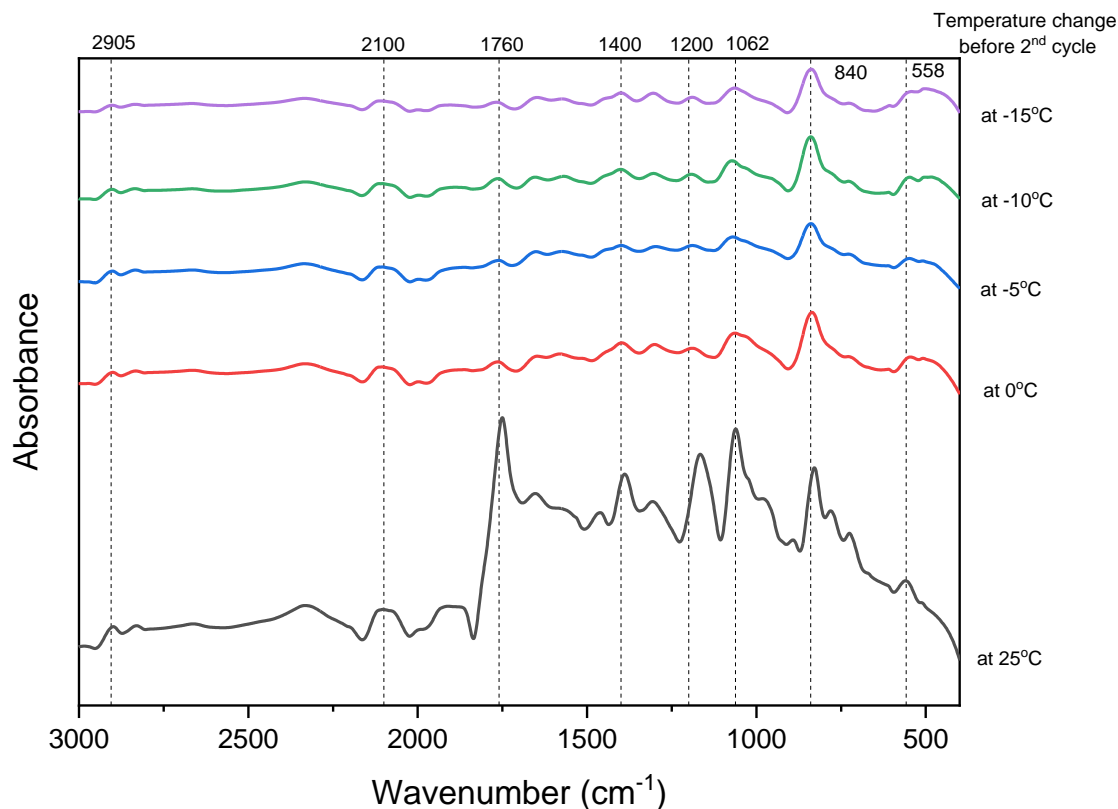

Figure 6-7: Average FTIR spectra of artificial graphite anodes from Li/graphite half-cells using LP30 electrolyte based on temperatures changed in 2nd cycle. They are the average data of the cells.

It showed that the 25°C data had the highest peak of 558 cm^{-1} which represents ROLi component on the SEI layer, but this peak faded away as the temperature decreased. This component is soluble and further reactions can be occurred based on literature [16]. From this, it can be assumed that this functional group of ROLi component does not form as it is highly affected by the electrolyte phase. As shown in Table 6-6 below, 840 cm^{-1} peak represents either $(CH_2OCO_2Li)_2$ or $ROCO_2Li$ component. It can be stated that both SEI components are not highly affected by the low-temperature as clear peak were visible on all FTIR spectra.

However, average FTIR data at 25°C had a highest peak at 1062 cm^{-1}, but it decreased at low-temperatures. It represents four SEI components; $(CH_2OCO_2Li)_2$, $ROCO_2Li$, and ROLi. Since some SEI components are similar to the 840 cm^{-1} peak, it can be assumed that same SEI component ($(CH_2OCO_2Li)_2$ or $ROCO_2Li$), but different functional group is relatively less formed at low-temperature. This can be due to low diffusivity of Li-ions occurred by unstable electrolyte phase at low-temperature. The peak of the PVDF (1200 cm^{-1}), a non-SEI component, was only seen at 25°C although the peak was slightly off to the right the height of the PVDF peak was decreased as the temperature decreased. Based on the 1400 cm^{-1} peak, it can be stated that as the cycle number decrease, the SEI layer can have the reduced relevant functional groups of SEI components; $(CH_2OCO_2Li)_2$, $ROCO_2Li$, ROLi and Li_2CO_3. Except for the unknown peak in 1760 cm^{-1} and 2100 cm^{-1}, most of the peaks were gradually lowered as the cycle temperature is decreased. This is possibly due to reduced ionic conductivity of LP30 electrolyte especially when the cycling temperature drops closer to the possible complete freezing point, -21.9°C [92]. Since the cell is fabricated with LP30 electrolyte, it is expected to have $(CH_2OCO_2Li)_2$, and Li_2CO_3 as a main SEI components since they are mostly formed in EC-based electrolytes [35]. In addition, a DMC reduction product appears as a ROLi component in the SEI layer [102]. However, the SEI layer in this experiment might not have a $ROCO_2Li$ component because it exists at the outer layer of the SEI formed in propylene carbonate (PC) containing electrolyte [35].

Table 6-6: Possible SEI components based on FTIR data in Figure 6-6 referred from Literatures [35]

Wavenumber (cm^{-1})	Possible SEI components
558	ROLi [98]
840	$(CH_2OCO_2Li)_2$, $ROCO_2Li$ [99]
1062	$(CH_2OCO_2Li)_2$ [99], $ROCO_2Li$ [98, 100], ROLi [98]
1200	PVDF [35, 96]
1400	$(CH_2OCO_2Li)_2$ [100, 101], $ROCO_2Li$ [97, 100], Li_2CO_3 [47]
2905	$ROCO_2Li$ [97, 100], ROLi [98]
1760, 2100	Unknown

6.4.2.3 Types of electrolytes – 5 cycles at 25°C and 5 cycles at 0°C

Figure 6-8 represents the average FTIR data of the 10 cycled Li/graphite half-cells with three electrolytes at 0°C. Their quantitative data (capacity, coulombic efficiency etc) were already presented in previous section 5.4.2. The five cycles were done at 25°C to allow SEI formation and the cycling temperature was lowered before 6th cycle. From this, the effect of electrolyte at low-temperature (0°C) on SEI formation can be understood. Unlike previous Figure 6-6 and 6-7, 11 noticeable peaks were aligned so that possible SEI components can be referred from literature values as shown in Table 6-7 below. Since they had five cycles at 25°C before the temperature was lowered to 0°C, it was expected to have better SEI formation than previous results in 6.4.2.2 which had only one cycle at 25°C.
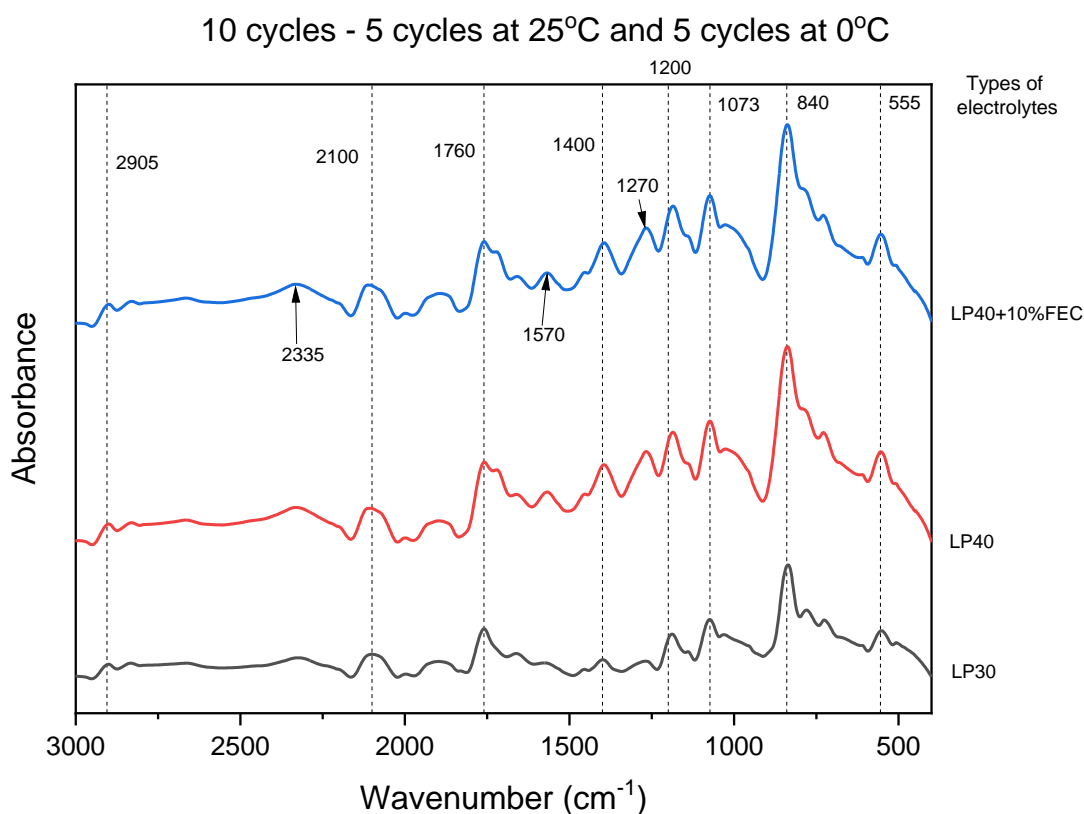
Figure 6-8: Average FTIR spectrum of artificial graphite anodes from Li/graphite half-cells based on temperatures changed in 6th cycle at 0°C with three electrolytes; LP30, LP40, and LP40 with 10 % FEC additive. They are the average data of the cells.

All FTIR spectra had a peak at 555 cm^{-1} that represents the ROLi component. It can be assumed that this soluble SEI component is also the most commonly found component in EC or DEC electrolyte although it is expected as DMC or EMC reduction product [16]. This peak was increased in LP40 with 10% FEC additive. From this, it can be hypothesised that FEC additive allow further development of ROLi component as well as LiF. Since all of the LP30, LP40 and LP40 with 10% FEC additive electrolytes contain EC solvent, it can be estimated that one of the SEI components is $(CH_2OCO_2Li)_2$ because it is

mostly formed in EC based electrolytes [35]. To explain, all FTIR data had peaks in 840 cm^{-1}, 1073 cm^{-1}, and 1400 cm^{-1} which means the SEI layer has a $(CH_2OCO_2Li)_2$ component but with different function group [35, 100]. LP30 electrolyte had the lowest absorbance peak in 840 cm^{-1} whereas the other two electrolytes had relatively higher peaks. From this, it can be expected that the functional group of $(CH_2OCO_2Li)_2$ at 840 cm^{-1} in the SEI layer is expected to dominate on the DEC based electrolyte. The PVDF peak that is a non-SEI component was visible in 1200 cm^{-1} [96] but in this experiment, it was detected at lower wavenumber. Another peak was visible in 1570 cm^{-1} which showed an increase in peak on LP40 with 10% FEC additive. Based on the literature, it can be the RCOOLi SEI component because it has a peak in a range of 1500 -1700 cm^{-1} [35, 47] but it still needs to be further investigated. The small peak in 2905 cm^{-1} was also visible in Figure 6-7 and 6-8 which can be either ROLi or ROCO$_2$Li component which is formed in the outer layer of the SEI [103] but it is still unsure because this is mostly occurs in PC containing electrolytes [35].

Table 6-7: Possible SEI components based on FTIR data in Figure 6-8 referred from Literatures [35]

Wavenumber (cm^{-1})	Possible SEI components
555	ROLi [98]
840	$(CH_2OCO_2Li)_2$, ROCO$_2$Li [99]
1073	$(CH_2OCO_2Li)_2$ [99], ROCO$_2$Li [98, 100], ROLi [98]
1200	PVDF [35, 96]
1400	$(CH_2OCO_2Li)_2$ [100, 101], ROCO$_2$Li [97, 100], Li$_2$CO$_3$ [47]
1570	ROCO$_2$Li [47]
2905	ROCO$_2$Li [97, 100], ROLi [98]
1760, 2100	Unknown
1270, 2335	Possibly LiF

There was an unknown peak in 1270 cm^{-1} which was mainly visible on the DEC contained electrolyte whereas, in LP30, it was not seen. From this, it can be hypothesised that they represent LiF component because relatively higher peaks were seen in LP40 with 10 % FEC additive. Another unknown peak at 1760 cm^{-1} was clearly shown in the FTIR data. This unknown peak was visible on all FTIR data but in low-temperature cycles, it was not as clear as the room temperature cycles. Instead, there was another miscellaneous peak formed next to the 1760 cm^{-1} peak based on DEC contained electrolytes. In previous Figure 6-6 using LP30 electrolyte, this peak was increased over cycle at room temperature. Hence, it can be concluded that the peak in 1760 cm^{-1} is easy to find in LP30 electrolyte at room temperature cycles, but in DEC contained electrolyte, an extra small peak is formed near 1760 cm^{-1} possibly another SEI component. Similarly, 2100 cm^{-1} and 2335 cm^{-1} were unknown literature values

but were more clear in Figure 6-8. From this, it can be assumed as LiF peak because the highest peak was shown in LP40 with 10% FEC electrolyte. Other electrolytes did not have the LiF additive, but this can still form because LP30 and LP40 are comprised of $LiPF_6$ salts. This peak was also increased over at room temperature based on Figure 6-6. However, these peaks were decreased as the cycling temperature decreased until -15°C based on Figure 6-7. Hence, it can be stated that they are the temperature-dependent peaks affected by the condition of the SEI layer formed on graphite anode.

6.4.2.4 Effect of the SEI formation at -5°C

Figure 6-9 represents the FTIR data from the average Li/graphite half-cells with LP30 electrolytes based on SEI formation before the temperature is lowered to -5°C. The black graph had 2 cycles in total; 1st cycle at ambient temperature and 2nd cycle at -5°C. The red graph had 10 cycles in total; 1st to 5th cycle at room temperature and 6th to 10th cycle at -5°C, and the blue graph had 15 cycles overall; 1st to 5th cycle at 25°C, 6th to 10th cycle at 0°C, and 11th to 15th cycle at -5°C. Their quantitative experimental data were already shown in previous Chapters 5.3, 54 and 5.6. Again, similar straight lines were used to indicate the noticeable peak which is similar to the Figure 6-6 peaks, but these values were slightly adjusted depending on the off-positions of the peaks. The possible SEI components based on the FTIR peaks were estimated from the Table 6-8 below.
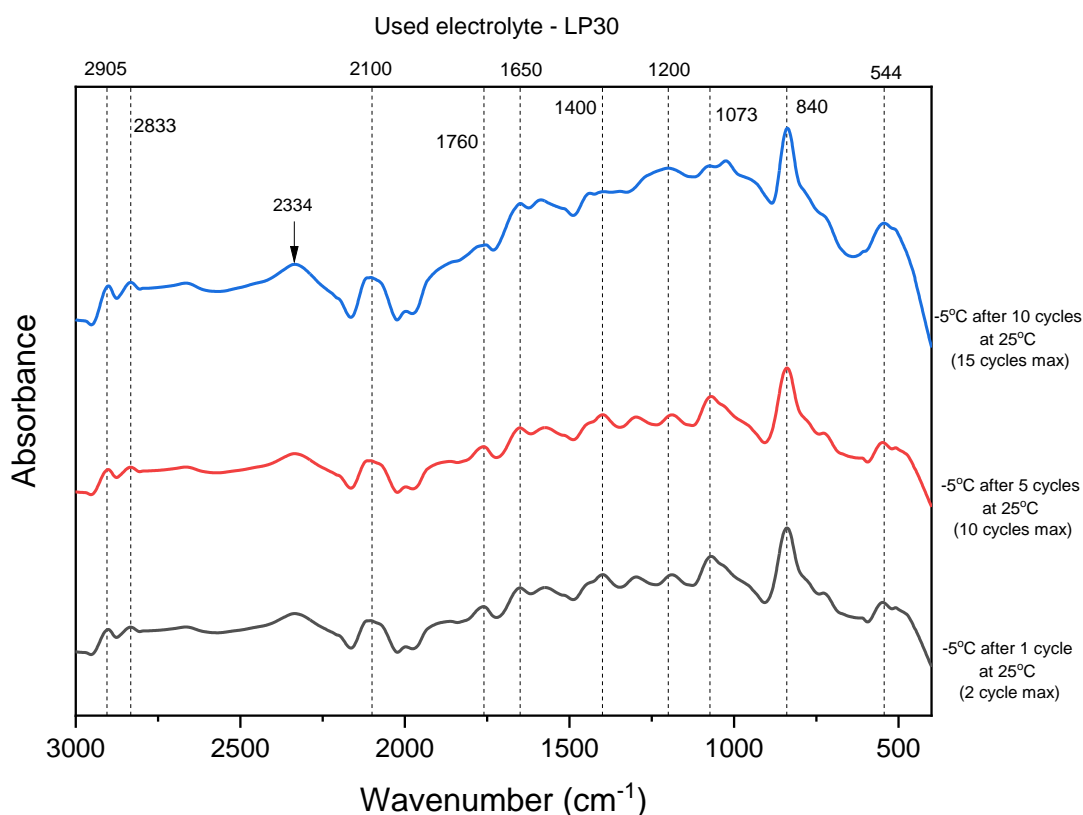

Figure 6-9: Average FTIR spectrum of artificial graphite anodes from Li/graphite half-cells based on the SEI formation. Multiple cycle numbers before the temperature change to -5°C might allow better SEI formation. They are the average data of the cells

Since only LP30 electrolyte was used, it can be stated that the SEI layer will have $(CH_2OCO_2Li)_2$ and ROLi components because of EC solvent [35]. The possible peaks in 544 cm^{-1} represent the ROLi component on the SEI layer that is increased over cycle although few cycles were assigned at low temperature (-5°C). From this, it can be stated that ROLi at 544 cm^{-1} is one of the common SEI component and increase as more SEI growth occurs over cycle in LP30 and LP40 electrolyte. Once again, all FTIR spectra had a clear peak at 840 cm^{-1} which can be either $(CH_2OCO_2Li)_2$ or $ROCO_2Li$ but it was difficult to determine which FTIR had comparatively better peak. It can be hypothesised that either $(CH_2OCO_2Li)_2$ or $ROCO_2Li$ components are not heavily affected by the SEI growth having multiple cycles at 25°C or the electrolyte phase. In addition, the peak at 1073 cm^{-1} can be the following SEI components; $(CH_2OCO_2Li)_2$ $ROCO_2Li$ or ROLi. It can be same or different functional group of $(CH_2OCO_2Li)_2$ $ROCO_2Li$ or ROLi compared to previous 544 cm^{-1} and 840 cm^{-1}. This peak was relatively higher in 2 cycle and 10 cycle data. Since LP30 electrolyte was used, $(CH_2OCO_2Li)_2$, $ROCO_2Li$ or ROLi are expected SEI components because they are formed depending on the type of the electrolyte. They are mostly formed in the outer layer of the SEI [103] and present in EC based electrolyte [35] or as a DMC reduction product [102].

The non-SEI component, PVDF peak was visible in 1200 cm^{-1} [96] but it was not as clear as previous Figures 6-6 and 6-8. It was assumed that this peak is strongly affected by the temperature because in 15 cycle data, it did not show as clear peak as the other two (2 and 10 cycle data). The peak at 1400 cm^{-1} can be similar or different functional groups of $(CH_2OCO_2Li)_2$ and $ROCO_2Li$ or Li_2CO_3. This peak was clearly seen in 2 and 10 cycle data whereas it either disappeared or shifted to higher wavenumber in 15 cycle data. Hence, it can be assumed that this represents Li_2CO_3 because it is formed in EC based electrolyte but not always present [36]. The peak at 1650 cm^{-1} can be assumed as similar or different functional group of $ROCO_2Li$ component. There was a new identified peak at 2833 cm^{-1} which can be either $ROCO_2Li$ or ROLi component. It can be hypothesised that this peak depends on the SEI formation because increase in peak was seen in 15 cycle data than 2 and 10 cycle data. Similarly, the peak at 2905 cm^{-1} can be explained as previous hypothesis because increase in peak was seen over cycle possibly due to better SEI formation.

There were three unknown peaks at 1760 cm^{-1}, 2100 cm^{-1}, and 2334 cm^{-1} shown in all three FTIR spectra. Based on Figure 6-9 above, these peaks were increased over cycle which can be assumed as they represents the determination of the SEI formation. If good SEI layer is formed, then dominant peaks are expected.

Table 6-8: Possible SEI components based on FTIR data in Figure 6-8 referred from Literatures [35]

Wavenumber (cm^{-1})	Possible SEI components
544	ROLi [98]
840	$(CH_2OCO_2Li)_2$, $ROCO_2Li$ [99]
1073	$(CH_2OCO_2Li)_2$ [99], $ROCO_2Li$ [98, 100], ROLi [98]
1200	PVDF [35, 96]
1400	$(CH_2OCO_2Li)_2$ [100, 101], $ROCO_2Li$ [97, 100], Li_2CO_3 [47]
1650	$ROCO_2Li$ [47]
2833	$ROCO_2Li$ [97] , ROLi [98]
2905	$ROCO_2Li$ [97, 100], ROLi [98]
1760, 2100	Unknown
2334	Possibly LiF

6.4.3 Conclusion

This section was introduced to understand the effect of the cycle number, temperature, and types of electrolytes on possible diverse SEI components formed on artificial graphite anode. Based on the average FTIR spectra, the major possible SEI components were $(CH_2OCO_2Li)_2$, Li_2CO_3, and ROLi because they are mostly present due to the EC based electrolyte or DMC solvent. Since LP30 electrolyte was used in cell fabrication in this thesis, it can be estimated that they are mostly formed as SEI components. Other peaks can represent the other SEI components such as $ROCO_2Li$ which had similar FTIR peaks as $(CH_2OCO_2Li)_2$ by sharing a similar range of FTIR vibrations. However, the possibility in this thesis can be low because it mostly occurs in PC containing electrolytes [35]. There were some unknown peaks at 1760 cm^{-1}, 2100 cm^{-1} and 2335 cm^{-1} which was estimated as possible LiF component of the SEI layer because these peaks were dominant especially on LP40 with FEC additive data. These peaks were also visible on all FTIR graphs because of $LiPF_6$. It is the fluorinated salt comprised in all of the electrolytes used in this thesis [35] so small LiF component can be formed in SEI layer. Hence, it can be concluded that the SEI layer is a temperature-dependent layer and is closely related to the ionic conductivity of the electrolyte. They are highly affected at low temperatures and might reduce some of the SEI components. This leads to poor battery performance due to not only the reduced ionic conductivity of the electrolyte but also less SEI components can be formed if the battery was continuously cycled at low-temperature due to imperfect SEI formation at room temperature cycles.

6.5 AFM

In this section, the qualitative data of the artificial graphite electrode were introduced to understand the before and after the SEI formation on the surface of the electrode using an AFM. It is an experimental technique that produces qualitative data of the scanned tested sample by producing a morphological 3D image. However, it can produce only the 3D image of the scanned surface of the artificial graphite anode.   The main focus of this experiment is the comparative study of the effect of the temperature as well as the cycle number and the types of electrolytes.

6.5.1 Experimental setup

Once the Li/graphite half-cells completed the designated battery cycles (refer to section 3.1.2), it was disassembled in a glovebox to obtain the artificial graphite electrode with the SEI layer formed. A detailed experimental setup was explained in section 3.2.2. These electrodes were washed with DMC to remove $LiPF_6$ and kept for a few days to dry them. The electrodes were scanned on the ex-situ AFM using a Bruker dimension icon in ScanAsyst mode. Obtained 3D images were analysed with Bruker software and Gwyddion software.

6.5.2 Results

Figure 6-10 represents the AFM scanned images of the pure artificial graphite anode without the additional SEI layer from the initial cycle and the battery cycle. Both 2D and 3D images were obtained by the Gwyddion software for further analysis. It can be seen that the surface of the uncycled artificial graphite anode is very rough, and the height of the graphite is randomly disordered. Figure 6-11 shows another AFM scanned image of the 1 cycled artificial graphite anode with some SEI layer formed on the surface of the electrode using LP30 electrolyte. By comparing with an uncycled pure graphite anode, it had a relatively smooth surface due to the SEI layer formed by filling a space from the randomly distributed height of the graphite.
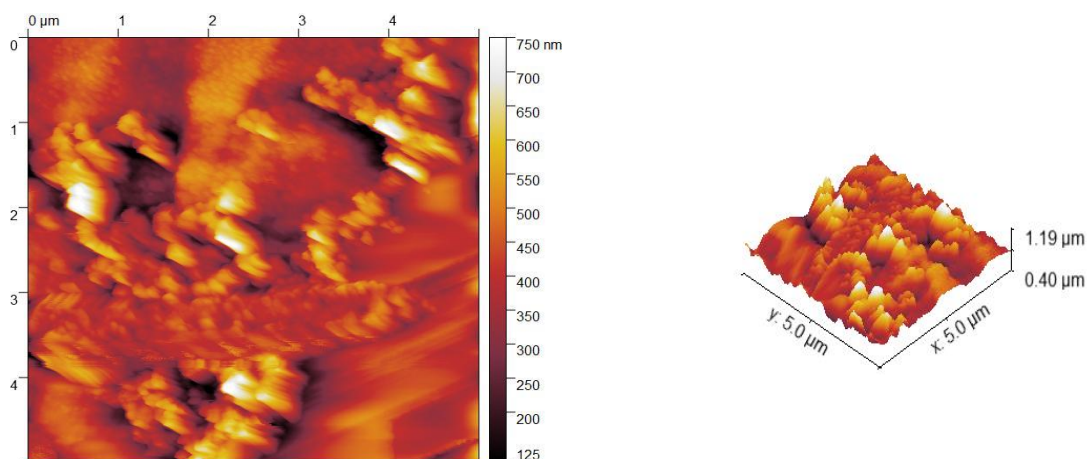

Figure 6-10: AFM images of an uncycled pure artificial graphite anode. No SEI is detected.
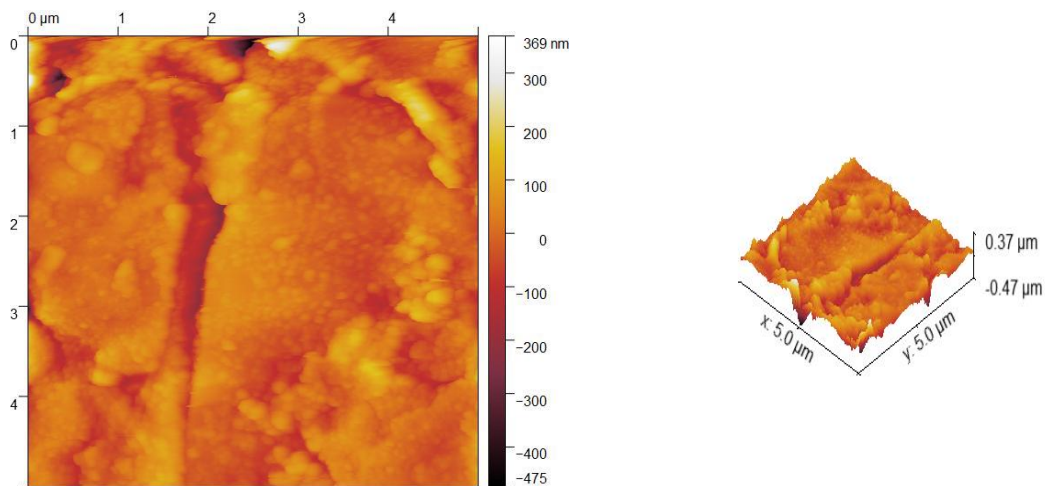
Figure 6-11: AFM images of a 1 cycled pure artificial graphite anode using LP30 electrolyte. Possible SEI is formed from 8 hours of ageing time and 1 cycle at 25ºC.

Figure 6-12 indicates the AFM images of scanned artificial graphite electrodes which had 2 cycles using LP30 electrolyte at room temperature. Relatively less roughness of the scanned surface area was seen because more SEI layer was formed in 2 battery cycles. More SEI formation was occurred than previous Figure 6-10 and 6-11 because it had 2 cycles at 25ºC beside 8 hours of ageing time. Based on the 3D image of Figure 6-12, it can be stated that the height difference was decreased over increase in cycle because more SEI components can fill in the space of the randomly disordered graphite surface. In addition, the height difference might decrease by the overlap of the SEI components like the battery cycle increase. This clearly justifies that most of the SEI layer is formed in 1st cycle but it continuously form over cycle [35] if an adequate SEI layer is not achieved. It was assumed that it can be formed roughly up to 30th cycle based on Chapter 4 and 5.
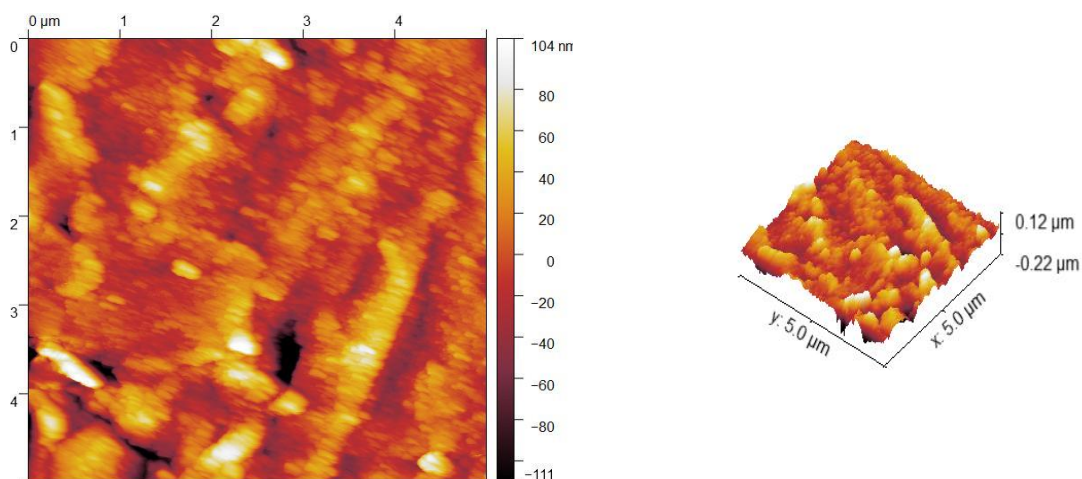

Figure 6-12: AFM images of a 2 cycled pure artificial graphite anode using LP30 electrolyte. Possible SEI is formed from 8 hours of ageing time and 2 cycle at 25ºC. Possibly better SEI formation than Figure 6-10 and 6-11.

Figure 6-13 represents the designated scanned texture of the roughness by the AFM probe based on the cycle number of the battery using LP30 electrolyte. The scanned surface of same textures were shown in previous Figure 6-10, 6-11, and 6-12. The sets of the data were obtained starting from 0 μm to 4 μm on the X-axis and fixed 2.5 μm on the Y-axis of the 2D image so that the roughness of the texture can be calculated using the Gwyddion software. From this, the height variations on the middle of the scanned surface can be estimated.
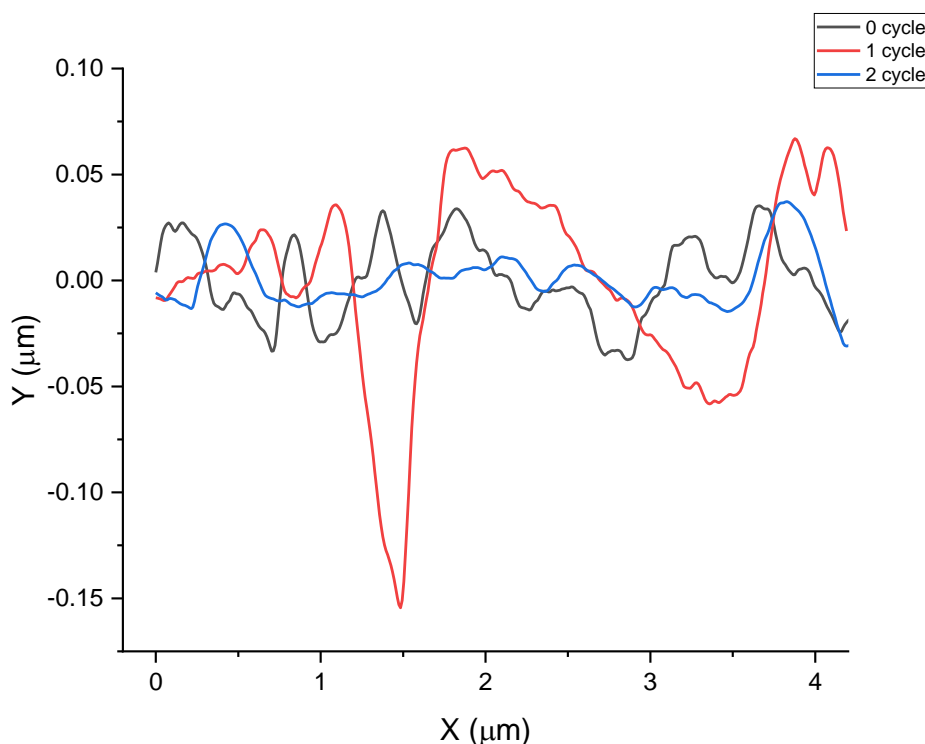

Figure 6-13: Texture difference of the graphite anode surface based on cycle number at 25°C.

It clearly shows that the graphite anode without the SEI formation (black) owns high roughness compared to others by having multiple variations of positive and negative heights. The negative height, in this case, means the scanned surface on that position was located lower than the neutral position of the AFM probe. Table 6- 9 was introduced below to show the roughness parameters of the texture from Figure 6-13 and the overall roughness of the scanned area of the electrode. Root mean square roughness (RMS) is the mean value of the height of the surface. RMS overall means it is the mean roughness value of the entire scanned area and RMS texture means the designated roughness measured from 0 μm to 4 μm on the X-axis and fixed 2.5 μm on the Y-axis of the 2D image.

The uncycled pure artificial graphite electrode had the highest RMS roughness overall. Better surface roughness was achieved over increase in cycle based on the RMS overall. The difference of RMS overall in between 0 and 1 cycles was 32.74 nm whereas the difference in 1 and 2 cycles was 26.84 nm. In

addition, the 2 cycles (blue) graph in Figure 6-13 had the relatively smoother height of the peaks. From this, it can be stated that more SEI components were filled in the space of the pure graphite anode in 1st cycle. In addition, the SEI formation continuously occurred in the 2nd cycle so that the better condition of the layer is expected to be formed. The RMS texture showed a similar phenomenon, but a relatively higher RMS texture was obtained in 1 cycle. This was possibly due to the small gap was seen around the 2 μm of the X-axis based on Figure 6-11.

Table 6-9: Roughness parameters based on the cycle number at room temperature

Cycle number	RMS (S_q) texture (nm)	RMS (S_q) overall (nm)
0	18.42	89.51
1	40.70	56.77
2	13.04	29.93

Figures 6-14 and 6-15 represent the scanned surface of the 10 cycled artificial graphite anode using LP30 and LP40 electrolytes. It was expected to have a decent SEI layer because it had 5 cycles with good ionic conductivity of both electrolytes at 25°C. However, the temperature was lowered to 0°C from the 6th onwards so relatively reduced ionic conductivity of the electrolytes were expected. Unlike previous room temperature cycled graphite anode surfaces in Figure 6-12, the small particles of the SEI components were not clearly seen based on the 2D image of Figure 6-14 and 6-15. From this, it can be assumed that the low-temperature affected the surface condition of the SEI layer. This cell had 5 cycles at 25°C to allow more SEI formation to occur before 5 cycles at 0°C compared to previous uncycled, 1, and 2 cycled cells. Overall, Figure 6-15 also had an unclear image of the SEI particles but there were some of the SEI components formed around the 3 to 5 μm region on the X-axis. Based on the ionic conductivity of two electrolytes shown in previous Chapter 6.2, LP30 has relatively higher ionic conductivity than LP40 electrolyte on both temperatures. It can be seen that the 3D image of the LP30 had a relatively smoother surface compared to the LP40 electrolyte based on the Z-axis of the 3D image because it had a relatively smaller height difference. From this, it can be stated that LP30 had better SEI formation compared to LP40 because the SEI components were highly temperature-dependent materials that are closely affected by ionic conductivity at 25°C and 0°C.
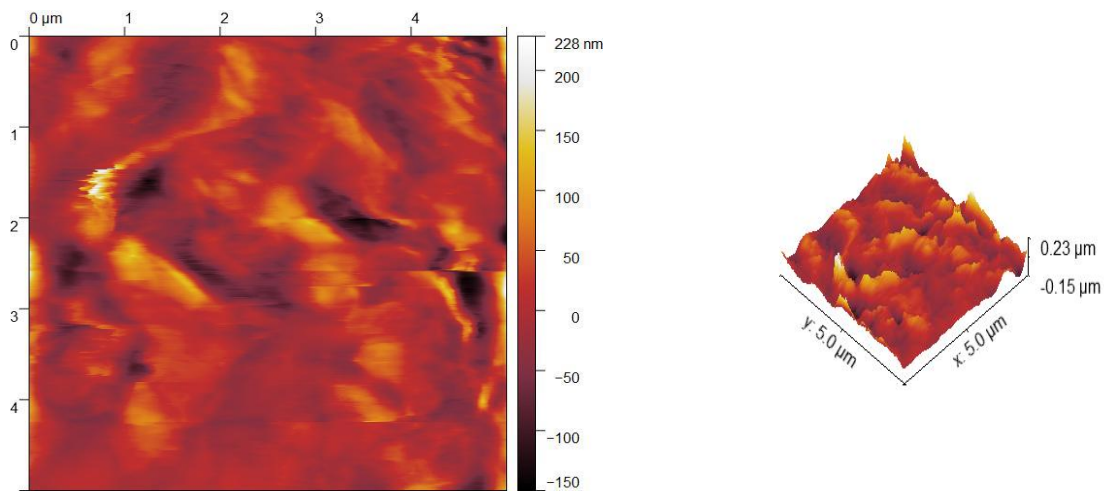
Figure 6-14: AFM images of 10 cycled artificial graphite anode using LP30 electrolyte based on cycling temperature. 1st to 5th at 25oC to allow SEI formation and 6th to 10th at 0oC.
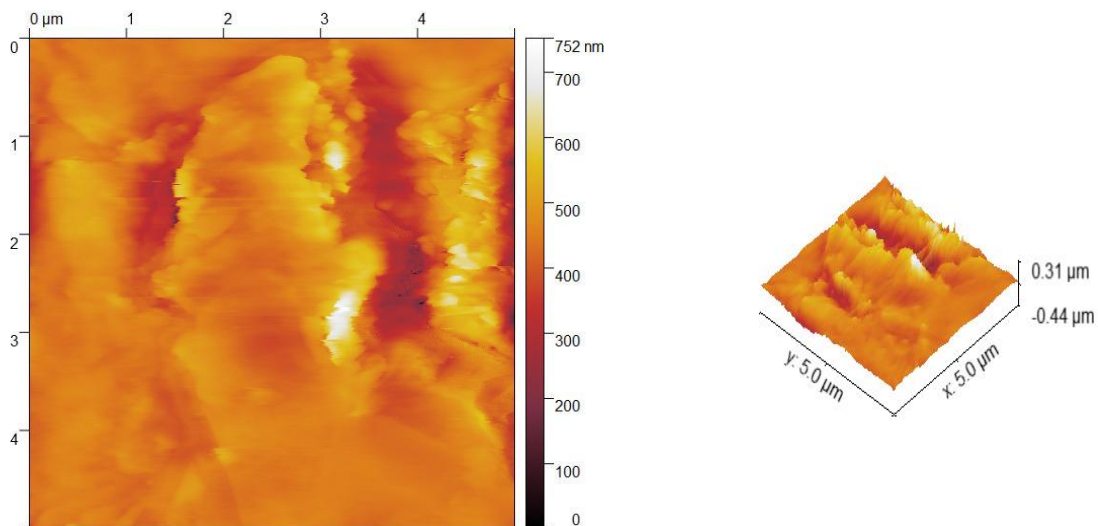

Figure 6-15: AFM images of 10 cycled artificial graphite anode using LP40 electrolyte based on cycling temperature. 1st to 5th at 25oC to allow SEI formation and 6th to 10th at 0oC.

Figure 6-16 shows the scanned surface of the 10 cycled artificial graphite anode using LP40 with 10% FEC additive based on cycling temperature. It was expected to have a good image of the graphite anode surface with SEI layer. The FEC additive improves the stability and elasticity of the SEI layer [28] and the ionic conductivity of LP40 electrolyte by forming LiF components to the SEI layer [95]. In addition, it should have a decent SEI layer on graphite anode because 5 cycles were assigned at 25°C although the cycling temperature was lowered to 0°C from the 6th cycle onwards. The 2D image visualised the various SEI components formed on the graphite electrode surface which possibly includes the LiF component. Hence, it can be concluded that the FEC additive improves the SEI layer by having another component, LiF, which can improve the ionic conductivity of the LP40 electrolyte [95]. These SEI components in Figure 6-16 were widely distributed all over the surface area whereas other electrolytes (LP30 and LP40) had possibly partial forming on a certain region.
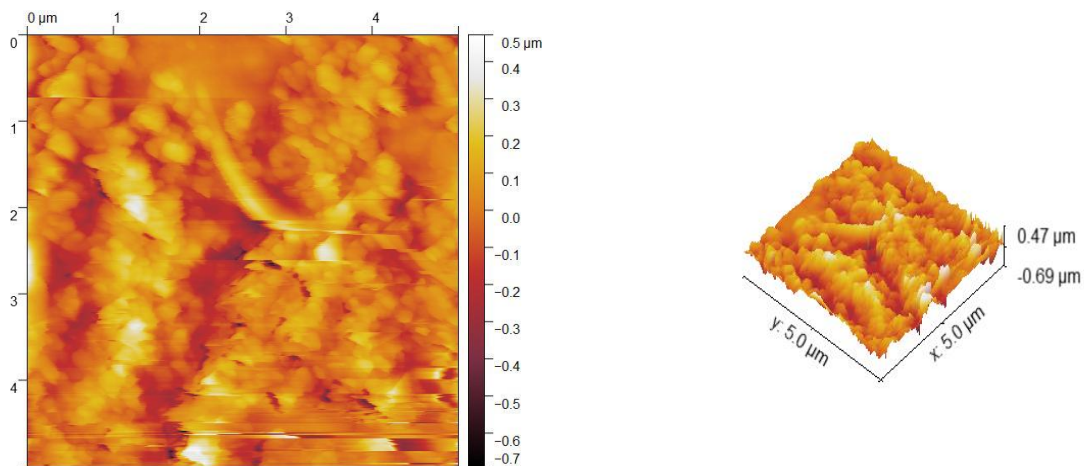
Figure 6-16: AFM images of 10 cycled artificial graphite anode using LP40 with 10% FEC additive based on cycling temperature. 1st to 5th at 25°C to allow SEI formation and 6th to 10th at 0°C.

Figure 6-17 was introduced below to understand the roughness of the scanned region of the texture by the AFM probe based on the electrolytes. The same scanned surface of these textures were shown in previous Figure 6-14, 6-15, and 6-16. The graphite electrode had 5 cycles at 25°C and 5 cycles at 0°C to allow decent SEI formation at room temperature before low-temperature cycles. Without the SEI layer, poor low-temperature was shown which was already mentioned in previous Chapter 5.2. The sets of the data were obtained from the Gwyddion software starting from 0 μm to 5 μm on the vertical X-axis and fixed 2.5 μm on the Y-axis of the 2D image.
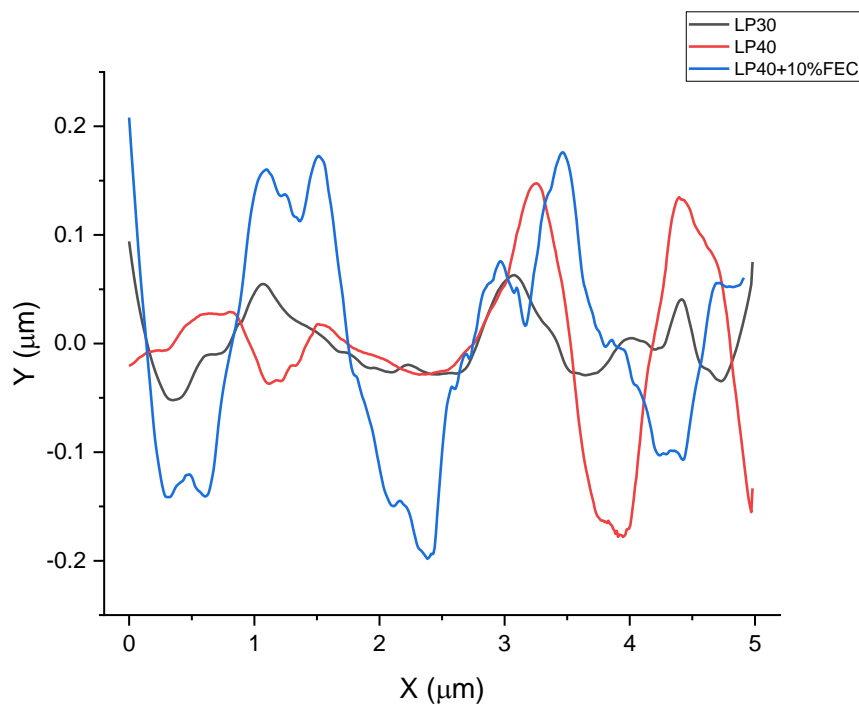

Figure 6-17: Texture difference of the 10 cycled graphite anode surfaces using three electrolytes based on cycling temperature. 1st to 5th at 25°C to allow SEI formation and 6th to 10th at 0°C.

It clearly shows that the LP30 had relatively smooth roughness of the texture compared to other electrolytes. LP40 had small peaks on the 0–2 μm but high peak variances were seen on the 3-5 μm region which was also shown in the 2D image of Figure 6-15. LP40 with 10% FEC additive showed the highest peak variances possibly due to relatively better formation of the SEI components compared to LP30 and LP40 electrolytes.

Table 6-10 was shown below to quantitatively understand the change in roughness based on the electrolytes. LP30 electrolyte had a much smoother surface compared to other electrolytes because it had better RMS texture and overall values. From this, it can be hypothesised that the melting point of LP30 electrolyte is higher than LP40 electrolyte. It can be assumed as either less amount of certain SEI components exist in SEI layer or less thickness of the SEI layer itself can be expected. LP40 with 10% FEC had the highest RMS roughness, and this is possibly due to ease of the SEI formation compared to the electrolyte on its own by forming the LiF component. However, this is information cannot be 100% accurate because the AFM only visualises the scanned surface of the electrode and does not tell the exact composition of the material.

Table 6-10: Roughness parameters based on the electrolytes

Electrolyte	RMS (S_q) texture (nm)	RMS (S_q) overall (nm)
LP30	26.84	38.59
LP40	68.53	57.01
LP40+10%FEC	74.66	113.5

6.5.3 Conclusion

This section was focused on the AFM analysis of the artificial graphite anode surface based on the cycle number, temperature, and types of electrolytes. Based on the 2D and 3D images produced by AFM, it was known that a relatively smoother surface was seen compared to the surface of the uncycled pure graphite electrode which had an extremely rough surface by having high RMS roughness. This value decreased over cycle because of the SEI layer possibly fills in the empty space from the rough graphite surface. Although most of the SEI layer is formed in 1st cycle, the SEI layer can continuously form over cycle which was also mentioned in previous Chapter 4.2. The type of electrolyte was important because it possibly affects the surface roughness. After all, not only the SEI components were highly dependent, but they also decides the ionic conductivity of the electrolyte based on the cycling temperature. FEC additive produced a better SEI layer than the LP30 and LP40 electrolyte on its own by possibly adding more LiF components to the SEI layer [95]. The highest RMS roughness was obtained by the LP40 with 10% FEC additive possibly having various SEI grains formed

on the surface of the graphite electrode based on the 3D image. However, further researches need to be done to investigate the exact SEI components because the limitation of AFM was it was only able to visualise the scanned surface on 2D and 3D images.

Chapter 7 - Conclusion and future work

This chapter introduces some crucial experimental results obtained in this thesis. In addition, outlined promising further researches are listed and explained to guide how and why they need to be investigated further.

7.1 Conclusion

The main scope of the thesis was to understand the formation of the SEI layer and its relationship with the temperature in the Li-ion battery system. Mainly, low-temperatures were fixed to 0^oC, -5^oC, -10^oC, and -15^oC. It was found that the SEI layer is a temperature-dependent layer. The compositions of the SEI layer were mainly decided by the compositions of the electrolyte because their physical properties such as freezing and melting points were highly dependable by the temperature. When the temperature is lowered to a certain extent, the partial freezing of the electrolyte occurs, and significantly poor ionic conductivity is achieved compared to room temperature. The SEI layer was crucial especially for the low-temperature battery cycle because, without the SEI layer, poor battery performance was seen in Chapter 5.2. The battery had a much better low-temperature performance with the SEI layer formed on the graphite anode. Due to the reduced ionic conductivity of the battery electrolyte, poor low-temperature battery performance was still observed although the SEI layer exists. The cycling performance including the capacity, coulombic efficiency, irreversible capacity loss, and capacity loss was poor at low-temperature. FEC additive can be used to improve the capacity loss and obtain good coulombic efficiency, but it does not affect the capacity produced. Some of the analytical techniques were used such as EIS, ATR-FTIR, and AFM to understand the behaviour or the SEI layer based on the temperature. EIS and ATR-FTIR were used to find out the possible resistance of the SEI layer (R_{sei}) and the SEI components by producing an FTIR spectrum. Based on the FTIR data compared with the literature values [35], $(CH_2OCO_2Li)_2$, Li_2CO_3, and ROLi are the most commonly observed SEI components because EC based electrolyte was mainly used in this thesis. Possibly in an electrolyte with an FEC additive, the LiF component can be additionally formed to the SEI component. AFM produced images of the SEI layer formed on the graphite electrode because it visualises the scanned surface of the sample.

This research has lots of potential in the future because the relationship between the SEI layer and the low temperature still needs to be investigated further. Once its relationship is fully found, then this would be vital in future low-temperature Li-ion battery manufacturing in diverse applications where the battery needs to be exposed to a cold environment.

7.2 Future work

The relationship of the SEI layer and the low-temperature is crucial for the future low-temperature Li-ion battery because of not enough information. Researchers were focused on findings of the best electrolyte compositions that are fully in a liquid state at extremely low temperatures $<-30^oC$ [48] or using different Lithium salt ($LiBF_4$) instead of $LiPF_6$ in the electrolyte to improve the low-temperature performance [41]. Most of the researches were mainly focused on chemical studies only to develop

cathode or anode material, electrolyte composition, Lithium-ion diffusivity, and so on. However, there was not enough physical study of the SEI layer. The experiment done in this thesis was mostly a proof of concept that the SEI layer is a temperature-dependent layer and the relationship between its layer with the low temperature. More significant work needs to be done especially on the temperature-based physical study of the SEI layer.

7.2.1 Improve formation of SEI layer

The composition of SEI layer in this thesis was limited due to only anode material (Artificial Graphite) and Lithium-based salt ($LiPF_6$) electrolyte were used. It is already known that the electrode material and electrolyte are the two key factors affecting the SEI layer composition [35] because the SEI components will be either organic or inorganic components on the surface of graphite as shown in Chapter 2, Table 2-3.

Although this stage of experiment was only limited to 90% artificial graphite in anode electrode composition, it is understood that controlling the formation of SEI layer can be the key aspect of low-temperature battery performance. Hence, it would be interesting to see how SEI layer forms when the graphite composition of electrode is changed to 80%, 85%, 95% and it affects the low-temperature battery performance. It can be expected that the more graphite composition in graphite electrode, the better formation of the SEI layer because the more Li-ions can react with graphite to form more inhomogeneous layer. Good SEI layer leads to better battery performance because it prevents the graphite exfoliation.

Another method to improve SEI formation is pre-lithiation technique in which the graphite electrode has direct contact with pure Li material with battery electrolyte as shown in Figure 7.1 below. Normally, pre-lithiation needs around 24-48 hours because it forcefully allow the Li material to react with graphite electrode and electrolyte. It is expected to have better SEI formation because less Li-ions will be involved on SEI formation at 1st cycle and further cycles in which prevents initial irreversible capacity loss. In addition, the capacity fade will occur later than 40th cycle (thesis specific result) as more Li-ions will be available for intercalation process in battery discharge/charge. However, this technique should be carefully monitored because the extra excess amount of unused Li will be over on the surface of the graphite electrode that leads to dendrite growth having major concern on safety issues of the battery.
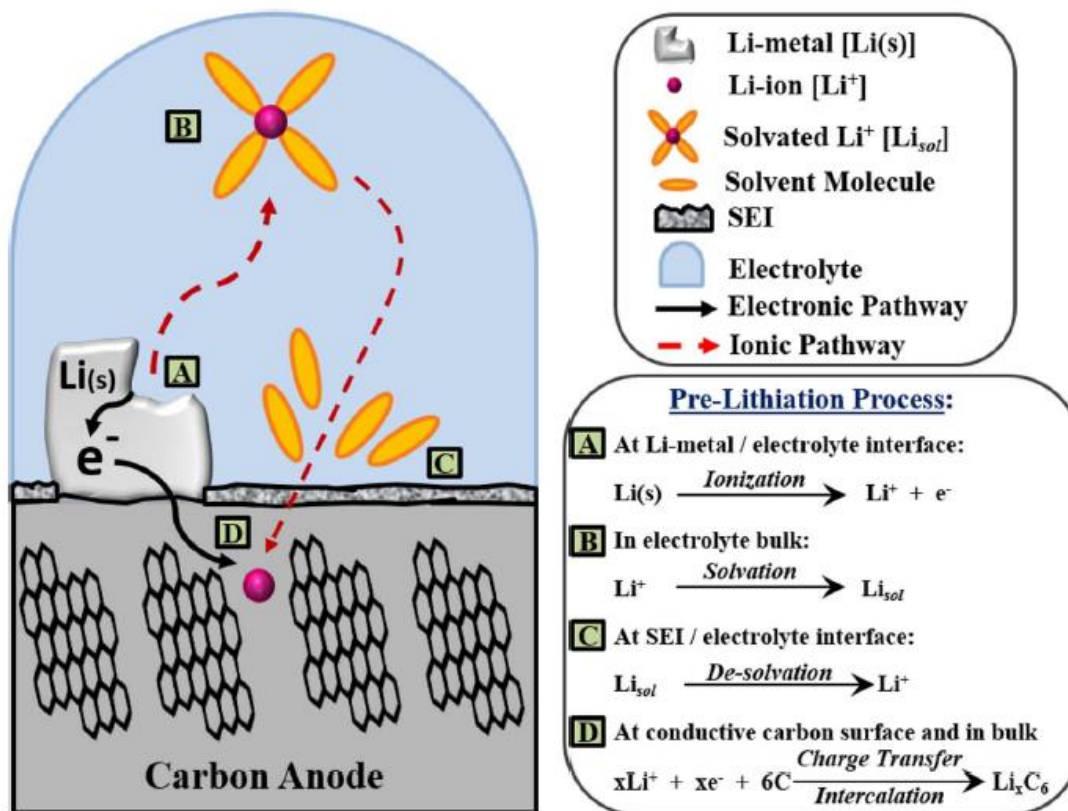
Figure 7-1: An example of how pre-lithiation works and its electrochemical reaction [104]

Varying graphite composition (80 – 95%) or pre-lithiation cannot be guaranteed whether they will solve the puzzle of low-temperature battery performance, but it is definitely promising topics as the relationship between SEI layer and the low-temperature battery performance can be dealt with.

7.2.2 Changing electrolyte

In this thesis, the type of electrolyte was limited to only the $LiPF_6$ salt in EC-based electrolyte (LP30) which is most commonly used electrolyte in battery system. In addition, it is understood that amongst various electrolyte available, having EMC solvent is more ideal for low-temperature battery systems due to its low melting point. FEC was used as an additive to mainly improve the quality of SEI layer forming LiF on graphite anode.

$LiBF_4$ (Lithium tetrafluoroborate) has smaller density (0.852 g/cm^3) than $LiPF_6$ (2.84 g/cm^3) so it would be interesting to see how an electrolyte with $LiBF_4$ salt performs at low-temperature. It can be hypothesised that $LiBF_4$ salt based electrolyte can perform better than $LiPF_6$ due to not only its better solubility in water but also smaller mass. Low-temperature battery performance and the quality of SEI layer with two salts can be compared from the further research in future and prove which salt performs better and why.

The physical property of a solvent becomes a key aspect in low-temperature battery system which were shown in Chapter 5 and also shown in previous research by Huang et al [48]. At low-temperature, most of electrolyte will be in full liquid state due to low melting point solvents; DEC and EMC. From this, it can be hypothesised as the composition of electrolytes can be differed having low melting point (DEC, EMC, and PC) with EC or DMC solvents. Further research needs to be done about low-temperature performance related to formation of SEI layer using various compositions of electrolytes. It would be interesting to see how the quality of SEI layer affects the low-temperature battery performance with various compositions of electrolytes. Although electrolytes consists of DEC and EMC solvents are 100% liquid state [48] at low-temperature, it is expected to have decreased capacity because electrolyte phase is not the only factor affecting the poor low-temperature battery performance.

Most of Li-ion batteries with an EC based electrolyte have a low initial coulombic efficiency due to the formation of SEI layer but this can be much improved using FEC or VC (Vinylene Carbonate) additive. In this particular thesis, it was understood that FEC additive had strong impact on not only reducing the capacity loss during change in cycling temperature but also improving the quality of SEI layer that leads to better initial coulombic efficiency. However, it had a little effect on the capacity in which can be hypothesised that the weight and the composition of electrode material are key factors determining the capacity. The role of FEC was already investigated by previous researchers [26, 27] but they were limited to battery performance and SEI layer of graphite and Si electrodes respectively. Hence, further investigation can be done relating with battery cycling low-temperatures and types of additives. From this, the correlation between the formation of SEI layer based on types of additives with cycling temperature can be understood to realise the main issue beside the electrolyte phase causing the limited low-temperature battery performance.

7.2.3 Investigation techniques

Few experimental techniques (EIS, AFM, FTIR) were used in this thesis due to the limited accessibility and availability in the lab. It is well-known that SEI layer is a very sensitive and thin layer that is only few Å. Since some of SEI components are partially soluble in the electrolyte, it becomes more difficult to investigate the SEI layer using experimental techniques. Hence, it needs to be investigated with techniques that minimise the damage of SEI layer.

There is a non-destructive technique that allows to understand the thermal decomposition behaviour of SEI layer called Differential Scanning Calorimetry (DSC). It can provide the thermal decomposition graph showing at which temperature does either endothermic or exothermic reaction taking place with a temperature range from -60 up to few hundreds °C. From this, more detailed SEI components

of the tested sample can be analysed easily. For example, $ROCO_2Li$ is one of the SEI components but R was difficult to identify. Previous research [105] narrow downed the R to either CH_3 or C_2H_5 using DSC technique.

For example, the resistance of the SEI layer after the discharge cycle can be compared with the charge cycle at a low cycling temperature. From this, it is expected to understand the correlation between the temperature and the discharge/charge cycle with the SEI layer from the change in resistance. Another possible physical study of the SEI layer is that to investigate the change in thickness and height of the SEI components based on low-temperature cycles by using X-ray diffraction (XRD) because it is a non-destructive experimental technique to deeply analyse the thin surface structure.

References

1. Whittingham, M.S., *History, evolution, and future status of energy storage.* Proceedings of the IEEE, 2012. **100**(Special Centennial Issue): p. 1518-1534.
2. Linden, D. and T.B. Reddy, *Handbook of batteries 3rd edition.* TRD: McGraw-Hill, 2002.
3. PANalytical, *Lithium ion battery works.* 2015, PANalytical.
4. Amatucci, G., et al., *Materials' effects on the elevated and room temperature performance of CLiMn2O4 Li-ion batteries.* Journal of power sources, 1997. **69**(1-2): p. 11-25.
5. Edstroem, K., T. Gustafsson, and J.O. Thomas, *The cathode–electrolyte interface in the Li-ion battery.* Electrochimica Acta, 2004. **50**(2-3): p. 397-403.
6. Winter, M., et al., *Insertion electrode materials for rechargeable lithium batteries.* Advanced materials, 1998. **10**(10): p. 725-763.
7. Ramadass, P., et al., *Capacity fade of Sony 18650 cells cycled at elevated temperatures: Part I. Cycling performance.* Journal of power sources, 2002. **112**(2): p. 606-613.
8. Ohzuku, T., et al., *Innovative insertion material of LiAl1/4Ni3/4O2 (Rm) for lithium-ion (shuttlecock) batteries.* Journal of Power Sources, 1997. **68**(1): p. 131-134.
9. Arai, H., et al., *Characterization and cathode performance of Li1− xNi1+ xO2 prepared with the excess lithium method.* Solid State Ionics, 1995. **80**(3-4): p. 261-269.
10. Ohzuku, T., A. Ueda, and M. Nagayama, *Electrochemistry and structural chemistry of LiNiO2 (R3m) for 4 volt secondary lithium cells.* Journal of the Electrochemical Society, 1993. **140**(7): p. 1862.
11. Huang, H., S.-C. Yin, and L.s. Nazar, *Approaching theoretical capacity of LiFePO4 at room temperature at high rates.* Electrochemical and Solid State Letters, 2001. **4**(10): p. A170.
12. Kominato, A., et al., *Analysis of surface films on lithium in various organic electrolytes.* Journal of power sources, 1997. **68**(2): p. 471-475.
13. Nitta, N., et al., *Li-ion battery materials: present and future.* Materials today, 2015. **18**(5): p. 252-264.
14. Dahn, J., et al., *Lithium Batteries, New Materials, Developments and Perspectives, .* G. Pistoia, Ed., Elsevier, Amsterdam 1994. **1**.
15. von Sacken, U., et al., *Comparative thermal stability of carbon intercalation anodes and lithium metal anodes for rechargeable lithium batteries.* Journal of power sources, 1995. **54**(2): p. 240-245.
16. Aurbach, D., et al., *On the correlation between surface chemistry and performance of graphite negative electrodes for Li ion batteries.* Electrochimica acta, 1999. **45**(1-2): p. 67-86.
17. Jung, Y., et al., *Lithium insertion into disordered carbons prepared from organic polymers.* Journal of the Electrochemical Society, 1998. **145**(9): p. 3123.
18. Béguin, F., et al., *Correlation of the irreversible lithium capacity with the active surface area of modified carbons.* Carbon, 2005. **43**(10): p. 2160-2167.
19. Crabtree, G., E. Kocs, and L. Trahey, *The energy-storage frontier: Lithium-ion batteries and beyond.* MRS Bulletin, 2015. **40**(12): p. 1067-1078.
20. Nishi, Y., *The development of lithium ion secondary batteries.* The Chemical Record, 2001. **1**(5): p. 406-413.
21. Wang, S., et al., *Direct visualization of solid electrolyte interphase on Li 4 Ti 5 O 12 by in situ AFM.* RSC Advances, 2016. **6**(81): p. 77105-77110.
22. Lan, C.-K., et al., *Improvement of the Ar/N 2 binary plasma-treated carbon passivation layer deposited on Li 4 Ti 5 O 12 electrodes for stable high-rate lithium ion batteries.* RSC Advances, 2015. **5**(112): p. 92554-92563.
23. Huang, S., et al., *Li4Ti5O12/Ag composite as electrode materials for lithium-ion battery.* Solid State Ionics, 2006. **177**(9-10): p. 851-855.
24. Chan, C.K., et al., *High-performance lithium battery anodes using silicon nanowires.* Nature nanotechnology, 2008. **3**(1): p. 31-35.

25. Zhang, S.S., K. Xu, and T.R. Jow, *Study of LiBF4 as an electrolyte salt for a Li-ion battery.* Journal of The Electrochemical Society, 2002. **149**(5): p. A586-A590.

26. McMillan, R., et al., *Fluoroethylene carbonate electrolyte and its use in lithium ion batteries with graphite anodes.* Journal of Power Sources, 1999. **81**: p. 20-26.

27. Nakai, H., et al., *Investigation of the solid electrolyte interphase formed by fluoroethylene carbonate on Si electrodes.* Journal of The Electrochemical Society, 2011. **158**(7): p. A798.

28. Hou, T., et al., *The influence of FEC on the solvation structure and reduction reaction of LiPF6/EC electrolytes and its implication for solid electrolyte interphase formation.* Nano Energy, 2019. **64**: p. 103881.

29. Shkrob, I.A., J.F. Wishart, and D.P. Abraham, *What makes fluoroethylene carbonate different?* The Journal of Physical Chemistry C, 2015. **119**(27): p. 14954-14964.

30. Smart, M., B. Ratnakumar, and S. Surampudi, *Electrolytes for Low-Temperature Lithium Batteries Based on Ternary Mixtures of Aliphatic Carbonates.* Journal of the Electrochemical Society, 1999. **146**(2): p. 486-492.

31. Zhang, X., et al., *Electrochemical and infrared studies of the reduction of organic carbonates.* Journal of The Electrochemical Society, 2001. **148**(12): p. A1341.

32. Delp, S.A., et al., *Importance of reduction and oxidation stability of high voltage electrolytes and additives.* Electrochimica Acta, 2016. **209**: p. 498-510.

33. Borodin, O., et al., *Towards high throughput screening of electrochemical stability of battery electrolytes.* Nanotechnology, 2015. **26**(35): p. 354003.

34. Peled, E., *The electrochemical behavior of alkali and alkaline earth metals in nonaqueous battery systems—the solid electrolyte interphase model.* Journal of The Electrochemical Society, 1979. **126**(12): p. 2047-2051.

35. Verma, P., P. Maire, and P. Novák, *A review of the features and analyses of the solid electrolyte interphase in Li-ion batteries.* Electrochimica Acta, 2010. **55**(22): p. 6332-6341.

36. Edström, K., M. Herstedt, and D.P. Abraham, *A new look at the solid electrolyte interphase on graphite anodes in Li-ion batteries.* Journal of Power Sources, 2006. **153**(2): p. 380-384.

37. Peled, E. and S. Menkin, *SEI: past, present and future.* Journal of The Electrochemical Society, 2017. **164**(7): p. A1703-A1719.

38. Zheng, T., A.S. Gozdz, and G.G. Amatucci, *Reactivity of the solid electrolyte interface on carbon electrodes at elevated temperatures.* Journal of The Electrochemical Society, 1999. **146**(11): p. 4014-4018.

39. MacNeil, D., D. Larcher, and J. Dahn, *Comparison of the reactivity of various carbon electrode materials with electrolyte at elevated temperature.* Journal of the electrochemical society, 1999. **146**(10): p. 3596-3602.

40. Du Pasquier, A., et al., *Differential Scanning Calorimetry Study of the Reactivity of Carbon Anodes in Plastic Li-Ion Batteries.* Journal of the Electrochemical Society, 1998. **145**(2): p. 472-477.

41. Zhang, S., K. Xu, and T. Jow, *A new approach toward improved low temperature performance of Li-ion battery.* Electrochemistry communications, 2002. **4**(11): p. 928-932.

42. Zhang, S., K. Xu, and T. Jow, *Low temperature performance of graphite electrode in Li-ion cells.* Electrochimica acta, 2002. **48**(3): p. 241-246.

43. Zhang, S., K. Xu, and T. Jow, *Electrochemical impedance study on the low temperature of Li-ion batteries.* Electrochimica acta, 2004. **49**(7): p. 1057-1061.

44. Plichta, E.J. and W.K. Behl, *A low-temperature electrolyte for lithium and lithium-ion batteries.* Journal of Power Sources, 2000. **88**(2): p. 192-196.

45. Smart, M., B. Ratnakumar, and S. Surampudi, *Use of organic esters as cosolvents in electrolytes for lithium-ion batteries with improved low temperature performance.* Journal of The Electrochemical Society, 2002. **149**(4): p. A361-A370.

46. Zhuang, G.V., et al., *A study of electrochemical reduction of ethylene and propylene carbonate electrolytes on graphite using ATR-FTIR spectroscopy.* Electrochemical and Solid State Letters, 2005. **8**(9): p. A441.

47. Zhuang, G.V. and P.N. Ross Jr, *Analysis of the chemical composition of the passive film on Li-Ion battery anodes using attentuated total reflection infrared spectroscopy.* Electrochemical and Solid State Letters, 2003. **6**(7): p. A136.

48. Huang, C.K., et al., *The limits of low-temperature performance of Li-ion cells.* Journal of the Electrochemical Society, 2000. **147**(8): p. 2893-2896.

49. Shiao, H.-C.A., et al., *Low temperature electrolytes for Li-ion PVDF cells.* Journal of power sources, 2000. **87**(1-2): p. 167-173.

50. Nagasubramanian, G., *Electrical characteristics of 18650 Li-ion cells at low temperatures.* Journal of applied electrochemistry, 2001. **31**(1): p. 99-104.

51. Plichta, E., et al., *Development of low temperature Li-ion electrolytes for NASA and DoD applications.* Journal of power sources, 2001. **94**(2): p. 160-162.

52. Herreyre, S., et al., *New Li-ion electrolytes for low temperature applications.* Journal of power sources, 2001. **97**: p. 576-580.

53. Behl, W.K. and E.J. Plichta, *An Electrolyte for Low Temperature Applications of Lithium and Lithium-Ion Batteries.* 1998, ARMY RESEARCH LAB ADELPHI MD.

54. Lin, H.-P., et al., *Low-temperature behavior of Li-ion cells.* Electrochemical and solid state letters, 2001. **4**(6): p. A71.

55. Zhang, S., K. Xu, and T. Jow, *The low temperature performance of Li-ion batteries.* Journal of Power Sources, 2003. **115**(1): p. 137-140.

56. Lingane, P.J. and D.G. Peters, *Chronopotentiometry.* 1971.

57. Shu, Z., R. McMillan, and J. Murray, *Electrochemical intercalation of lithium into graphite.* Journal of The Electrochemical Society, 1993. **140**(4): p. 922.

58. Marks, T., et al., *A guide to Li-ion coin-cell electrode making for academic researchers.* Journal of The Electrochemical Society, 2010. **158**(1): p. A51.

59. Atkins, P., *J. dePaula.* Physical chemistry, 2006. **9**.

60. Analytical, R., *Conductivity. Theory and Practice.* 1992: Radiometer Analytical SAS.

61. Baykara, M.Z. and U. Schwarz, *Atomic force microscopy: Methods and applications*, in *Encyclopedia of Spectroscopy and Spectrometry*. 2017, Elsevier.

62. Jagtap, R. and A. Ambre, *Overview literature on atomic force microscopy (AFM): Basics and its important applications for polymer characterization.* 2006.

63. Baykara, M.Z., et al., *Three-Dimensional Atomic Force Microscopy–Taking Surface Imaging to the Next Level.* Advanced materials, 2010. **22**(26-27): p. 2838-2853.

64. Zhang, J., et al., *Direct observation of inhomogeneous solid electrolyte interphase on MnO anode with atomic force microscopy and spectroscopy.* Nano letters, 2012. **12**(4): p. 2153-2157.

65. Demirocak, D.E. and B. Bhushan, *In situ atomic force microscopy analysis of morphology and particle size changes in lithium iron phosphate cathode during discharge.* Journal of colloid and interface science, 2014. **423**: p. 151-157.

66. Ramdon, S., B. Bhushan, and S.C. Nagpure, *In situ electrochemical studies of lithium-ion battery cathodes using atomic force microscopy.* Journal of Power Sources, 2014. **249**: p. 373-384.

67. Cresce, A.v., et al., *In situ and quantitative characterization of solid electrolyte interphases.* Nano letters, 2014. **14**(3): p. 1405-1412.

68. Eaton, P. and P. West, *Atomic force microscopy.* 2010: Oxford University Press.

69. Kaemmer, S.B., *Introduction to Bruker's ScanAsyst and PeakForce tapping AFM technology.* Bruker application note. Bruker Nano Inc., Santa Barbara, CA, 2011.

70. Scientific, T., *Introduction to FTIR spectroscopy.* 2018, Viitattu.

71. Forensics, G., *How does Fourier Transform Infrared (FTIR) Spectroscopy Work?*

72. Ausili, A., M. Sánchez, and J.C. Gómez-Fernández, *Attenuated total reflectance infrared spectroscopy: A powerful method for the simultaneous study of structure and spatial orientation of lipids and membrane proteins.* Biomedical Spectroscopy and Imaging, 2015. **4**(2): p. 159-170.

73. Corporation, B., *ATR Basics – Principles of Attenuated Total Reflectance Spectroscopy*. 2019, Bruker Corporation: ETTLINGEN.

74. Matsui, M., et al., *In-operando FTIR Spectroscopy for Composite Electrodes of Lithium-ion Batteries.* Electrochemistry, 2015. **83**(10): p. 874-878.

75. Wu, C., Y. Bai, and F. Wu, *Fourier-transform infrared spectroscopic studies on the solid electrolyte interphase formed on Li-doped spinel Li 1.05 Mn 1.96 O 4 cathode.* Journal of Power Sources, 2009. **189**(1): p. 89-94.

76. Lu, W., et al., *Identification of solid electrolyte interphase formed on graphite electrode cycled in trifluoroethyl aliphatic carboxylate-based electrolytes for low-temperature lithium-ion batteries.* Ionics, 2016. **22**(11): p. 2095-2102.

77. Tensor, B., *FT-IR & OPUS Data Collection Program.* Bruker Optics, Milan, Italy. Google Scholar: p. 30.

78. Instruments, G., *Basics of electrochemical impedance spectroscopy.* G. Instruments, Complex impedance in Corrosion, 2007: p. 1-30.

79. Choi, W., et al., *Modeling and Applications of Electrochemical Impedance Spectroscopy (EIS) for Lithium-ion Batteries.* Journal of Electrochemical Science and Technology, 2020. **11**(1): p. 1-13.

80. Jiang, S., J. Love, and S.P. Badwal. *Electrochemical techniques in studies of solid ionic conductors*. in *Key engineering materials*. 1997. Trans Tech Publ.

81. Andre, D., et al., *Characterization of high-power lithium-ion batteries by electrochemical impedance spectroscopy. II: Modelling.* Journal of Power Sources, 2011. **196**(12): p. 5349-5356.

82. Krewer, U., et al., *dynamic models of Li-Ion batteries for diagnosis and operation: A review and perspective.* Journal of The Electrochemical Society, 2018. **165**(16): p. A3656.

83. Ratnakumar, B., M. Smart, and S. Surampudi, *Effects of SEI on the kinetics of lithium intercalation.* Journal of power sources, 2001. **97**: p. 137-139.

84. Momma, T., et al., *Ac impedance analysis of lithium ion battery under temperature control.* Journal of Power Sources, 2012. **216**: p. 304-307.

85. Bryngelsson, H., et al., *How dynamic is the SEI?* Journal of Power Sources, 2007. **174**(2): p. 970-975.

86. Aurbach, D., *Review of selected electrode–solution interactions which determine the performance of Li and Li ion batteries.* Journal of Power Sources, 2000. **89**(2): p. 206-218.

87. Glazier, S., et al., *Determining Parasitic Reaction Enthalpies in Lithium-Ion Cells Using Isothermal Microcalorimetry.* Journal of The Electrochemical Society, 2018. **165**(14): p. A3449.

88. Shi, F., et al., *Lithium metal stripping beneath the solid electrolyte interphase.* Proceedings of the National Academy of Sciences, 2018. **115**(34): p. 8529-8534.

89. Birkl, C.R., et al., *Degradation diagnostics for lithium ion cells.* Journal of Power Sources, 2017. **341**: p. 373-386.

90. Fan, J., *On the discharge capability and its limiting factors of commercial 18650 Li-ion cell at low temperatures.* Journal of Power Sources, 2003. **117**(1-2): p. 170-178.

91. Uhlemann, M., et al., *In-Depth Study of Li4Ti5O12 Performing beyond Conventional Operating Conditions.* ACS Applied Materials & Interfaces, 2020. **12**(33): p. 37227-37238.

92. Cho, Y.-G., et al., *Enabling the Low-Temperature Cycling of NMC|| Graphite Pouch Cells with an Ester-Based Electrolyte.* ACS Energy Letters, 2021. **6**(5): p. 2016-2023.

93. Xiao, L., et al., *Optimization of EC-based multi-solvent electrolytes for low temperature applications of lithium-ion batteries.* Electrochimica acta, 2004. **49**(27): p. 4857-4863.

94. Alliata, D., et al., *Electrochemical SPM investigation of the solid electrolyte interphase film formed on HOPG electrodes.* Electrochemistry communications, 2000. **2**(6): p. 436-440.

95.   Zhu, Z., et al., *Fluoroethylene Carbonate Enabling a Robust LiF-rich Solid Electrolyte Interphase to Enhance the Stability of the MoS2 Anode for Lithium-Ion Storage.* Angewandte Chemie, 2018. **130**(14): p. 3718-3722.

96.   Aurbach, D., et al., *Failure and stabilization mechanisms of graphite electrodes.* The Journal of Physical Chemistry B, 1997. **101**(12): p. 2195-2206.

97.   Aurbach, D., Y. Ein-Ely, and A. Zaban, *The surface chemistry of lithium electrodes in alkyl carbonate solutions.* Journal of The Electrochemical Society, 1994. **141**(1): p. L1-L3.

98.   Aurbach, D., Y. Gofer, and J. Langzam, *The correlation between surface chemistry, surface morphology, and cycling efficiency of lithium electrodes in a few polar aprotic systems.* Journal of the Electrochemical Society, 1989. **136**(11): p. 3198.

99.   Aurbach, D., et al., *A comparative study of synthetic graphite and Li electrodes in electrolyte solutions based on ethylene carbonate-dimethyl carbonate mixtures.* Journal of the Electrochemical Society, 1996. **143**(12): p. 3809.

100.   Aurbach, D., et al., *A comparative study of synthetic graphite and Li electrodes in electrolyte solutions based on ethylene carbonate-dimethyl carbonate mixtures.* Journal of The Electrochemical Society, 1996. **143**(12): p. 3809-3820.

101.   Aurbach, D., et al., *The behaviour of lithium electrodes in propylene and ethylene carbonate: Te major factors that influence Li cycling efficiency.* Journal of Electroanalytical Chemistry, 1992. **339**(1-2): p. 451-471.

102.   Aurbach, D., *Electrode–solution interactions in Li-ion batteries: a short summary and new insights.* Journal of power sources, 2003. **119**: p. 497-503.

103.   Peled, E., et al., *An advanced tool for the selection of electrolyte components for rechargeable lithium batteries.* Journal of the electrochemical Society, 1998. **145**(10): p. 3482.

104.   Shellikeri, A., et al., *Investigation of pre-lithiation in graphite and hard-carbon anodes using different lithium source structures.* Journal of The Electrochemical Society, 2017. **164**(14): p. A3914.

105.   Ryou, M.-H., et al., *Effects of lithium salts on thermal stabilities of lithium alkyl carbonates in SEI layer.* Electrochimica acta, 2012. **83**: p. 259-263.